

STUDIES OF LOW FIELD
MAGNETIZATION IN ALLOYS

Thesis submitted
for the degree of Doctor of Philosophy
at the University of London

by

WILLIAM HOWARTH

The Blackett Laboratory
Imperial College of Science and Technology
London S.W.7.

October 1978.

ABSTRACT

Since the discovery in 1971 that the a.c. susceptibility of AuFe alloys exhibited extremely sharp peaks as a function of temperature, the study of spin glass ordering in materials has continued to expand, both theoretically and experimentally. We discuss in detail the development of this field up to the present time. At the outset of this work it was still not known whether the sharp cusps obtained in these spin glass materials were an artefact of the a.c. technique of measurement or not and so we approached the problem by designing a sensitive low field apparatus to make similar measurements in a d.c. field, details of which are presented.

We have used this apparatus to make a detailed study of the low field (~ 2 Oe) magnetization in a series of Palladium Manganese alloys with concentrations between 8.5 at%Mn and 1.3 at%Mn. From these, and additional resistivity, measurements, we have shown conclusively the spin glass ordering occurring in those alloys with greater than 4.0 at%Mn and we discuss the nature of the approach to ferromagnetic ordering as the Manganese concentration is decreased.

We also show that the apparatus is not only capable of measuring the dipole moment of a sample but in principle of giving signals from higher multipoles in an expansion of the sample magnetization. An important extension of

this for the use of a SQUID magnetometer to observe the sublattice magnetization of a layer antiferromagnet is given.

Finally, we present related low field magnetization measurements on PdFe and PdCo alloys, which, although not complete, throw up intriguing points of discussion related to the magnetic ordering in dilute Palladium alloys, and suggest many areas for additional work.

ACKNOWLEDGEMENTS

This dissertation is submitted for the degree of Doctor of Philosophy in the University of London. The research was carried out between October 1974 and September 1977 in the Physics department of Imperial College, London, under the supervision of Professor B.R. Coles. It is my great pleasure to thank him for his constant advice and guiding influence and for his many hours of valuable discussion.

I would like to express my deepest gratitude to Dr. C.N. Guy who has not only taught me many things relating to the practical side of research but who has, throughout the whole of the time, been constantly interested in this work and been the source of many fruitful discussions.

Similarly, I thank Dr. N.Rivier, not only for his contagious enthusiasm, but also for many stimulating ideas and for being so friendly and helpful at all times.

Dr. H.E.N. Stone has been a source of invaluable advice on all metallurgical matters related to this work and I thank him very much for his great willingness to always be of assistance. I would also like to thank all the other members of the Metal Physics and Solid State Physics Groups at Imperial College for their help and for making three years of research so pleasurable.

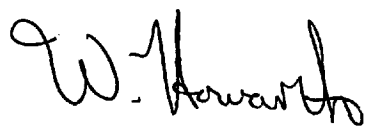
I acknowledge the financial support of the Science Research Council during the three years spent at Imperial College as they provided me with a research studentship.

I should also like to thank my new colleagues in the

Department of Metallurgy and Materials Science, Cambridge University, especially Dr. J.E. Evetts and Dr. R.E. Somekh, for their help and moral support during the trying time of completing the write up of this thesis. My thanks also go to Mrs C. Bishop and Mrs S. Hessey for their typing of this manuscript.

The essence of education is to prepare oneself for the future and there are other things to life than research alone. I should therefore like to give a mention to several authors, whose works that I've read in the past four years have had the most influence on me and given me the greatest pleasure, these are: C.P. Snow, A. Huxley, Shakespeare, E. Hemmingway, M. Renault, Charles Dickens and A. Malreaux.

Finally I should like to thank my parents for their constant, but not over-pressurizing, interest in all of my education and for all of the sacrifices they have made for my sake. To them I dedicate this thesis.



William Howarth

Department of Metallurgy and Materials Science,
University of Cambridge.
September, 1978.

CONTENTS

	<u>Page</u>
Abstract	1
Acknowledgements	3
Contents	5
<u>Chapter 1</u>	<u>Magnetic Alloys</u>
1.1	Introduction 8
1.2	The Single Impurity Limit 9
1.3	Interactions Between Solute Atoms
1.	Introduction 13
2.	RKKY Interaction 14
3.	Short Range Interactions 21
4.	Exchange Enhanced Hosts 23
1.4	The Spin Glass
1.	Introduction 27
2.	Behaviour of Spin Glass Systems 29
3.	Theories of Spin Glasses 41
4.	Conclusions 54
	References 56
<u>Chapter 2</u>	<u>Previous Work on the PdMn System</u>
2.1	Introduction 63
2.2	Resistivity 67
2.3	Specific Heat 68
2.4	Magnetization Measurements 69
2.5	Electron Paramagnetic Resonance 71
2.6	Low Field Susceptibility 73
2.7	Neutron Scattering 74
2.8	Nuclear Orientation 79
	References 80
<u>Chapter 3</u>	<u>Experimental</u>
3.1	Magnetic Measurements 82
3.2	Force Method 82

	<u>Page</u>	
3.3	Induction Methods	
	1. Introduction	84
	2. Mutual Inductance Techniques	85
	3. SQUID Magnetometers	89
	4. Vibration Magnetometers	93
3.4	The Vibrating Sample Magnetometer	
	1. Introduction	94
	2. Mechanical Design	96
	3. Electrical Design	
	i) Circuit Description	100
	ii) The Pick-up Coils	102
	iii) The Magnetic Field Coils	109
	4. Temperature Measurement	110
	5. Usage and Performance	114
3.5	Resistivity Apparatus	119
3.6	Sample Preparation	121
	References	124
<u>Chapter 4</u>	<u>Investigation of the PdMn Magnetic Phase Diagram</u>	
4.1	1. Low Field Magnetization Measurements	126
	2. Resistivity Measurements	141
	3. Discussion	143
4.2	Observation of unusual Remanent Behaviour	165
	References	169
<u>Chapter 5</u>	<u>Re-Analysis of the VSM Signal for Non-Uniform Magnetization</u>	
5.1	Introduction	170
5.2	Experimental Verification	172
5.3	Studies of the Remanent State of Magnetically Ordered Materials	
	1. Introduction	182
	2. Results for Iron, Nickel & Cobalt	182
	3. Results on Haematite & Ferrite	186
	4. Palladium Alloys	186
	5. Discussion	189

	<u>Page</u>
5.4	Numerical Analysis of the $\epsilon(z_0)$ Curves 192
5.5	Sublattice Magnetization Measurements 195
	References 200
 <u>Chapter 6</u>	
6.1	Introduction 201
6.2	Copper Manganese 201
6.3	Palladium Iron and Palladium Cobalt
	1. Results 206
	2. Discussion 217
6.4	Platinum Nickel 220
	References 225
 <u>Chapter 7</u>	 Suggestions for further work 227
 Appendix A	 Calculation of pick-up coil field derivatives 230
 Appendix B1	 Programme for HP 9820 to do the field derivative calculations 233
 Appendix B2	 Orthogonalization Programme 234
 Appendix B3	 Least squares fitting programme 235

CHAPTER 1

MAGNETIC ALLOYS

1.1. Introduction

The ancient Chinese knew of the existence of magnetic materials as long ago as 2500B.C. and the production of magnetic fields by electric circuits was first noted by Oersted in 1820. The understanding of such magnetic phenomena has made great advances in the last century due to the inception of Relativity and Quantum Mechanics. These two great leaps in our quest for comprehension of the physical world are both intricately tied up with the study of magnetism. A current carrying wire produces a magnetic field around it. This is now understood as a consequence of the Lorentz transformation of the electrostatic force between charges which are moving with respect to an observational frame of reference. The study of the magnetic order present in the pure elements is inseparable from Quantum Mechanics.

Although our understanding is greatly aided by these powerful tools, the answer to the question; Why is iron (for example) magnetic? still eludes us. The magnetic ordering of pure elements is a very complex phenomenon because of the many interactions which play a role. With the ultimate solution to this problem in mind, progress has been made by examining the interactions taking place in alloys of magnetic elements with those elements which

are non-magnetic. The study of systems where a small concentration of a magnetic element is dissolved in a non-magnetic host can give indications as to how the magnetic properties of the isolated magnetic atom are affected by interactions with the surrounding conduction electrons. Extending to a study of the magnetic properties as a function of the concentration of the magnetic solute atoms can then provide information about the interactions occurring between these atoms.

1.2. The Single Impurity Limit

When we substitute an atom, which has a net magnetic moment in the free state, into some bulk material, the outcome is very dependent on the solvent matrix and on the particular shell responsible for the moment of the free atom. If the unfilled shell remains well localized and tightly bound, as in the case of substitution into non-magnetic insulators, the host has little effect on the magnetic state of the impurity. For the rare earth magnetic impurities this will even be the case when the host is a non-magnetic metal because the 4f shell, which is responsible for the magnetic moment, is well hidden inside the outer bonding shells and so retains its atomic properties.

The substitution of 3d transitional magnetic elements such as Fe, Co and Mn into metallic hosts, however, is complicated by the fact that the 3d energy level generally falls within the conduction band of the host. The 3d

electrons responsible for the moment of the free atom can then go into the conduction band and extend throughout the crystal. Two questions then arise: whether the moment is maintained in the alloy and the extent of its location. This has been the source of a great deal of theoretical and experimental attention for quite some time now. Experimentally, a variety of electrical and magnetic behaviour is shown when 3d atoms are dissolved in metallic hosts, Daybell and Steyert (1.1). Models to explain the formation of localized moments on the 3d impurity atom in metals, by Anderson (1.2), Wolff (1.3) and Clogston et al. (1.4) are all based on the idea of the Virtual Bound State (VBS) which was proposed by Friedel (1.5). Friedel was the first to consider the fact that the 3d electrons could not be truly localized and he suggested that a resonance could be built-up around the impurity from the continuum of the conduction states. A review discussing moment formation in metals is given by Heeger (1.6). Although this is a very important consideration when transition elements are substituted into metals, a preliminary study of the magnetic properties of many metallic systems can be made by assuming that a localized moment does exist on the impurity. Kondo (1.7) made such an assumption and treated the interaction of the conduction electrons with the localized moment, which can be characterized by a spin S , by means of the so-called s-d exchange Hamiltonian;

$$H_{\text{ex}} = - J \sum_{\mathbf{r}} \mathbf{S} \cdot \mathbf{s}(\mathbf{r})$$

first proposed by Zener (1.8) in the different context of moment interaction in insulators. V is the volume over which the localized moment extends, $s(o)$ is the spin density of the conduction electrons at the impurity site and J is the s - d exchange coupling constant. By calculating the effect of this interaction on the scattering amplitude of the conduction electrons, to second order in J , Kondo was able to give an explanation to the long-standing problem of the resistance minimum, occurring as a function of temperature in several metallic alloys (de Haas et al. (1.9a), Van den Berg (1.9b)). It had been shown that such a minimum occurred in alloys which had a strongly temperature dependent susceptibility, Sarachik et al. (1.10), thus indicating that the magnetic moment was instrumental in causing this phenomenon. Kondo showed that spin-flip scattering could produce interference between scattering amplitudes of up and down spin electrons, leading to a term in the resistance proportional to $J \ln T$. For negative J this is an increasing function with decreasing temperature which, in conjunction with the conventional phonon term, decreasing as T^5 , yields a resistance minimum. There is obviously a lower limit to the temperature for which this holds since $\ln T$ diverges as $T \rightarrow 0$. This occurs where the perturbative method employed by Kondo breaks down and subsequent theories, all starting with the assumption of a localized moment and using the s - d Hamiltonian, have shown that a bound state can form between the impurity and the conduction electrons

below a certain temperature, Nagaoka (1.11a), Yosida (1.11b), Wilson (1.11c). This temperature is the Kondo temperature, T_K , below which the correlation between the conduction electrons and the impurity moment is so large that a perturbative calculation can no longer be valid. Indeed, a non-magnetic bound state is formed below that temperature, Nozières (1.12). For a good discussion of the Kondo problem, as this is called, see the reviews by Nozières (1.12), Heeger (1.6) and Kondo (1.13).

Although we know that a magnetic atom in a metal may lose its magnetic moment at sufficiently low temperatures we shall, in this thesis, consider essentially magnetic impurities i.e. those for which $T > T_K$. T_K is still a difficult quantity to evaluate theoretically, being the temperature of cross-over between the high temperature, magnetic, and low temperature, non-magnetic, behaviour, Nozières (1.12). The magnetic behaviour is indicated by a temperature-dependent susceptibility (essentially Curie-Weiss) and a resistance which increases logarithmically with temperature as the temperature is decreased.

Considerable success having been achieved in understanding the magnetic state of single impurities, the interest has swung in the last few years to a study of the magnetic properties of alloys with higher concentrations of magnetic impurity where inter-impurity interactions must be considered.

1.3. Interactions Between Solute Atoms

1.3.1. Introduction

When two moment bearing atoms are brought together, an interaction between the spins arises out of the nature of the quantum mechanical description of the joint system, Heisenberg (1.14). This so called 'Exchange Interaction' strongly couples their spins and gives a preference for them to be parallel or antiparallel, depending on the sign of the interaction. Dirac (1.15) showed that the interaction between the spins of electrons localized in different orthogonal orbitals, $\psi_i(\mathbf{r})$ and $\psi_j(\mathbf{r})$, can be written;

$$V_{\text{ex}} = - \sum_{i,j} J_{ij} \underline{S}_i \cdot \underline{S}_j \quad (\text{I.1})$$

where the exchange integral J_{ij} is given by;

$$J_{ij} = \int d\mathbf{r}_1 \int d\mathbf{r}_2 H(\mathbf{r}_1, \mathbf{r}_2) \psi_i^*(\mathbf{r}_1) \psi_j(\mathbf{r}_1) \psi_j^*(\mathbf{r}_2) \psi_i(\mathbf{r}_2)$$

Equation (I.1) is called the Heisenberg Exchange interaction between spins s_i and s_j . The concept of exchange arose originally in the context of the Heitler-London (1.16) approximation for the Hydrogen molecule but in general 'exchange' is not to be taken as a physical phenomenon of the electrons actually swapping with each other because these quantum mechanical electrons are indistinguishable.

The importance of the contributions to the exchange

interaction between moment bearing atoms in a host is very dependent on the environment of the impurities. In insulators the major contributions are short ranged, direct exchange and kinetic exchange arising from direct overlap of the individual wavefunctions and superexchange being an indirect interaction via some perturbation in the wavefunction of an intermediary, non-magnetic, atom. For a review of these exchange interactions in insulators, along with other much smaller interactions such as polarization exchange and various higher order effects, see Anderson (1.17).

1.3.2. RKKY Interaction

In metals, a long range oscillatory spin polarization is induced in the conduction electrons as a result of the interaction between a localized moment and the conduction electrons. A second impurity atom situated within the range of this spin polarization will be influenced by the spin state of the first, thus leading to a correlation between the spins of the two atoms. This interaction between the solute atoms occurs over large distances and is therefore the major interaction in dilute alloys; it is called the Ruderman-Kittel-Kasuya-Yosida (RKKY) interaction. Kasuya (1.18) and Yosida (1.19) investigated the interaction between localized moments along similar lines to those followed by Ruderman and Kittel, (1.20), who had previously considered the problem of the response of the conduction electrons to a nuclear moment

and had explained the broadening of the nuclear magnetic resonance lines to be a result of the indirect coupling of the nuclear spins.

Yosida (1.19) calculated the effect of the perturbation to the conduction electron wavefunction $\phi_k^0 = \sqrt{\frac{1}{V}} e^{i\mathbf{k}\cdot\mathbf{r}}$ caused by the s-d exchange interaction with a localized spin \underline{S}

$$H_{sd} = -J(\underline{k}, \underline{k}') \underline{S} \cdot \underline{s}$$

where $J(\underline{k}, \underline{k}') = \int \psi_d^*(\underline{r}_1) \phi_k^0(\underline{r}_2) V(\underline{r}_1, \underline{r}_2) \psi_d(\underline{r}_2) \phi_{k'}^0(\underline{r}_1) d\underline{r}_1 d\underline{r}_2$

ψ_d is the localized wavefunction of the solute atom and $V(\underline{r}_1, \underline{r}_2)$ is the interaction potential.

The wavefunction becomes perturbed to ϕ_k and is given by;

$$\phi_k = \phi_k^0 + \sum_{k'} \frac{H_{sd}}{E_k - E_{k'}} \phi_{k'}^0$$

to first order in perturbation

The screening of the localized charge by other electrons means that the interaction potential is considerably shorter ranged than coulombic, and is generally approximated to be a δ -function type of interaction. Making the assumption that $V(\underline{r}_1, \underline{r}_2) = \delta(\underline{r}_1 - \underline{r}_2)$ gives;

$$J(\underline{k}, \underline{k}') = \int \psi_{\underline{d}}^*(\underline{r}) \psi_{\underline{d}}(\underline{r}) e^{i(\underline{k}-\underline{k}') \cdot \underline{r}} d\underline{r} = J(\underline{k}-\underline{k}')$$

$$\therefore J(\underline{k}, \underline{k}') = J(\underline{q}) \quad \text{where } \underline{q} = \underline{k}-\underline{k}'$$

The spin polarization around the impurity moment is then given by

$$\rho_{\pm}(\underline{r}) = \rho_0 \left\{ 1 \pm \frac{3}{8E_F N} \int_0^{\infty} J(q) f(q) s^z (e^{i\underline{q} \cdot \underline{r}} + e^{-i\underline{q} \cdot \underline{r}}) dq \right\}$$

$$\text{where } f(q) = 1 + \left\{ \frac{4k_F^2 - q^2}{4k_F q} \right\} \ln \left(\frac{2k_F + q}{2k_F - q} \right)$$

and N is the total number of lattice points.

and the final form for the spin polarization depends on the final form taken for $J(q)$. Yosida takes $J(q)f(q) = 2J(0)$ for $q < 2k_F$ and zero for q above this. This then leads to a polarization of the form;

$$\rho_{\pm}(\underline{r}) = \rho_0 \left\{ 1 \pm \frac{36}{E_F} \left(\frac{n}{N} \right) J(0) S_z F(2k_F r) \right\}$$

$$\text{where } F(Y) = \frac{Y \cos Y - \sin Y}{Y^4}$$

and $2n$ is the total number of electrons.

For $y \gg 1$, $F(Y)$ is oscillatory in nature as shown in Figure 1.1 for $y > 10$. Therefore the spins of the conduction electrons around an impurity are polarized in an

Figure 1.1 : The spin polarization of the conduction electrons around a magnetic impurity follows a form proportional to $F(Y) = [Y \cos Y - \sin Y] / Y^4$. This is the so called RKKY polarization and is of the oscillatory form shown in the figure for $Y > 10$ radians. This means that the sign of the interaction between this impurity and another moment some distance away can be of either sign.

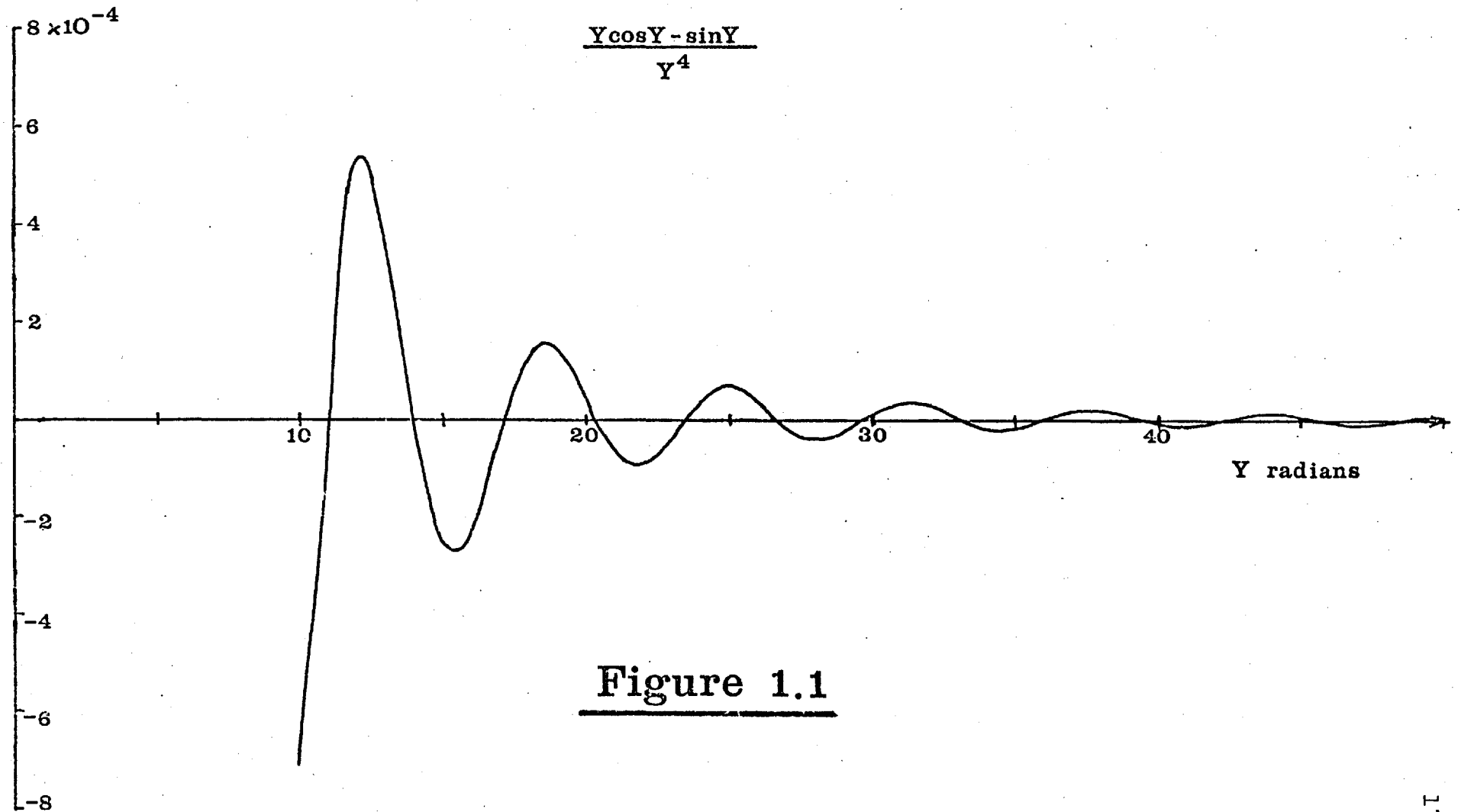


Figure 1.1

oscillatory manner, the magnitude of the polarization slowly decaying with increasing distance from the impurity ($\frac{1}{r^3}$). This can be viewed as the diffraction of de Broglie waves having a maximum wave-vector of k_F , resulting from a sharp cut-off at the Fermi surface.

The effect of the spin polarization about an impurity situated at $\underline{r} = 0$, on another impurity at $\underline{r} = \underline{R}$, is to couple the two spins with an energy

$$E(\underline{R}) = \frac{9\pi}{8} \left(\frac{n}{N}\right)^2 \frac{J^2(0)}{E_F} F(2k_F R) \underline{S}(0) \cdot \underline{S}(\underline{R})$$

This interaction between the two moments can be represented by a Hamiltonian of the form;

$$H = -j(-\underline{R}) \underline{S}(0) \cdot \underline{S}(\underline{R})$$

ie. a Heisenberg Exchange Hamiltonian between the two spins with an exchange constant, $j(\underline{R})$, which is oscillatory in nature.

In general, for any number of moments coupling via the RKKY interaction, we can write

$$H = -\frac{1}{2} \sum_{ij} j(\underline{R}_i - \underline{R}_j) \underline{S}_i \cdot \underline{S}_j$$

or, taking the Fourier Transform;

$$H = - \sum_{\underline{q}} j(\underline{q}) \underline{S}_{\underline{q}} \cdot \underline{S}_{-\underline{q}} \quad (\text{I.2})$$

$$\text{where } j(q) = \frac{1}{2} \sum_{ij} j(\underline{R}_i - \underline{R}_j) e^{iq \cdot (\underline{R}_i - \underline{R}_j)}$$

The randomness of the impurity substitution and the long range oscillatory interaction amongst impurities in dilute alloys leads to a particular type of magnetic ordering at low temperatures which has been the source of a great deal of attention in the last few years. Long range ordering does not occur but the effective field which each solute atom sees leads to the spins being frozen in random orientations below a certain temperature. Alloys which exhibit this type of ordering are called 'spin glasses' (1.21) and will be discussed in detail in Section 1.4.

As well as being the dominant interaction between moments well separated from each other, the RKKY interaction is important in discussing the properties of the rare earth elements. For concentrations of transition metal impurities such that the probability for one transition metal impurity to have a nearest neighbour which is also a transition metal impurity is larger than the probability for it to sit by itself, short range interactions such as d-d covalent admixture and direct exchange largely determine the magnetic ordering which occurs. However, the 4f moments in rare earths interact very little in a direct manner so that the intermediary conduction electron interaction remains an important

mechanism. The nature of the ordering amongst a regular array of spins interacting via a Heisenberg Exchange interaction of the form of Equation (I.2) is dependent on the shape of $j(q)$. If $j(q)$ has a maximum at $q = Q$, say, the stable configuration (that of minimum energy) will be magnetic ordering corresponding to a modulation of the spins with a wave vector Q . If $Q = 0$, ferromagnetic ordering occurs; if $Q = \frac{n\pi}{a}$, the coupling alternates between positive and negative from one spin to the next, giving antiferromagnetic ordering. If Q is non-commensurate with the lattice, a helical or some other modulated spin structure occurs. Neutron diffraction studies have confirmed the existence of this type of spin structure in rare earth elements (1.22). This is no longer true for a disordered array of spins (where in fact $j(q)_{\text{RKKY}}$ has a maximum at $q = 0$, but no long range order occurs).

In the above derivation of the RKKY interaction we have assumed that a localized moment is interacting with a 'sea' of independent conduction electrons which are represented by plane waves. The effect of a strong exchange interaction in the conduction band of the host metal is important in considerably modifying the spatial distribution of the spin polarization around an impurity moment from that calculated above. This is discussed more fully in Section 1.3.4, in relation to the occurrence of 'giant moments' and the severe modification to the nature of the interactions between impurities in such hosts.

A reduced conduction electron mean free path also affects the nature of the RKKY interaction. As shown by De Gennes (1.23), a damping of the strength of the RKKY interaction by a factor $e^{-r/\lambda}$, where λ is the mean free path, is expected to occur. Buchmann et al. (1.24) have recently shown that the temperature of the maximum in the resistivity of thin films of AuFe, in the concentration range of 0.24 to 6.0 at%Fe, where the RKKY interaction is thought to be dominant, increases with increasing annealing temperatures. Increasing the annealing temperature has the effect of removing some of the structural defects and considerably increases the mean free path of the conduction electrons. Thus, by reference to a theory by Larsen (1.25), which relates the impurity interaction strength to the resistivity maximum, it is concluded that the reduction of the mean free path considerably reduces the interaction between the impurity moments.

1.3.3. Short Range Interactions

As the concentration of the solute is increased there soon comes a sizable probability of having nearest neighbour impurities and for transition metals the direct interaction between nearby moments is large. This interaction is largely governed by the nature of the d-d covalent admixture since direct exchange is relatively small. Moriya (1.26) has shown that the effective energy between two similar, adjacent, five-fold degenerate

orbitals, varies with the number of localized electrons in the manner shown in Figure 1.2.

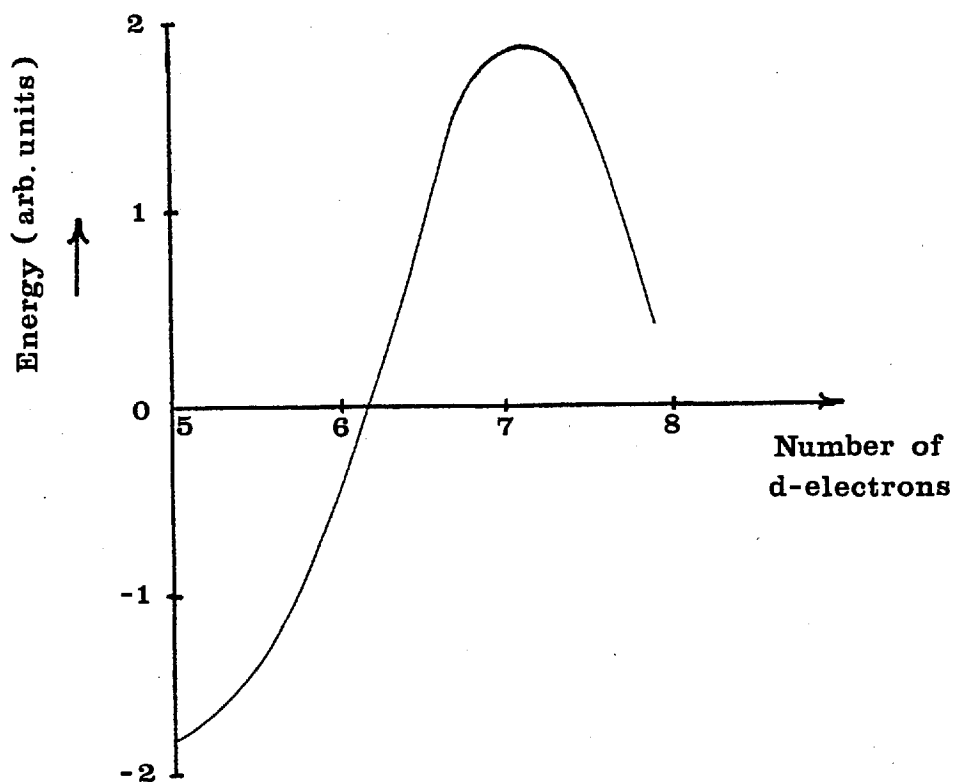


Figure 1.2

Atoms with nearly half-filled d-shells have a tendency to couple antiferromagnetically and as the number of d-electrons is increased there is an increasing tendency for ferromagnetic coupling to occur. On this basis, the interaction between near neighbour iron atoms, for example, will cause them to align parallel to one another while the coupling between manganese atoms will be antiferromagnetic.

The short range interaction between moments, therefore, links together the spins of impurities that are near

neighbours. As the solute concentration increases from the dilute limit, where the random long range interaction describes the nature of the ordering (conditional on there being no Kondo quenching of the moment), first the spins of a few atoms and then a progressively larger number, become correlated by this short range interaction, leading eventually to long range ordering occurring between the moments. The critical concentration for the onset of long range order can be evaluated by 'percolation' theories, which try to calculate the concentration of solute necessary to set up an infinite chain of nearest neighbour impurities in a host metal.

1.3.4. Exchange Enhanced Hosts

Moriya (1.27) has shown that when the exchange enhancement of the susceptibility of the host is large, the spatial extension of the induced polarization is determined by the spatial dependence of the zero frequency generalized susceptibility of the host metal. Within the random-phase approximation (RPA), the susceptibility is given by (1.28)

$$\chi(q,w) = \frac{\chi^0(q,w)}{1-\gamma\chi^0(q,w)} \quad (\text{I.3})$$

where $\chi^0(q,w)$ is the susceptibility without any exchange enhancement and γ is the measure of the intra-atomic interactions.

$$\text{Now } \chi^0(q, w) = \chi_p U(q, w)$$

where χ_p is the Pauli spin susceptibility for free electrons and $U(q, w)$ is the Lindhard function (1.29) with $U(0, 0) = 1$. For $w = 0$ we have that;

$$U(q, 0) = \frac{1}{2} \left[1 + \frac{1-\lambda^2}{2\lambda} \ln \frac{1+\lambda}{1-\lambda} \right] \quad (\text{I.4})$$

$$\text{where } \lambda = \frac{q}{2k_F}$$

A measure of the ferromagnetic tendency is the Stoner factor, S , given by;

$$S = \frac{1}{1-\gamma\chi^0(0, 0)} = \frac{1}{1-\gamma\chi_p} \quad (\text{I.5})$$

For the case where $\gamma = 0$, the static non-local response is described by $\chi^0(q, 0)$, the Fourier transform of which leads to the RKKY polarization. When electron-electron interactions occur, $\chi(q, 0)$ is strongly enhanced for small q and the polarization around a magnetic impurity is considerably more extended than in the RKKY case. The oscillations in the spin density then only appear at a larger distance (1.30). $\chi(q, 0)$ is shown in Figure 1.3 for $S = 10$ (as band calculations for the density of states at the Fermi surface (1.31) have shown to be the value in Pd) and $S = 1$ (no electron-electron interaction).

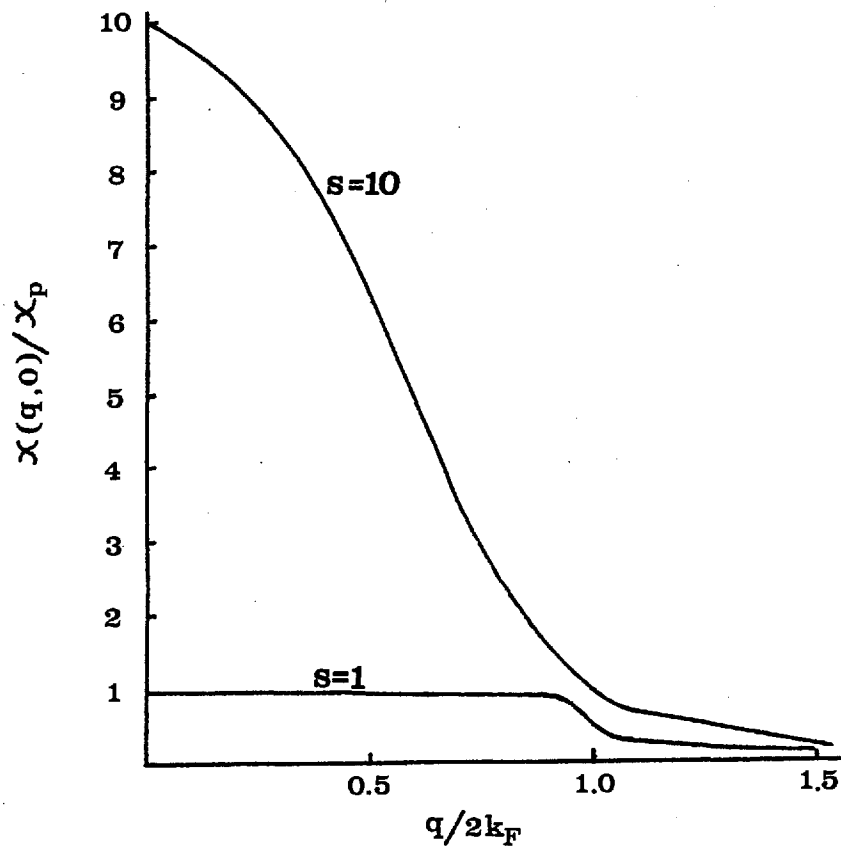


Figure 1.3

Figure 1.3 indicates that the susceptibility is the largest at $q = 0$ and that the first long range magnetic instability to be expected is ferromagnetic. Hence, we are interested in the neighbourhood of $q = 0$ only i.e. the long-wavelength nature of the susceptibility is of main interest (1.32). For $q \ll 2k_F$, Equation I.4 becomes

$$U(q,0) = \frac{1}{1 + \frac{1}{3} \left(\frac{q}{2k_F} \right)^2} \quad (\text{I.6})$$

by using the fact that $\frac{1}{1+x} \approx 1-x$, for $x \ll 1$.

Substituting Equation (I.6) into Equation (I.3) gives the

static susceptibility to be;

$$\chi(q,0) = \frac{\chi_p}{1 - \gamma \chi_p + \frac{1}{3} \left(\frac{q}{2k_F}\right)^2} = \frac{\chi_p}{\frac{1}{S} + \frac{1}{3} \left(\frac{q}{2k_F}\right)^2} \quad (\text{I.7})$$

Taking the Fourier Transform of this leads to the spatial dependence;

$$\chi(r,0) \propto \frac{e^{-r\sigma}}{r} \quad (\text{I.8})$$

$$\text{where } \sigma^2 = \left(\frac{3}{S}\right) (2k_F)^2$$

which is of the form of a Yukawa strong interaction (1.33), which can be mediated by a meson obeying the Klein-Gordon equation.

Neutron diffraction experiments of Low and Holden (1.34) on dilute alloys of Fe in Pd have indirectly observed the spin polarization around the impurity moments. These results indicated the large spatial extent of this polarization, showing appreciable effects out to about 10\AA from the impurity moment. This agreed with the spatial extent of the moment inferred by Crangle and Scott (1.35) from their magnetization measurements, although the form of the polarization deduced from the neutron results did not agree with that given by Equation (I.8), the evidence pointing to saturation effects. The conduction electron polarization thus covers some 200 Pd atoms around the iron impurity, each one adding a small moment and the whole acting as a 'giant moment'. A giant

moment of $10\mu_B$ was reported for Fe and Co in Pd by MacDougald and Manuel (1.36) and other giant moment systems include Fe in Pt (1.37) and Fe in $ZrZn_2$ (1.38). Techniques such as NMR, Mössbauer and neutron diffraction show that the moment on the impurity itself is much smaller than the obtained giant moment and indicate that the giant moment is due more or less entirely to the polarization of the host.

1.4. The Spin Glass

1.4.1. Introduction

Spin glasses, as they are now called, have been studied for a long time. Prior to the discovery of a sharp peak in the a.c. magnetic susceptibility (1.39), the physical properties of spin glasses, such as the prototype systems AuFe and CuMn, were generally consistent with a wide distribution of internal fields among the randomly positioned spins indirectly coupled by a long range oscillatory interaction. A model in which the local molecular field at some impurity moment is represented by a smooth distribution function $P(H)$ was used by Marshall (1.40) and Klein and Brout (1.41) to explain the linear term that had been found at low temperatures in the specific heat of AgMn (1.42) and CuMn (1.43). At high temperatures $P(H)$ is a single-peaked, symmetric Lorentzian distribution but at lower temperatures the spin correlations lead to a $P(H)$ which is a double-peaked Lorentzian with a reduced probability at $H = 0$, Figure 1.4.

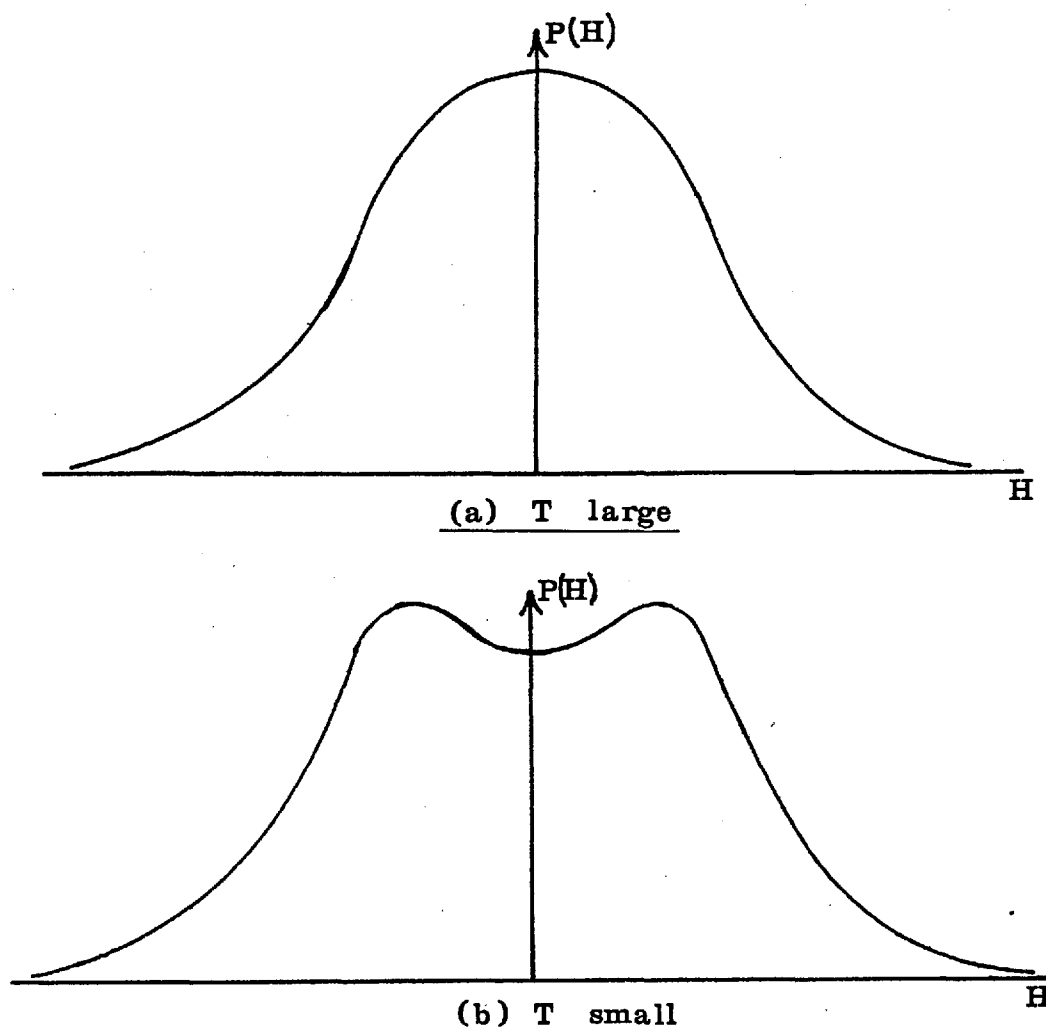


Figure 1.4

With this wide distribution of fields, a broad maximum in $\chi(T)$, as had been hitherto observed in CuMn and AgMn (1.44) and AuFe (1.45), is easily explained. These susceptibility measurements, however, were made in finite fields (>200 Oe) and the current interest in spin glasses has sprung mainly from the observation of a sharp, cusp-like, peak in the magnetic susceptibility of these alloys (1.39), (1.46), when measured by an a.c. method in low fields. This may suggest a sharp transition to a new phase at the temperature of the cusp, T_g , or at least a sudden blocking (freezing) of some of the magnetic degrees of freedom. Neutron scattering experiments (1.47), however, have shown that no long-range magnetic order

occurs at low temperatures and a transition does not show up in the measurements of many other bulk properties such as the resistivity or specific heat. There is also the occurrence of irreversible magnetic behaviour (remanent and time dependent magnetization) below T_g . The important question to be answered is whether a phase transition occurs at T_g or not. Different theoretical approaches have attacked the problem of the spin freezing and successfully obtained a cusp in $\chi(T)$. These will be discussed in Section 1.4.3 after some of the experimental measurements on these systems, which any theory must duplicate, are considered in the next section.

1.4.2. Behaviour of Spin Glass Systems

At the present time there are a variety of opinions as to what exactly defines a spin glass. It is generally accepted that there must be a freezing of the moments below some temperature but with no long range magnetic order occurring. Different views are held as to whether certain experimental properties are necessary to designate a spin glass. Operationally, it has been observed that the characteristic temperature (obtained by some experiment) as a function of the concentration (and also the temperature dependence of the electron resistivity, $(\rho_{4K} - \rho_{1K})$) exhibits noticeable qualitative changes in behaviour at the concentration for which isolated impurity effects give way to spin glasses or spin glasses to long range magnetic order. For example, a Tari-Coles plot

ie. $(\rho_4 - \rho_1)$ as a function of impurity concentration, is shown in Figure 1.5 for AuFe. Some workers restrict the term 'spin glass' to the very dilute alloys ($C_K < C < 1$ at%, where C_K is a minimum concentration such that Kondo compensation of the moment does not occur before the spin glass freezing) and other terms such as 'cluster glass'

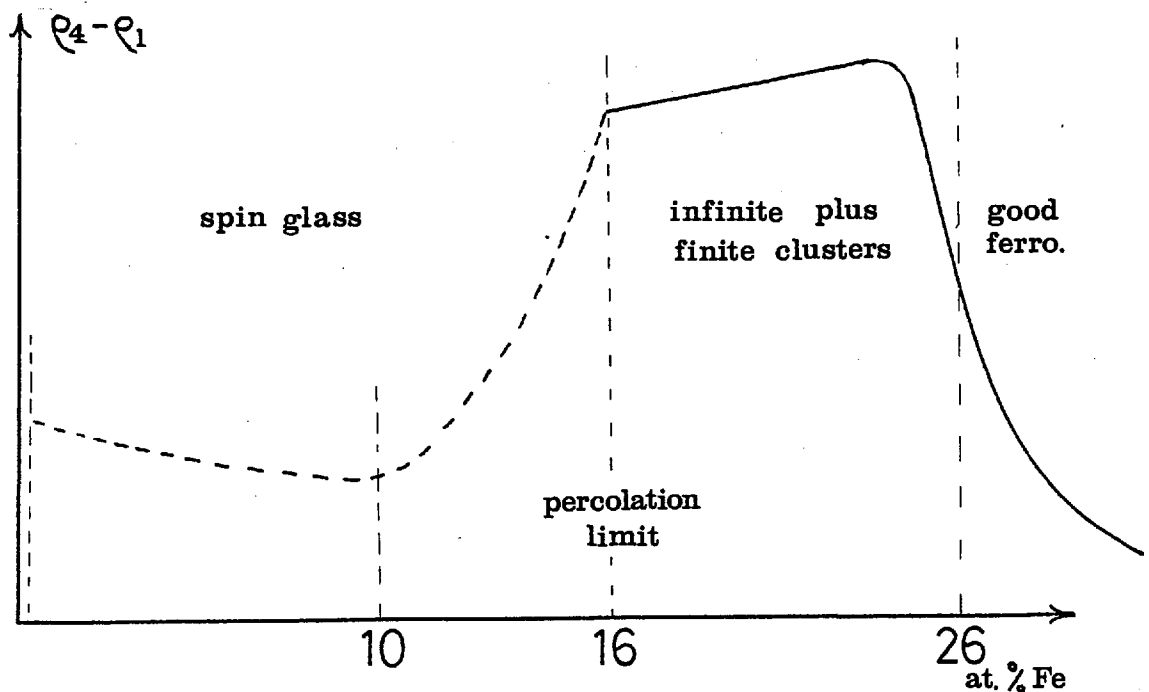


Figure 1.5

and 'mictomagnet' are often used to describe systems where large correlated 'clusters' of spins interact with one another via an oscillatory, long range interaction, as in the above systems once short range interactions begin to dominate ($C > 10$ at%) or where atomic ordering occurs. I shall use the term spin glass to represent the whole of the concentration range of solute from C_K upto the concentration where long range ordering first occurs

(for impurities where the direct coupling is ferromagnetic the percolation limit in an f.c.c. structure is approximately $C_p = 15$ at% (1.48), whereas a much larger concentration is required when the spins couple antiferromagnetically, $C_p \approx 45$ at% (1.49)). This general use of the term spin glass is consistent with the current theoretical ideas, where the essence of the phenomenon is that interactions of random sign occur (1.50).

Some or all of the moments in a spin glass freeze at random when cooled in zero external field to below T_g and the occurrence of irreversible magnetization effects reflect the viscous nature of the freezing process. If a spin glass is cooled to a temperature below T_g in zero field and then a field is applied, a certain magnetization is initially obtained which increases with time (1.51, 1.52). When the field is removed, a time dependent isothermal remanence (IRM) is seen. Tholence and Tournier (1.53) showed that the method of measurement yields qualitatively different susceptibilities owing to the existence of this remanent magnetization below T_g . In particular, in cooling to $T < T_g$ in a small field, the magnetization in the field remains almost constant below T_g instead of showing a peak. A thermoremanent magnetization (TRM) occurs, under these conditions, below T_g and it increases in magnitude linearly with $(T_g - T)$ when the temperature decreases. Thus the total susceptibility can be considered as being made up of two parts, a reversible part which is measured by the a.c. technique and an irreversible part which

is not detected by a fast a.c. method. For dilute spin glasses in the concentration range $C_K < C < 1$ at%, Souletie and Tournier (1.54) have shown that reduced quantities such as the specific heat $\frac{C_m}{C}$ and Magnetization $\frac{M}{C}$, follow universal functions of the variables $\frac{T}{C}$ and $\frac{H}{C}$ and that the freezing temperature T_g is proportional to C . This 'scaling' arises from the $\frac{1}{r^3}$ decay of the RKKY interaction and the statistical independence of the spin positions and it breaks down at concentrations greater than 1 at% solute due to the occurrence of near neighbour interactions and the loss of statistical independence. The IRM and TRM have been shown to saturate at the same value of σ_{rs} (1.53) and σ_{rs} obeys the scaling laws. This has led Tholence and Tournier (1.53, 1.55) to eliminate the assumption that the remanence is due to clustering effects (an assumption made by Kouvel (1.44) to explain the shifted hysteresis loops produced by field cooling to below T_g) and to develop a phenomenological model, based on the work by Néel (1.56), which describes spin glass behaviour in terms of the blocking of large antiferromagnetic clusters. They suggest that at temperatures well below T_g a spin glass can be represented by an assembly of magnetic 'clouds'. Within a cloud the spins are strongly coupled to one another by the RKKY interaction but different clouds are not strongly interacting, so that each cloud behaves like a superantiferromagnetic particle with a particular anisotropy energy to a net spin rotation. Holtzberget al. (1.57) discuss the possibility of the dipolar interaction

giving rise to this anisotropy between clouds. The anisotropy energy leads to a blocking temperature for each individual cloud and since the anisotropy energy varies from cloud to cloud there will be a distribution of blocking temperatures. These ideas have been used by Wohlfarth (1.58) and Guy (1.52) to draw the analogy with results from rock magnetism and Rivier (1.59) has presented a microscopic origin for the Néel anisotropy which is analogous to the attractive electron-electron interaction occurring in ordinary polaron theory, and allowed him to give a model for slowly relaxing remanence in spin glasses.

A systematic study of the resistivity of the most favourable noble metal - 3d impurity spin glasses (ie. AuMn, CuMn, AgMn and AuCr) has shown that they follow the same overall behaviour (1.60). The magnetic contribution to the resistivity, $\Delta\rho$, in these systems starts with a large zero temperature contribution, $\Delta\rho_0$, due to the disorder scattering from the frozen moments. The initial temperature dependence is proportional to $T^{3/2}$ and the constant of proportionality decreases slowly with increasing concentration up to the maximum concentration studied in each system (~ 10 at% solute). The AuFe system was studied further by Mydosh et al. (1.61) and up to about 10 at%Fe the coefficient of $T^{3/2}$ similarly decreased with increasing concentration, then for a further increase in concentration, a $T^{3/2}$ behaviour was still followed at low temperatures but with an increasing coefficient

with concentration. This initial $T^{3/2}$ behaviour has been interpreted by Rivier and Adkins (1.62) to result from the long-wavelength, diffusive, excitations which occur in a spin glass. At higher temperatures, $\Delta\varrho$ for all of these systems first begins to increase more linearly then slows down and shows a maximum at some temperature much higher than T_g (obtained from the peak in the a.c. susceptibility). For the AuFe system, Mydosh et al. (1.61) showed that there was reasonable correspondence between the maximum in $\frac{d\Delta\varrho}{dT}$ and T_g , but this seems to have been more fortuitous than a general property of spin glasses since the extended study of the other four systems (1.60) has shown that no such correspondence occurs, the maximum falling somewhat lower than T_g . The cross-over into the long-range ordering regime, as the concentration is increased, is distinguishable by the form of $\Delta\varrho(T)$ at the ordering temperature. A sharp 'knee' is obtained at a ferromagnetic transition while a smooth curve occurs for spin glass alloys, Figure 1.6.

Schilling et al. (1.63) have studied the effects of pressure on the impurity-impurity interactions in spin glass alloys by making measurements of the electrical resistivity on very dilute AuFe, AuMn, CuMn and MoFe at pressures upto 100Kbar. In all these alloys the resistivity at atmospheric pressure shows a minimum at some temperature due to the Kondo effect and at a lower temperature a maximum occurs, arising from the interactions

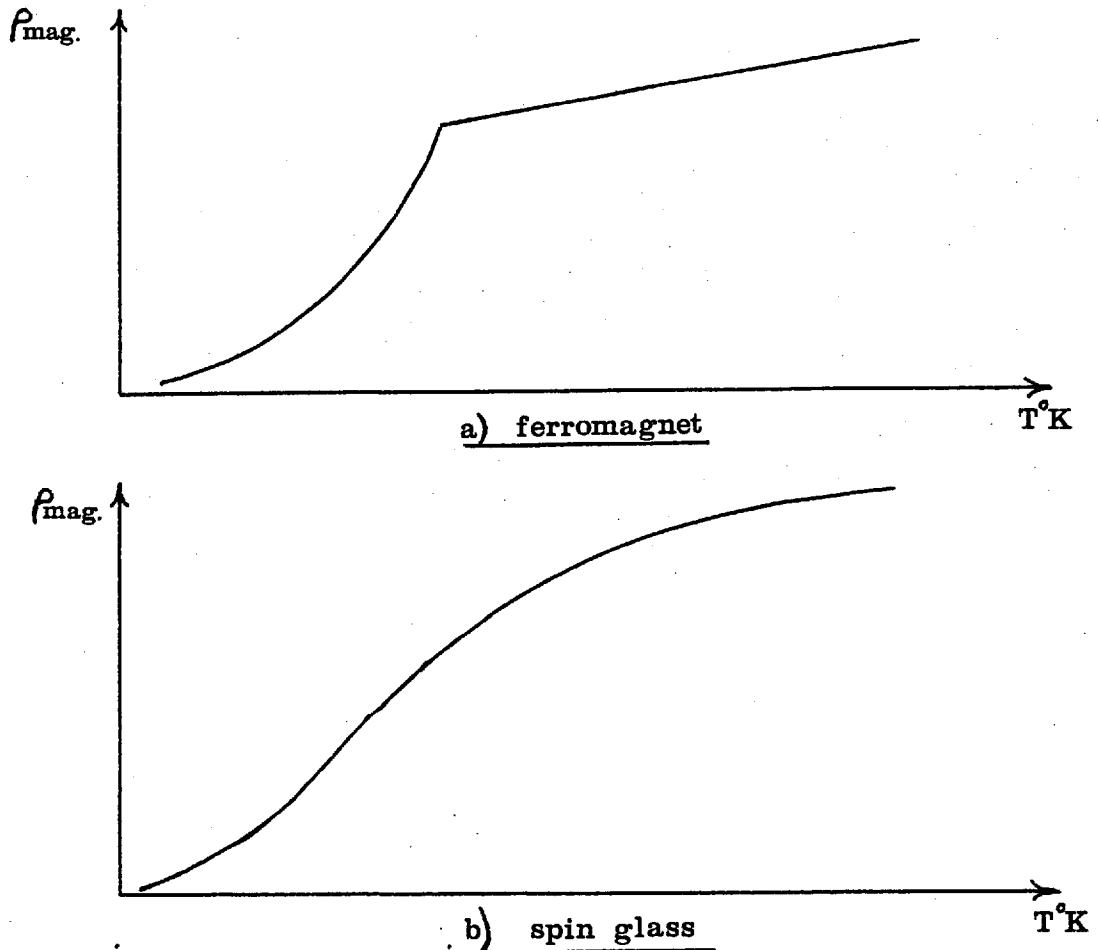


Figure 1.6

between the moments. The temperature of this maximum occurs at a temperature higher than T_g . By applying pressure the temperature of this maximum changes in a complicated manner. The direction and amount of the shift is highly dependent on the alloy system and the impurity concentration of the specimen. A theory by Larsen (1.25), relating the temperature of the maximum to the Kondo temperature and to the root-mean-square RKKY interaction, accounts for these different properties as measured by Schilling et al. (1.63) and they conclude that the RKKY interaction is indeed responsible for the properties of these dilute alloys.

The resistivity of spin glasses, therefore, shows

no characteristic anomaly at T_g . The specific heat of spin glasses, further, has provided no evidence of any phase transition at T_g . Experimentally, a very precise measurement is necessary to accurately determine the magnetic contribution to the specific heat, C_m , but recent results of Wenger and Keesom (1.64) have shown that any anomaly in C_m at T_g is less than 1% of the total magnetic contribution. At low temperatures C_m is linear in T (1.42, 1.43, 1.65, 1.66) and then shows a broad maximum centred well above the susceptibility peak temperature. Wenger and Keesom (1.64) further showed that the change of magnetic entropy from absolute zero to T_g [ie. $\Delta S_m = \int_0^{T_g} \frac{C_m}{T} dT$] amounted to less than one third of the expected value $\Delta S_m = CR \ln(2S+1)$ which would be the entropy change of a concentration, C , of spins, S , between a completely ordered state and one of complete disorder. This indicates, therefore, that the system is not completely disordered above T_g .

Early investigations of spin glasses by Mössbauer spectroscopy include those of Gonser et al. (1.67) and Violet and Borg (1.68, 1.69) on the AuFe system using the Fe^{57} isotope. These results lend strong support to the transition at T_g since there is a splitting of the spectra from a paramagnetic line to a six line structure at roughly the same temperature as the peak in the a.c. susceptibility. However, considerable broadening of the paramagnetic line occurs above T_g , Violet and Borg (1.69), and they suggested that this could be due to a

persistence of short range magnetic order above T_g .

Very recent muon depolarization experiments (1.70) have also been used to indicate a sharp onset of depolarizing fields. In these experiments, polarized μ^+ particles are used to probe the internal fields at random positions. The μ^+ is stopped at a random interstitial site and feels the effect of the polarizing field and any net field at the site from the atoms around. The muon spin precesses about the effective field direction until it decays, emitting positrons along the direction of the spin at that time. At high temperatures, when the extra field produced at the interstitial site averages to zero, there will be an oscillating rate of detection at a counter placed at an angle to the polarizing field. This oscillation will have a well defined frequency. As the field at the site no longer averages to zero over the lifetime of the muon once freezing takes place, and as the field at any site will be random in direction and magnitude, the oscillations in the count rate at the detector will no longer occur.

In essence, therefore, this muon experiment is the same as the Mössbauer experiment in that it senses the onset of a local field which does not average to zero over the muon lifetime. The results of Murnick et al. (1.70) show a large increase in depolarizing field around the temperature of the peak in the a.c. susceptibility but the question as to whether a sudden onset occurs at T_g is not clear. These results seem to indicate finite

depolarizing fields at temperatures above T_g .

MacLaughlin and Alloul (1.71) show that no abrupt change occurs in the Cu^{63} NMR linewidth of a series of dilute CuMn alloys with between 0.1 and 0.4 at%Mn. An extension to higher concentration CuMn alloys (1.72) similarly indicates a continuous variation of linewidths across T_g , instead of the expected sharp increase by a factor of four to five at T_g , if all the spins suddenly froze.

The NMR results suggest that even at $T < T_g$ a sizeable fraction of the impurity spins are still rapidly fluctuating. Neutron experiments also support this view. Murani and Tholence (1.73) have carried out neutron scattering experiments on a CuMn alloy with 8 at%Mn. They find a continuous increase in the elastic cross-section and a continuous decrease in the integrated quasi-elastic cross-section with decreasing temperature below 80°K , suggesting a gradual decrease in the number of fast relaxing spins rather than a sudden freezing of them all. The temperature of the susceptibility maximum obtained from these neutron results turns out to be significantly higher than the peak in the a.c. susceptibility ($\sim 52^\circ\text{K}$ c.f. $\sim 39^\circ\text{K}$) which is ascribed to be due to the difference in the time scale of the two measurements, $\sim 10^{-11}$ secs for neutrons and $\sim 10^{-2}$ for the a.c. susceptibility measurements. Murani (1.74) has further shown that the temperature of the peak in the scattering from AuFe alloys with 10 and 13 at%Fe is wavevector dependent by using low

angle diffuse neutron scattering. The temperature of the peak increases as the wavevector, q , is decreased. Murani argues that the discontinuity in the scattering intensity directly reflects a discontinuity in $\chi(q)$ and hence there is a q dependent freezing temperature obtained from these measurements. This, he suggests, is due to the fact that with neutrons of wavevector q , one is looking at clusters of dimension $\sim \frac{1}{q}$, so that the lower q is, the larger the cluster being observed and the higher the freezing temperature of this cluster.

A study of the thermal expansion of a series of CuMn alloys with concentrations of manganese between 0.54 and 7.6 at% and AgMn alloys with between 1 and 6.5 at%Mn has been carried out by Khan (1.75). Plots of the excess coefficient of linear expansion divided by temperature, $\frac{\alpha(\text{Mn})}{T}$, versus temperature, show a smooth peak at the same temperature as the a.c. susceptibility maximum.

Hurd and McAlister (1.76) have studied the anomalous Hall resistivity in a Au8.1 at%Mn alloy. The anomalous component is a large additional part to the Hall resistivity (over the Lorentz component) which was originally seen in several dilute alloys of transition metals dissolved in noble hosts (1.77). This has been attributed to the asymmetric (or 'skew') scattering of conduction electrons due to the spin-orbit coupling during the scattering from a magnetic ion (1.78, 1.79). A measurement of this anomalous or skew component, therefore, should give some indication of any internal magnetic

re-arrangement in a spin glass. Hurd and McAlister (1.76) measured the variation of the Hall resistivity with temperature in various applied fields. These measurements peak at the same temperature as the peak in the a.c. susceptibility, ($\sim 25^{\circ}\text{K}$), and the height of the peak increases with increasing field. Magnetic fields of 250 Oe to 1,000 Oe are used (thus the skew component to the Hall resistivity dominates the much smaller Lorentz contribution) in order to observe the effect but, they say, without completely disrupting the spin glass state. In plotting ρ_H/B , where ρ_H is the total Hall resistivity and B is the magnetic field, the curves at different fields come together at a temperature of about 42°K . They assert that above this temperature the skew scattering is dominated by single moments and that the differences in the curves below this temperature arise from the formation of clusters.

Ultrasonic investigations would be expected to show a critical anomaly for a cooperative type of phase transition. The temperature dependence of the sound propagation is simply related to that of the specific heat and a similar maximum in the ultrasonic attenuation is expected at a phase transition. No evidence has been found of any sharp anomaly in the ultrasonic velocity in a Au₈at%Fe single crystal (1.80) and only a weak indication of any velocity minima at T_g occurs in an investigation of several AuCr alloys (1.81), in agreement with specific heat data.

At the present time, most spin glass systems are composed of 3d solute atoms and the majority of experimental work has been carried out on these systems. Rare earth impurities interact via the RKKY interaction and so offer the opportunity of studying spin glass ordering when alloyed in appropriate hosts. There are problems in that the interaction is weaker and that crystal field effects are important but Sarkissian and Coles (1.82) have reported interesting spin glass behaviour in Y-RE and SC-RE alloys. Sarkissian (1.83) further reports spin glass behaviour in PrTb alloys with a concentration of Tb greater than about 2 at%.

$\text{La}(\text{Gd})\text{Al}_2$ offers an excellent opportunity of studying the effect of the RKKY interaction between moments without the problem of nearest neighbour overlap. The LaAl_2 - GdAl_2 system has a continuous range of solid solutions and a systematic study by Bennett and Coles (1.84) has shown that for alloys with upto about 16%Gd substitution, spin glass ordering occurs, before a more long range ordering sets in.

1.4.3. Theories of Spin Glasses

Several theories now exist to attempt to explain the properties of spin glasses and recent reviews by Heber (1.85) and Fischer (1.86) discuss some of these approaches.

A probabilistic mean field theory by Adkins and Rivier (1.87) was one of the first attempts at explaining the sharp cusp in the a.c. susceptibility. In this approach,

Adkins and Rivier extended the ideas of Marshall (1.40) and Klein and Brout (1.41), obtaining a distribution $P(H)$ of molecular fields from first principles by using a random walk technique.

The field seen by any given spin, \underline{S}_i , is the sum of contributions from all the other spins in the alloy:

$$H(\underline{R}_i) = \sum_{j(\neq i)} J(\underline{R}_i - \underline{R}_j) \underline{S}_j$$

This field is dependent on the orientations of all the other spins, each of which is dependent on the orientation taken by the first spin i . There is thus a conditional probability distribution for the field at site i . By using the random walk calculation on a spin $\frac{1}{2}$ Ising system the probability distribution is given by:

$$P(H_z) \propto \int d\mathbf{k} e^{-i\mathbf{k}H_z} e^{\frac{ic}{a^3} \int dR \frac{1}{2} (p_+ - p_-) \sin \frac{1}{2} \mathbf{k} J} e^{\frac{c}{a^3} \int dR \sum_{\pm} p(\pm \frac{1}{2}) 2 \sin^2 \frac{\mathbf{k} J S_z}{2}}$$

where $p_\sigma(R, H)$ is the conditional probability that a spin, distant R from the origin (position of spin i that the field is being calculated for), has a direction σ , given H at the spin.

The last exponential in this expression is very nearly independent of the directions of the spins around. This term determines the width of the distribution of fields seen by spin i . The second exponential, however, is dependent on the ordering taken by all the other spins.

Adkins and Rivier introduce an order parameter $q(T)$ ($m(T)$ in 1.87) which breaks the 'chain' of higher correlation functions necessary to calculate $P_\sigma(R,H)$. Within a correlation length, ξ , of the spin, all the other spins are linked to it in a definite orientation;

$$\begin{aligned} (p_+ - p_-)(R, H_z) &= \text{sign}(H_z) \cdot 2q(T) & R < \xi \\ &= 0 & R > \xi \end{aligned}$$

$P(H_z)$ and $q(T)$ are coupled and by obtaining a self consistent solution for $q(T)$, Adkins and Rivier showed that for $T < T_g$ a non-zero solution for $q(T)$ occurs and that for zero external field $q(T) \propto (T - T_g)^{\frac{1}{2}}$, near T_g , (see Figure 1.7).

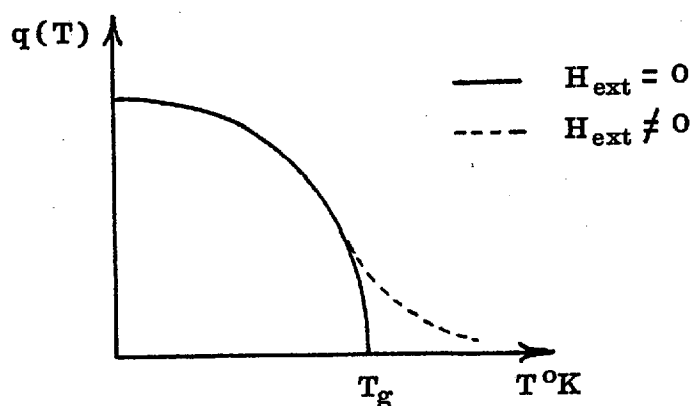


Figure 1.7

This short range order parameter arises from considering the interactions with all the other spins in the alloy and so even though no long range order exists the local ordering is a collective effect. For zero external field there is a sudden onset of $q(T)$ below T_g

and a finite $q(T)$ leads to a change in the distribution function $P(H_z)$ from a single Lorentzian function, symmetrical about $H = 0$, to an increased probability of high fields. The sudden onset of a finite $q(T)$ below T_g leads to a cusp in the susceptibility. For finite external field, $q(T)$ is modified as shown in Figure 1.7 and this causes a rounding of the cusp in the susceptibility.

Much theoretical effort has recently gone into studying a model first proposed by Edwards and Anderson (1.88). In this model, instead of randomly positioned spins with a fixed exchange, the spins lie on a regular lattice and the interaction between nearest neighbour pairs is assumed to be an independent random variable.

The Hamiltonian for the Edwards and Anderson model with Ising spins is written as

$$H = - \frac{1}{2} \sum_{i \neq j} J_{ij} S_i \cdot S_j$$

and the interaction J_{ij} is between nearest neighbours and each J_{ij} is a random, independent quantity obeying a Gaussian distribution.

$$P(J_{ij}) = P_0 e^{-J_{ij}^2/2J^2}$$

Such a continuous symmetrical distribution prevents the possibility of any periodic magnetic order but allows a spin glass ordering. In this system, a ground state

occurs in which any particular spin is aligned in some direction, but a direction which varies randomly from spin to spin so that the net magnetization is zero. An order parameter for this transition, which could be taken as $q = \langle S_i(t_1)S_i(t_2) \rangle$ when $(t_1 - t_2) \rightarrow \infty$, is found self consistently from the configuration-averaged free energy. The free energy is proportional to $\ln Z = \ln \text{Tr} e^{-\beta H}$ and an average of this function was achieved by Edwards and Anderson (1.88) by using the so-called $n \rightarrow 0$ 'trick', since the following identity is used:

$$\ln Z = \lim_{n \rightarrow 0} \frac{1}{n} (Z^n - 1)$$

Averaging Z^n is easily achieved, leading to;

$$\begin{aligned} \langle Z^n \rangle &= \left\langle \prod_{\alpha=1}^n \text{Tr} e^{\frac{1}{2}\beta \sum_{i \neq j} J_{ij} S_i(\alpha) S_j(\alpha)} \right\rangle \\ &= \left\langle \text{Tr}_n \text{ times } \text{Tr} e^{\frac{\beta}{2} \sum_{\alpha=1}^n \sum_{i \neq j} J_{ij} S_i(\alpha) S_j(\alpha)} \right\rangle \\ &= \text{Tr}_n e^{\frac{\beta^2}{4} J^2 \sum_{i \neq j} \sum_{\alpha \beta} S_i(\alpha) S_i(\beta) S_j(\alpha) S_j(\beta)} \end{aligned}$$

$$\text{since } \int dJ_{ij} e^{-\frac{1}{2}J_{ij}^2 - KJ_{ij}} \propto e^{\frac{1}{2}K^2}$$

Thus, averaging Z^n over $P(J_{ij})$ has caused an effective interaction between different replicas, α , of the system.

Hence,

$$\langle Z^n \rangle = \text{Tr}_n e^{-\beta H_{\text{eff}}}$$

$$\text{where } H_{\text{eff}} = - \sum_{i \neq j} \sum_{\alpha \beta} \frac{\beta J^2}{4} S_i(\alpha) S_i(\beta) S_j(\alpha) S_j(\beta)$$

and Edwards and Anderson proceed by making a mean field approximation to treat the effective Hamiltonian. They obtain a self-consistent equation for the order parameter, $q_{\alpha\beta} = \langle S_i(\alpha) S_i(\beta) \rangle$, which measures the correlation between the same spin in different replicas. This is assumed to behave in the same way as the time correlation $q_{t_1, t_2} = \langle S_i(t_1) S_i(t_2) \rangle$, at large time intervals. This is an order parameter which represents the probability that a spin at a particular site points in the same direction when observed at different times, ie. an auto-correlation which corresponds to the idea of freezing.

Figure 1.8 shows a schematic diagram of the time evolution of $\langle S_i(0) S_i(t) \rangle$ for two cases; a) $T < T_g$: there is a correlation between the spin direction at a later time t which tends to a value q and b) $T > T_g$: the auto-correlation is lost within the time scale of any measurement.

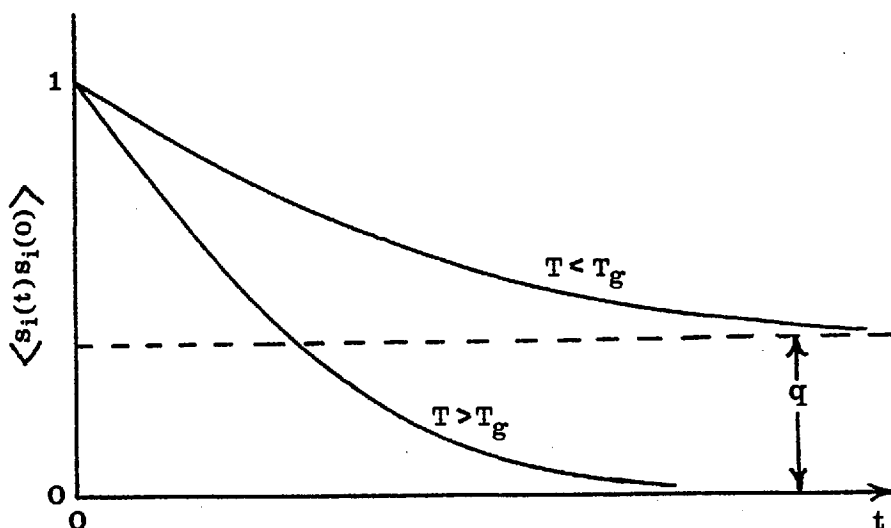


Figure 1.8

The variation of q with temperature is shown in Figure 1.9.

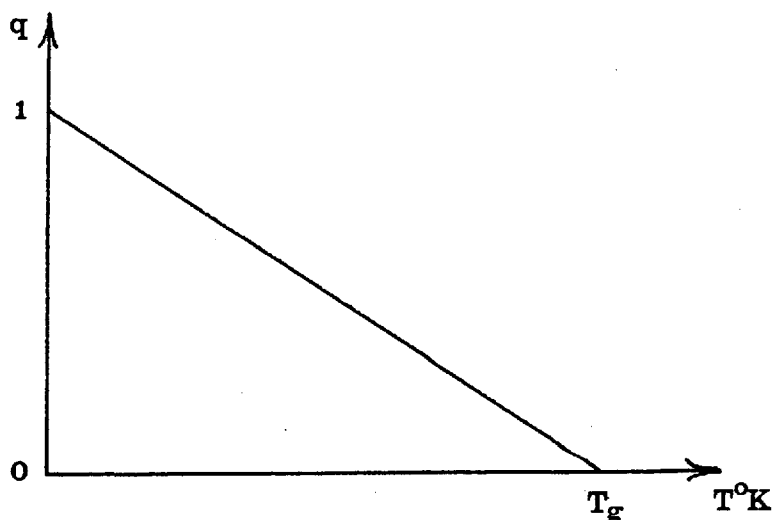


Figure 1.9

At $T = 0$, therefore, $q = 1$ and the spins stay in their preferred orientation for all time, while for $T > T_g$, the preferred orientation is lost within a short time.

This theory predicts a transition to the ground state at T_g , a cusp in the susceptibility which is rounded in a field and a specific heat which persists above T_g . However, it also predicts a cusp in the specific heat and a negative entropy for $T \rightarrow 0$.

Similar approaches have been made by Sherrington and Kirkpatrick (1.89) and Fischer (1.90) and similar predictions to those of Edwards and Anderson are obtained. The theory of Sherrington and Kirkpatrick extends the ideas of Edwards and Anderson to the case where J_{ij} covers, with equal probability distribution, all sites, ie. an infinite ranged J_{ij} . This is then exact in the mean field

approach above T_g but gives completely unphysical results below T_g . The problem here arises from taking the limit $N \rightarrow \infty$ (where N is the number of neighbours, and taking $N \rightarrow \infty$ makes the mean field theory exact) before the $n \rightarrow 0$ limit. Fischer (1.91) and Sherrington and Southern (1.92) have further extended the Edwards and Anderson model to consider quantum mechanical systems, leading to improvements at low temperatures and generally giving similar behaviour to the classical theories.

A recent attempt to obtain solutions below T_g has been made by Thouless et al. (1.93) by bypassing the $n \rightarrow 0$ 'trick'. They use a diagram expansion for the free energy and find similar behaviour to the Sherrington and Kirkpatrick approach (1.89) above T_g , showing that in the mean field theory the results are correct for $T > T_g$. They obtain a different low temperature behaviour, albeit with several approximations in order to make the diagram series converge below T_g . Using a spherical model of a spin glass, Kosterlitz et al. (1.94, 1.95) have obtained the same results with and without using the $n \rightarrow 0$ method but this appears to be the case for this model only.

Young and Stinchcombe (1.96) have investigated the Edwards and Anderson spin glass model by a real space renormalization group calculation instead of the replica technique. The renormalization techniques predict a spin glass phase transition for a three dimensional system but no transition is predicted for two dimensions, whereas computer simulations suggest that a phase transition

also occurs in two dimensional systems (1.97).

Computer 'experiments' have proved very useful in comparing the results predicted by an Edwards-Anderson model of a spin glass with both experimental results and RKKY descriptions of spin glasses. These Monte Carlo simulations of spin glasses set up an initial situation and pick a spin at random. The amount by which the energy of the system changes, if the spin is changed, is calculated. If this change, ΔE , is negative, the spin is changed, while if ΔE is positive the spin is only changed with a probability $e^{-\Delta E/k_B T}$, ie. this simulates thermal fluctuations of the system. After this step, another spin is selected at random and the process repeated. Binder and Schröder (1.97) discuss a Monte Carlo run on a thousand RKKY Ising spins distributed randomly in a cube of length $50/k_F$ and show that the distribution of exchange energies was roughly symmetric about $J_{ij} = 0$, where it is a maximum. Other smaller maxima occur, however, so that a Gaussian distribution is not obtained. These authors further calculated the susceptibility and specific heat for a two dimensional Ising model with nearest neighbour interactions following the Edwards and Anderson Gaussian distribution. The susceptibility shows a sharp cusp while the specific heat has a broad maximum at some temperature higher than the cusp in the susceptibility, in general agreement with results on real spin glasses. Binder and Stauffer (1.98) show that similar results are obtained on a three dimensional simulation of a spin glass except

that the specific heat is more sharp in the three dimensional case. A three dimensional Heisenberg Edwards-Anderson spin glass model has been simulated by Binder (1.99) and here the situation is less clear. Two methods of calculating the specific heat (looking at energy fluctuations and by differentiation of the energy) give different results. This inconsistency makes the results unreliable and so the susceptibility peak may be a nonequilibrium effect. Thus Binder concludes that T_g for this case may possibly be zero.

From these computer simulations, Binder and Stauffer (1.98) have obtained information on the time decay of the magnetization and temperature variation of the order parameter, q , and have been successful in duplicating the physical behaviour of real spin glasses to a reasonable extent. Binder (1.100) obtains a hysteresis loop for a two dimensional Ising model that is almost symmetric and shows that $P(H_{\text{eff}})$ seems to have a slight minimum at $H_{\text{eff}} = 0$ [$P(H_{\text{eff}})$ is the distribution of the effective fields seen at the sites of the spins].

By starting with the same initial state and going through the Monte Carlo process at $T = 0$ several times, different metastable ground states have been found (1.101). Such a system of local minima in the energy can well explain the time effects found in spin glasses, which may arise from tunneling from one such metastable state to one slightly higher when a field supplies a little energy. Since looking at $T = 0$ involves less computing time, more

complicated spin glass models than the Edwards-Anderson one may be looked at in this case. Rozario et al. (1.102) have looked at Heisenberg spins distributed randomly throughout a three dimensional continuum interacting via the RKKY force. In this simulation the energy is minimized by holding one spin fixed and successively aligning all the other spins in the field existing at their sites. Convergence towards an overall minimum was typically found after about 1,000 repetitions. This simulated ground state was found to be almost random in the direction of the spins but with a slight ferromagnetic alignment. The internal field distribution is shown to lead to a T^3 term in the specific heat in disagreement with experiment. Walker and Walsdedt (1.103) consider a simulation of a dilute spin glass consisting of spins distributed randomly on a f.c.c. lattice. They determine the $T = 0$ equilibrium configuration and excitations from it, for an isotropic RKKY coupling between the spins. The systems studied had concentrations of spin of 0.3% and 0.9%. In this, they find that the system of spins very quickly drop to a state of 'quasiequilibrium' but there then follows a long slow energy decrease which occurs mainly due to an increase in the average magnitude of the exchange fields. The equilibrium configuration thus generated, for random starting arrangements, is said to consist of different arrangements of identical subregions containing approximately 20 spins each. By

treating the elementary excitations as bosons Walker and Walstedt (1.103) obtain quantitative agreement with the measured low temperature specific heats of spin glasses.

Finally, theoretical descriptions of spin glasses based on the formation of clusters have been proposed by Smith (1.104). In these, a magnetic cluster is defined as a connected group of spins coupled by the RKKY interaction. Members of a cluster are spins that interact strongly enough so that the exchange interaction is greater than the thermal energy, and hence the size of any clusters increases as the temperature is reduced. Such clusters then act in an analogous way to the monodomain ferromagnetic particles in Neel's theory (1.56) of magnetism in rocks. The ideas involved there are that the rotation of the magnetic moment of such a particle may be impeded by an anisotropy potential. There is a relaxation time for a transition over this barrier and if the temperature is less than a certain value, the particle is effectively 'blocked' within the time scale of a measurement. This blocking temperature, T_b , will vary depending on the size of the particle and the time of the measurement (the longer the time of measuring the lower T_b is). In applying Neel's theory to spin glasses, large clusters are necessary in order to produce the long relaxation times which occur. In Smith's approach (1.104), clusters form and grow as the temperature is reduced. The temperature at which the first infinite cluster appears for a long time measurement (essentially $t \rightarrow \infty$) is regarded

as the spin glass temperature, T_g . In assuming that all the other finite clusters are free, a cusp in the susceptibility is obtained at the temperature of the formation of this first (long-time) infinite cluster. Smith obtains (1.104) a susceptibility which goes to zero as $T \rightarrow 0$ in contradiction with experimental results, which show that the susceptibility extrapolates to a fairly large $T = 0$ value (see, for example, Cannella and Mydosh (1.46) or Guy (1.105), which show results by an a.c. technique and d.c. technique, respectively). The specific heat behaviour near T_g is not given from this approach.

Binder (1.99) shows that a cluster model can be reduced to a model of an Edwards-Anderson type of spin glass and justifies the use of the simpler Edwards-Anderson model in the computer simulations.

Soukoulis and Levin (1.106) use a cluster model but include the internal dynamics of a cluster. By then using the replica technique of Edwards and Anderson (1.88) they follow the same mean field decoupling of the configuration-average Free Energy and find an order parameter involving the spin of a cluster. The susceptibility shows a peak in a similar way to that obtained by Edwards and Anderson but the specific heat has two contributions, an inter cluster term which shows a peak and an additional term arising from the intracluster contribution which has a rounded maximum as a function of temperature (any $P(H)$ would also give a similar sort of

behaviour).

1.4.4. Conclusions

It is not clear from the experimental results whether a phase transition occurs or whether the spin glass transition should be considered as a freezing phenomenon. Theories along the lines of a phase transition include those of Adkins and Rivier (1.87) and Edwards and Anderson (1.88) and they lead to an anomaly in the magnetic specific heat which is experimentally not found. Other theories follow the line of explanation in terms of a freezing phenomenon (eg. Tholence and Tournier (1.53)) which require some mechanism to prevent thermodynamic equilibrium being reached by the system such as a blocking of the spins by magnetic anisotropy fields. The magnetic blocking of clusters of spins can be used as an explanation of the time dependent magnetization and remanent effects observed in spin glasses (Guy (1.51)); an effect unexplained on the basis of the phase transition models (a recent paper by Kinzel and Fischer (1.107) considers the dynamics of single Ising spins, interacting with a heat bath but does not include clustering, blocking or anisotropy).

Further investigation is thus necessary into the size and dynamics of magnetic clusters and the magnetic anisotropy between them, for different treatments given to a spin glass. Neutron measurements are proving worthwhile as measurements by Murani (1.74) have shown and

further work in this direction is awaited. Neutron scattering work should prove informative on the character of the freezing process at T_g and on the build up of clusters as $T \rightarrow T_g$. Information on the spin wave excitations can also be obtained this way.

The wide field of metallic glasses also offers the possibility of studying spin glass behaviour. In metallic glasses, the metal is cooled very rapidly from the liquid state and the random atomic arrangement of the liquid is 'frozen' into the solid, if cooled at a high enough rate. Certain alloy systems should show spin glass behaviour as, for example, shown by Harris and Zobin (1.108) and discussed by Klein (1.109) and further effort is needed in this direction.

A continuation of the study of the spin glass properties of systems with rare-earth impurities will also be of value where more complicated systems are available to test the varying properties.

REFERENCES

- 1.1 DAYBELL M.D. and STEYERT W.A.
Rev. Mod. Phys. 40, 380 (1968).
- 1.2 ANDERSON P.W.
Phys. Rev. 124, 41 (1961).
- 1.3 WOLFF P.A.
Phys. Rev. 124, 1030 (1961).
- 1.4 CLOGSTON A.M., MATTHIAS B.T., PETER M., WILLIAMS H.J.,
CORENZWIT E. and SHERWOOD R.C.,
Phys. Rev. 125, 541 (1962).
- 1.5 FRIEDEL J.
Can. J. Phys. 34, 1190 (1956).
- 1.6 HEEGER A.J.
Solid State Physics 23, 283 (1969), (Seitz F.,
Turnbull D. and Ehrenreich H., eds.), Acad. Press,
New York.
- 1.7 KONDO J.
Prog. Theor. Phys. 32, 37 (1964).
- 1.8 ZENER C.,
Phys. Rev. 81, 440 (1951).
- 1.9(a) DE HAAS W.J., DE BOER J. and Van Den BERG G.J.
Physica 1, 1115 (1934).
- 1.9(b) Van Den BERG G.J.
Low Temp. Phys. LT9, (part B), 955 (1965).
- 1.10 SARACHIK M.P., CORENZWIT E. and LONGINOTTI L.D.
Phys. Rev. 135, A1041 (1964).
- 1.11(a) NAGAOKA Y.
Prog. Theor. Phys. 37, 13 (1967).
- 1.11(b) YOSIDA K.
Phys. Rev. 147, 223 (1966).
- 1.11(c) WILSON K.G.
Rev. Mod. Phys. 47, 773 (1975).
- 1.12 NOZIERES P.
Low Temp. Phys. LT14, Vol.5, 339 (1975).
- 1.13 KONDO J.
Solid State Physics 23, 183 (1969), (Seitz F.,
Turnbull D. and Ehrenreich H., eds.), Acad. Press,
New York.

- 1.14 HEISENBERG W.
Z. Physik 49, 619 (1928).
- 1.15 DIRAC P.A.M.
Proc. Roy. Soc. A123, 714 (1929).
- 1.16 HEITLER W. and LONDON F.
Z. Physik 44, 455 (1927).
- 1.17 ANDERSON P.W.
Solid State Physics 14, 99 (1963), (Seitz F. and
Turnbull D., eds.), Acad. Press, New York.
- 1.18 KASUYA T.
Prog. Theor. Phys. 16, 45 (1956).
- 1.19 YOSIDA K.
Phys. Rev. 106, 893 (1957).
- 1.20 RUDERMAN M.A. and KITTEL C.
Phys. Rev. 96, 99 (1954).
- 1.21 COLES B.R.
Quoted by P.W. Anderson, Mat. Res. Bull. 5, 349 (1970).
- 1.22 COOPER B.R.
Solid State Physics 21, 393 (1968), (Setiz F.,
Turnbull D. and Ehrenreich H., eds.), Acad. Press,
New York.
- 1.23 DE GENNES P.G.
J. Phys. Radium 23, 630 (1962).
- 1.24 BUCHMANN R., FALKE H.P., JABLONSKI H.P. and
WASSERMAN E.F., Physica 86-88B, 835 (1977).
- 1.25 LARSEN U.
Phys. Rev. B14, 4356 (1977).
- 1.26 MORIYA T.
Prog. Theor. Phys. 33, 157 (1965).
- 1.27 MORIYA T.
Prog. Theor. Phys. 34, 329 (1965).
- 1.28 IZUYAMA T., KIM D.J. and KUBO R.
J. Phys. Soc. Japan 18, 1025 (1963).
- 1.29 LINDHARD J.
Dan. Mat. Fys. Medd. 28, no. 8, (1954).
- 1.30 GIOVANNINI B., PETER M. and SCHRIEFFER J.R.
Phys. Rev. Letts. 12, 736 (1964).

- 1.31 ANDERSEN O.K.
Phys. Rev. B2, 883 (1970).
- 1.32 SCHRIEFFER J.R.
J. Appl. Phys. 39, 642 (1968).
- 1.33 YUKAWA H.
Prog. Phys. Math. Soc. Japan 17, 48 (1935).
- 1.34 LOW G.G. and HOLDEN T.M.
Proc. Phys. Soc. 89, 119 (1966).
- 1.35 CRANGLE J. and SCOTT W.R.
J. Appl. Phys. 36, 921 (1965).
- 1.36 McDOUGALD M. and MANUEL A.J.
J. Appl. Phys. 39, 961 (1968); and J. Phys. C 3, 147 (1970).
- 1.37 BOZORTH R.M., DAVIS D.D. and WERNICK J.H.
J. Appl. Phys. (suppl.) 17, 112 (1962).
- 1.38 FONER S.
J. Appl. Phys. 39, 411 (1968).
- 1.39 CANNELLA V., MYDOSH J.A. and BUDNICK J.I.
J. Appl. Phys. 42, 1689 (1971).
- 1.40 MARSHALL M.
Phys. Rev. 118, 1519 (1960).
- 1.41 KLEIN M.W. and BROUT R.
Phys. Rev. 132, 2412 (1963).
- 1.42 De NOBEL J. and Du CHATENIER F.J.
Physica 25, 969 (1959).
- 1.43 ZIMMERMAN J.E. and HOARE F.E.
J. Phys. Chem. Sol. 17, 52 (1960).
- 1.44 KOUVEL J.S.
J. Phys. Chem. Sol. 21, 57 (1961) and Ibid. 24, 795 (1963).
- 1.45 LUTES D.S. and SCHMIDT J.S.
Phys. Rev. 134, A676 (1964).
- 1.46 CANNELLA V. and MYDOSH J.A.
Phys. Rev. B6, 4220 (1972).
- 1.47 ARROTT A.
J. Appl. Phys. 36, 1093 (1965).
- 1.48 DUFF K. and CANNELLA V.
Amorphous Magnetism p.207, edited by Hooper H.O. and De Graaf A.M., Plenum, N.Y., (1973).

- 1.49 SATO H. and KIKUCHI R.
AIP Conf. Proc. 18, 605 (1974).
- 1.50 ANDERSON P.W.
Amorphous Magnetism II, p.1, edited by Levy R.A.
and Hasegawa R., Plenum, N.Y., (1977).
- 1.51 GUY C.N.
J. Phys. F7, 1505 (1977).
- 1.52 GUY C.N.
J. Phys. F5, L242 (1975).
- 1.53 THOLENCE J.L. and TOURNIER R.
J. de Physique 35, C4-229, (1974).
- 1.54 SOULETIE J. and TOURNIER R.
J. Low Temp. Phys. 1, 95 (1969).
- 1.55 THOLENCE J.L. and TOURNIER R.
Physica 86-88B, 873 (1977).
- 1.56 NÉEL L.
Adv. Phys. 4, 191 (1955).
- 1.57 HOLTZBERG F., THOLENCE J.L. and TOURNIER R.
Amorphous Magnetism II, p.155, edited by Levy R.A.
and Hasegawa R., Plenum, N.Y. (1977).
- 1.58 WOHLFARTH E.P.
Physica 86-88B, 852 (1977).
- 1.59 RIVIER N.
Amorphous Magnetism II, p.55, edited by Levy R.A.
and Hasegawa R., Plenum, N.Y., (1977).
- 1.60 FORD P.J. and MYDOSH J.A.
Phys. Rev. B14, 2057 (1976).
- 1.61 MYDOSH J.A., FORD P.J., KAWATRA M.P. and WHALL T.E.
Phys. Rev. B10, 2845 (1974).
- 1.62 RIVIER N. and ADKINS K.
J. Phys F. 5, 1745 (1975).
- 1.63 SCHILLING J.S., FORD P.J., LARSEN U. and MYDOSH J.A.
Phys. Rev. B14, 4368 (1977).
- 1.64 WENGER L.E. and KEESOM P.H.
Phys. Rev. B11, 3497 (1975), and Ibid. B13, 4053 (1976).
- 1.65 SMITH F.W.
Phys. Rev. B9, 942 (1974).

- 1.66 DREYFUS B., SOULETIE J., TOURNIER R. and WEIL L.
Comptes Rendues 259, 4266 (1964).
- 1.67 GONSER U., GRANT R.W., MECHAN C.J., MUIR A.H. and
WIEDERSICH H., J. Appl. Phys. 36, 2124 (1965).
- 1.68 VIOLET C.E. and BORG R.J.
Phys. Rev. 149, 540 (1966).
- 1.69 VIOLET C.E. and BORG R.J.
Phys. Rev. 162, 608 (1967).
- 1.70 MURNICK D.E., FIORY A.T. and KOSSLER W.J.
Phys. Rev. Letts. 36, 100 (1976).
- 1.71 MACLAUGHLIN D.E. and ALLOUL H.
Physica 86-88B, 839 (1977).
- 1.72 MACLAUGHLIN D.E. and ALLOUL H.
Phys. Rev. Letts. 38, 181 (1977).
- 1.73 MURANI A.P. and THOLENCE J.L.
Solid State Comms. 22, 25 (1977).
- 1.74 MURANI A.P.
Phys. Rev. Letts. 37, 450 (1976).
- 1.75 KHAN J.A.
Thesis, University of London, (1976), unpublished.
- 1.76 HURD C.M. and McALISTER S.P.
Amorphous Magnetism II, p.47, edited by Levy R.A.
and Hasegawa R., Plenum, N.Y., (1977).
- 1.77 ALDERSON J.E.A. and HURD C.M.
J. Phys. Chem. Sol. 32, 2075 (1971).
- 1.78 HURD C.M.
Contemp. Phys. 16, 517 (1975).
- 1.79 FERT A. and FRIEDERICH A.
Phys. Rev. B13, 397 (1976).
- 1.80 HAWKINS G.F., MORAN T.J. and THOMAS R.L.
AIP Conf. Proc. 29, 235 (1976).
- 1.81 HAWKINS G.F., MORAN T.J. and THOMAS R.L.
Amorphous Magnetism II, p.117, edited by Levy R.A.
and Hasegawa R., Plenum, N.Y., (1977).
- 1.82 SARKISSIAN B.V.B. and COLES B.R.
Commun. Phys. 1, 17 (1977).
- 1.83 SARKISSIAN B.V.B.
Physica 86-88B, 865 (1977).

- 1.84 BENNETT M.H. and COLES B.R.
Physica 86-88B, 844 (1977).
- 1.85 HEBER G.
Appl. Phys. 10, 101 (1976).
- 1.86 FISCHER K.H.
Physica 86-88B, 813 (1977).
- 1.87 ADKINS K. and RIVIER N.
J. de Physique C4, 237 (1974).
- 1.88 EDWARDS S.F. and ANDERSON P.W.
J. Phys. F5, 965 (1975).
- 1.89 SHERRINGTON D. and KIRKPATRICK S.
Phys. Rev. Letts. 35, 1792 (1975).
- 1.90 FISCHER K.H.
Solid State Comms. 18, 1515 (1976).
- 1.91 FISCHER K.H.
Phys. Rev. Letts. 34, 1348 (1975).
- 1.92 SHERRINGTON D. and SOUTHERN B.W.
J. Phys. F5, L49 (1975).
- 1.93 THOULESS D.J., ANDERSON P.W. and PALMER R.B.
Phil. Mag. 35, 593 (1977).
- 1.94 KOSTERLITZ J.M., THOULESS D.J. and JONES R.C.
Physica 86-88B, 859 (1977).
- 1.95 KOSTERLITZ J.M., THOULESS D.J. and JONES R.C.
Phys. Rev. Letts. 36, 1217 (1976).
- 1.96 YOUNG A.P. and STINCHCOMBE R.B.
J. Phys. C 9, 4419 (1976).
- 1.97 BINDER K. and SCHRÖDER K.
Phys. Rev. B14, 2142 (1976).
- 1.98 BINDER K. and STAUFFER D.
Phys. Letts. 57A, 177 (1976).
- 1.99 BINDER K.
Z. Physik B26, 339 (1977).
- 1.100 BINDER K.
Physica 86-88B, 871 (1977).
- 1.101 SHERRINGTON D.
AIP Conf. Proc. 29, 224 (1975).
- 1.102 De ROZARIO F.A., SMITH D.A. and JOHNSON C.H.J.
Physica 86-88B, 861 (1977).

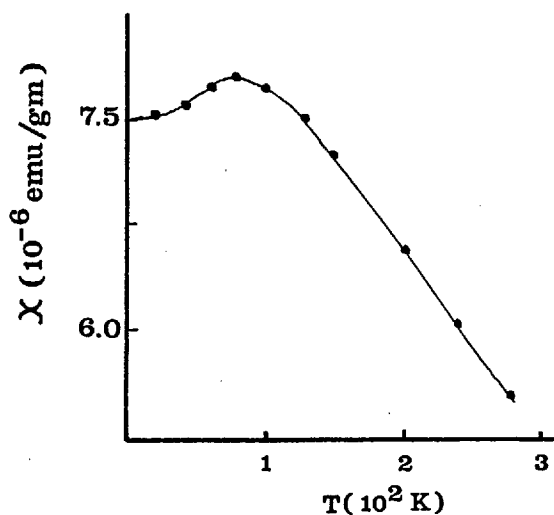
- 1.103 WALKER L.R. and WALSTEDT R.E.
Phys. Rev. Letts. 38, 514 (1977).
- 1.104 SMITH D.A.
J. Phys. F4, L266 (1974), and Ibid 5, 2148 (1975).
- 1.105 GUY C.N.
Physica 86-88B, 877 (1977).
- 1.106 SOUKOULIS C.M. and LEVIN K.
Phys. Rev. Letts. 39, 581 (1977).
- 1.107 KINZEL W. and FISCHER K.H.
J. Phys. F7, 2163 (1977).
- 1.108 HARRIS R. and ZOBIN D.
AIP Conf. Proc. 29, 156 (1976).
- 1.109 KLEIN M.W.
J. Phys. F7, 1699 (1977).

CHAPTER 2

PREVIOUS WORK ON THE PALLADIUM MANGANESE SYSTEM

2.1. Introduction

Pure palladium has atomic number 46 and the 5s and 5p hybridized conduction band overlaps with the narrow 4d band, resulting in there being 0.36 unoccupied d-states per atom, Hodges et al. (2.1). The Pauli susceptibility, obtained from band structure calculations, should be about $0.75 \cdot 10^{-6}$ emu/gm for Pd, Anderson (2.2), but as the χ vs. T plot of Figure 2.1 shows, the actual susceptibility is some ten times larger than this at its maximum.



after Hoare & Matthews(2.3)

Figure 2.1

An explanation has been attempted by assuming that there is a large exchange interaction between the d-band electrons. This can account for the increased level of the

susceptibility but not the anomalous peak which occurs. Such an assumption has also proved important in explaining the magnetic properties of alloys of palladium such as PdMn and PdFe and Giovannini et al. (2.4) were able to obtain quantitative agreement with esr data on rare earth alloys of palladium by this assumption.

Misawa (2.5) has explained the anomalous peak in the susceptibility of Pd as the effect of the many-body correlations inherent in a Fermi liquid. He had previously shown that the magnetic susceptibility $\chi(T)$ of any normal paramagnetic Fermi liquid at low temperatures is given by;

$$\chi(T) = a - bT^2 \ln\left(\frac{T}{T^*}\right) + \dots$$

Misawa (2.6), where a, b and T^* are constants. This, therefore, predicts a maximum in $\chi(T)$ at $T = T^*/\sqrt{e}$ and Misawa (2.5) was able to fit the experimental data for Pd very well by assuming that

$$\frac{\chi}{\chi(T=0)} = 1 - \left(\frac{T}{312}\right)^2 \ln\left(\frac{T}{132}\right) + \left(\frac{T}{331}\right)^4 \ln\left(\frac{T}{142}\right)$$

The justification for a $T^4 \ln(T)$ term coming next instead of a $T^3 \ln(T)$ term, as predicted by Barnea (2.7) from a microscopic theory, being given later by Misawa (2.8).

As discussed in Section 1.3.4, exchange interactions between the conduction electrons considerably modifies the nature of the polarization around a moment bearing impurity. A large increase in the polarization at the site of the

impurity and a pushing out of the first change in sign of the polarization, from that expected in the RKKY calculation, results. In such 'giant moment' systems, therefore, the critical concentration for the occurrence of an infinite chain of ferromagnetically coupled impurities is greatly reduced from the critical concentrations expected in non-enhanced systems such as AuFe. Manganese, Iron and Cobalt all maintain their magnetic moments when dissolved in palladium and PdFe, PdCo and PdMn have all been shown to order ferromagnetically above about one part in a thousand of solute, Nieuwenhuys (2.9).

PdMn differs from both PdFe and PdCo in that for increasing concentration of solute the direct impurity-impurity interactions become more important and the Mn-Mn coupling is antiferromagnetic while the Fe-Fe and Co-Co couplings are both ferromagnetic (as discussed in Section 1.3.3). In PdMn, therefore, there is a competition between the direct antiferromagnetic interaction and the ferromagnetic interaction between the impurity moments via the polarized electrons of the host. As a consequence, for concentrations greater than 3 at%Mn the ordering temperature decreases before the Mn-Mn interactions win out and spin glass ordering occurs (see Figure 2.2, after Coles et al. (2.10)). Thus we have a rare opportunity of observing the approach to long range order as a function of decreasing concentration by studying the palladium manganese system.

The phase diagram for PdMn, Watanabe (2.11), shows that Mn is soluble in Pd upto about 26 at%. The ordered

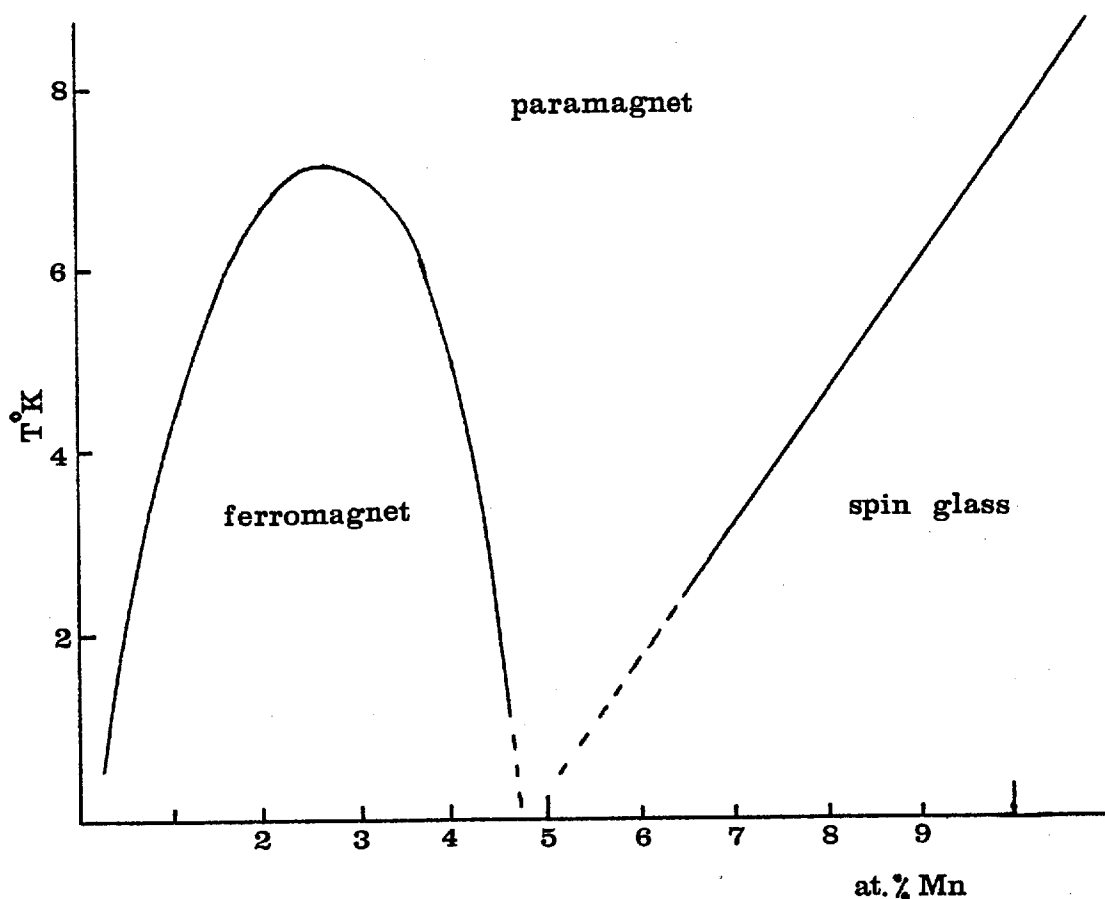


Figure 2.2

structure Pd_3Mn is difficult to obtain, as demonstrated by Chakrabati (2.12). Starting with a disordered solid solution of 25 at%Mn in Pd, Chakrabati (2.12) showed that a susceptibility peak was obtained at about 30°K . This falls on an extrapolation of the spin glass line in the magnetic phase diagram, Figure 2.2, indicating that the disordered Pd 25 at%Mn alloy is a spin glass. Progressive atomic ordering was achieved by longer heat treatments at a temperature just below 650°C and resulted in a reduction of the susceptibility peak. Only after a very long heat treatment did the susceptibility measurements indicate the antiferromagnetic transition expected in ordered Pd_3Mn (Cable et al. (2.13)).

The major interest in the PdMn system has focussed on the magnetic properties of the dilute manganese concentration alloys (with less than 3 at%Mn) and Nieuwenhuys (2.9) reviews the experimental work carried out on dilute Pd based alloys with Co, Fe and Mn. In the following sections we shall consider the major results relevant to a later discussion about the magnetic ordering in PdMn alloys.

2.2. Resistivity

Resistivity measurements on PdMn alloys include those of Sarachik and Shaltiel (2.14), Williams and Loram (2.15), Williams et al. (2.16), Zweers and Van den Berg (2.17) and Coles et al. (2.10). The low concentration results of Sarachik and Shaltiel (2.14) and Williams and Loram (2.15) defined the transition temperatures, T_c , as the temperature at which a sharp 'kink' occurred in the resistivity as a function of temperature (in these measurements the change was abrupt but higher resolution measurements by Nieuwenhuys and Boerstael (2.18) on a Pd 1.0 at%Mn alloy showed a small amount of rounding). These low concentration results, carried out for concentrations of manganese between 0.5 and 2.91 at%, showed that T_c was roughly proportional to the concentration, c . Measurements on lower concentration alloys by Nieuwenhuys (2.9) showed that this is no longer true below 0.5 at%Mn and he further found that the transition broadens with decreasing concentration.

The magnetostriction measurements of Williams et al. (2.16) on a Pd 2.91 at%Mn alloy showed that the difference between the contribution from the totally disordered state and the $T = 0^\circ\text{K}$ state to $\Delta\epsilon$ was field dependent. This is inconsistent with the incremental resistivity at $T = 0^\circ\text{K}$, in zero applied field, being due to the scattering from the fully ordered state. This led Williams et al. (2.16) to the assumption that there was still a considerable effect from antiferromagnetically coupled near neighbour manganese atoms in this alloy. Above this concentration these antiferromagnetically coupled impurity moments become more important and result in a reduction in the ordering temperature, Coles et al. (2.10). The resistivity measurements of Zweers and Van den Berg (2.17) reflect this effect in that for concentrations above 3 at%Mn the resistivity versus temperature curves no longer exhibit the sharp change in slope seen in the lower concentration alloys.

2.3. Specific Heat

Specific heat measurements have been reported on low concentration PdMn alloys ($c < 2.45$ at%Mn) by Boerstoeel et al. (2.19) and on alloys with Mn concentrations between 2.7 and 9.5 at% by Zweers and Van den Berg (2.17). The specific heat measurements of Boerstoeel et al. (2.19) showed that the variation of the magnetic contribution to the specific heat in zero external magnetic field has a much sharper peak than observed in any other dilute magnetic system. They

showed that the fairly sharp peaks were broader than, but had a close relationship with, the λ -type peaks observed in pure ferromagnetic or antiferromagnetic materials. They further, compared their results on the specific heat as a function of temperature and applied magnetic field with numerical calculations based on the molecular field model. Those alloys studied below 0.5 at%Mn could be well fitted by the model, for the larger applied magnetic fields, when a value of $5/2$ was taken for the magnetic quantum number. This value of $5/2$ was close to the average value of 2.3 that Boerstoeel et al. (2.19) deduced from the entropy content of the specific heat (obtained by graphical integration of $\frac{\Delta C}{T}$ vs T plots; for data where reliable extrapolations to $T = 0$ and $T = \infty$ could be made). Zweers and Van den Berg (2.17) investigated the specific heat of higher concentration PdMn alloys and found that above 2.45 at%Mn the peak broadens upto 4.0 at%Mn before becoming relatively narrower for less dilute alloys of 5.5, 8.0 and 9.5 at%Mn.

2.4. Magnetization Measurements

Rault and Burger (2.20) carried out high field magnetization measurements on PdMn alloys with upto 25 at%Mn and they found a decreasing Curie-Weiss temperature, θ , in going from 3 to 8 at%Mn, before antiferromagnetic-like ordering was obtained.

Star et al. (2.21) carried out a study of the magnetization of a series of dilute PdMn alloys ($0.05 < c < 2.45$)

as a function of field and temperature. From this work they determined a saturation moment of about $7.5\mu_B$ per Mn atom, ie. larger than the free manganese atom, showing the effect of the polarization of the Pd host around the impurity moment. In assuming $s = 5/2$ (consistent with the specific heat results of Boerstoele et al. (2.19)) the saturation moment leads to an effective g value for the Mn moment of about 3. Using these values the field dependent magnetization of the low concentration curves ($c = 0.05, 0.054$ and 0.08 at%Mn) could be well fitted to the Brillouin function. The more concentrated alloys could not be fully saturated, even in fields as high as 210 KOe. This they attributed to the near-neighbour Mn-Mn antiferromagnetic interactions which have a very high energy of interaction so that even a field of 210 KOe is not enough to overcome the interaction and align all the moments. The spontaneous and high field magnetizations were used to estimate the energy of the direct Mn-Mn interactions and to obtain the number of Mn atoms involved in the pairing. From this, Star et al. (2.21) determined a coordination number, n , which is defined such that a Mn atom that has no neighbours within a sphere containing n lattice sites interacts ferromagnetically with all the others, while a Mn atom that has one or more neighbours in that range interacts antiferromagnetically with these neighbours. For the 1.35 at%Mn alloy they found that $n = 32$ and for the 2.45 at%Mn specimen they obtained $n = 43$. They conclude from this that up to third nearest neighbour

Mn impurities can interact antiferromagnetically.

The work of Star et al. (2.21) further showed that these PdMn alloys did not exhibit any magnetic hysteresis. The low field M versus H plots had a sharp linear increase in magnetization upto about 200 Oe before a sharp knee occurred, followed by a long gradual increase for a further increase in magnetic field. Their measurements showed this process to be completely reversible for all fields applied.

2.5. Electron Paramagnetic Resonance

The results of Boerstael et al. (2.19) and Star et al. (2.21) showed that in order to consistently describe the magnetization and specific heat of dilute paramagnetic PdMn alloys the giant moment of Mn needs to be considered as having an effective g value of $g_{\text{eff}} = 3$ while having a 'normal' spin $s = 5/2$. However, electron paramagnetic resonance measurements of Shaltiel and Wernick (2.22) indicated a positive g-shift of +0.105 for a Pd 2.0 mole%Mn alloy. From their EPR measurements, Coles et al. (2.10) found that alloys with less than 3 at%Mn gave a minimum in the line width at a temperature very close to the transition temperature and positive paramagnetic g-shifts of about +0.15 were obtained. These g-shifts are thus considerably smaller than the g_{eff} expected from magnetization and specific heat results. This discrepancy is thought to be due to the dynamic effects operative in EPR measurements which are not relevant to the static

measurements. In EPR a local moment is excited to a higher energy level, causing the absorption of energy from the exciting field, and then relaxation back to the equilibrium level occurs. The possible relaxation paths for a local moment are via the conduction electrons to the lattice and the direct relaxation of the local moment to the lattice. The reverse transfer of energy from the conduction electrons to the local moment can cause a 'bottleneck' in the energy flow. For a review of EPR techniques and results see Taylor (2.23). If the impurity moment has a large g value then a large g -shift would occur if the conduction electron-lattice relaxation time were short compared with the conduction electron-local moment relaxation time. As the observed g shift is smaller than expected in the PdMn alloys this could be due to a long moment-lattice relaxation time. This, however, would result in a bottlenecked resonance which Coles et al. (2.10) do not find. It is thus difficult to reconcile the two g values obtained, one from the static measurements of the specific heat and magnetization and the other from the EPR measurements.

As the temperature is reduced the paramagnetic resonance line for Mn in the spin glass region broadens and shifts to lower fields at temperatures well above the expected spin glass freezing temperatures (as obtained from the susceptibility maxima), Coles et al. (2.10). For these spin glass alloys no field cooling effects were observed in the EPR measurements.

2.6. Low Field Susceptibility

During the course of their investigation into hydrogenated PdMn alloys, Burger and McLachlan (2.24) reported low field a.c. susceptibility results on two PdMn alloys, one with 3.0 at%Mn and the other with 10.0 at%Mn. The 3.0 at%Mn specimen was found to have a susceptibility variation with temperature of the form shown in Figure 2.3. This is characteristic of a ferromagnetic transition and the temperature at which the sharp decrease in susceptibility occurs is assigned to be the ordering temperature, T_c . Burger and McLachlan (2.24) found $T_c = (6\frac{1}{2} \pm \frac{1}{2})^\circ\text{K}$ for the 3 at%Mn alloy. In contrast to this behaviour, the Pd 10.0 at%Mn alloy exhibited a peak in the susceptibility, plotted as a function of temperature. The peak occurred at a temperature of 9°K , agreeing well with the predicted spin glass ordering temperature for an alloy of this particular concentration of Mn, obtained from the higher field magnetization measurements of Coles et al. (2.10).

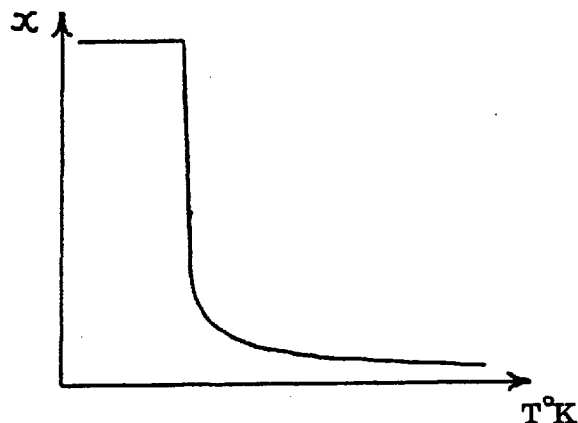


Figure 2.3

2.7. Neutron Scattering

Diffuse neutron scattering experiments by Low and Holden (2.25), on PdFe and PdCo alloys in the ferromagnetic phase, proved very successful in probing the spatial distribution of the moments associated with the Fe or Co magnetic impurities. Similar measurements on the PdMn system have only been attempted more recently. De Pater et al. (2.26) carried out diffuse neutron scattering measurements on a Pd 0.23 at%Mn alloy at a temperature of 1.4°K . Resistivity measurements on an alloy with this concentration of Manganese indicate a ferromagnetic ordering temperature of 0.4°K so that at a working temperature of 1.4°K the alloy will be in the paramagnetic phase. A difference counting technique was used; the contribution to the scattering cross-section in a large magnetic field applied along the direction of the scattering vector being subtracted from the contribution in zero field, this being achieved by switching the field on and off at a period of 20mins. The applied field of 9.5 KOe was sufficient to achieve 90% of the saturation magnetization. Neutrons of wavelength $\lambda = 2.56\text{\AA}$ were selected using a pyrolytic graphite crystal and the magnetic cross-section was obtained as a function of the scattering angle, K .

From the large angle results, a bare moment of $5.5\mu_{\text{B}}$ was determined for the Mn impurity, a value consistent with the $s = 5/2$ predicted from the specific heat data. At low angles, however, a problem arose. In their measurements,

Low and Holden (2.25) obtained the diffuse magnetic cross-section $\left(\frac{d\sigma}{d\Omega}\right)_K$ down to about $K = 0.15\text{\AA}^{-1}$ and then an extrapolation of the curve was made to coincide with the $K = 0$ cross-section estimated from the saturation magnetization of the alloy. The Fourier Transform of this curve then gave the spatial extent of the polarization of the Pd matrix in the vicinity of an impurity moment. The data obtained by De Pater et al. (2.26) for the Pd 0.23 at%Mn alloy was similarly taken down to about 0.15\AA^{-1} by which point the magnetic cross-section was larger than the $K = 0$ cross-section estimated from the saturation magnetization results of Star et al. (2.21). A straightforward extrapolation was not possible for such a situation. This unexpectedly large low angle scattering was thought to result from critical scattering effects while another possible explanation, the effect of fluctuations of the polarization clouds, was not discounted.

Verbeek et al. (2.27) extended this work to include measurements of the diffuse magnetic cross-section for a Pd 0.46at%Mn alloy. They measured the angular dependence of the magnetic diffuse scattering at 4.2°K between $K = 0.1$ and 1.5\AA^{-1} and also the temperature dependence of the scattering at a fixed angle of $K = 0.11\text{\AA}^{-1}$, by the same difference counting technique employed by De Pater et al. (2.26). The K dependence of the magnetic diffuse scattering was found to be very similar to that obtained on Pd 0.23 at%Mn by De Pater et al. (2.26); an enhanced peak in the forward direction rising to a value much larger

than the cross-section for $K = 0$ estimated from the saturation magnetization. The temperature dependence of the low angle scattering was investigated in an attempt to identify any critical scattering occurring. Any fluctuations in the magnetization due to the alloy being close to the transition temperature would become progressively less important as the temperature is increased away from this point and hence reduce any critical scattering that was taking place. Incomplete saturation of the sample magnetization itself gave a temperature dependence to the diffuse scattering cross-section and after making allowance for this the results of Verbeek et al. (2.27) indicated that no other temperature dependence of the scattering was occurring. From this they concluded that critical scattering was not playing a role in the enhancement of the forward scattering peak and as an alternative explanation they considered further the possibility of fluctuations in the polarization cloud. However, upon making an energy analysis at small K they could find no broadening of the elastic peak, within the energy resolution available.

This enhanced forward peak has therefore caused considerable problems to the people working on the neutron scattering from PdMn alloys. Current work in this direction (B.D. Rainford, private communication) now points once more to explanation on the basis of critical scattering effects. Measurements on PdFe have shown that the scattering intensity at small angles is very dependent on the magnetic

field applied to the sample. The intensity for zero applied field differs from that in a large field, even at temperatures well above the magnetic ordering temperature, showing that the higher fields tend to suppress the critical scattering which occurs in the low field measurements.

(This may explain why Verbeek et al. (2.27) failed to obtain any change of critical scattering as a function of temperature since they had a large field applied to the sample). It has been found during the course of this recent work that the measurements of the scattering intensity from PdFe varies at different azimuthal angles for the same K value. Intensity measurements were made within the plane perpendicular to the axis of the neutron beam and for external fields applied to the sample in one direction within this plane. It was found that the intensity varies with the angle α that the scattering direction makes relative to the applied magnetic field direction as

$$I = A(r) + B(r) \cos^2 \alpha$$

$B(r)$ is very small but is proportional to the magnetic scattering cross-section while $A(r)$ is suppressed isotropically as the magnetic field increases. This has enabled the determination of the magnetic scattering cross-section without any critical scattering contribution. The results for PdFe indicate a behaviour at small K different from that predicted by Low and Holden (2.25) in

their smooth extrapolation of the $K = 0$ value. It is found that the magnetic cross-section remains roughly constant for $0.02 < K < 0.1$ at a value lower than the $K = 0$ value predicted from the saturation magnetization of the alloys studied. It is expected that a similar analysis for PdMn will remove the excessively large low-angle scattering, but there is still work to be done in this direction to clarify these points.

In order to investigate the Mn moment without the problems of critical scattering effects, Cable and David (2.28) used a polarized-neutron diffuse-scattering method. In this method the sample is magnetized perpendicular to the scattering plane and the scattering cross-sections for incident neutrons polarized parallel and antiparallel to the magnetization are obtained. Measurements were carried out on four alloys, with 0.23, 0.46, 0.99 and 1.91 at%Mn at a temperature of 4.2°K . A field of 45 KOe was applied to the samples, producing over 0.9 of the saturation magnetization for the three lower concentration alloys and 85% of the saturation magnetization for the 1.91 at%Mn specimen. These measurements show a moment of only $4\mu_{\text{B}}$ on the Mn atoms compared with the $5.5\mu_{\text{B}}/\text{Mn}$ atom deduced from the unpolarized neutron measurements (2.26). Evidence of antiparallel Mn-Mn couplings are found in the results of the two higher concentration alloys.

2.8. Nuclear Orientation

Experimental limitations (increased difficulty in going to lower temperatures) have generally set a limit on the lower concentration of PdMn alloys studied; a limit which has meant all low concentration alloys which have been measured in one way or another have indicated a ferromagnetic transition. Interesting questions arise as to whether in the very low concentration limit the giant moment around a Mn atom is the same as in the higher concentration alloys, if spin glass ordering occurs over some region of concentration and whether a Kondo-like coupling exists. Flouquet et al. (2.29) have approached this problem by making nuclear orientation measurements on the Mn⁵⁴ isotope included in Palladium. They find that a giant moment exists down to 10 mK and that no concentration effects on this moment occur above this temperature. They also find evidence for a spin glass type coupling at these very low concentrations.

REFERENCES

- 2.1 HODGES L., WATSON R.E. and EHRENREICH H.
Phys. Rev. B5, 3953 (1972).
- 2.2 ANDERSON O.K.
Phys. Rev. B2, 883 (1970).
- 2.3 HOARE F.E. and MATHEWS J.C.
Proc. Roy. Soc. A212, 137 (1952).
- 2.4 GIOVANNINI B., PETER M. and SCHRIEFFER J.R.
Phys. Rev. Letts. 12, 136 (1964).
- 2.5 MISAWA S.
Phys. Letts. 32A, 514 (1970).
- 2.6 MISAWA S.
Phys. Letts. 32A, 153 (1970).
- 2.7 BARNEA G.
J. Phys. C8, L216 (1975).
- 2.8 MISAWA S.
J. Phys. C8, L403 (1975).
- 2.9 NIEUWENHUYS G.J.
Adv. in Phys. 24, 515 (1975).
- 2.10 COLES B.R., JAMIESON H., TAYLOR R.H. and TARI A.
J. Phys. F5, 565 (1975).
- 2.11 WATANABE D.
Trans. Jap. Inst. Metals 3, 234 (1962).
- 2.12 CHAKRABATI D.J.
Int. J. of Magnetism 6, 305 (1974).
- 2.13 CABLE J.W., WOLLAN E.O., KOEHLER W.C. and CHILD H.R.
Phys. Rev. 128, 2118 (1962).
- 2.14 SARACHIK M.P. and SHALTIEL D.
J. Appl. Phys. 38, 1155 (1967).
- 2.15 WILLIAMS G. and LORAM J.W.
Solid State Comms. 7, 1261 (1969).
- 2.16 WILLIAMS G., SWALLOW G.A. and LORAM J.W.
Phys. Rev. B7, 257 (1973).
- 2.17 ZWEERS H.A. and Van Den BERG G.J.
J. Phys. F5, 555 (1975).

- 2.18 NIEUWENHUYS G.J. and BOERSTOEL B.M.
Phys. Letts. 33A, 281 (1970).
- 2.19 BOERSTOEL B.M., ZWART J.J. and HANSEN J.
Physica 57, 397 (1972).
- 2.20 RAULT J. and BURGER J.P.
Comptes Rendues 269B, 1085 (1969).
- 2.21 STAR W.M., FONER S. and McNIFF E.J.
Phys. Rev. B12, 2690 (1975).
- 2.22 SHALTIEL D. and WERNICK J.H.
Phys. Rev. 136, A245 (1964).
- 2.23 TAYLOR R.H.
Adv. in Phys. 24, 681 (1975).
- 2.24 BURGER J.P. and MCLACHLAN D.S.
Solid State Comms. 13, 1563 (1973).
- 2.25 LOW G.G. and HOLDEN T.M.
Proc. Phys. Soc. 89, 119 (1966).
- 2.26 DE PATER C.J., VAN DIJK C. and NIEUWENHUYS G.J.
J. Phys. F5, L58 (1975).
- 2.27 VERBEEK B.H., AMUNDSEN T. and VAN DIJK C.
Physica 86-88B, 482 (1977).
- 2.28 CABLE J.W. and DAVID L.
Phys. Rev. B16, 297 (1977).
- 2.29 FLOUQUET J., RIBAUD M., TAURIAN O., SANCHEZ J. and
THOLENCE J.L., To be published (see reference in
Phys. Letts. 38, 81 (1977)).

CHAPTER 3

EXPERIMENTAL

3.1. Magnetic Measurements

The methods available for directly determining magnetic moments can be split into two classes; i) those which measure the force acting on a sample when placed in an inhomogeneous field and ii) those which measure the induced voltage in a circuit due to a change in flux linkage. There are also numerous indirect techniques for measuring magnetic moments such as the Faraday effect, the ferromagnetic Hall effect and ferromagnetic resonance and where applicable these indirect techniques can be extremely sensitive and can add valuable information to systems which have been studied by other methods. However, they rely on some particular phenomenon which occurs in only a limited number of materials and so a piece of apparatus employing one of the direct methods of measurement is more generally useful.

3.2. Force Method

If a sample of magnetic moment \underline{M} is placed in an inhomogeneous field, $\underline{H}(\underline{r})$, then there will be a force, \underline{F} , acting on the sample given by;

$$\underline{F} = \nabla(\underline{M} \cdot \underline{H})$$

If the sample can be approximated by a dipole moment \underline{M} then;

$$\underline{F} = \underline{M} \cdot \nabla \underline{H}$$

and if the demagnetizing field is small:

$$F = m \chi \underline{H} \cdot \nabla \underline{H}$$

where m is the mass of the sample and χ emu/gm is the mass susceptibility.

The Faraday balance is an apparatus for measuring the magnetization of samples using this method. Accurately known field and field gradients are produced at the sample position and the force upon the sample is measured. This force can then be directly related to the sample moment after appropriate calibration. For a comprehensive discussion of the design of a Faraday balance see Bell (3.1) or Male (3.2). The sensitivity of this type of apparatus is limited by the force detection, moment changes of 10^{-10} emu/gm have been measured by use of automatic vacuum microbalances. This, however, is for large field and field gradients and where low field measurements are required on low susceptibility samples the sensitivity is much reduced below this. There is an additional problem in that it is difficult to measure the magnetization in a uniform field since the field gradient is necessary to produce a force.

3.3. Induction Methods

3.3.1. Introduction

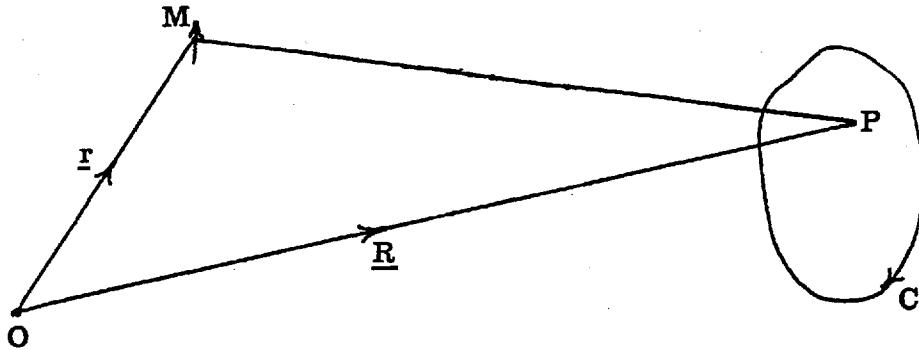


Figure 3.1

Consider any two dimensional circuit, C , and some point, P , at position \underline{R} relative to an origin O , Figure 3.1. If an infinitesimal dipole moment \underline{M} is at position \underline{r} then the vector potential at P due to \underline{M} is given by;

$$\underline{A} = \frac{\mu_0}{4\pi} \frac{\underline{M} \wedge (\underline{R} - \underline{r})}{|\underline{R} - \underline{r}|^3}$$

and since $\underline{B} = \nabla \wedge \underline{A}$ we can easily show that the flux through C is;

$$\phi = \frac{\mu_0}{4\pi} \oint_C \underline{M} \cdot \frac{(\underline{R} - \underline{r}) \wedge d\underline{l}}{|\underline{R} - \underline{r}|^3} \quad (\text{III.1})$$

Now, if a current, i , was to pass through the circuit C , in the absence of \underline{M} the field at \underline{r} would be given by;

$$\underline{H}(\underline{r}-\underline{R}) = \frac{1}{4\pi} \oint_C \frac{(\underline{R}-\underline{r}) \wedge d\underline{l}}{|\underline{R}-\underline{r}|^3}$$

∴ Equation III.1 becomes:

$$\phi = \frac{\mu_0}{1} \underline{M} \cdot \underline{H}(\underline{r}-\underline{R}) \quad (\text{III.2})$$

This is one of the reciprocity theorems of electromagnetism. Thus, the flux cutting a circuit due to a moment \underline{M} is given by $\phi = \mu_0 \underline{M} \cdot \underline{h}(\underline{r}-\underline{R})$, where \underline{h} is the field that would be produced at the position of the moment, with the moment absent, if unit current were to pass through the circuit.

Any change in the flux linkage in a circuit will lead to an e.m.f., $\epsilon = \frac{-d\phi}{dt}$, being produced in the circuit which can then, in principle, be used to obtain information about the magnetization of any material in close proximity to the circuit. There are a wide number of variations on this basic theme, all designed to give accurately and easily the required magnetic moment, some of which will now be considered.

3.3.2. Mutual Inductance Techniques

Consider any two circuits, 1 and 2, say. If a current I_1 flows in circuit 1 then there will be a certain flux linkage with circuit 2 depending on their relative positions and environment. If I_1 changes, the flux cutting the second circuit will alter and an e.m.f., ϵ_{21} ,

will be induced in this second circuit. The mutual inductance of these two circuits is then defined as the ratio of the e.m.f. induced in one of the circuits to the time rate of change of current in the other circuit;

$$\text{ie.} \quad M_{12} = - \frac{\epsilon_{21}}{dI_1/dt}$$

If a magnetic sample is in the vicinity of the second circuit then any change in the susceptibility of this sample will cause a change in the flux linkage in circuit 2 and hence alter the mutual inductance of these circuits. Thus, the temperature dependence of the sample susceptibility can be determined if the temperature variation of the mutual inductance, without the sample, is known.

The mutual inductance coils generally consist of concentrically wound primary and secondary solenoid coils, with the magnetic sample being placed in the bore of these coils. The incremental change of mutual inductance when a sample is moved in, is a very small fraction of the empty coil inductance, so that, in order to obtain greater sensitivity, the secondary can be made from two identical, oppositely wound, coils thus making the overall mutual inductance small.

Giauque and MacDonald (3.3) were able to measure the variation of the susceptibility of a paramagnetic salt and use this as a method of monitoring the temperature. This was possible as only a measure of the mutual

inductance relative to that at a known temperature, eg. 4.2°K , was needed. However, absolute values of the susceptibility were not possible due to the fact that the empty coil mutual inductance was not repeatable with temperature cycling. McKim and Wolff (3.4) described an improvement of this method to enable the absolute susceptibility to be determined. They constructed a system which allowed for the movement of the sample in and out of the coils so that at each temperature the additional mutual inductance due to the sample could be found.

The measurement of the mutual inductance is done by means of a mutual inductance bridge, generally of a form based on the traditional bridge of Hartshorn (3.5). For this type of measurement these bridges usually work somewhere within the frequency range 15 Hz-1500 Hz; the lower limit being set by the magnitude of the e.m.f. produced in the secondary while the effects of the self capacity of the primary and secondary and the capacity between them sets the upper limit. The essential operation of such a bridge is shown in Figure 3.2.

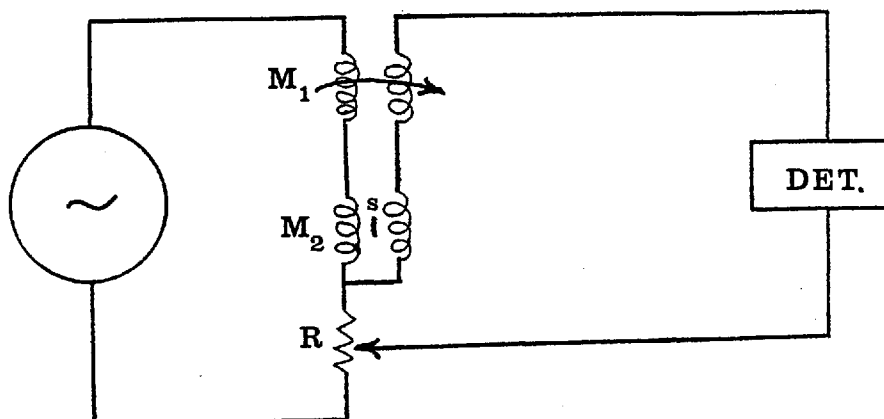


Figure 3.2. Hartshorn Bridge

An alternating current is produced in the primary windings of the mutual inductors M_1 and M_2 by the oscillator and the variable mutual inductance M_1 is varied to balance that of M_2 . However, the change in mutual inductance of M_2 , when the sample is inserted, also has an imaginary part due to the losses in the material associated with dissipative processes such as eddy currents and therefore to balance the bridge a variable potentiometer, R , also needs adjusting to obtain a null at the detector.

Commercial bridges are available based on a modified version of the Hartshorn bridge suggested by Pillinger et al. (3.6), in which the variable mutual inductance is replaced by a fixed inductor with a resistive potential divider, the primary current in the fixed compensating mutual inductance being varied to give the balance condition. The advantage of this is that the secondary self-impedance remains constant, in comparison with the Hartshorn bridge where the mutual inductance of the coils may not be linearly proportional to the reading of the variable mutual inductance.

Mutual inductance methods have long been in use for magnetic measurements but special interest in this field was generated by the discovery of Cannella and Mydosh (3.7) who found that the temperature dependent susceptibility of dilute alloys of AuFe showed a sharp cusp. These measurements were made by an a.c. mutual inductance apparatus, Cannella (3.8), employing the

techniques described above. It is now known that alloys such as AuFe fall into the spin glass group of magnetic materials for certain concentrations of iron, Section 1.4, and the cusp is related to the response of the spins to the applied field, which in the mutual inductance method is alternating at the frequency set by the bridge. It was essential, therefore, to make a study of the susceptibility of these alloys in a similarly small but steady field (the alternating field at the sample position in the measurements of Cannella and Mydosh was ~ 5 gauss r.m.s.) where the other induction techniques to be discussed are of more use.

3.3.3. SQUID Magnetometers

The Superconducting Quantum Interference Device (SQUID) depends for its operation upon the long range quantum mechanical coherence which exists in superconductors and the Josephson tunnelling possible across a 'weak link' between two superconductors. A SQUID basically consists of a superconducting loop, generally less than 1 cm^2 in area, in series with one or more weak links, across which coherence of the wavefunction is possible upto a critical supercurrent of a few tens of microamps. Zimmerman et al. (3.9) discuss the requirements of a useful SQUID and they describe the design of a particularly stable and robust two hole point-contact SQUID.

When a magnetic field is applied to a superconductor,

supercurrents are set up so as to oppose the applied field, leading to the well known Meissner effect. When a field is applied to a SQUID, a supercurrent will be set up to oppose the field but the size of the allowed current is limited by the weak link. When the critical current is reached the weak link will become 'normal', thus destroying the supercurrent and admitting a flux quantum. This process will then be continuously repeated for further increases in the field. Hence, changes in the flux incident on a SQUID can be monitored by suitable external circuits resulting in a flux detector whose response can be periodic in the flux quantum, $\phi_0 = 2 \cdot 10^{-7}$ gauss cm².

Two methods have been devised to measure the total circulating current in the SQUID in order to use its periodic variation with applied field so as to provide a sensitive magnetometer. One way is to use a second weak link and to measure the critical current, i_{cp} , of the pair. It is found that the current, i_{cp} , at which a voltage appears across the two weak links, is modulated by the periodic variation of the circulating current, which is periodic in ϕ_0 . The quantum interference properties of double Josephson Junctions are discussed by Fulton et al. (3.10). The second method, developed by Silver and Zimmerman (3.11), uses a tuned circuit, resonant at about 20 MHz, inductively coupled to the SQUID. The theory of the response of a SQUID to the applied rf field is discussed in the papers of Zimmerman et al. (3.9) and Silver and

Zimmerman (3.11) and a good general discussion is given by Lounasmaa (3.12). For completeness a short description will be given but for full details reference should be made to one of these papers. The variation of the voltage, V_L , across the inductance of the resonant circuit when driven at the resonant frequency, as a function of the amplitude of the rf current I_{rf} , and applied flux, ϕ_a , is shown in Figure 3.3.

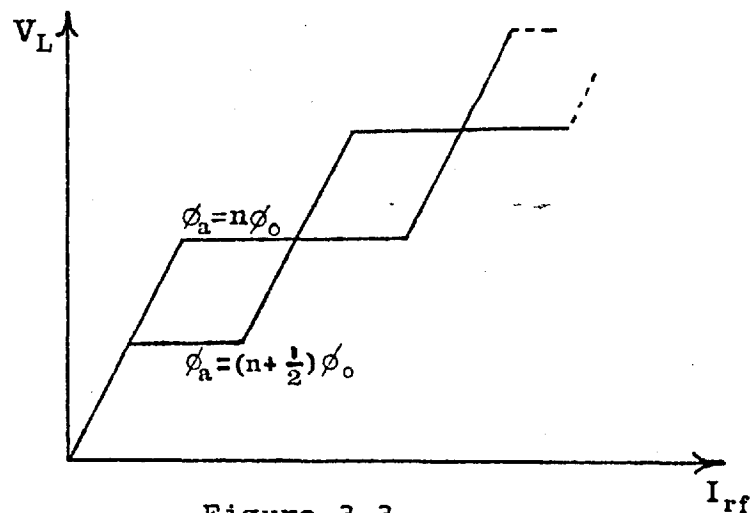


Figure 3.3

A block diagram of the components used for rf detection is given in Figure 3.4.

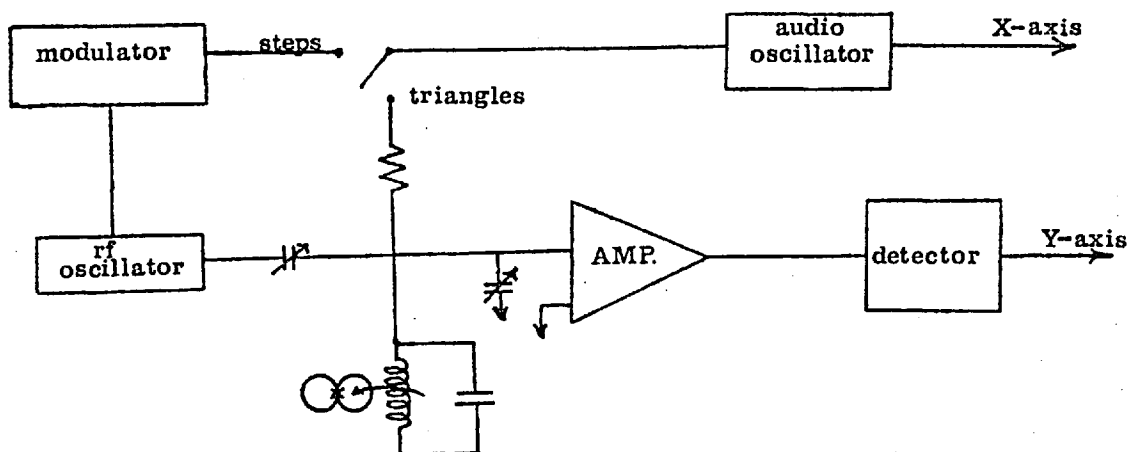


Figure 3.4

The circuit is driven at its resonant frequency by an rf oscillator weakly coupled to it via a capacitor. The voltage across the resonant circuit is amplified and detected. If the amplitude of the rf driving voltage is modulated by an audio voltage and the audio signal taken to the horizontal deflection of an oscilloscope then the 'step' or 'staircase' pattern, Figure 3.3, will be obtained if the signal, V_L , is taken to the y deflection of the oscilloscope. Alternatively, if the average current through the resonant circuit is made to vary at the audio frequency and superimposed on this is a constant rf level, the voltage detected decreases linearly for a change in applied flux from $\phi_a = n\phi_0$ to $\phi_a = (n+\frac{1}{2})\phi_0$ and then increases linearly for a further change from $\phi_a = (n+\frac{1}{2})\phi_0$ to $\phi_a = (n+1)\phi_0$. The resultant pattern on the oscilloscope will then be triangular since the horizontal deflection is now proportional to the average magnetic flux in the SQUID.

In a SQUID magnetometer the pick-up coils, tightly twisted shielded connecting leads and coil located in a hole of the SQUID, form a continuous superconducting loop. This 'flux transformer' produces a flux change in the SQUID equal to the change of flux in the pick-up coils. If this occurs because of a variation in susceptibility of a sample located in the pick-up coils it is then necessary to be able to measure the change in flux incident upon the SQUID to obtain a measure of the variation of the sample susceptibility. This may be done by using the SQUID as a

null detector in a negative feedback loop. After setting a certain flux and closing the feedback loop any deviation of the average flux in the SQUID is corrected for by an equal and opposite feedback flux produced by a current fed to the rf coil. By measuring the feedback current, therefore, in this 'flux-locked loop' the change in flux can be measured very accurately.

SQUID magnetometers have come into wide use in the last few years and enable very sensitive magnetization measurements to be made. With commercially available SQUIDS and associated electronics such a system is now comparatively easy to set up. The noise limitations of such a SQUID measuring system are discussed by Gifford et al. (3.13). A noise level of about $10^{-4} \phi_0$ per root Hz is found, thus giving a very high flux sensitivity for these systems. Several uses of SQUID magnetometers have been described by De Bruyn Ouboter and De Waele (3.14).

3.3.4. Vibration Magnetometers

As the emf induced in a pick-up coil is proportional to the magnetization of a moving sample in close proximity to the coil we can obtain a measure of the sample magnetization by detecting this emf. Many different arrangements have been used in practise in order to suit a particular investigation, two of the most widespread being the oscillatory coil or sample techniques. For the vibrating signal-coil systems the magnetizing fields need to be extremely uniform otherwise unwanted signals will be

produced in the coils. For this reason it is usual to vibrate the sample relative to fixed coils and the vibrating sample magnetometer (VSM) has found great favour in magnetization measurements, Foner (3.15), Murani (3.16), Springford et al. (3.17). The usual sensitivity of this type of apparatus is about 10^{-6} emu. However, many people incorrectly assume this is a limiting value for VSM's when arguing in favour of force methods. As Foner (3.18) pointed out, this is not the case since suitable coil design can increase the efficiency of the coupling of the sample to the detection coil, giving several orders of magnitude better sensitivity if required. For most measurements, however, 10^{-6} emu is more than adequate.

3.4. The Vibrating Sample Magnetometer

3.4.1. Introduction

An important limitation to the sensitivity of a Vibrating Sample Magnetometer is the production of spurious signals from the movement of the detection coils relative to the magnetizing field, which arises due to the difficulty in totally isolating the system from sympathetic vibrations. In the VSM designed by Foner (3.15) the pick-up coils were rigidly attached to the pole faces of the electromagnet, eliminating the problem of coil vibration but at the expense of reducing the sensitivity by restricting the coupling possible between the sample and the detection coils. For low temperature

work, in order to allow the sample to coil coupling to increase, the detection coils need to be placed inside the dewars. To overcome the problem of the vibration of the detection coils in the magnetizing field we also took the field producing coils inside the cryostat. This considerably limits the field that can be achieved but for the present low field investigations this is not a drawback.

Instead of directly detecting the emf produced in the sample pick-up coils, a null method is employed in order to obtain a measurement which is directly proportional to the sample magnetization and which is independent of small changes in the frequency or amplitude of vibration. To achieve this a reference signal is produced in a second detection coil located around a small coil wound onto the vibration rod at some position well isolated from the sample. When a current flows through this coil it duplicates a dipole moment thus inducing the reference signal in the detection coil around it. A fraction of this reference signal is taken to balance out the signal produced in the sample pick-up coils, the fraction necessary then being a direct measure of the sample magnetization, once calibration has been carried out.

With suitable design of the pick-up coil arrangement (Section 3.4.3) and by rigidly connecting the field producing coils to the pick-up coils we have designed an apparatus capable of measuring moments of 10^{-6} emu.

3.4.2. Mechanical Design of the Apparatus

Figure 3.5 shows the major features of the magnetometer. The design centres on the requirement to be able to make magnetization versus temperature measurements in the liquid helium temperature range. The standard double dewar system is used; allowing pre-cooling of the sample to about 78°K when liquid nitrogen is placed in the outer dewar, followed by cooling to 4.2°K when liquid helium is transferred into the inner dewar. The nitrogen in the outer dewar then acts as a good baffle to radiation; cutting down this source of heat input by about 99%, so allowing a much more economical use to be made of the liquid helium.

A leak tight helium enclosure is required so as to be able to reduce the pressure above the liquid helium surface when going to temperatures below 4.2°K . This is achieved by means of the brass hat shown in Figure 3.6. The hat has two strips of angle iron hard soldered onto the brim at either end of a diameter and is supported upon a framework at the ends of these strips of angle iron. Both dewars are suspended from the hat by means of cages which tightly fit around the outside of the dewars and which each screw into the base plate of the hat at three positions. The inner dewar just fits into the hat and a rubber annulus separates the top of the dewar from the brass, forming a vacuum seal. The opening at the top of the hat permits the magnetometer to be placed through this gap until plate, P, Figure 3.5, comes to rest on top of

Figure 3.5 : Diagram of the top portion of the low field Vibrating Sample Magnetometer. Not shown at the bottom of the apparatus is just an extension of the vibration rod and the pick-up coil and field coil assembly (which are shown separately in figures 3.12 and 3.13, respectively). These are suitably connected via a small piece of brass to the outer stainless steel tube to enable the turn rod to move the pick-up coil former up and down relative to the sample position.

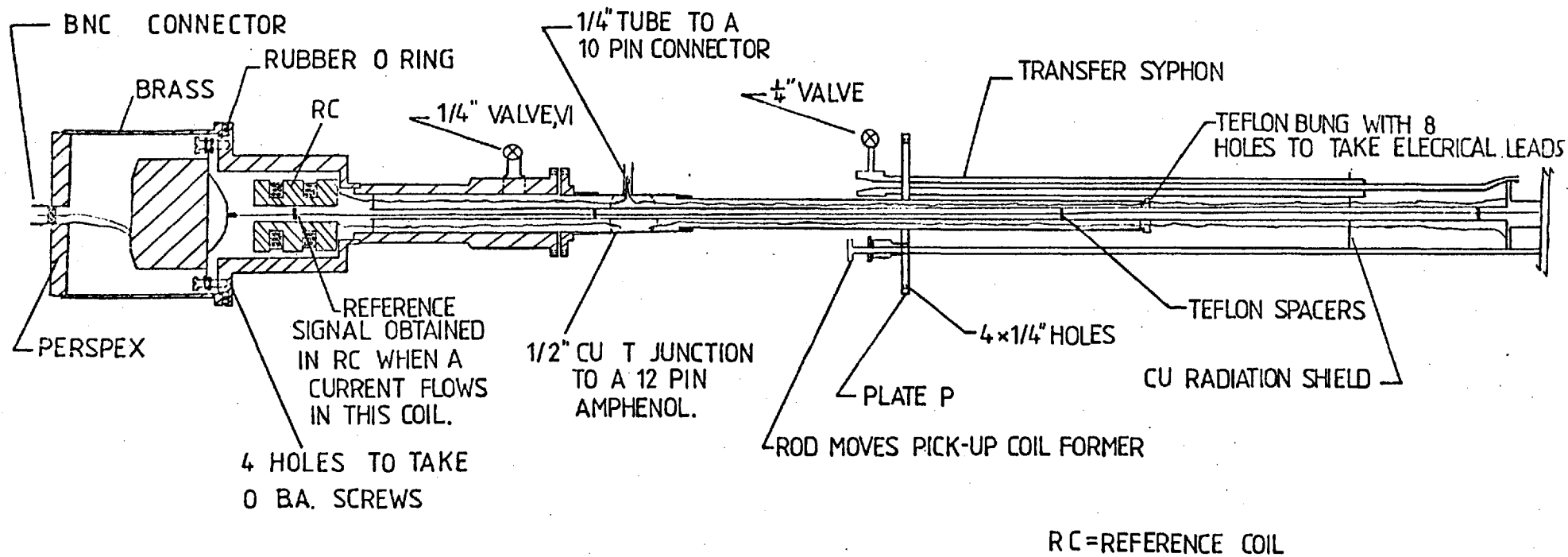


Figure 3.5

Figure 3.6 :

Brass hat from which the two glass dewars are suspended. The magnetometer can then be inserted into the dewars and plate P, figure 3.5, screwed into the top of the hat to form a vacuum tight seal.

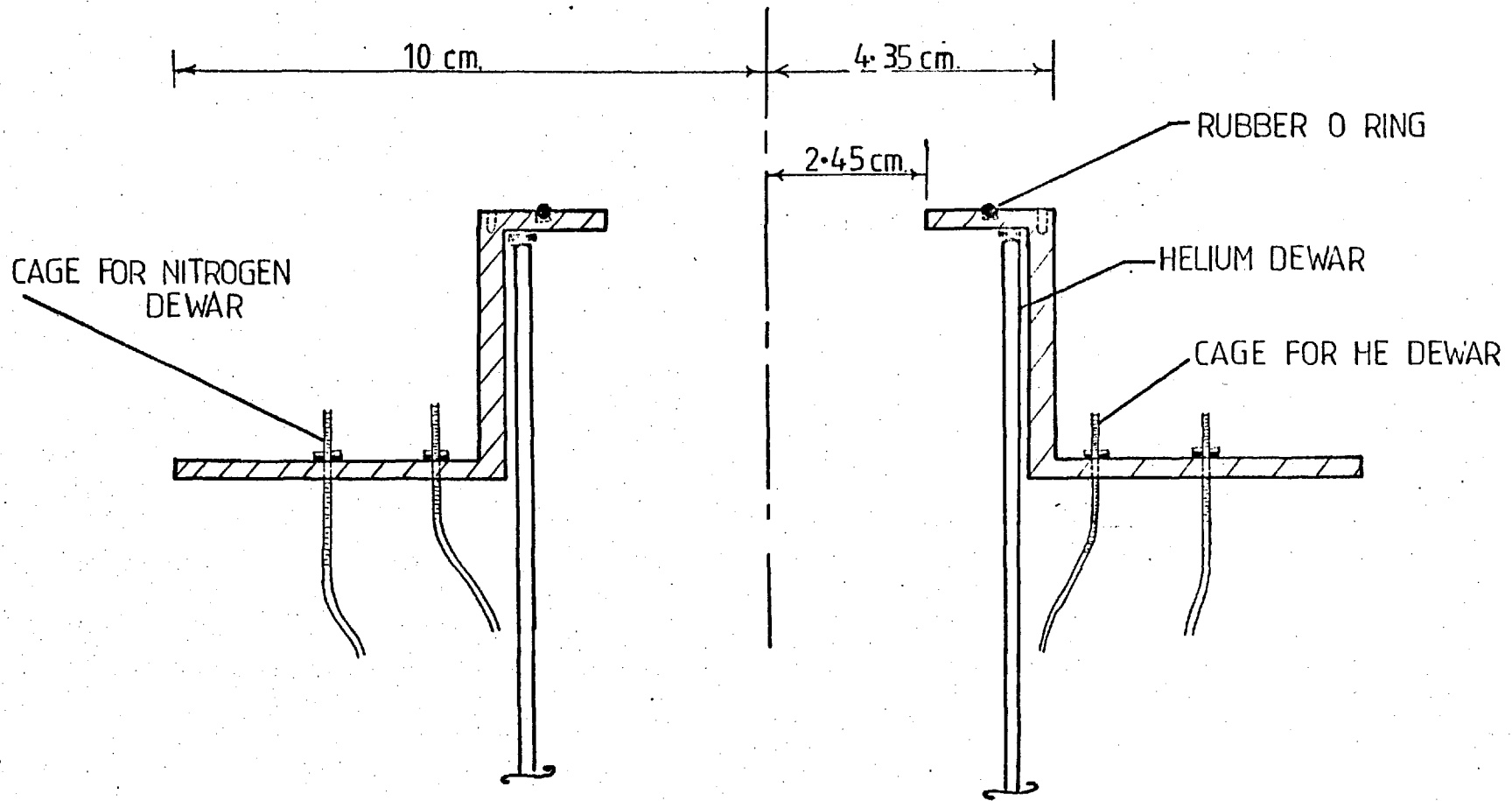


FIGURE 3.6

the hat. The two are then tightly screwed together, the 'O' ring between creating a good leak tight seal.

A Ling Dynamic systems 101 Vibration generator is housed in a de-mountable vacuum enclosure of brass and is joined via a long thin walled stainless tube to the sample at the bottom. The vibration generator is shock mounted onto the outer vacuum enclosure on 'O' rings in order to reduce the transmission of vibrations via the body of the apparatus to the dewars and lower portions of the apparatus. A bnc lead-through sealed into the perspex top enables the wire carrying the signal from the oscillator, which drives the vibration generator, to be easily connected and disconnected. The vibration tube runs inside a wider stainless tube and has teflon washers along its length to prevent sideways motion of the sample. The sample is fixed onto a tufnol rod which extends to a point well outside the pick-up coils before joining onto the end of the stainless vibration rod. Tufnol has a low diamagnetic susceptibility variation with temperature of magnitude $(-0.2 + \frac{2.5}{T}) \cdot 10^{-6}$ emu/gm, Commander and Finn (3.19), and as the mass of tufnol within the sphere of influence of the pick-up coils is much less than a gram, the contribution from this sample holder can be ignored. A blank run showed this to be a valid appraisal.

All the necessary electrical wires are taken through two side ports via vacuum lead-through plugs. The wires are run in pairs through PTFE tubing to the bottom of the magnetometer; being connected to a small peg-board,

from which all relevant connections are then made. Two side ports in the brass hat, Figure 3.6, allow for the return of helium gas and for the connection of a manostat for pumping on the inner space.

A double-walled, evacuated, transfer syphon tube is an integral part of the magnetometer, passing through the plate, P, Figure 3.5, via a soldered leak tight seal to a point nearer the bottom of the dewar; below a nitrogen radiation shield.

The pick-up coil and field producing coil unit (discussed more fully in Section 3.4.3) is moveable to enable sample changes to be made from the bottom end.

3.4.3. Electrical Design

i) Circuit Descriptions

Figure 3.7 shows a schematic diagram of the arrangement used. The vibration generator is driven by a Ling Dynamic Systems TPO 20 audio oscillator, a signal from which is also taken through a Brookdeal MS320 phase shifter to the reference of a Brookdeal FL355 Lock-in amplifier.

The d.c. current, I_{ref} , in the coil C, was provided by a battery and could be varied where necessary to suit the size of sample signal obtained. An amount, K, of the reference signal thus induced in the pick-up coils is taken from a ten turn $10,000\Omega$, wirewound potentiometer which is sub-divided into 1,000 divisions. A fraction $K \cdot 10^{-3}$ of the reference signal is therefore obtained if the

Figure 3.7 : Schematic diagram of the measuring principle employed in the apparatus. The vibration of the rod is run from an oscillator at $\sim 70\text{Hz}$. The signal from the sample pick-up coils is taken to a differential amplifier along with a fraction, K , of the reference signal and the difference signal taken to a P.S.D. A null is looked for by varying the fraction K .

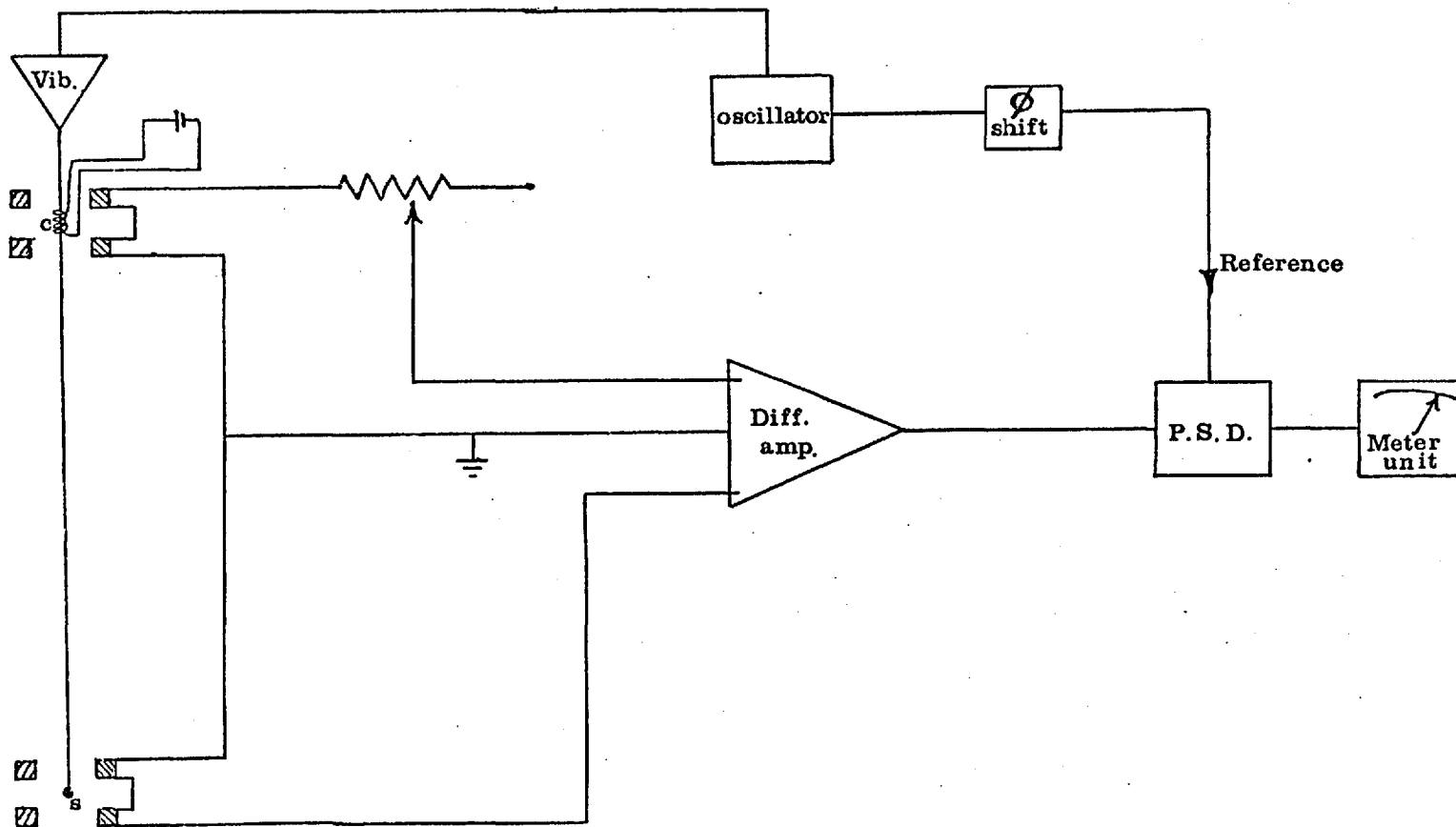


Figure 3.7

output of the potentiometer is exactly linear. Checks on this linearity showed only very slight deviations ($<0.5\%$) from linearity. This fraction of the reference signal is taken, along with the full sample signal, to a differential amplifier, the circuit for which is given in Figure 3.8. By then taking this difference signal to the lock-in amplifier referenced at the vibration frequency we obtain an output which is a measure of the difference between the two signals at this frequency. Following the P.S.D. is a Brookdeal MS 320 meter unit which smooths the difference signal by means of one of a set of time constants available and which indicates the magnitude of the difference signal.

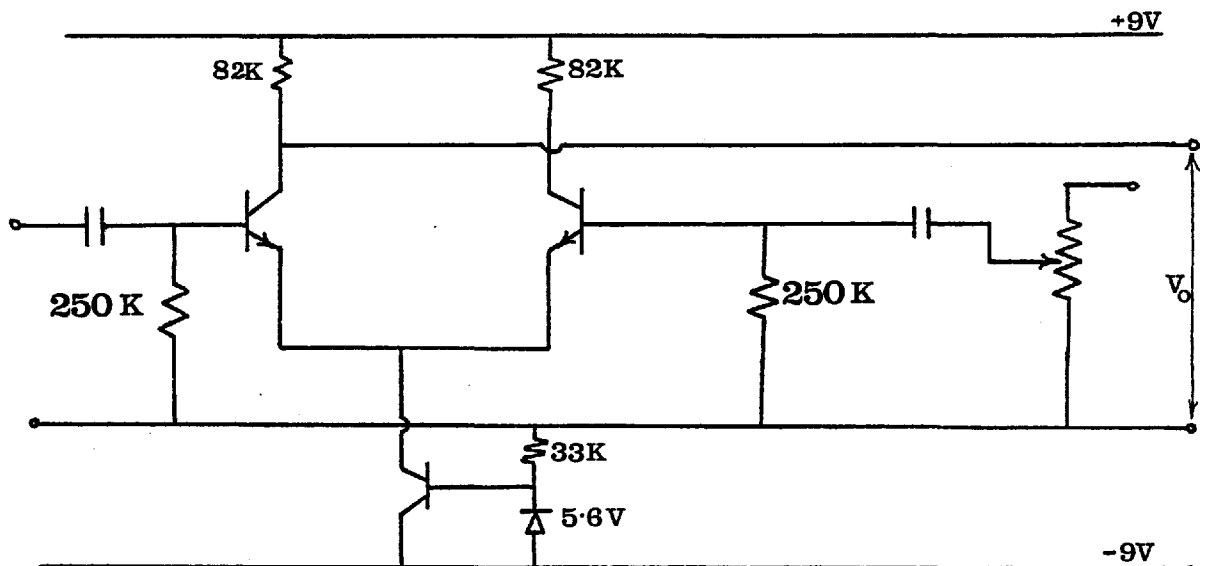


Figure 3.8

ii) The pick-up Coils

Foner (3.15) obtained empirically the most useful pick-up coil arrangements by observing the signal variation with sample position, for various geometries of the

detection coils. Pairs of circular or oval coils connected in series-opposition were found to be suitable since a pair such as that shown in Figure 3.9 minimized the effects of sample positioning and greatly reduced the background noise due to instabilities in the magnetic field or vibrations of the magnet and coil system. For Figure 3.9 the applied field was perpendicular to Z and positioning was relatively insensitive to variations in all directions about O.

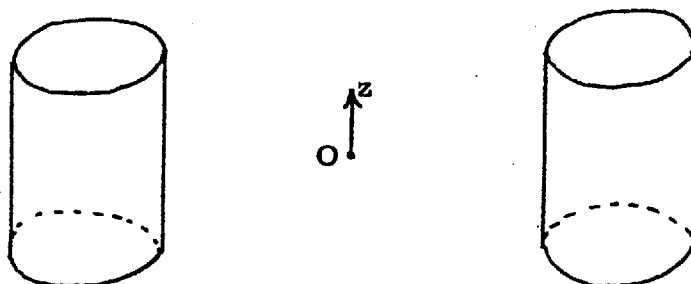


Figure 3.9

Mallinson (3.20) approached the problem more mathematically. He demonstrated that a reciprocity theorem of electromagnetism, Equation III.2, permits the discussion of the coil properties in terms of the spatial variation of the magnetic field that would be produced if a current were to flow through the coils. He showed that the signal was proportional to the gradient of this field and therefore one wishes to obtain a situation where the field gradient remains constant over as large a region as possible.

In preference to the arrangement of Figure 3.9 we

have adopted that shown in Figure 3.10 in order to increase the sample to coil coupling. The sample is made to vibrate within a pair of oppositely wound coils. Vibration takes place in the direction of, and on, the axis of the coils and hence the system possesses rotational symmetry about the vibration rod. The pair of coils are wound onto a tufnol former with a hole drilled through the centre in order to take the vibrating sample. The coils were wound with approximately the same number of turns and then the net flux linkage of the pair was adjusted to zero by varying the number of turns on one of the coils when the pair was located in a homogenous alternating magnetic field.

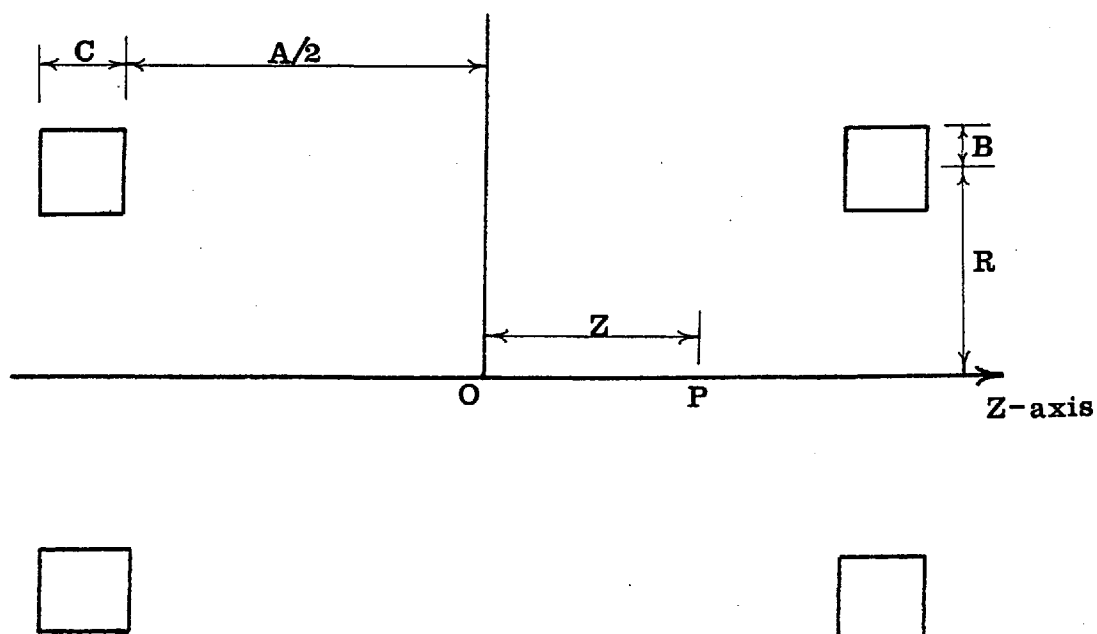


Figure 3.10

Following Guy, (3.21), a complete analysis of the signal produced in the detection coils can be given for the case when the sample may be approximated by a dipole moment in the Z-direction. Consider the vibration in the Z-direction of a dipole moment M_Z . If the frequency of vibration is ω_0 and the amplitude a_0 then the instantaneous position may be written $Z = Z_0 + a_0 e^{i\omega_0 t}$, where Z_0 is the mean position. By the reciprocity theorem, Equation III.2, the flux cutting the pick-up coils is given by;

$$\phi = \mu_0 M_Z h(Z)$$

where $h(Z)$ is the field that would be produced at a point on the axis of the coils, distant Z from the origin, if unit current were to flow through the coils.

The emf induced in the coil is therefore given by;

$$\epsilon = - \frac{\partial \phi}{\partial t} = -\mu_0 M_Z \frac{\partial h(Z)}{\partial t} \Bigg|_{Z=Z_0}$$

which can be shown to give:

$$\epsilon = -\mu_0 M_Z \left[i\omega_0 a_0 \frac{\partial h(Z)}{\partial Z} \Bigg|_{Z=Z_0} e^{i\omega_0 t} + i\omega_0 a_0^2 \frac{\partial^2 h(Z)}{\partial Z^2} \Bigg|_{Z=Z_0} e^{2i\omega_0 t} \right] + O(3)$$

Therefore, a signal at the vibration frequency

proportional to $a_{00} \omega_0 M_Z \left. \frac{\partial h(Z)}{\partial Z} \right|_{Z=Z_0}$ is obtained. This

term was also determined by Mallinson (3.20), but we can see that there are additional contributions to the total signal at higher harmonics of the vibration frequency, which Mallinson did not obtain. Possible applications of these higher harmonic signals are suggested by Guy (3.21) but for the present applications the sample moment may be determined merely by detecting at the vibration frequency.

The design of the coils therefore centres on a suitable choice of coil dimensions which will produce a large field gradient, constant over as large a distance as possible, while taking into consideration the compatibility with the geometrical constraints of the cryostat and the sensitivity required.

The calculation of the field, $h(Z)$, produced at a point P on the axis of the coil arrangement of Figure 3.10, is given in Appendix A. From this we can calculate the first derivative $\frac{dh(Z)}{dZ}$ and this is given in the appendix by Equation (A.4). We can therefore determine the shape of $\frac{dh(Z)}{dZ}$ for any particular set of coil parameters. Figure 3.11 shows three plots of $\frac{dh(Z)}{dZ}$, calculated for $B = 1.0$ mm, $C = 5.0$ mm and $R = 4.7$ mm, at different separations, A. These values of B, C and mean coil radius, R, were chosen within the above requirements of sensitivity and compatibility. By choosing $A = 5.4$ mm, therefore, we have a region of about four

Figure 3.11 : Calculated field derivatives for the pick-up coil geometry of figure 3.10. The curves were calculated for fixed values of $B = 1.0\text{mm}$, $C = 5.0\text{mm}$ and $R = 4.7\text{mm}$ and for different coil separations of $A = 4.5, 5.6$ and 6.5mm . From these curves we obtain the optimum coil separation (where there is a large central region with a constant $dh(Z)/dz$) of $\sim 5.4\text{mm}$.

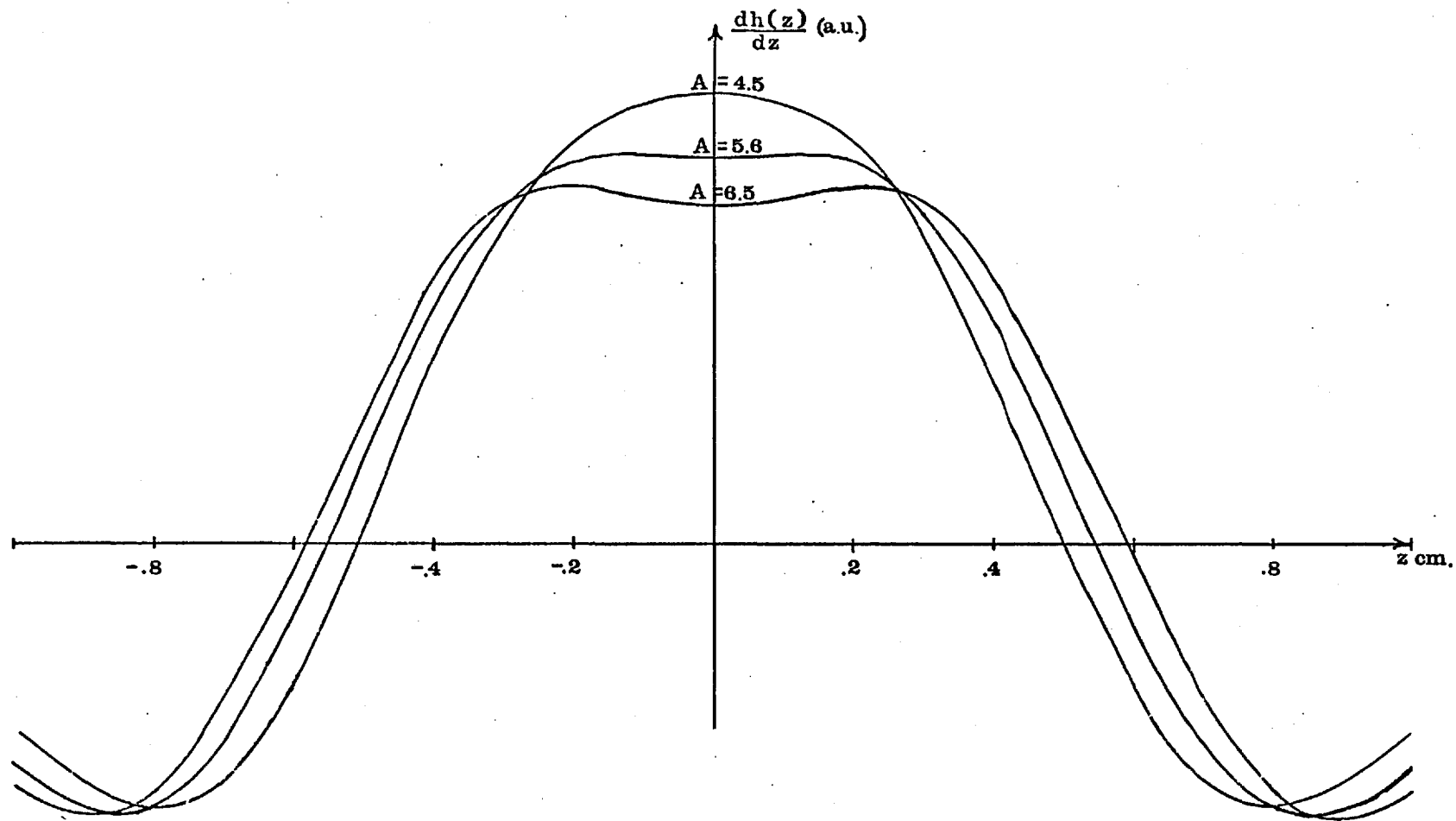


Figure 3.11

millimeters over which the signal from the dipole moment remains constant, thus allowing for any error in the placing of the sample. Figure 3.12 shows the coil former that was constructed, the dimensions being given in millimeters.

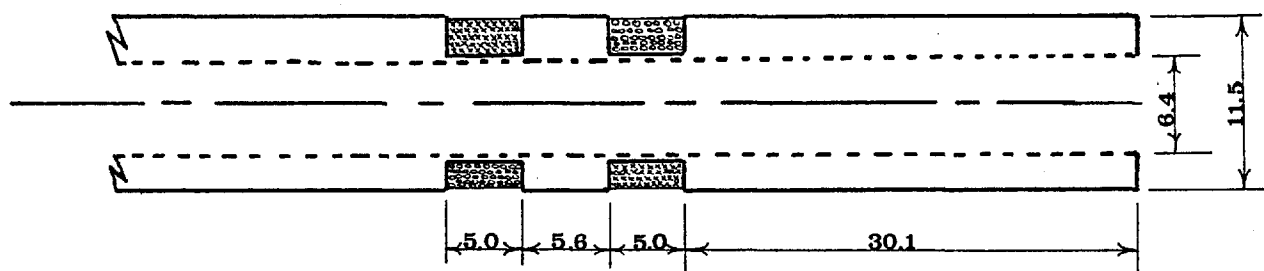


Figure 3.12

Each coil was separately wound from approximately 3,000 turns of 48 swg enamelled copper wire and the resistance of each then measured. Initial balancing was achieved by unwinding turns as necessary to try to balance the resistances of the two coils and then final balancing carried out in an alternating magnetic field. The four ends of the copper wires were then carefully laid in a small groove running along the tufnol former and connected to four metal tabs on the stem of the former.

It is not difficult to obtain a large reference signal so the design of the reference pick-up coils need not be so carefully considered. The dimensions were chosen

to conveniently fit in the recess available (see Figure 3.5) while again allowing for some misplacement from the centre of the coils. A small tufnol former was made and two coils wound with approximately 690 turns of 42 swg enamelled copper wire.

The d.c. coil, C, Figure 3.7, was made from 360 turns of 42 swg Cu wire wound onto a small former with a hole drilled through just wide enough to take the vibration rod. The coil is then fixed into position so that it sits centrally between the reference pick-up coils.

iii) The Magnetic Field Coils

As uniform a field as possible is required. A long solenoid is one possibility but we decided upon a Helmholtz pair as this permits temperature measuring probes to be more easily placed close to the sample (see Section 3.4.4). The coils, Figure 3.13, were wound on tufnol formers, circular in cross-section, with an 11.6 mm diameter hole drilled through the centre. A 6 mm square cross-section of coil is wound onto each former; 37 swg enamelled Cu wire was used for this and 700 turns were needed for each of the coils. The pair of coils were then slid over the reference coil former and fixed symmetrically about the central position of the pick-up coils. Equation A.3 was used to calculate the field produced by this Helmholtz pair and the optimum separation obtained to be 1.15 cm, giving a field that was constant to $\pm 1\%$ over a region of at least 1 cm.

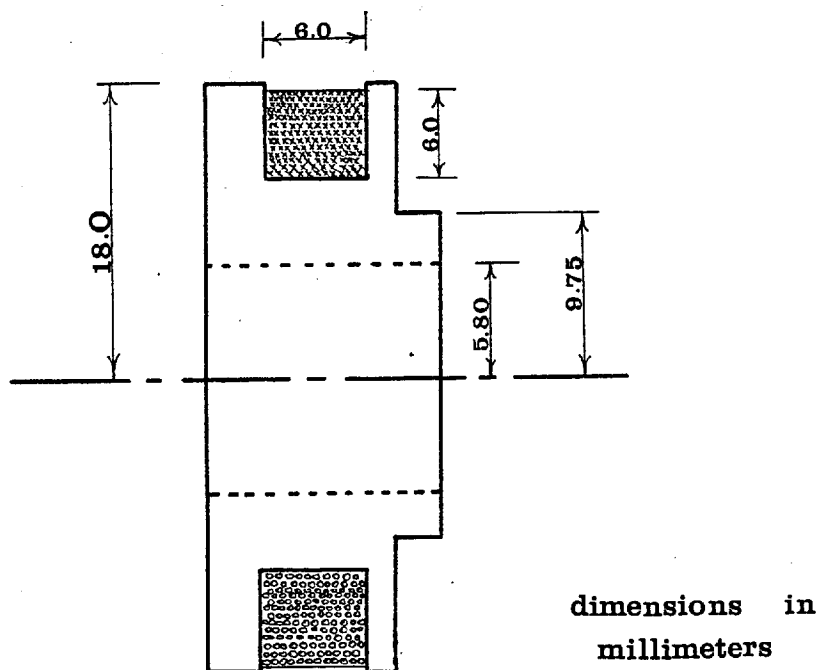


Figure 3.13

The d.c. current for the production of the field was provided by a stabilized power supply and the field-current relationship calibrated by means of a Hall probe.

3.4.4. Temperature Measurement

Two thermometers, a carbon resistance thermometer for the low temperature region below 20°K and a diode for temperatures above this, are used. An Allen Bradley, ½ Watt carbon resistor of 100 Ω nominal value at room temperature, was chosen to give a suitable resistance variation in the required region of 4°K - 20°K. Clement and Quinell (3.22) first showed that the resistance of these carbon resistors was reproducible at low temperatures and that it is possible to fit the resistance against temperature variation to the relationship;

$$\log R + \frac{K}{\log R} = A + \frac{B}{T} \quad (\text{III.3})$$

where T is the temperature, R the resistance and A, B and K are constants.

In order to determine the values of the constants A, B and K for the chosen carbon resistor we initially placed it in thermal contact with a Germanium resistance thermometer (GE 4498) calibrated from 3°K to 21°K and took readings of the resistance of each as a function of temperature. A, B and K were then obtained by using three points and solving simultaneously, a check then being made on the accuracy by comparing the temperature that Equation III.3 predicts, using the calculated values of A, B and K , with the temperature indicated by the Ge thermometer, when one of the other points is used. Three such fits over different portions of the whole range enable temperatures to be read by the carbon thermometer to within $\pm 0.1^{\circ}\text{K}$ over the calibrated region.

Figure 3.14 shows the circuit used to measure the resistance of the carbon thermometer.

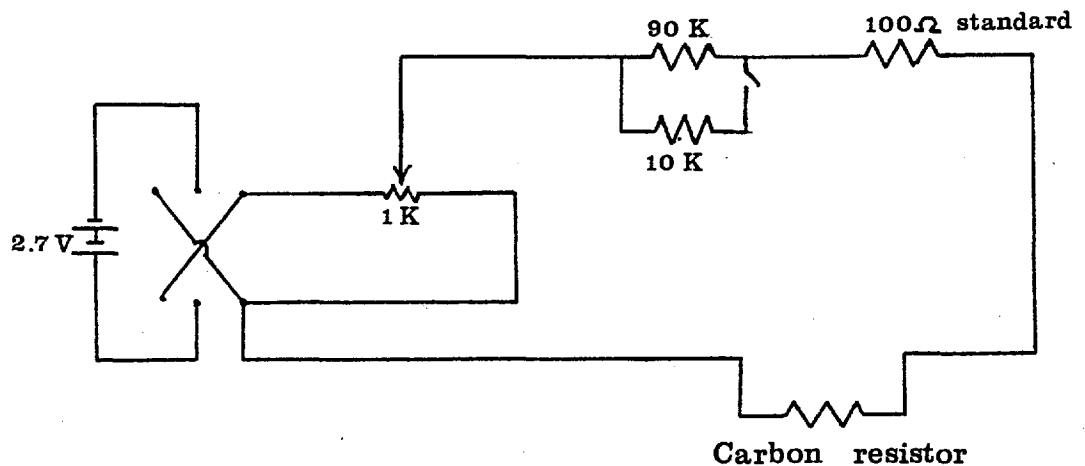


Figure 3.14

A reading of the voltage across a $100\ \Omega$ standard resistance placed in series with the carbon resistor gives a measure of the current in the circuit, thus allowing the resistance of the carbon thermometer to be calculated when a measurement of the voltage across it is made.

The reversing switch permits readings to be taken for current flowing in both directions in order to account for any thermal emf's in the circuit. The size of the current can be altered by means of the $1\ \text{K}\Omega$ variable resistor enabling a convenient value to be set as the resistance of the carbon thermometer changes. A larger change in current is achieved by switching in the $10\ \text{K}\Omega$ resistor in parallel with the $90\ \text{K}\Omega$ resistor. This is useful for temperatures greater than 15°K , where the carbon resistance has dropped below $250\ \Omega$.

A 1S922 silicon diode has been used for temperature measurement above 20°K . A constant current supply, Figure 3.15, was used to provide $10\ \mu\text{A}$ to the diode, the voltage drop across the diode giving a measure of the temperature.

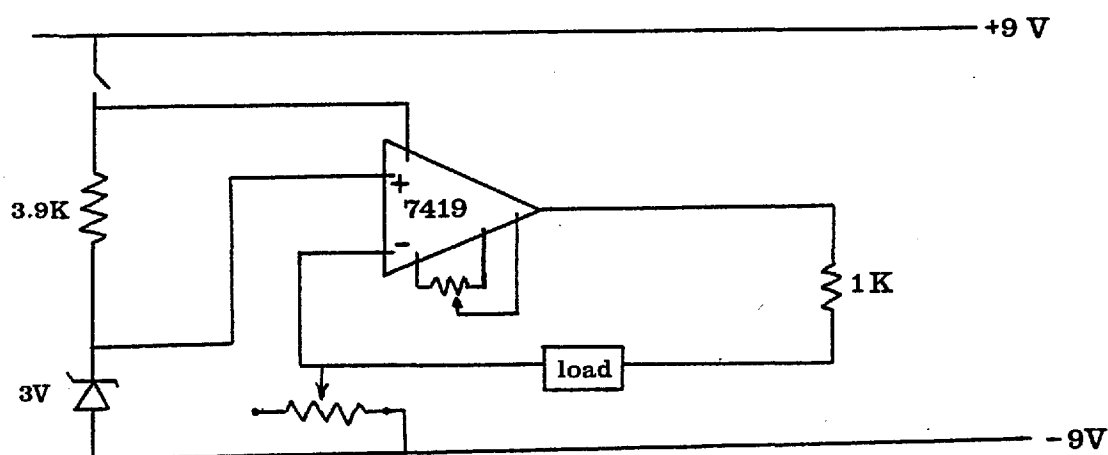


Figure 3.15

The voltage variation with temperature is almost linear down to about 40°K , below which it increases more rapidly. By taking the room temperature reading and the liquid nitrogen temperature reading, a linear extrapolation may be carried out. A check at several points over this range with a Cu-constantan thermocouple showed them to read the same temperatures to within $\pm 2^{\circ}\text{K}$ down to 40°K . The diode was further calibrated to lower temperatures against a Germanium resistance thermometer which was calibrated upto 100°K thus enabling the diode to be used for all temperatures above 20°K .

The placing of the temperature measuring probes in actual thermal contact with the sample is inconvenient due to the small amount of space within the inner walls of the pick-up coil former and also due to the contribution to the signal that any such probe would make. In preference to this, two small holes were drilled through the tufnol former mid-way between the pick-up coils. The two probes were then placed partly through these holes so that when the sample is positioned centrally between the pick-up coils these probes will only be about 2 mm away from the sample. There will always be a good flow of helium exchange gas between the sample and probes so that it may be expected that the readings given by the thermometers will accurately reflect the sample temperature. This has been shown to be the case by comparing the temperature reading as given by the carbon thermometer and that given by another calibrated probe

placed in the sample position.

3.4.5. Procedure in Usage and Performance

The field and pick-up coil block was moved upwards in order to make the end of the vibration rod accessible. After completely cleaning the end of the rod and the surrounding inner wall of the pick-up former with acetone soaked tissues, the sample was glued onto the end of the vibration rod with a little Durofix. Careful cleaning was essential because the slightest particle of ferromagnetic material in the vicinity of the sample would produce a large error signal. The block was then moved back down until the sample was positioned mid-way between the two pick-up coils. After carefully placing the cryostat into the inner dewar and screwing plate, P, Figure 3.5, into the hat, Figure 3.6, the continuity of all the circuits was checked and then the following cool down procedure was carried out;

- i) The inner dewar was evacuated and then filled with an atmosphere of helium gas. This was repeated a couple of times, finally leaving an over pressure of helium in the space by connecting a bladder full of the gas to one of the side ports. The gas acts as an exchange medium allowing the heat to be conducted away from the sample block after nitrogen was placed in the outer dewar. It was essential to exclude air from the inner dewar as any air solidifying around the vibration rod could cause the vibration to cease. The overpressure

was useful to prevent air getting in when the transfer syphon was placed into the dewar as, for the short time the connection was open, the helium gas flow outwards was dominant.

ii) The vacuum interspace of the inner dewar was evacuated and filled with nitrogen several times so as to flush out any helium which may have diffused through the glass wall from the previous run. An atmosphere of nitrogen was then left in this space while cooling towards 77°K . Once the temperature reached about 80°K , the interspace was evacuated ready for the transfer of liquid helium into the inner dewar. The time taken to cool straight down to liquid nitrogen temperature from room temperature was about one hour.

iii) If temperatures below 4.2°K are required the pressure above the helium is reduced. A reduction in the pressure means that more molecules are passing through the liquid-gas interface from the liquid than are passing back into the liquid from the gas. The loss of the more energetic molecules from the liquid thus causes the rest of the liquid to cool until equilibrium is again reached. The use of a monostat means that very controlled changes can be achieved and any pressure below atmospheric can be held with great stability. With our reasonably vacuum tight system, temperatures of 1.5°K could be reached by this means. This, however, causes the removal of a large amount of liquid helium so that, to cool the sample to 1.5°K and still have it immersed in the liquid helium, a

larger amount needed to have originally been transferred. The actual amount of helium transferred was therefore very dependent on the temperature range of interest. If a pump down was required, an average of $2\frac{1}{2}$ litres was used, of which about $\frac{1}{2}$ litre was used to cool from 77°K to 4.2°K , the rest filled the inner dewar to a suitable point. If temperatures above 4.2°K only were required then it was merely necessary to transfer a couple of inches of liquid into the tail of the dewar and to control the warm up.

Once the transfer had finished, the syphon was removed and a rubber tube placed between the top of the syphon extension and the $\frac{1}{4}$ " valve, VI (see Figure 3.5). This equalized the pressure between the main chamber of the inner dewar and the point high up the vibration rod guide tube and cut out oscillations which otherwise occurred along the length of the tube, causing the liquid helium to boil off very quickly.

There were two heaters available for use. The first was a resistor placed at the bottom of the tail of the inner dewar and which was used to put heat into the liquid helium. This served several purposes; a) to heat the helium back to 4.2°K after a pump down, b) to boil off unwanted helium to below the sample block when a warm up from 4.2°K was required, c) to boil off helium in order to re-cool to 4.2°K if required and if enough liquid helium remained in the tail and d) to boil helium gently to stabilize the temperature at required intervals to allow

measurements to be taken. The second heater was a manganin sample heater which was wound onto the ridge of the lower helmholtz field coil and which was used to speed up the rate of warming from 4.2°K . The supply for both these heaters was the output from a temperature controller. The controller was used in conjunction with the voltage from the diode to put a current into the sample heater and to stabilize at some pre-set voltage of the diode. A natural warm up from 4.2°K was extremely slow since the heat leaking into the system had been minimized by the use of stainless tubes and by the nitrogen shields. Of course, the warm up rate is very dependent on the level of the helium in the tail of the dewar so that if a large temperature range needed to be covered, a faster rate of warming was achieved by starting with a low level of helium. If the helium level was just below the sample block the time taken to warm from 4.2°K upto 6°K could be as long as two to three hours.

A resonance of the vibration system occurred at about 70 hz, so that maximum signal may be obtained at this setting of the vibration frequency. However, large sideways motions are easily induced at this frequency and variations in the signal due to amplitude changes are larger so that a frequency just off resonance, generally ~ 75 hz, was used. The amplitude of vibration was generally set at about 1 millimeter peak to peak, which is slightly less than half the possible maximum drive available. Prior to taking measurements, the phase of the reference

signal to the lock-in amplifier was varied until it was the same as the signal from the reference pick-up coils. Measurements were then taken of the sample magnetization, as a function of temperature, by taking a note of the reference current, I , and the dial setting, K , on the ten turn potentiometer. The absolute magnetic moment can then be obtained by using the conversion obtained by calibration, which relates a change in K , for a given I , to the magnetic moment.

Calibration was carried out by setting the reference current to 1 mA and measuring the value of K to null the signal produced by a 0.446 gm sample of manganese at room temperature. Mn has a room temperature susceptibility of 9.7×10^{-6} emu/gm, and readings were taken in various fields upto 40 Oe. For this setting of the reference current the calibration comes out at a change of 1 in K corresponds to 1.93×10^{-6} emu in magnetic moment. This has been rechecked occasionally and remained accurate. The only care to be taken is that if the vibration rod is disconnected from the vibration generator, when reconnection is made the reference coil may not be positioned exactly in the same place as before, and the calibration should then be rechecked.

The sensitivity of the measurement is limited by the noise level of the signal and this was normally such as to give an uncertainty of $\pm \frac{1}{2}$ in the reading of K , for a 1 mA reference current. This represents an ultimate sensitivity of $\sim 10^{-6}$ emu. The absolute accuracy of the

measurements cannot be relied on to better than an estimated 5% but within any particular run the relative accuracy of the data is better than 1%.

3.5. Resistivity Apparatus

Transport properties such as the electrical resistivity strongly reflect the magnetic nature of a material and we have supplemented the magnetization measurements on several samples by making a study of the variation of the resistivity with temperature. The apparatus described by Barber (3.23) has been used for this purpose.

A four terminal d.c. technique is employed in this apparatus. A current, stabilized to a few parts in 10^6 , is supplied to the specimens which are connected in series with one another and contained in an isothermal copper chamber. In series with the specimens is a high precision standard resistor, contained in oil and kept in a constant temperature bath. Up to six samples can be accommodated in the apparatus and the potential leads are brought out to a Tinsley stabomatic potentiometer via a low thermal selector switch. The potentiometric circuit uses a current controller to provide a stable current. By varying the capacitance dials of the potentiometer the potential drop across an internal standard resistance is varied and compared, by means of a photocell galvanometer amplifier and secondary galvanometer, with the potential drop across the sample. At a balance

position the two voltages are equal and zero current flows through the sample. Such a null method means that the sample potential leads carry no current in the balance position and thus the lead and contact resistances are not measured. By comparing the potential drop across a sample with the drop across the standard resistor the specimen resistance can be calculated. In order to cancel thermal emf's in the potential leads, measurements of the potentials were made for current flowing in the forward and reverse directions. The emf's in the potentiometer circuit are eliminated by using a thermal compensator in series with the galvanometer amplifier. By this method potentials could be measured to a nanovolt.

The temperature measurements were made by reading the resistance of a calibrated germanium thermometer for the temperature region upto 20°K and by means of a Cu-constantan thermocouple, referenced to Nitrogen, above this. These thermometers were heat sunk onto the central copper block which contains the current and potential posts to which the samples are connected. Surrounding the whole is a copper cylinder with a heater wound around it.

Platinum current leads were spot welded onto the ends of the samples and voltage leads, again of platinum, were spot welded a couple of millimeters inside the current leads.

3.6. Sample Preparation

All the alloys were prepared by argon arc melting appropriate amounts of the constituent elements on a water cooled copper hearth. 3N purity Palladium and 4N purity manganese were used for the PdMn alloys (the discussion of the other systems in Chapter 6 will include the particular preparations for those alloys). The standard practice of turning and remelting several times was carried out to aid homogeneity, care being taken on the first melt to ensure that the Pd flowed over the Mn in order to reduce the Mn loss. Upon the final melt the alloy was sucked into a casting mould producing an ingot about 2 cm long with a 3 mm square cross-section. The final weight was checked and in all cases the loss was less than 1% of the total weight so that the true composition will not be significantly different from the nominal value. All the compositions given in the following chapters are the nominal values.

For the magnetization measurements the amount of alloy required was small; the sensitivity of the apparatus was so great that for samples, such as PdMn, with large susceptibilities (giving moments very large compared with the limit of 10^{-6} emu) the signal was, if anything, larger than required so that there was no problem with measuring samples as small as 2 or 3 milligrams. The samples studied were either spherical or disc shaped, produced in the following ways;

i) Spherical Samples:- A small portion was taken from either end of the cast ingot and melted together in the arc furnace. The alloy was then allowed to cool in a small hemispherical crevice in the copper hearth, resulting in an almost perfectly spherical sample due to the small mass involved and to surface tension effects. It was expected that due to the very small size of the sample the cooling from the melt would occur so quickly throughout the volume of the sample that this was equivalent to quenching after a heat treatment i.e. that a further homogeneizing heat treatment was not necessary. Microprobe analysis of several such spherical samples showed that the homogeneity was indeed very good.

ii) Disc Shaped Samples:- A portion of the ingot was taken and wrapped in copper foil ready for rolling through a mill. The copper foil prevented impurities from becoming trapped in any folds produced at the sample edges during the rolling process and the sample was rolled through the mill until it was about 5-10 thousandths of an inch thick. It was then cleaned in aqua regia for two to three minutes. Two, 2 mm diameter discs were then cut from different portions of this slab by using an appropriate tool in a spark cutting machine. After enclosing the discs in an evacuated quartz tube they were then heated at 750°C for about 18 hours before being quenched into water.

The specimens for the resistivity measurements were prepared by one of the following two methods, each starting with an ingot of the alloy produced by sucking into a mould

in the arc furnace;

A) The ingot was rolled through a mill between a protective copper sheet until it was about 10-20 thousandths of an inch thick. A uniform rectangular cross-section was obtained by rubbing on emery cloth so that the dimensions were fairly uniform for each individual specimen, typical dimensions being 3 cm long by 2 mm wide. These samples were then placed in a quartz tube and pumped out to better than 3×10^{-6} torr before being sealed off and heated at 750°C for approximately 17 hours. As manganese has a high vapour pressure it is easy to lose manganese from the sample surface during heat treatment and so it was decided that it would be better if the temperature was kept down to 750°C instead of the more often used $1,000^{\circ}\text{C}$ for these alloys. After quenching in water a small layer of each surface was removed by careful rubbing on emery and then platinum potential and voltage leads were spot welded onto the samples.

B) The as cast ingot was rolled down until an approximately square cross-section of $1\frac{1}{2}$ mm was obtained then it was placed in aqua regia for about two minutes. Further cleaning by rubbing on emery cloth was followed by encapsulation, evacuation and heat treatment. The sample was heated at 750°C for three days before being quenched into water. After rubbing away the surface, the sample was drawn through a series of dies until a fine wire resulted. Cleaning was then followed by a stress-relieving anneal at 750°C for about half an hour and a final gentle rubbing of the surface after quenching completed the process.

REFERENCES

- 3.1 BELL A.E.
Thesis, University of London (1973), unpublished.
- 3.2 MALE S.E.
Thesis, University of London (1976), unpublished.
- 3.3 GIAUQUE W.F. and MACDONALD D.P.
Phys. Rev. 43, 768 (1933).
- 3.4 MCKIM F.R. and WOLF W.P.
J. Sci. Insts. 34, 64 (1957).
- 3.5 HARTSHORN L.
J. Sci. Insts. 2, 145 (1925).
- 3.6 PILLINGER W.L., JASTRAM P.S. and DAUNT J.G.
Rev. Sci. Insts. 29, 159 (1956).
- 3.7 CANNELLA V. and MYDOSH J.A.
Phys. Rev. B6, 4220 (1972).
- 3.8 CANNELLA V.
Thesis, Wayne State University (1973), unpublished.
- 3.9 ZIMMERMAN J.E., THIENE P. and HARDING J.T.
J. Appl. Phys. 41, 1572 (1970).
- 3.10 FULTON T.A., DUNKLEBERGER L.N. and DYNES R.C.
Phys. Rev. B6, 855 (1972).
- 3.11 SILVER A.H. and ZIMMERMAN J.E.
Phys. Rev. 157, 317 (1967).
- 3.12 LOUNASMAA O.V.
Experimental Principles and Methods Below 1 K
(Academic Press, New York, 1974).
- 3.13 GIFFORD R.P., WEBB R.A. and WHEATLEY J.C.
J. Low Temp. Phys. 6, 533 (1971).
- 3.14 De BRUYN OUBOTER and De WAELE A.TH.A.M.
Progress in Low Temperature Physics VI, p.243, edited
by C.J. Gorter, Acad. Press.
- 3.15 FONER S.
Rev. Sci. Insts. 30, 548 (1959).
- 3.16 MURANI A.
Thesis, University of London (1968), unpublished.

- 3.17 SPRINGFORD M., STOCKTON J.R. and WAMPLER J.
J. Phys. E4, 1036 (1971).
- 3.18 FONER S.
Rev. Sci. Instrs. 45, 1181 (1974).
- 3.19 COMMANDER R.J. and FINN C.B.P.
J. Phys. E3, 78 (1970).
- 3.20 MALLINSON J.
J. Appl. Phys. 37, 2514 (1966).
- 3.21 GUY C.N.
J. Phys. E9, 433 (1976).
- 3.22 CLEMENT J.R. and QUINELL E.H.
Phys. Rev. 79, 1028 (1952).
- 3.23 BARBER
Thesis, University of London (1974), unpublished.

CHAPTER 4

INVESTIGATION OF THE PdMn MAGNETIC PHASE DIAGRAM

4.1.1. Low-Field Magnetization Measurements

Only in recent years has interest focussed on PdMn alloys with concentrations of manganese greater than 3 at%. As shown by Coles et al. (4.1) the high field magnetization data of Rault and Burger (4.2) over-emphasised the ferromagnetic nature above about 5 at%Mn and they put forward a revised phase diagram (Figure 2.2) after measurements on the field cooling of these higher concentration alloys had indicated that a spin glass type freezing was occurring (see Chapter 2).

A more comprehensive study has been made during the course of this work on the spin glass freezing in alloys with concentrations from 8½ at%Mn downwards in order to discover the nature of the approach to long range order at the lower concentrations. The low field magnetometer was extremely useful for this purpose as very low fields (~ 2 Oe) have been used to accurately obtain the spin glass freezing temperatures.

The variation of the magnetization of the 8.5 at%Mn alloy, for an applied field of 2.4 Oe, is shown as a function of temperature in Figure 4.1. There is a peak centred on $5.8 \pm 0.4^\circ\text{K}$ and this is interpreted as the spin glass temperature, T_g . This agrees well with the spin glass line drawn in the magnetic phase diagram of Figure 2.2.

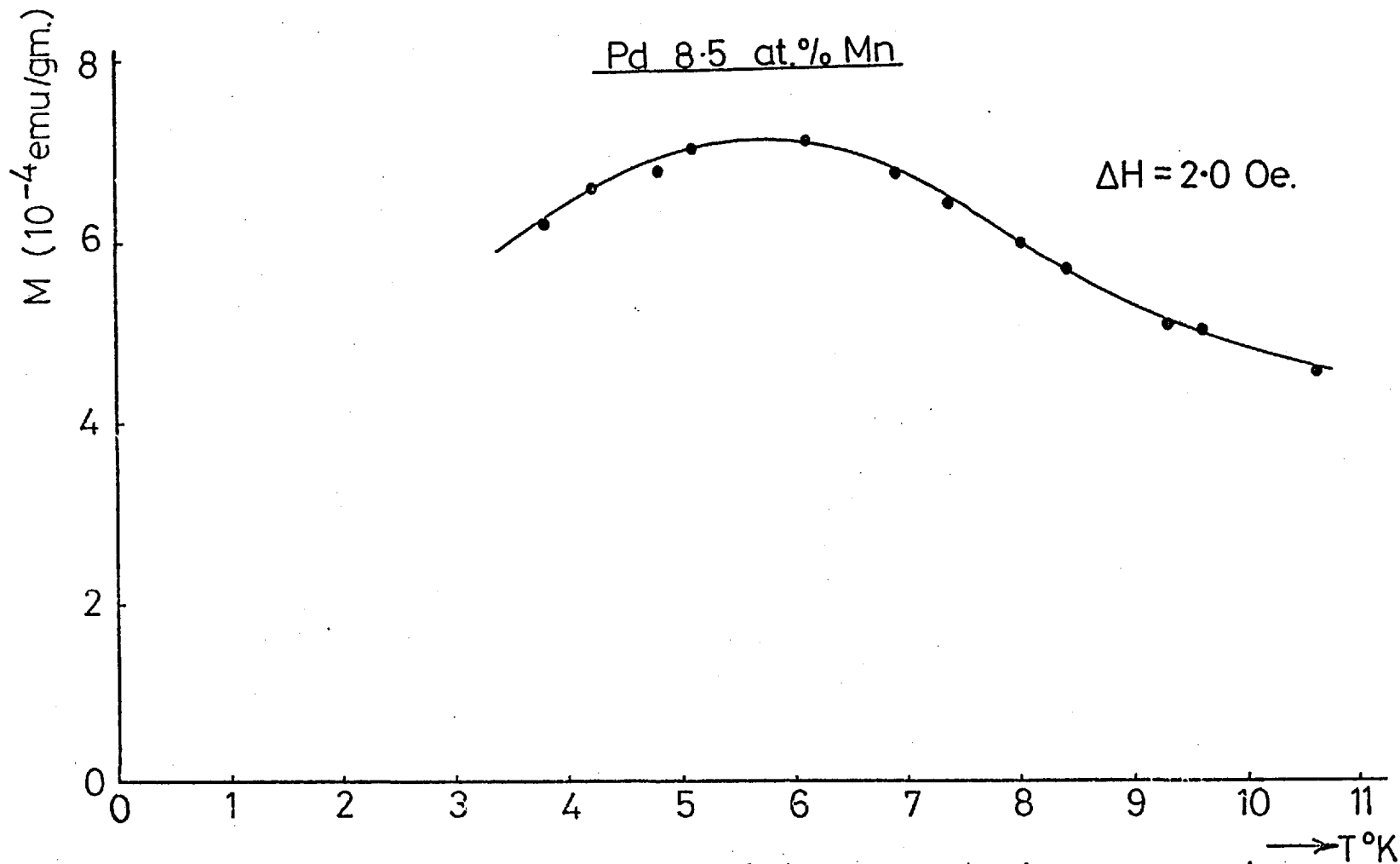


Figure 4.1 : Temperature variation of the magnetization measured in an incremental field of 2.0 Oe.

Similar magnetization versus temperature curves, all for an applied field of 2.4 Oe, are shown for alloys with 5.8, 5.35 and 4.9 at%Mn in Figure 4.2. Figures 4.3 and 4.4 show the results for alloys with 4.5 and 4.2 at%Mn respectively. These curves all have fairly sharp peaks and the temperatures of the peaks are given in Table 4.1.

Alloy	T_g	θ_p	P_{eff}
(at%Mn)	$^{\circ}K$	$^{\circ}K$	μ_B/Mn
8.5	5.8 ± 0.4	-	-
5.8	3.3 ± 0.05	1.8 ± 0.2	6.7 ± 0.2
5.35	2.95 ± 0.05	2.6 ± 0.2	6.7 ± 0.2
4.90	2.60 ± 0.05	4.1 ± 0.2	6.5 ± 0.3
4.5	2.58 ± 0.05	5.0 ± 0.3	7.2 ± 0.4
4.2	2.60 ± 0.15	-	-
4.0	2.60 ± 0.15	-	-

Table 4.1

All these samples had time dependent magnetization at temperatures below T_g , characteristic of spin glass behaviour (Section 1.4.2). The shape of the curve obtained thus depends upon the method of measurement. These measurements were all obtained by varying the temperature with the external measuring field removed, stabilizing the

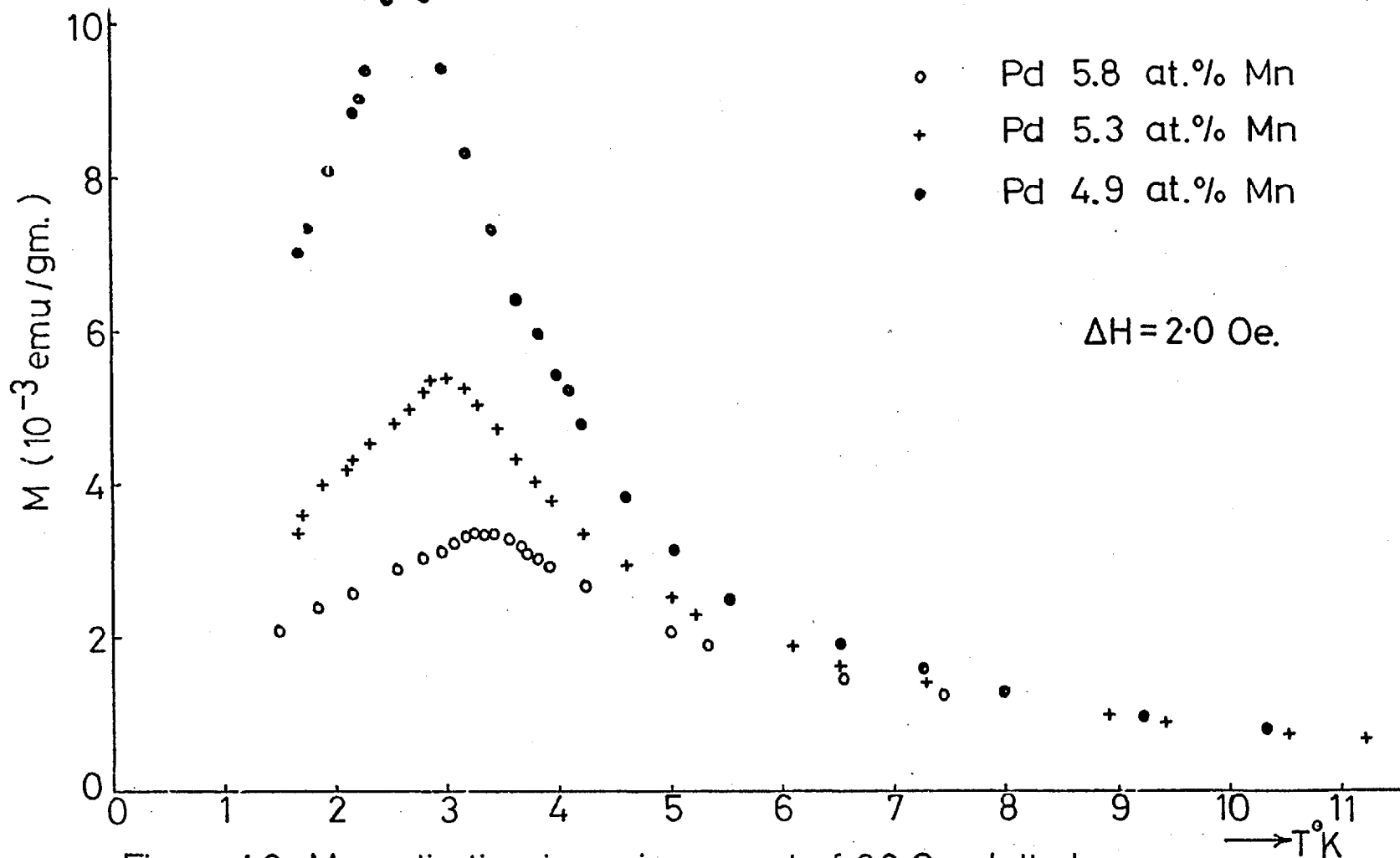
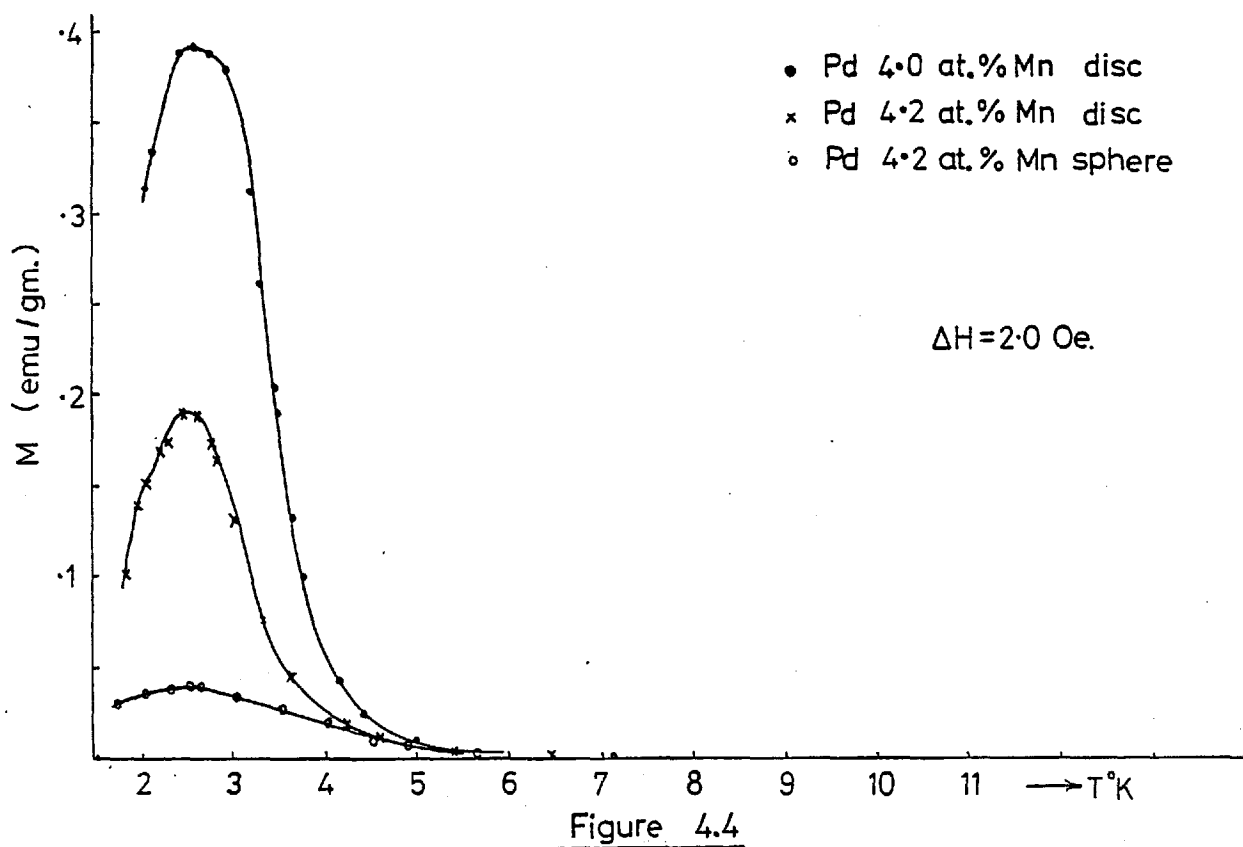
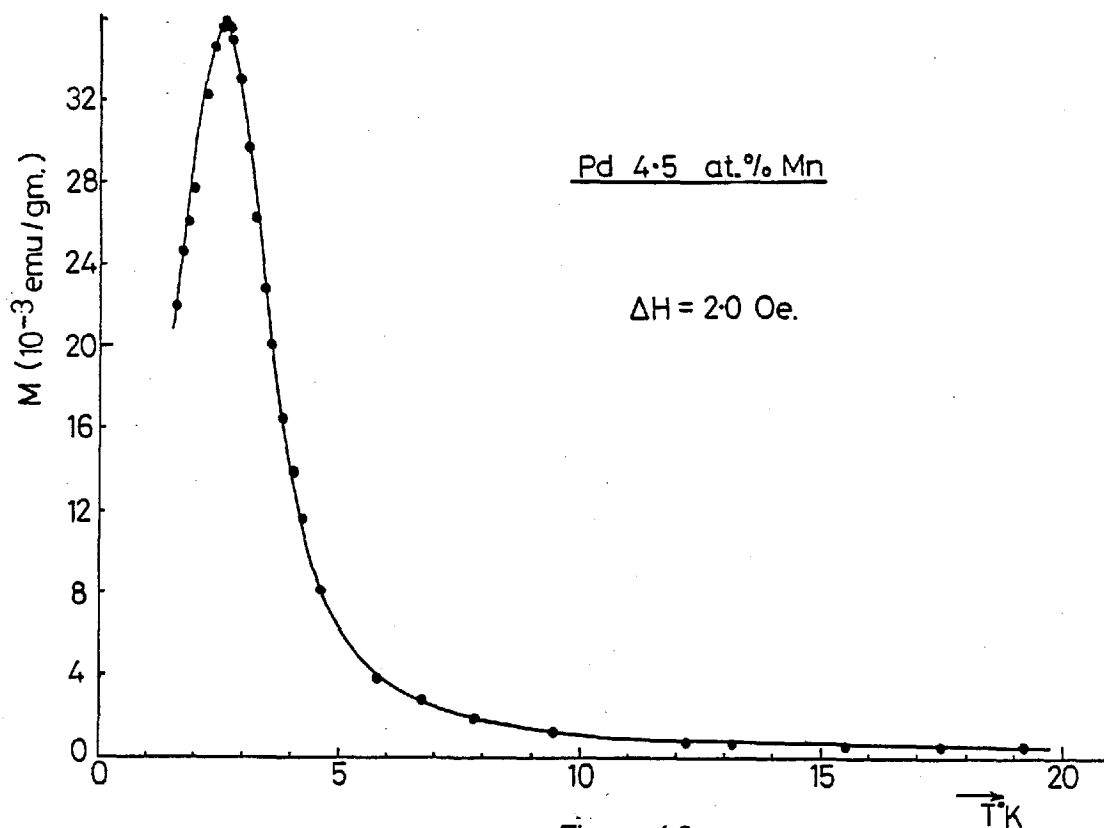


Figure 4.2: Magnetization in an increment of 2.0 Oe. plotted as a function of temperature for the 3 concentrations as shown.



temperature then applying the field and taking the reading as quickly as possible (~ 10 seconds, with some practise). The reading in the earth's field is then subtracted from the reading in the applied field. These curves, therefore, represent the response of the sample to the difference between the applied field of 2.4 Oe and the earth's field (~ 0.4 Oe) ie. 2.0 Oe. Thus the susceptibility is obtained by dividing these results by two.

These results were all obtained on spherical samples and in the composition range $C > 4.5$ at%Mn the absolute value of the susceptibility is small enough for the demagnetizing field to be ignored to first order. The extremely rapid rise in susceptibility with decreasing composition below 4.9 at%Mn makes the effect of the demagnetizing field increasingly important. The intrinsic volume susceptibility χ_0 is related to the observed susceptibility χ' by the relation

$$\chi_0 = \frac{\chi'}{1 - N\chi'}$$

where N is the demagnetization factor. The peak susceptibility of the 4.2 at%Mn alloy just fails to reach the limiting value of $\frac{1}{N} = 0.2387$ emu/cc (≈ 0.0199 emu/gm for Pd/Mn) so for this and lower concentration alloys we have prepared thin disc samples and made measurements with the specimens placed edge-on to the applied field. The demagnetization factor is thus considerably reduced and can be approximately calculated by assuming the disc to be a

spheroid of revolution; for which the demagnetizing field can be calculated exactly, Zijlstra (4.3).

The effect of the demagnetizing field is clearly seen by comparing the results shown in Figure 4.4 for disc and spherical shaped 4.2 at%Mn alloys. The peak for the disc occurs at roughly the same temperature, but is some five times larger at this maximum point, than for the sphere. The results for a Pd 4.0 at%Mn disc are also shown in Figure 4.4. This similarly exhibits a spin glass peak and has time effects below the peak, the temperature of the peak occurring at $2.6 \pm 0.15^\circ\text{K}$. The difference in the peak value of the magnetization for the two disc shaped specimens shown in Figure 4.4 is not a concentration effect but is related to the physical dimensions of the discs used for these measurements. These curves are still affected by the demagnetizing field once the temperature drops below about 3.2°K and the demagnetization factor for these discs is dependent on the ratio of the thickness to the diameter of the discs. This will shortly be discussed more fully concerning the limiting values reached by the magnetization for the lower concentration PdMn alloys.

The susceptibility data for the four alloys with 4.5, 4.9, 5.3 and 5.8 at%Mn (where demagnetization effects are not important) were fitted to the formula

$$\chi_i = \chi_0 + \frac{C}{T - \theta_p}$$

where the Curie constant $C = N\mu_B^2 p_{\text{eff}}^2 / 3k_B$. χ_i is the alloy susceptibility and χ_0 is the matrix susceptibility. However, upon alloying there is no reason why χ_0 should merely be the susceptibility of the pure palladium host and Star et al. (4.5)

showed that for the lower concentration PdMn alloys (with $C < 0.93$ at%Mn) χ_0 is the same as χ_{Pd} at low temperatures ($< 20^\circ K$) but that the increase in χ_0 from $20^\circ K$ to $80^\circ K$ is much less in the alloy than in pure Pd. Star et al. (4.5) employed a computer least squares fitting procedure in order to find the value of χ_0 which gave the best straight line for $(\chi_i - \chi_0)^{-1}$. Only the region $T < 40^\circ K$ is used in our fit so that any temperature dependence of χ_0 is much less than 1% of the change in χ_i , allowing the assumption of constant χ_0 to be made. At $T = 40^\circ K$, χ_i is approximately a factor of ten up on the value of the susceptibility of pure Pd at the same temperature so that the χ_0 term could have up to a 10% effect if neglected. At lower temperatures χ_0 becomes more and more insignificant when compared with $\frac{C}{T - \theta_p}$.

In figures 4.5 to 4.8 we show plots of $(\chi_i - \chi_0)^{-1}$ versus T , where χ_0 was taken to be $6.8 \cdot 10^{-6}$ emu/gm. This value was chosen so as to be in agreement with the values obtained by Star et al. (4.5) for their lower concentration alloys, although there is no real reason why this value holds at our higher concentrations. As a result, values of χ_0 equal to $7.6 \cdot 10^{-6}$ emu/gm. and zero were also used to obtain two extremes, determining the errors in the quoted values of θ_p and p_{eff} (table 4.1). The values of θ_p and p_{eff} were obtained by drawing the best straight line through the data of $(\chi_i - \chi_0)^{-1}$ versus temperature; the intercept on the temperature axis giving the paramagnetic Curie temperature, θ_p and the gradient leading to a value for p_{eff} . These values, as determined from figures 4.5 to 4.8, are given in table 4.1. The

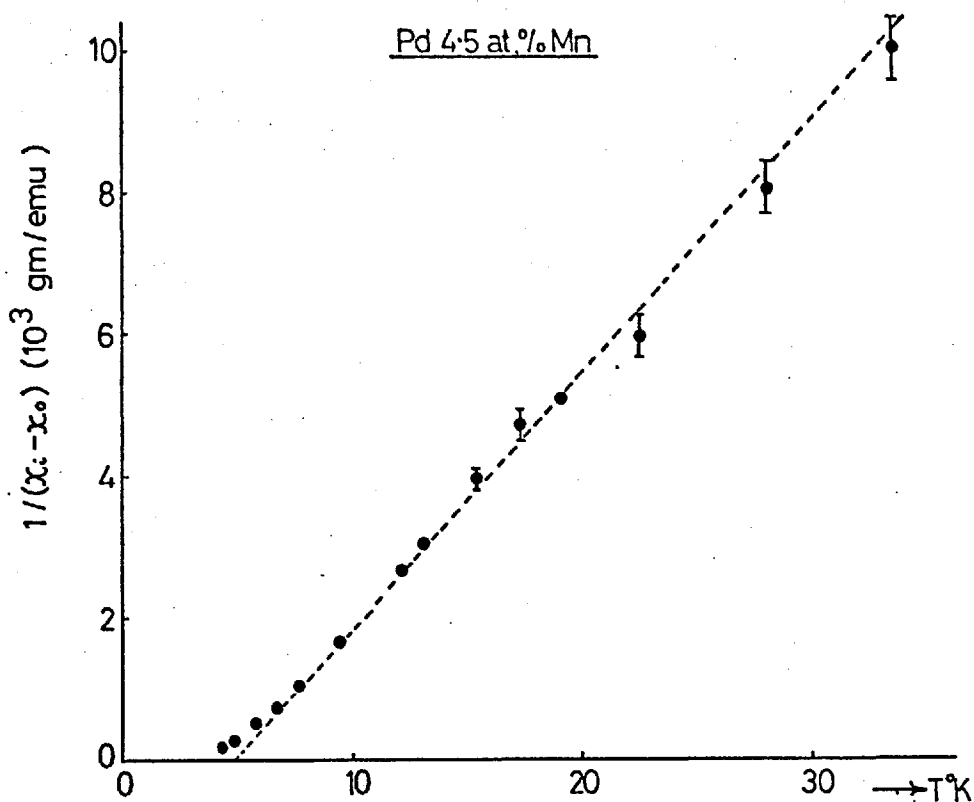


Figure 4.5 : Temperature dependence of the inverse of $(\chi_i - \chi_0)$ for the Pd 4.5 at.% Mn alloy. Here, and in the three following figures, with 4.9, 5.35, 5.8 at.% Mn respectively, χ_i is the measured susceptibility and $\chi_0 = 6.8 \cdot 10^{-6}$ emu/gm.

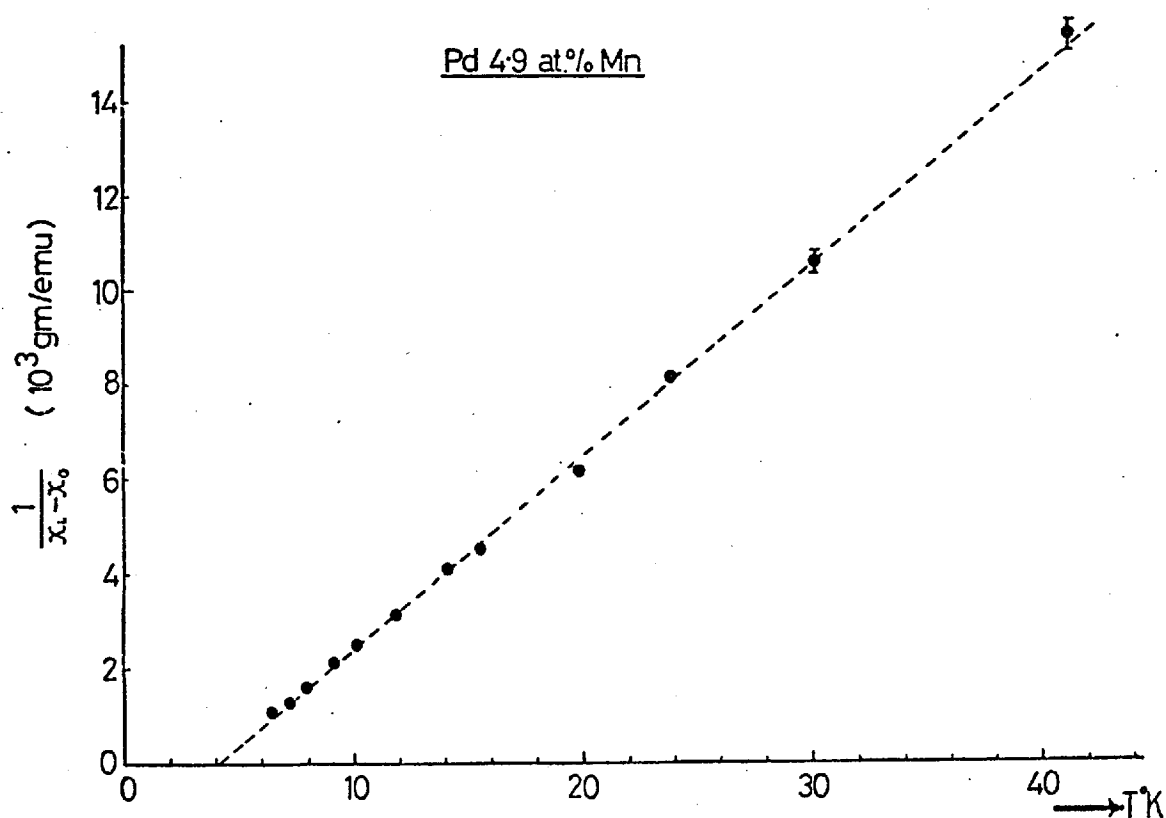


Figure 4.6 : Inverse susceptibility versus temperature.

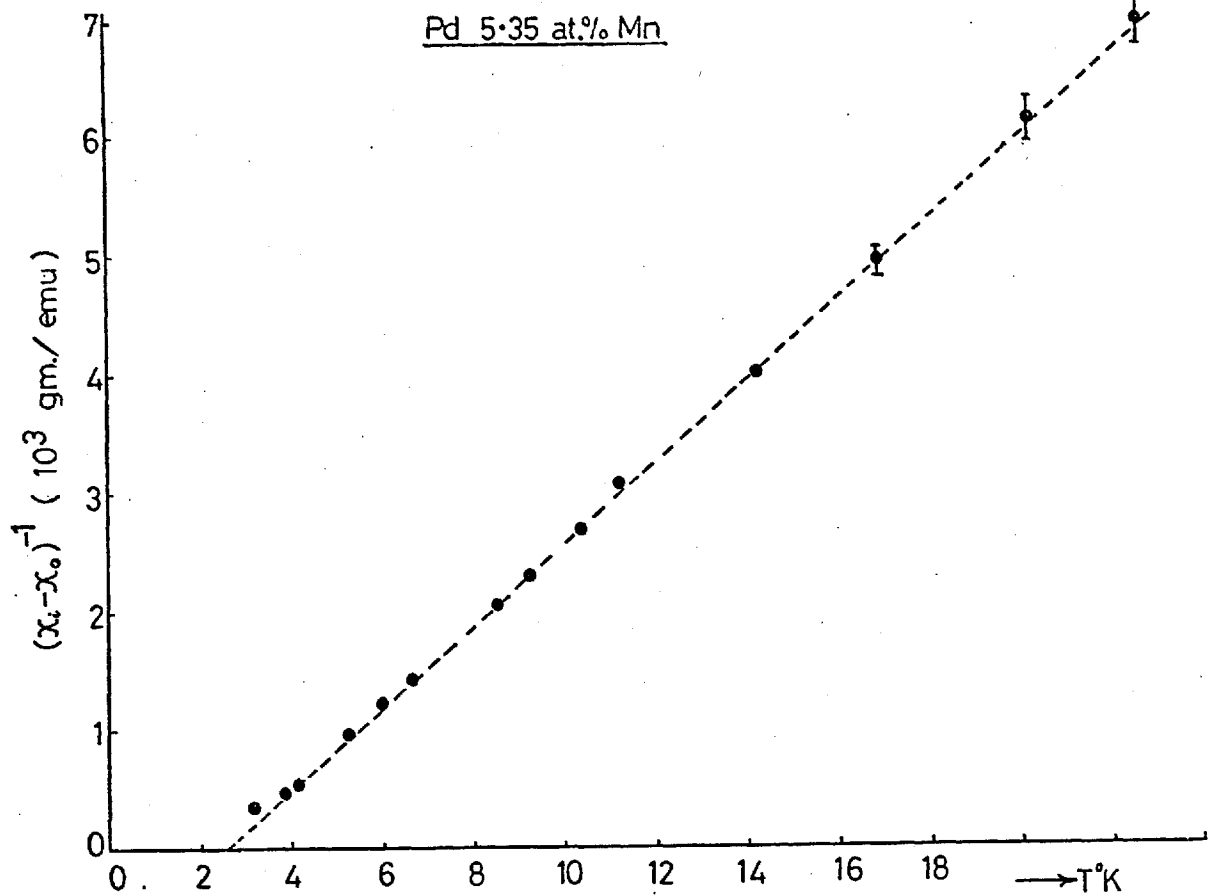


Figure 4.7

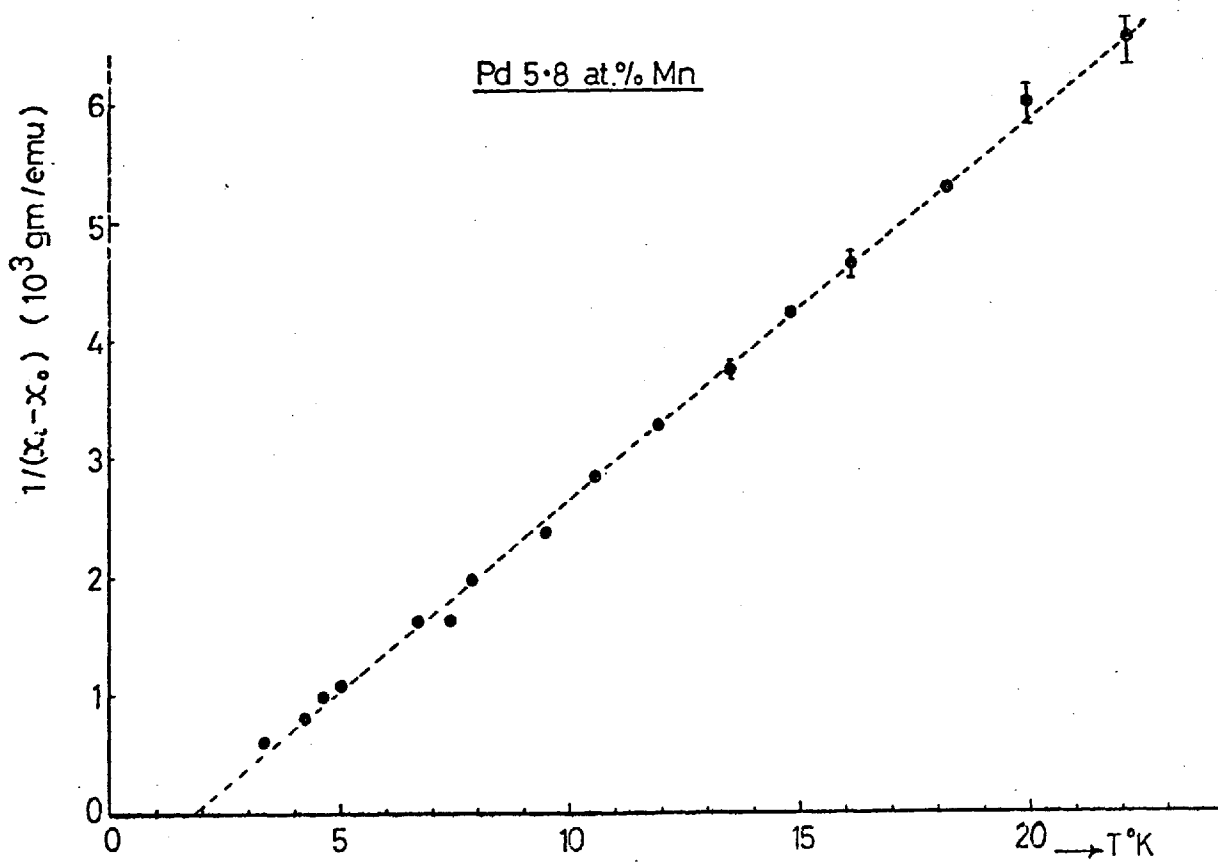


Figure 4.8

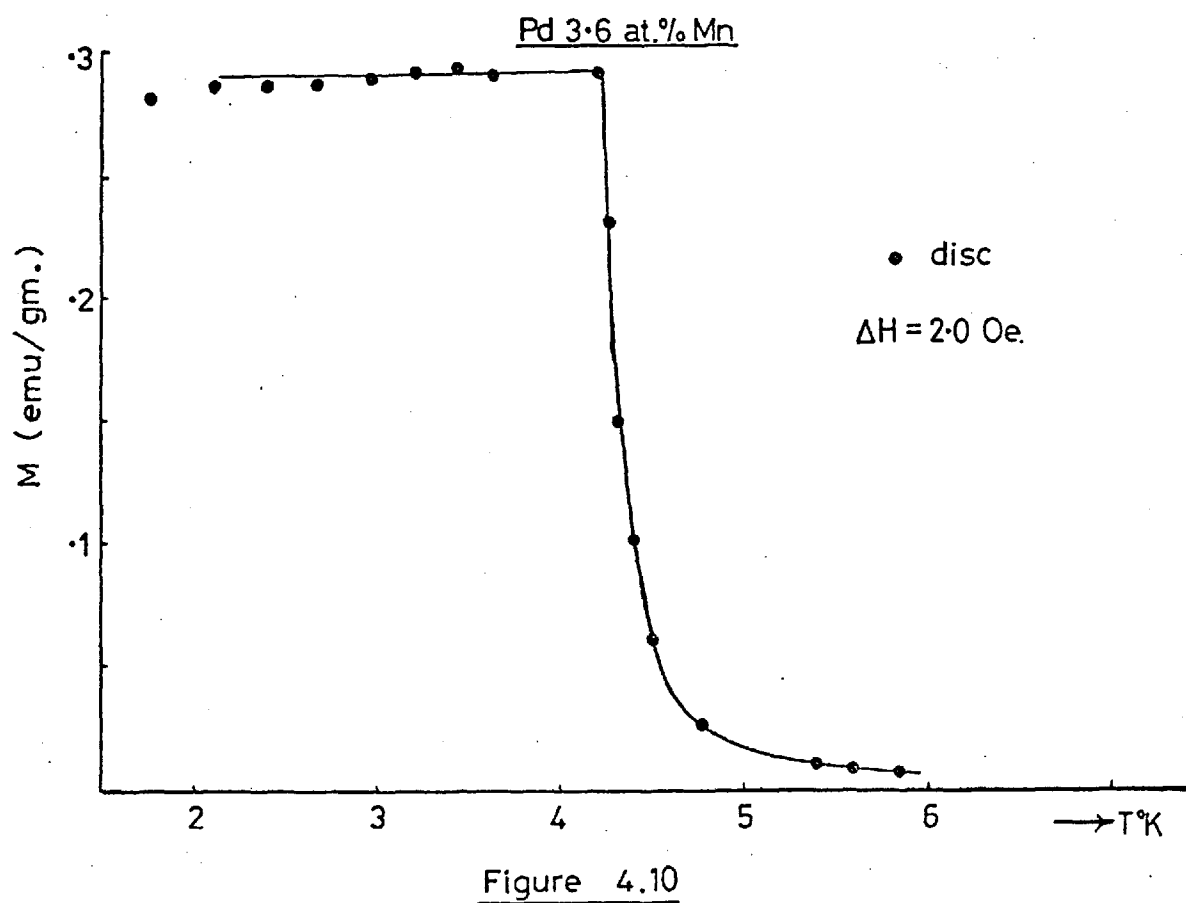
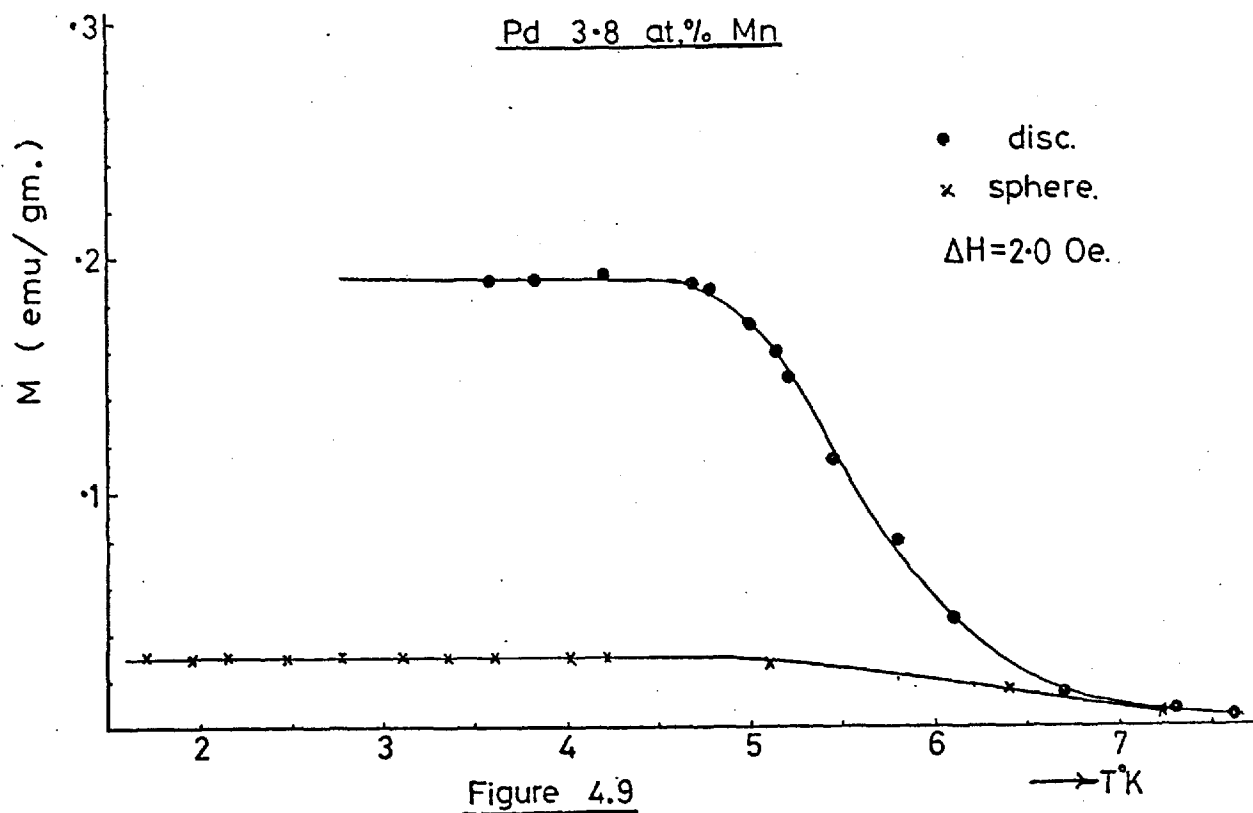
increasing importance of the direct Mn-Mn interaction with increasing concentration is reflected by the decrease in θ_p as well as by the decrease in the magnitude of the susceptibility at T_g .

For the 3.8 at%Mn alloy, shown in Figure 4.9, there is a distinct change in character from the higher concentration alloys, the magnetization remaining constant below a well defined temperature. The magnetization has now reached the demagnetizing limit of H_{app}/N . This is clearly indicated by the two curves in Figure 4.9, one for a spherical sample and one for a disc. The calculated limit of H_{app}/N for disc shaped samples is dependent on the dimensions of the disc and also on the angle which the disc makes with the applied field. The smallest demagnetization factor is when the circular faces of the disc are parallel to the field. However, due to the very large demagnetizing field perpendicular to the circular faces, the overall demagnetization factor is very sensitive to any deviation from this optimum angle. Although care was taken to position the disc shaped samples such that the circular faces were parallel to the vibration axis of the apparatus, small deviations from this were difficult to prevent, resulting in a limiting magnetization somewhat below the value calculated for samples at the optimum angle. A deviation of only 10° results in approximately a three-fold increase in the demagnetization factor for a disc with $\gamma = 20$ ($\gamma = \frac{c}{a}$; the ratio of the length of the axis of revolution of the

Figure 4.9 : Temperature variation of the magnetization of two Pd 3.8 at%Mn alloys measured in an increment of 2.0 Oe. above the earth's field.

• Disc shaped sample, × Spherical shaped sample. The differences in the two curves result from the reduction in the demagnetization factor in going from a spherical specimen to a disc shaped specimen.

Figure 4.10: Temperature variation of the magnetization of a Pd 3.6 at%Mn disc, in an incremental field of 2.0 Oe.

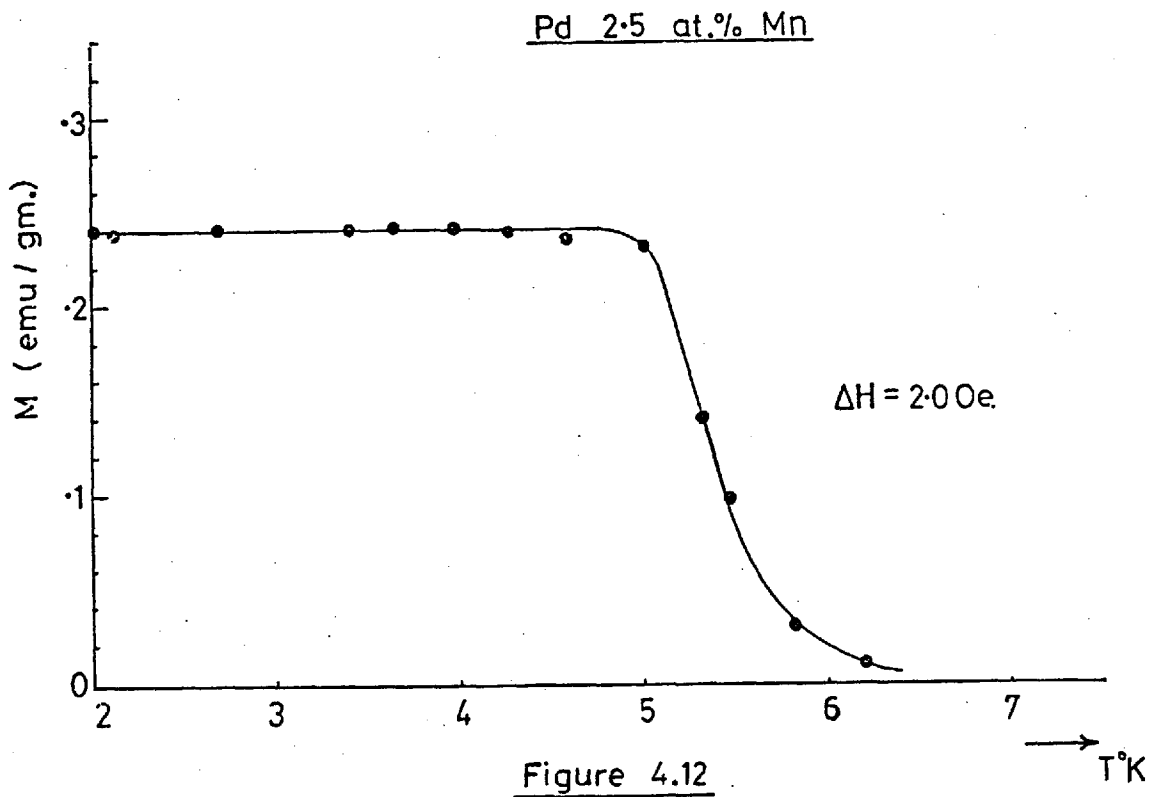
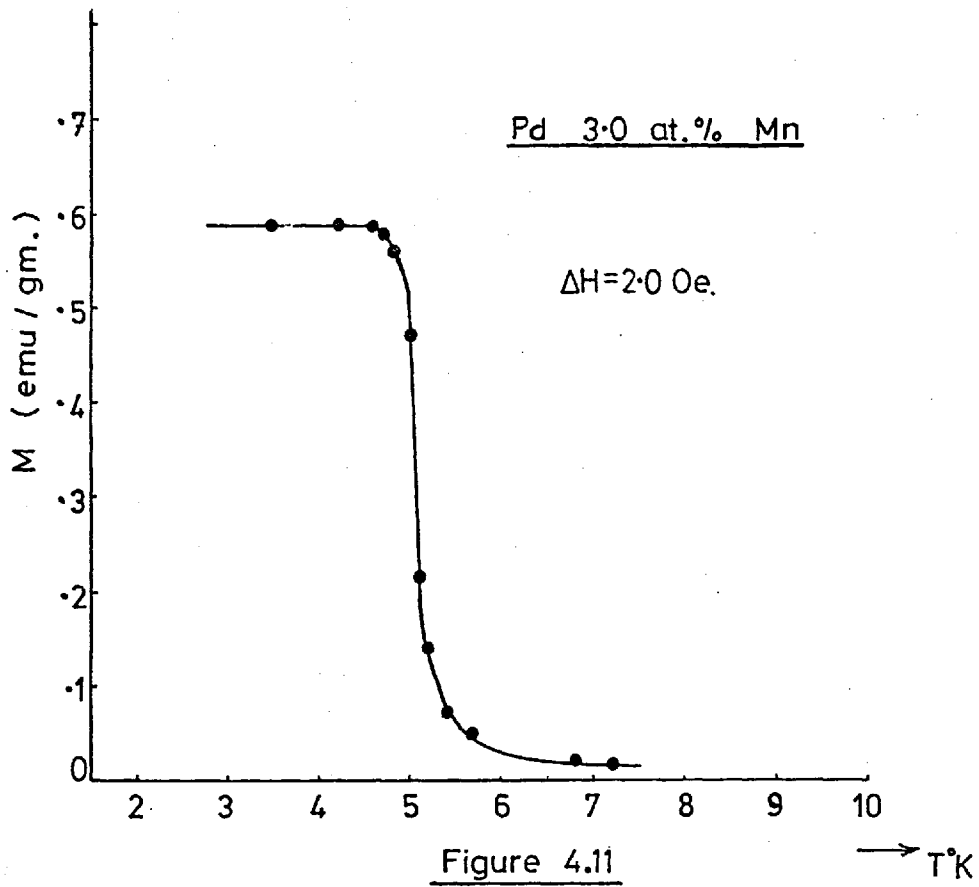


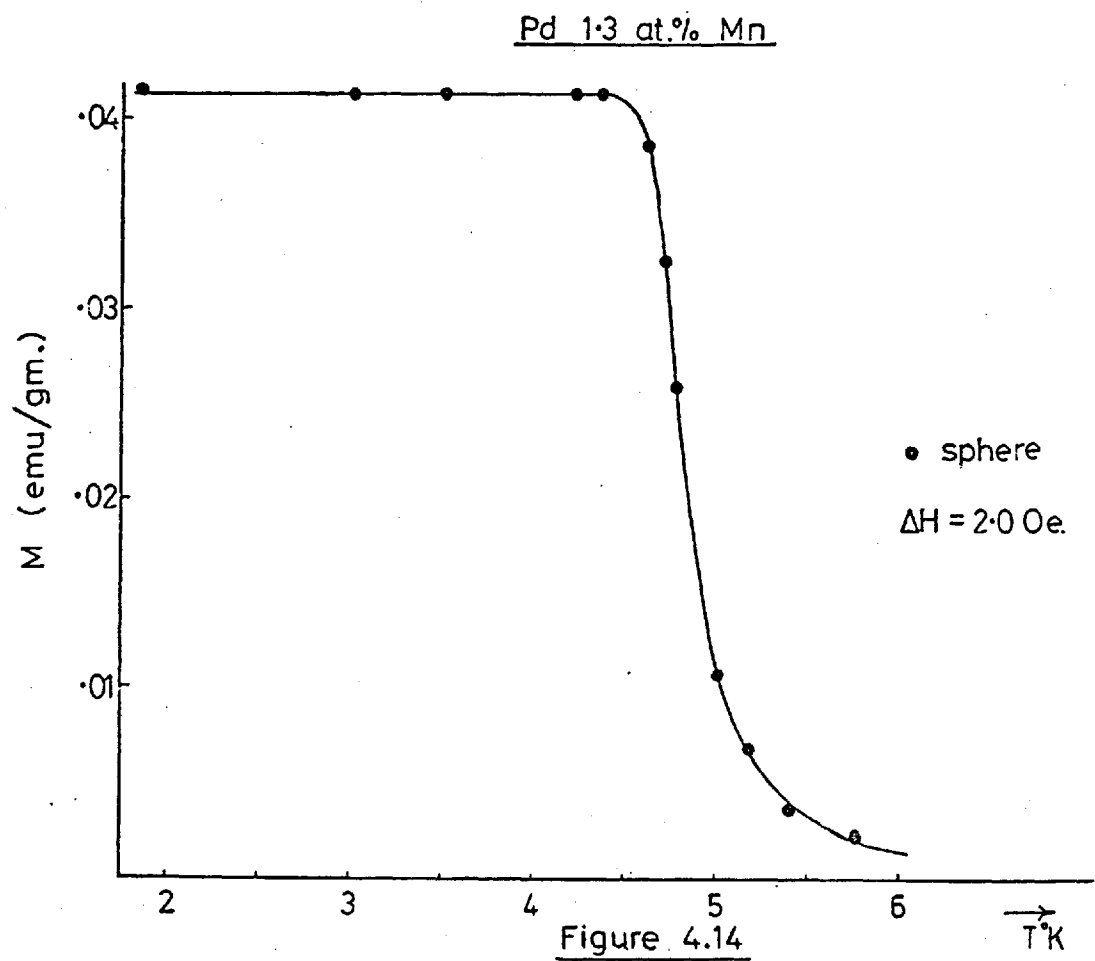
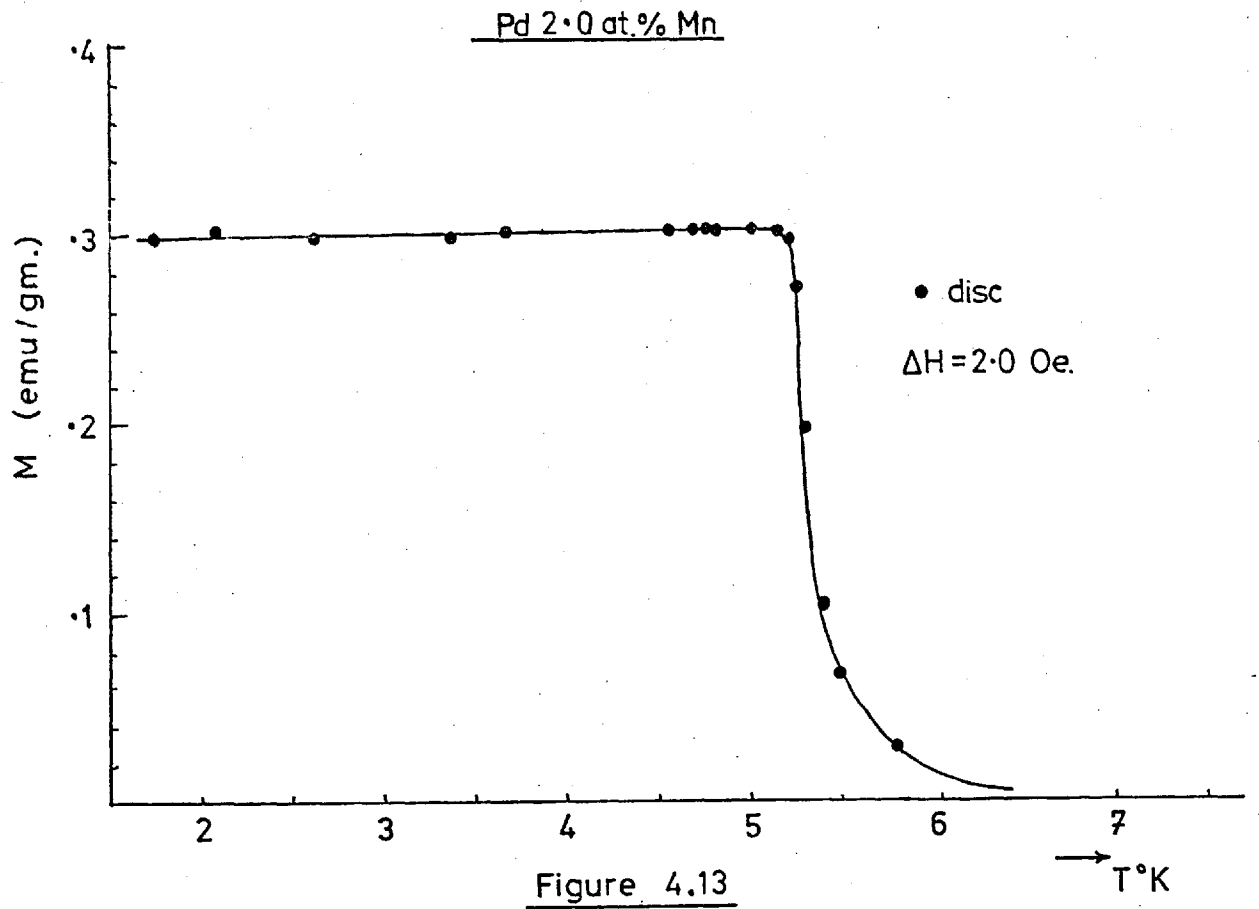
approximating spheroid to the length of the other axis, see Zijlstra (4.3)), thus giving a magnetization which only reaches a third the calculated optimum value.

The magnetization versus temperature curves for palladium alloys with 3.6, 3.0, 2.5 and 2.0 at%Mn are shown in Figure 4.10, 4.11, 4.12 and 4.13 respectively. The applied field was the same for all these results ($= 2.4$ Oe) and the samples were all discs 2 mm in diameter. The thickness of the disc, however, varied from about 8 thousandths of an inch ($\gamma \sim 10$) to 2 thousandths of an inch ($\gamma \sim 40$). Over this range of γ the transverse demagnetization factor (ie. perpendicular to the circular faces) remains constant while the axial demagnetization factor decreases by an order of magnitude (Zijlstra (4.3)). This fact, in conjunction with the variation due to the angle of placement explains the different levels of magnetization at which the curves flatten at low temperatures. The results for a spherical Pd 1.3 at%Mn sample are shown in Figure 4.14.

The temperature at which the magnetization first begins to drop is taken to be the relevant ordering temperature. This is not obviously so: there is no way to define exactly the ordering temperature from single M-T curves such as these. The usual method of obtaining an ordering temperature is to measure the magnetization as a function of field at many temperatures through the transition and to make Arrott plots (M^2 vs. $\frac{H}{M}$). The temperature at which $M^2 = 0$ for $\frac{H}{M} = 0$ is then the ordering temperature, for

Figures 4.11-4.14: Temperature variation of the magnetization of four PdMn alloys with 3.0, 2.5, 2.0 and 1.3 at%Mn respectively, each for the same field of 2.0 Oe. The Pd 1.3 at%Mn results in figure 4.14 are for a small spherical sample; the other three are disc shaped specimens.





ferromagnetic materials. However, as can be seen from the magnetization curves of these PdMn alloys, the magnetization increases so sharply that a transition temperature can be defined directly to within $\pm \frac{1}{2}^{\circ}\text{K}$, and much better than this in most cases. (A series of measurements, shown in Figure 4.15, of the magnetization versus field characteristics, at various temperatures, for the Pd 2.0 at%Mn alloy, allow such a set of Arrott plots to be made. This led to an ordering temperature of $5.09 \pm 0.1^{\circ}\text{K}$, agreeing well with that obtained by taking the temperature at which the curve first begins to drop).

It is clear from these magnetization curves that there is a discrepancy between the ordering temperatures obtained from these low field measurements and those suggested by the magnetic phase diagram, Figure 2.2. The magnetization results suggest a roughly constant ordering temperature of about $5\frac{1}{2}^{\circ}\text{K}$ for those alloys in the concentration range 2-3 at%Mn and that nowhere is a value approaching $7\frac{1}{2}$ - 8°K obtained. We have thus carried out a very careful series of resistivity measurements, firstly to check this point and secondly to obtain additional information on the nature of the change of the ordering as the concentration decreases from the spin glass regime through 4.0 at%Mn.

4.1.2. Resistivity Measurements

In Figures 4.16-4.20 we show the resistivity results for Pd 4.5, 4.2, 4.0, 3.6 and 3.0 at%Mn, respectively. All these specimens were prepared by method A (Section 3.6).

Figure 4.15: Field dependence of the magnetization of a Pd 2.0 at%Mn alloy, at various temperatures. As T is reduced below the ordering temperature the magnetization at low fields becomes demagnetization limited. As T is further reduced the magnetization follows further up the demagnetization line before curving over and increasing at a much reduced rate.

(The large fields produced here were obtained by setting up a large magnet coil around the outside of the dewars).

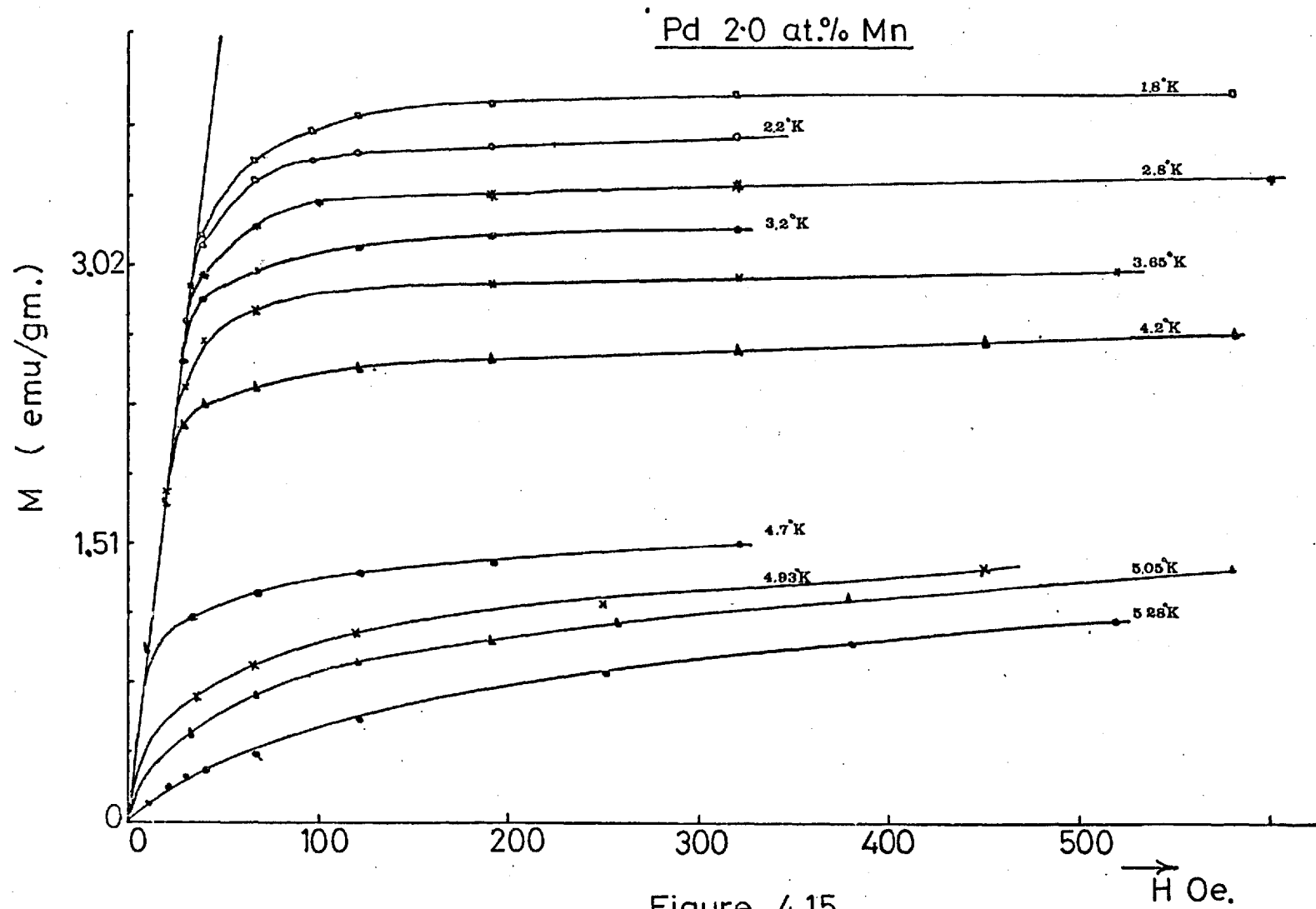


Figure 4.15

The results for the two highest concentration alloys show no noticeable anomaly at the temperature at which the low field magnetization peaked while the 4.0 at%Mn alloy shows a slight increase in gradient at $3\frac{1}{2}^{\circ}\text{K}$. None of the alloys show a sharp 'kink' in the resistivity but the 3.6 and 3.0 at%Mn specimens exhibit a large change in slope over about 1°K , something approaching a true 'kink' in behaviour. This change in slope is roughly centred on 5.5°K for the 3.0 at%Mn specimen and about 4.5°K for the 3.6 at%Mn alloy, results consistent with the magnetization measurements.

As a check on the method of preparation, method B (Section 3.6) was used for the 2.5, 2.0 and 1.5 at%Mn resistivity specimens. The results are given in Figures 4.21, 4.22 and 4.23, respectively.

4.1.3. Discussion

The low field magnetization results for the PdMn alloys with $C > 4.0$ at%Mn confirm the spin glass nature of these alloys. As discussed in Section 1.4.2, the original idea that isolated spins interacting in a random manner via the RKKY interaction constitute a spin glass has been superceded by the more general idea that any system with competing interactions should be a suitable candidate. This is well borne out by these results, which show the spin glass nature in PdMn arising from the competition of the indirect ferromagnetic coupling of Mn atoms with the increasing antiferromagnetic tendency as the concentration

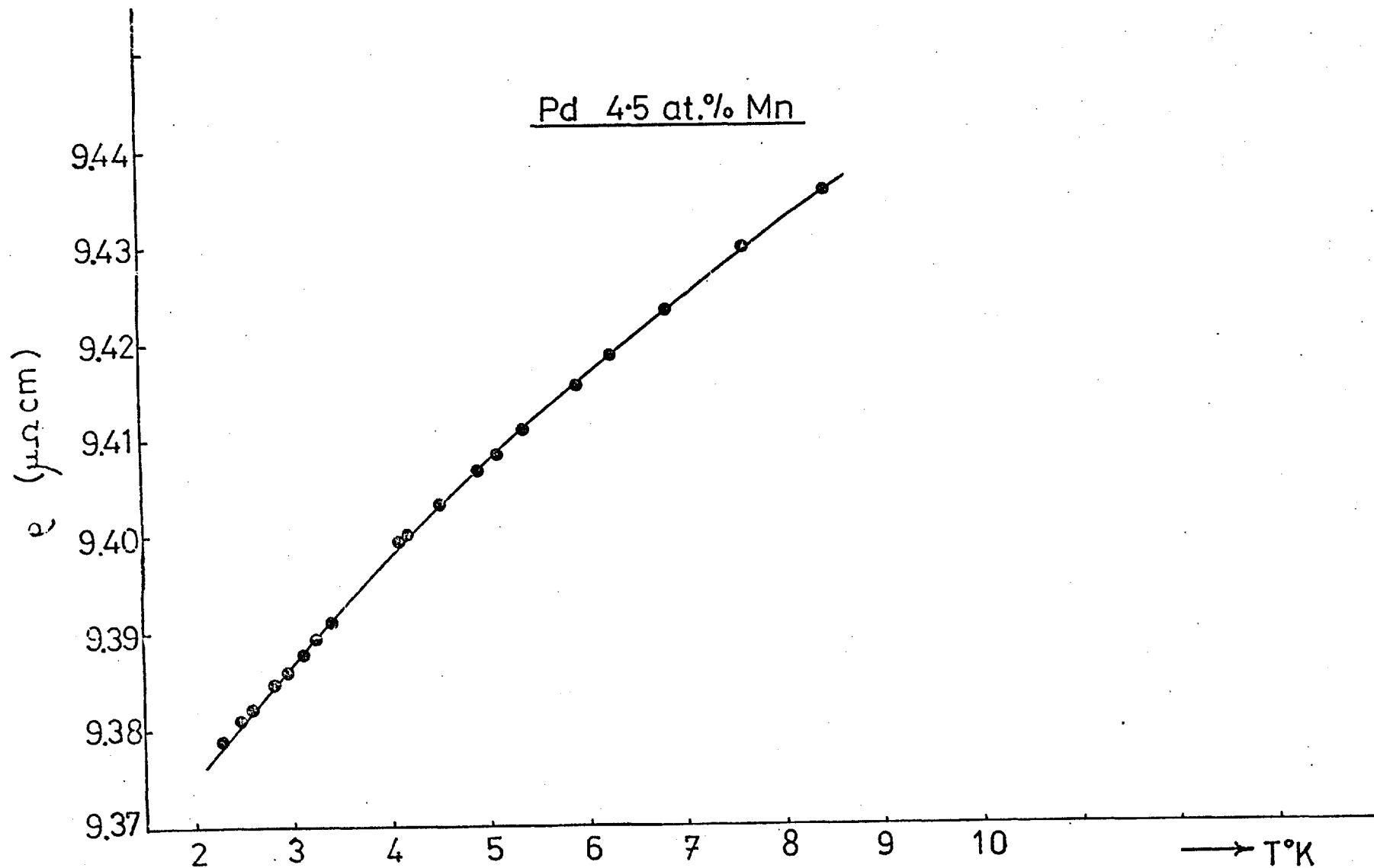


Figure 4.16 : Resistivity versus temperature for a Pd 4.5 at.% Mn alloy.

Figures 4.17-4.23: Temperature dependence of the resistivity for a series of PdMn alloys with 4.2, 4.0, 3.6, 3.0, 2.5, 2.0 and 1.5 at%Mn respectively. As we were interested only in the overall shape of these curves and not in the absolute value of the resistivity, the samples were not prepared with carefully uniform dimensions.

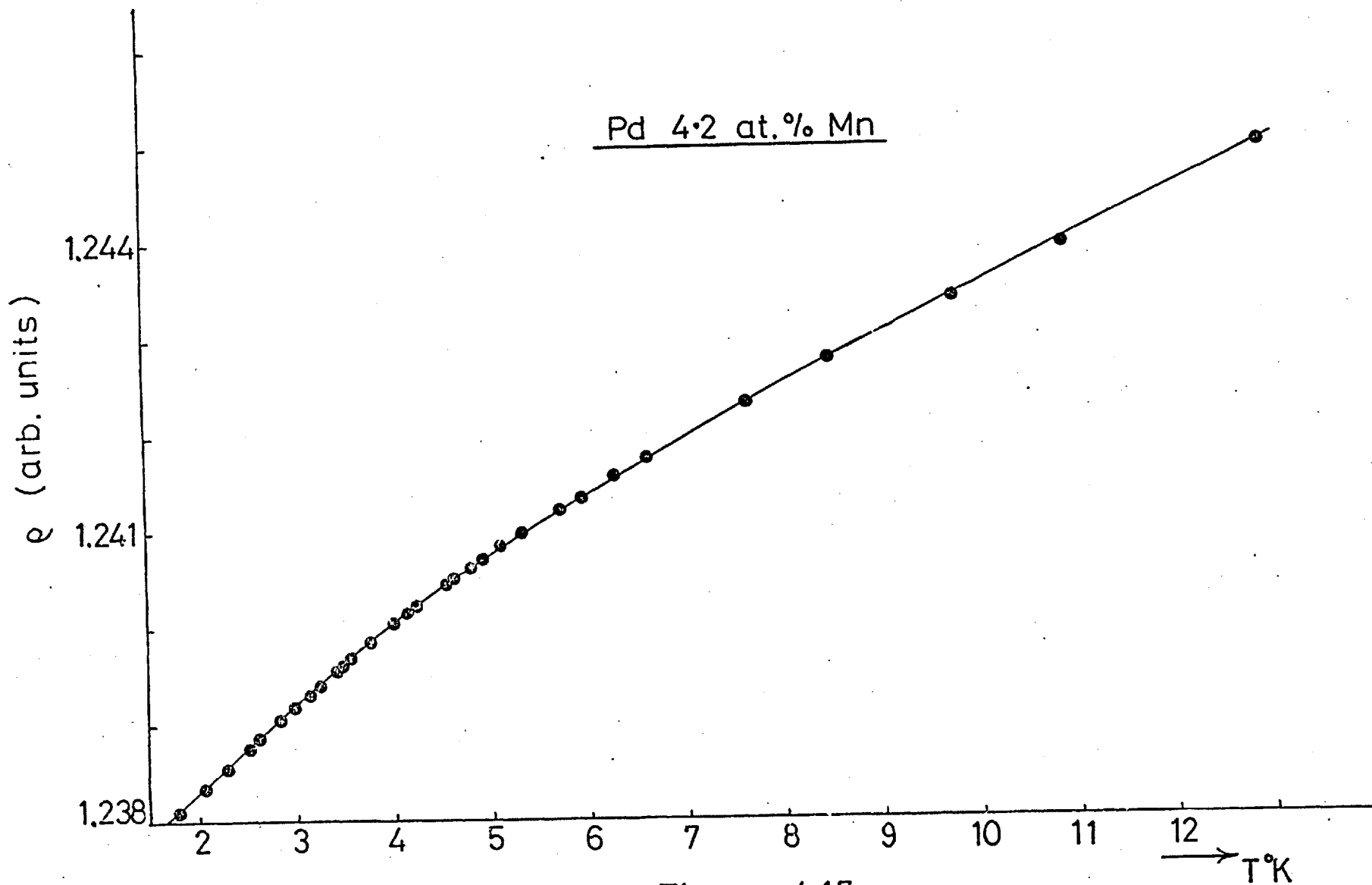
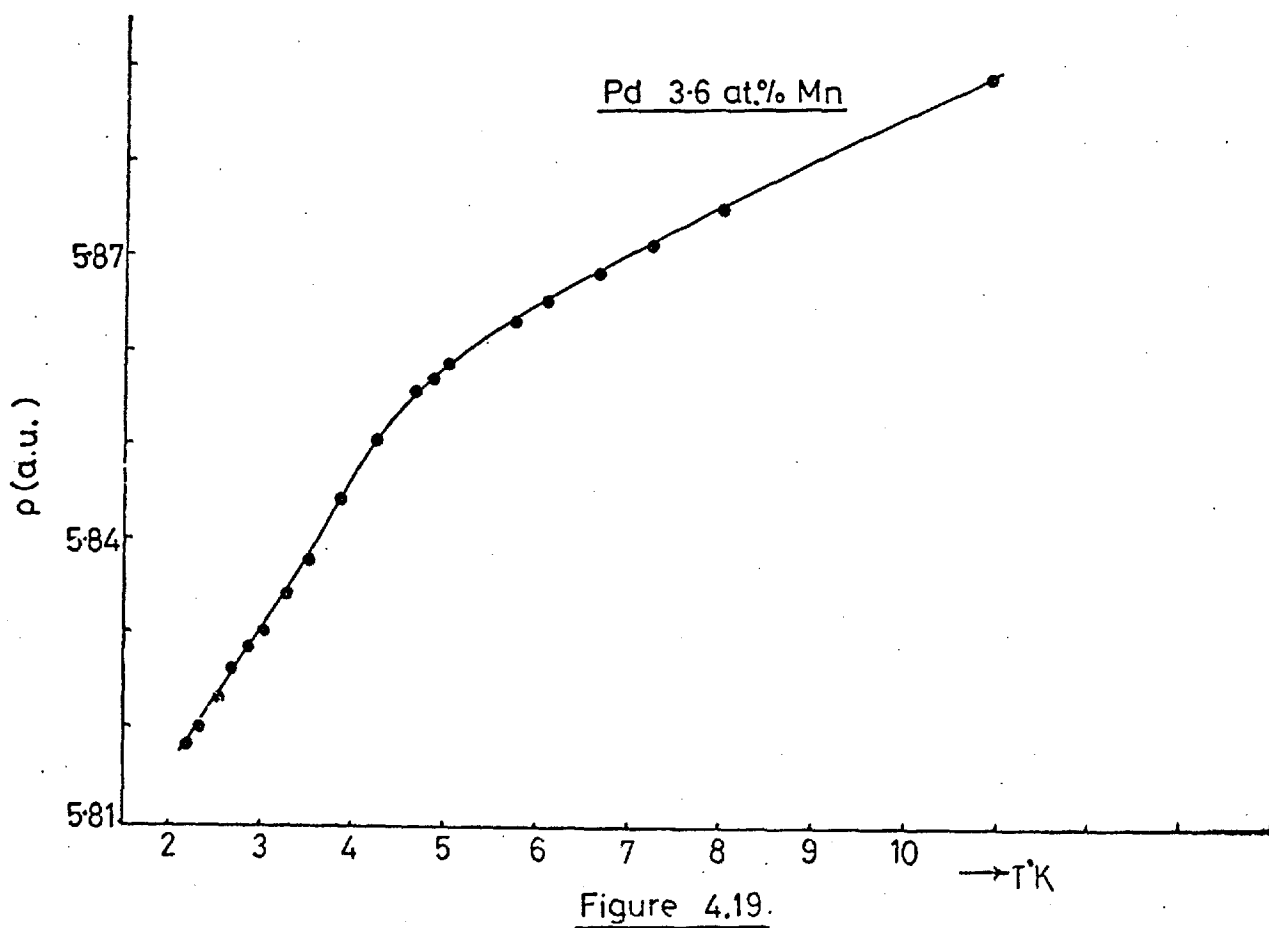
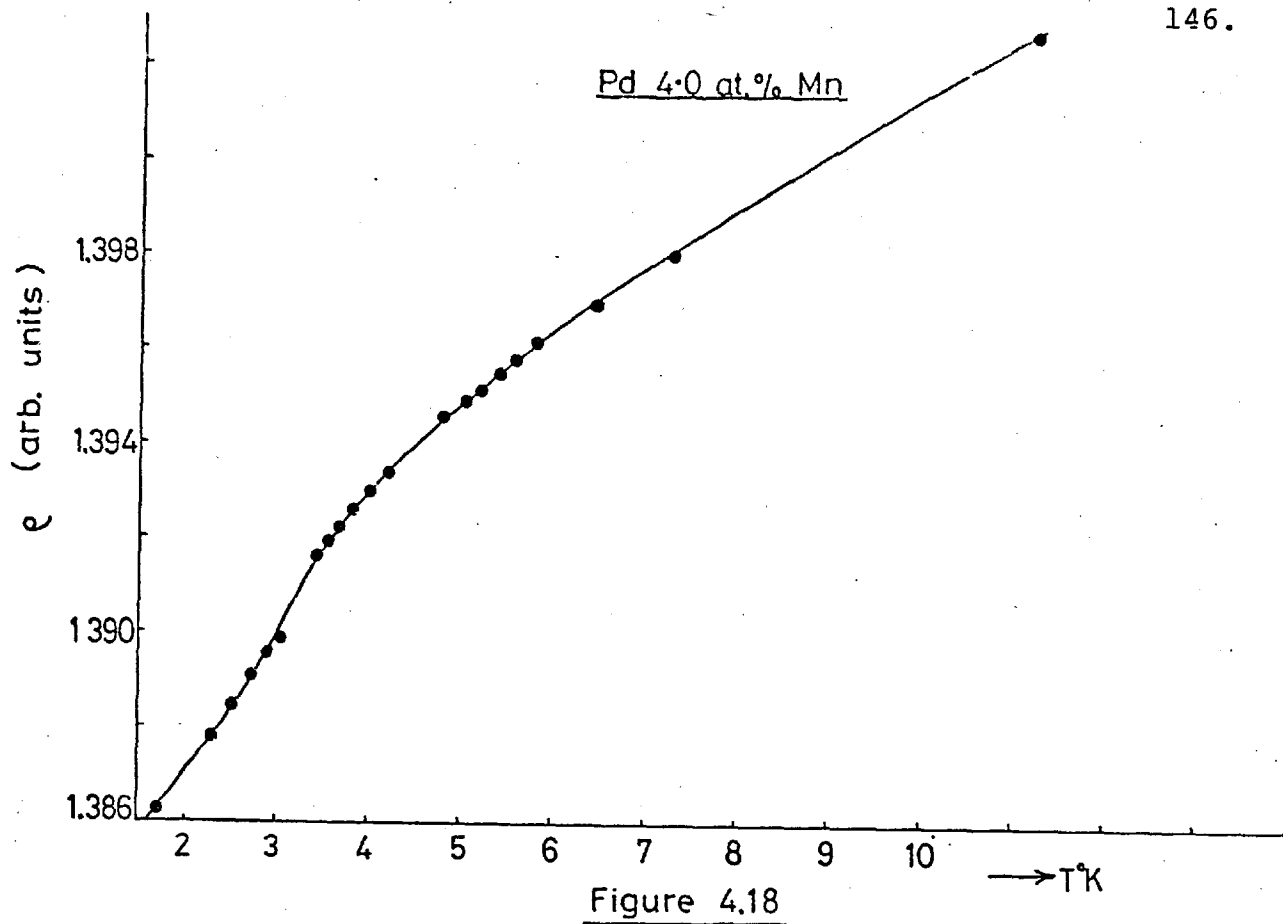
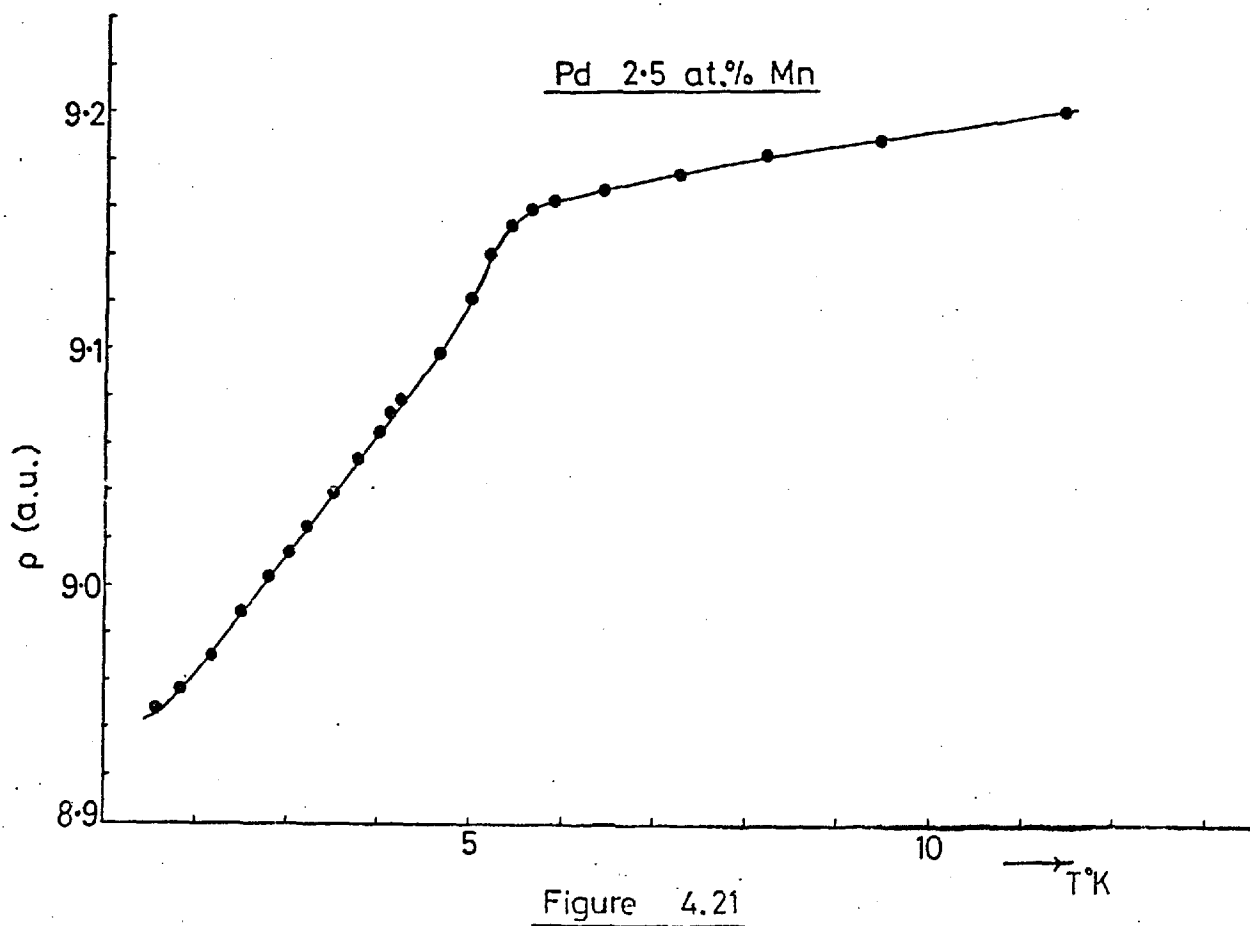
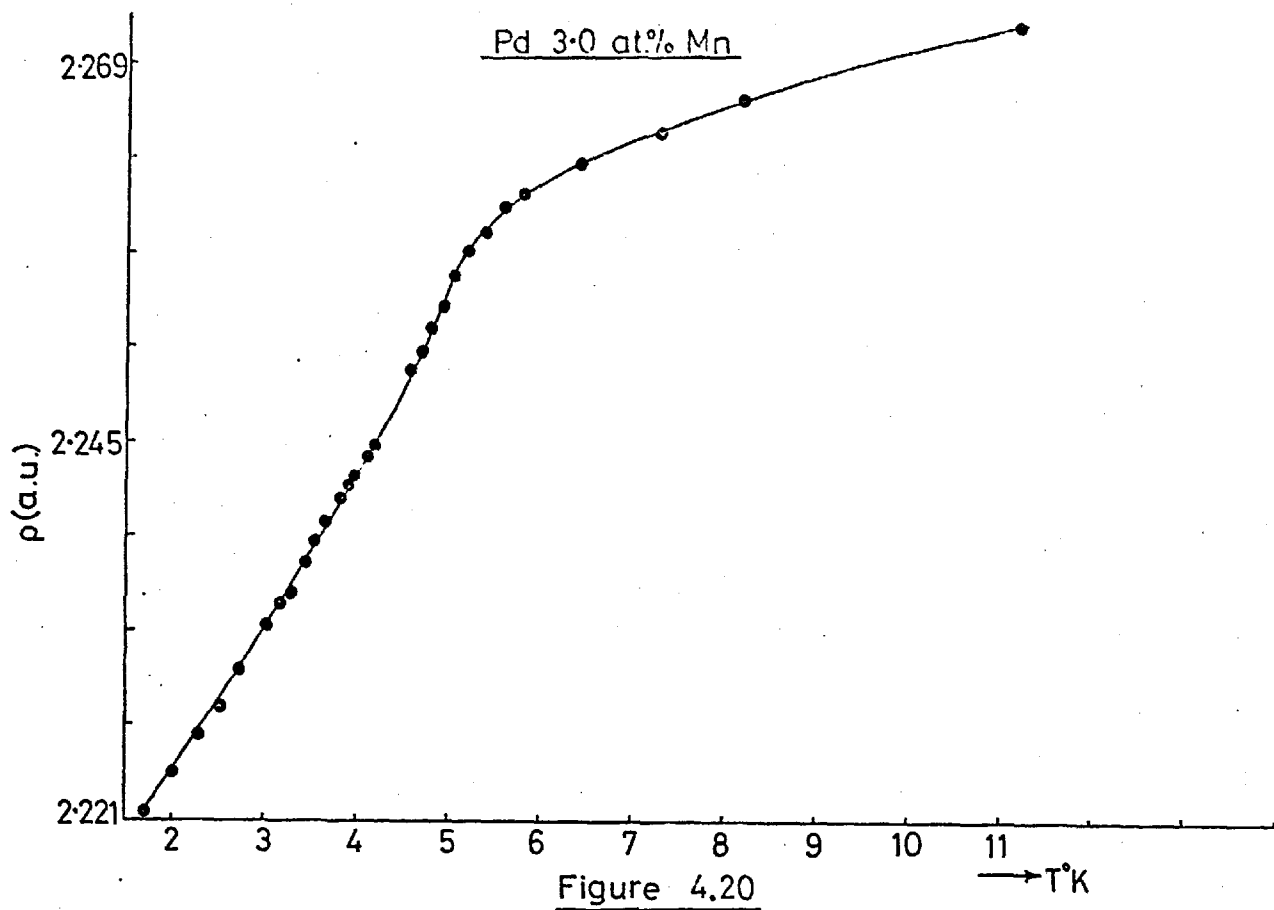
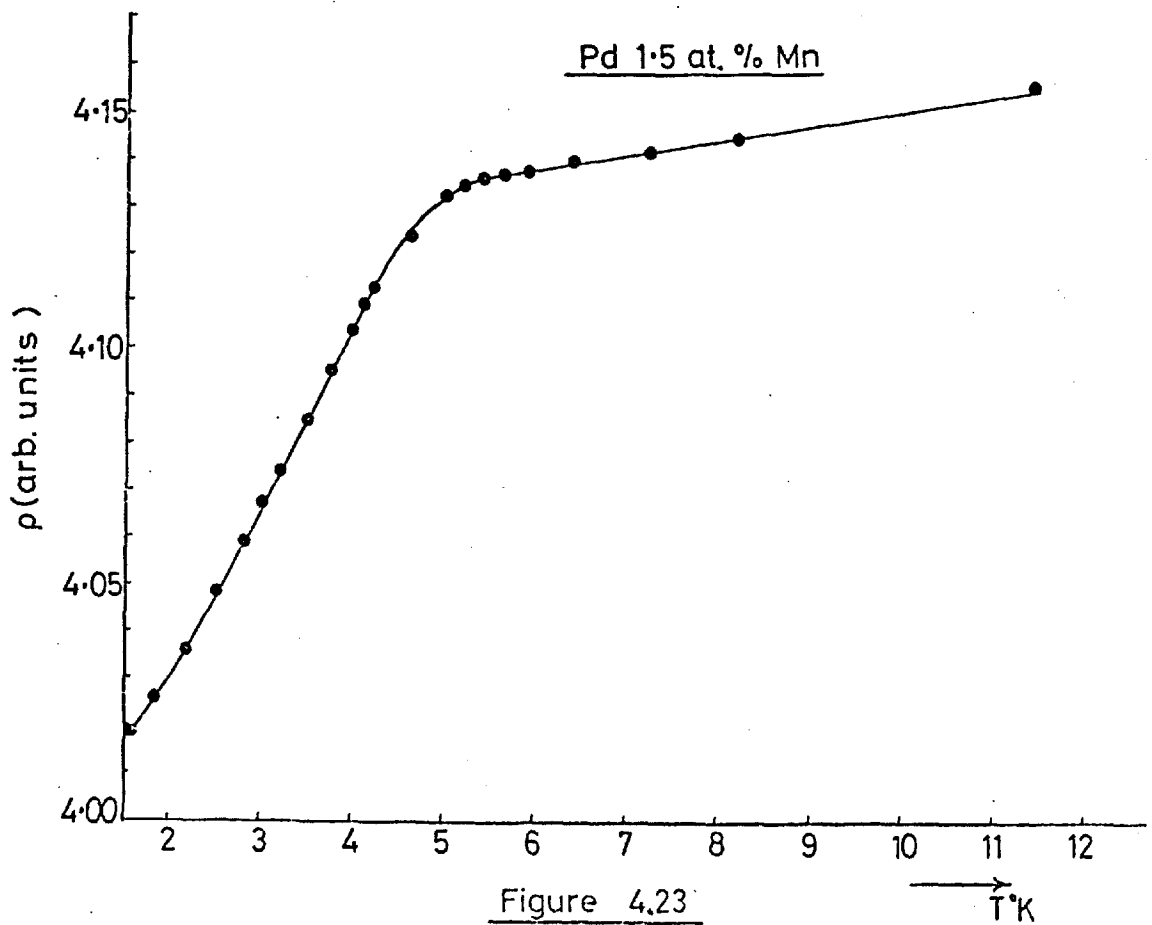
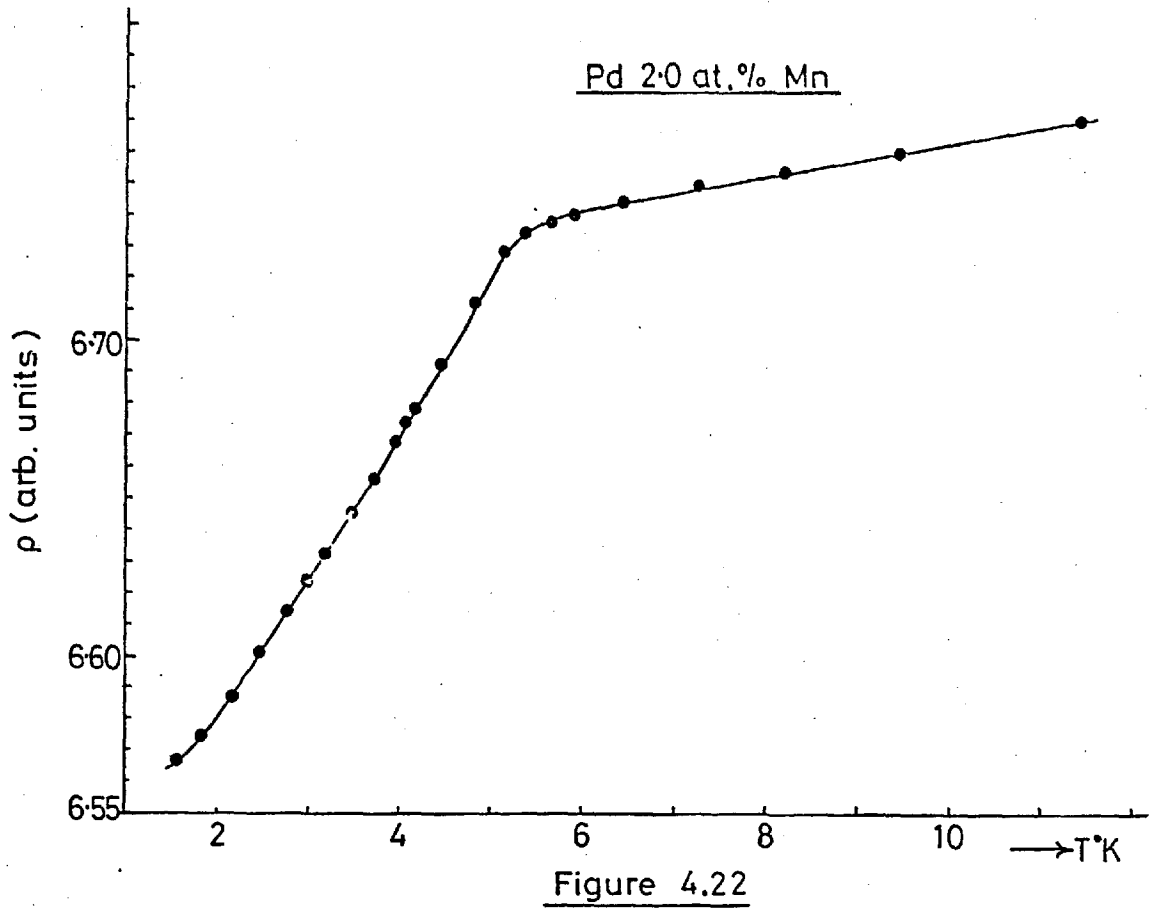


Figure 4.17







increases. Palladium Manganese thus offers a rare opportunity of studying the approach to long-range order through a spin glass regime as the solute concentration decreases. Decreasing the manganese concentration from 8.5 at%Mn results in a reduction of the spin glass temperature, T_g (Table 4.1), but not in the way predicted by Figure 2.2. The values of T_g flatten at about $2\frac{1}{2}^{\circ}\text{K}$ for $C < 5.0$ at%Mn and the sharply increasing peak magnetization for $C < 5.0$ at%Mn reflects the increasing ferromagnetic tendency. In this concentration regime the competing interactions must be of an approximately equal magnitude and a complex mixed regime must exist. In this region the ordering will depend to a larger extent on the precise distribution of the manganese atoms in the alloy, a fact which is clearly seen in the magnetization behaviour of the 4.5 at%Mn alloy with a different heat treatment. In Figure 4.24 we see the M-T curve for the 4.5 at%Mn sphere when a heat treatment to increase the atomic ordering had been given. This treatment involved heating the sample at 750°C for 1 day in vacuo and then instead of quenching to retain the random arrangement of Mn atoms, the temperature was very slowly reduced, over a period of two days, to room temperature, turning down 25°C at a time. Any atomic ordering occurring has thus increased the ferromagnetic nature of the alloy. This is reasonable because a small ordered region will result in the remaining Mn atoms being further spaced from each other, on average.

The results of a further investigation into the

Figure 4.24 : This shows the increase in the ferromagnetic nature of a Pd 4.5 at%Mn alloy due to a slow cooling heat treatment. Plotted is the magnetization of a sphere measured in an increment of 2.0 Oe; x As cast and,
● Heating at 750°C for 1 day and then slowly reducing the temperature at 25°C intervals to room temperature over a period of two days.

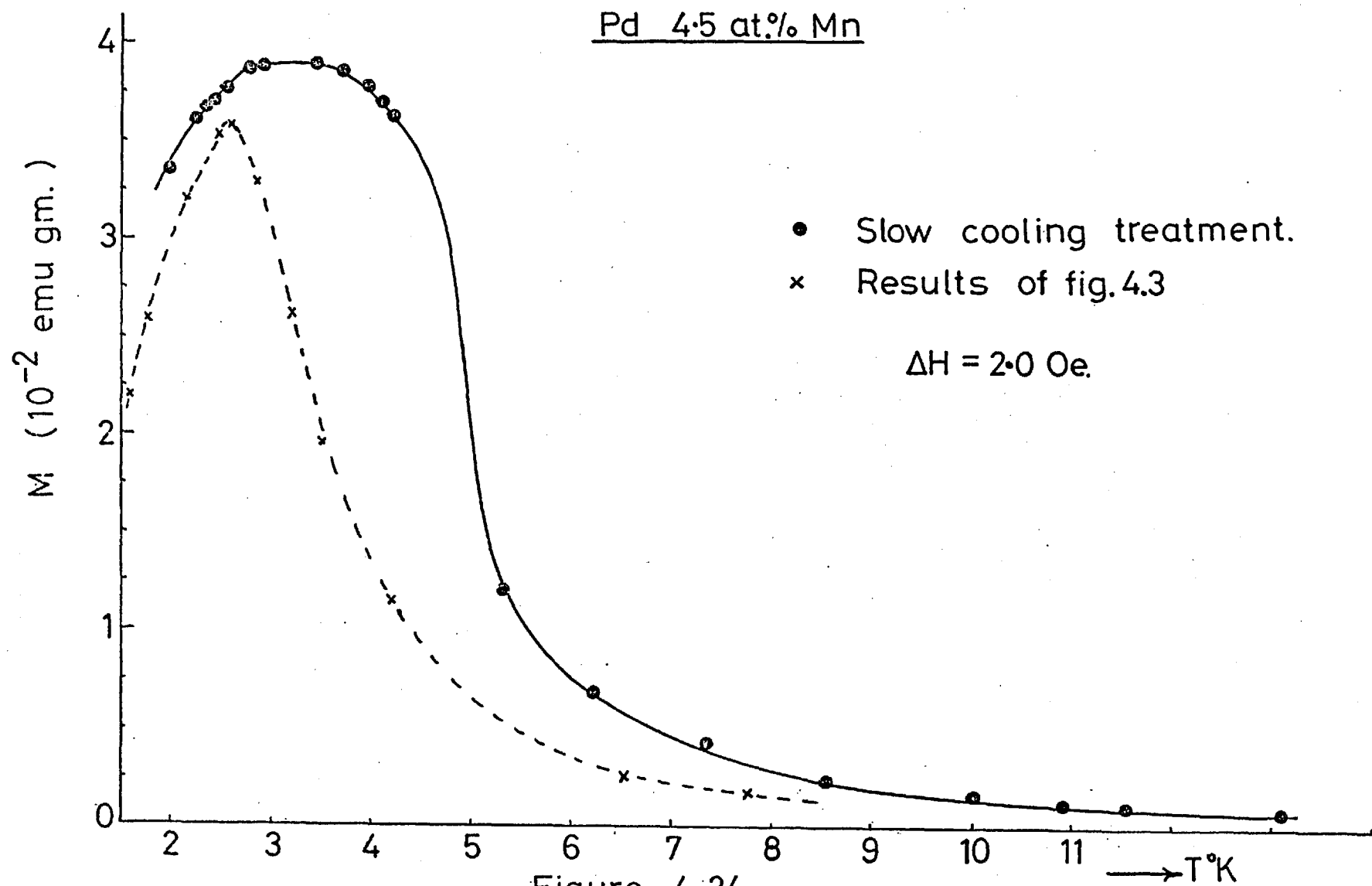
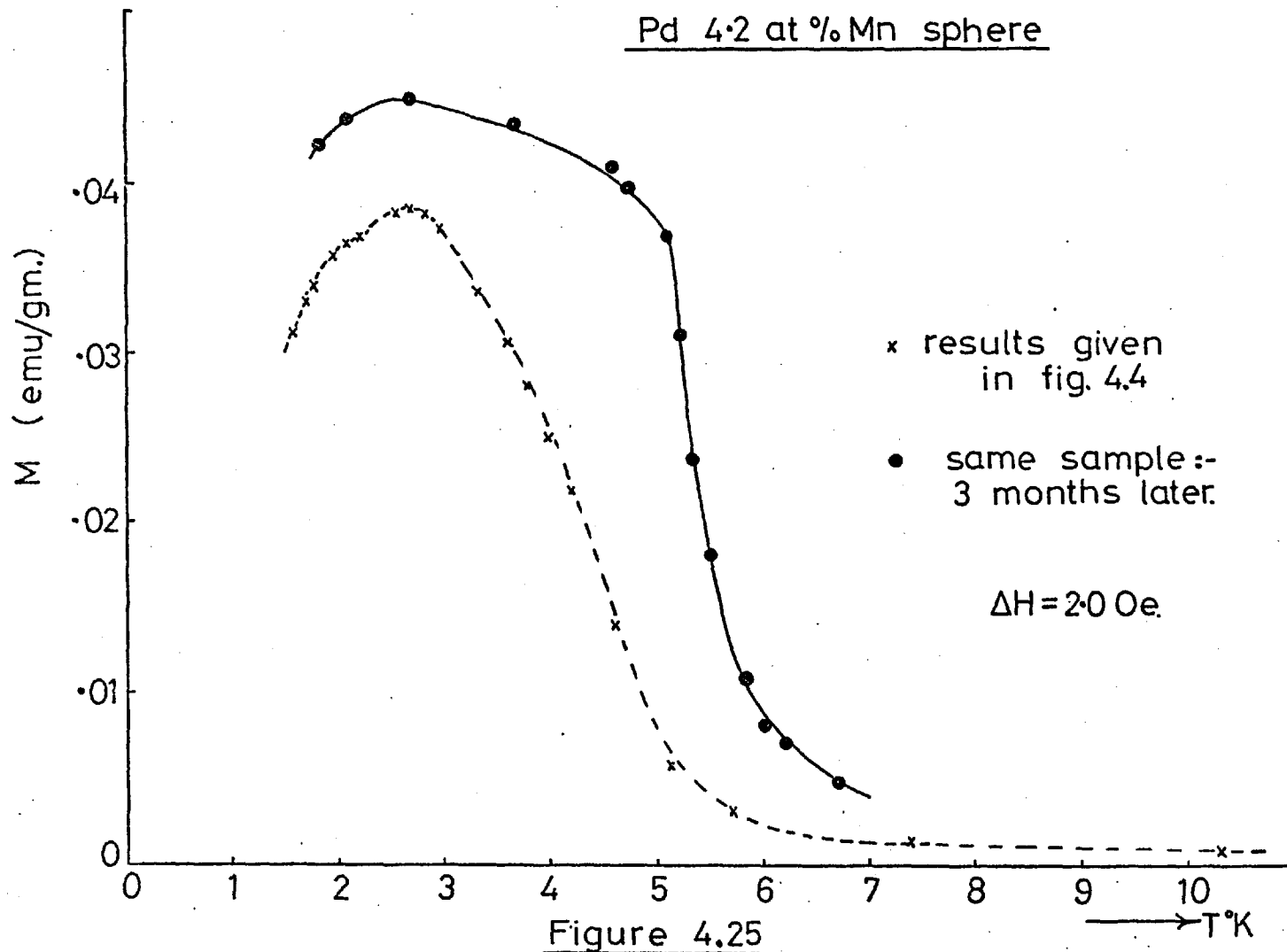


Figure 4.24

magnetization of the same Pd 4.2 at%Mn sphere as used for the results given in Figure 4.4 are shown in Figure 4.25. These were obtained three months after those of Figure 4.4 and they show increased ferromagnetic behaviour, so it appears that a small amount of room temperature annealing has occurred and which, because this is in the critical cross-over region, has a marked effect.

Some mention should be made here regarding the nature of the time dependence of the magnetization of the PdMn alloys with $C \geq 4.0$ at%Mn. The viscous nature of spin glasses has been studied by Guy (4.4) and we find a similar behaviour for all the alloys studied with concentrations greater than 4 at%Mn. However, the time dependence seems to be unusually fast in PdMn compared with other spin glasses. As mentioned previously, the magnetization of these spin glass PdMn alloys below the susceptibility peak was obtained by applying the field at a given temperature and obtaining the reading within several seconds. If a delay of only half a minute occurred between applying the field and obtaining the reading, the magnetization was much higher (approaching, but never greater than that at the temperature of the peak); and if all points were taken with such a sluggish response the susceptibility peak became much less sharp and the low temperature decrease in susceptibility much less than that for the curve when taken quickly. A systematic study of the time dependent susceptibility (such as the variation with time at different temperatures, and for different concentration alloys) has not been carried out but would certainly be useful for

Figure 4.25 : Difference in the magnetization curves for a Pd 4.2 at%Mn sphere after a period of three months, indicating increased ferromagnetic behaviour for the older sample.



future work. Another aspect of this unusually fast variation is seen in the complete loss of the susceptibility peak at higher fields. Again only a qualitative description can be given, as a complete study has not been carried out, but it seems certain that this is in some way related to the time response of the magnetization as a function of applied field, and again would be a fruitful field for a study of spin glass time effects. For those alloys with 4 at%Mn or more, the magnetization as the temperature was reduced failed to show any peak when fields of ~ 200 Oe were used. It did, however, increase at a much reduced rate below T_g (as obtained from the low field χ measurements). The time variation of the magnetization, below the temperature at which the magnetization in 2 Oe peaked, now seemed to be so fast that it always reaches the upper limit before being measured.

The usual criterion for defining an alloy as ferromagnetic is the establishment of an infinite chain of nearest neighbour impurities. The situation with PdMn is different since we are approaching the ferromagnetic regime as the concentration decreases. Thus, the near neighbour impurity - impurity interactions break up any ferromagnetic long-range order compared with the Fe-Fe interactions in AuFe, for example, which are responsible for the long range ordering. In PdMn, therefore, we require to know the concentrations of manganese for which an infinite chain of ferromagnetically coupled giant clouds is not broken by any antiferromagnetic Mn-Mn coupling along the line; a much more complex calculation

than the ordinary percolation calculations and which has not, to the present time, been achieved. From the magnetization results it appears as though the susceptibility has diverged for the 3.8 at%Mn alloy, but not for the 4.0 at%Mn alloy, thus marking the maximum concentration for long range ordering. The transition temperatures, as determined by these M-T plots are shown in Figure 4.26 along with the temperatures at which $\frac{d\rho}{dT}$ reach a maximum. The maximum of $\frac{d\rho}{dT}$ was chosen to characterise the resistivity results due to the lack of a sharp 'kink'. The resistivity and low field magnetization thus correspond quite well and so we believe that previous measurements on PdMn alloys with 2-3 at%Mn over estimated the ordering temperatures.

A relevant, but often neglected, aspect of the ferromagnetic properties of these PdMn alloys is the unusually soft magnetic nature they exhibit. Star et al. (4.5) have carried out a comprehensive high field magnetization study on alloys with concentrations up to 2.45 at% Manganese. They showed that the magnetization of these alloys has a linear increase as a function of applied field up to about 200 Oe and that there was then a sharp turn over, followed by a long gradual increase for higher fields which does not saturate, for the alloys above about 1 at%Mn, even in fields as large as 210 KOe. No hysteretic behaviour and hence no remanence was observed in their measurements. The lack of hysteresis in their measurements indicated a coercivity of something below 0.5 Oe. This in itself is a low value but indications are that the coercivity is at least an order of magnitude lower than this.

Figure 4.26 : Collection of the data presented in this chapter leading to this modified magnetic phase diagram of the PdMn system.

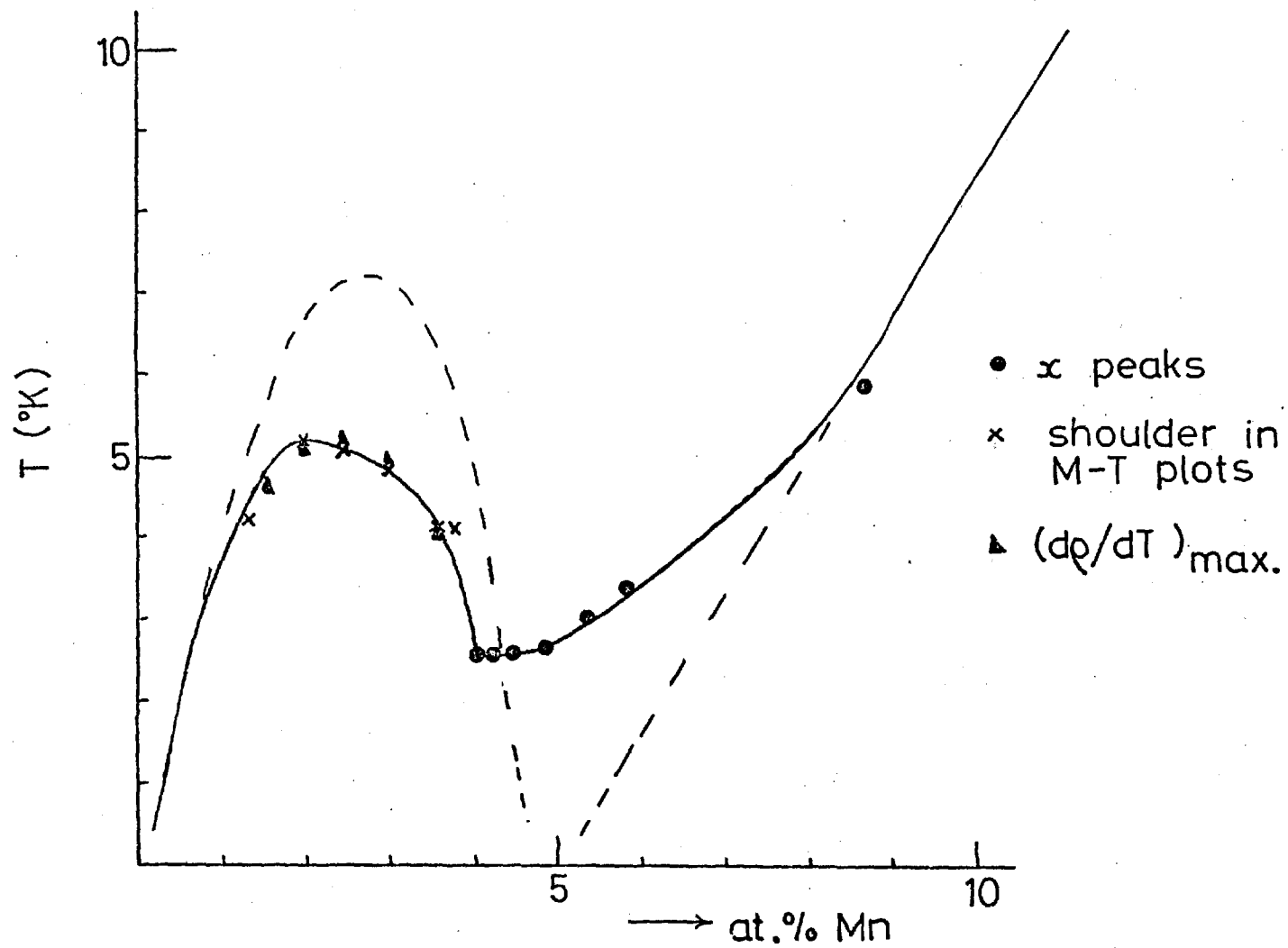


Figure 4.26

The magnetization process in ferromagnetic materials is of an extremely complex nature and the study of such things as domain structure and domain wall motion have added greatly to an understanding of the underlying processes influencing the magnetization. These studies also have great relevance to such commercial aspects as the production of materials with extremely low coercivity and high saturation magnetization for use in transformers and with high coercivity for use as permanent magnets. Ferromagnetic domain theory is discussed in great detail by Kittel and Galt (4.6) and by Craik and Tebble (4.7) while the book by Chikazumi (4.8) covers very well many aspects of the magnetization process.

A ferromagnetic material, such as iron, will in general have zero magnetization if cooled to below T_c in zero applied field. Thus, even though ferromagnetic ordering has occurred, the individual moments do not all align in one direction to give a large overall magnetic moment for the sample. In a polycrystalline sample this will be due in part to the random orientations of the separate crystallites but even a single crystal will not have all the moments aligned in one direction in zero applied field. This is due to the formation of domains in order to reduce the magnetostatic energy. Domain formation is thus an energy minimization process balancing magnetostatic and domain wall energies with one another. The nature of the domain structure formed is dependent on the magneto-crystalline anisotropy and any other induced anisotropies occurring in the material. When this ferromagnetic

material is subjected to an increasing external magnetic field the magnetization increases to saturation (when it is then a single domain) by a mixture of domain wall motion and domain rotation. In the initial permeability range, reversible domain wall motion is the major process but if H is increased beyond this initial region the magnetization increases much more rapidly, due mainly to irreversible domain wall motion. As a result, if the field is removed any time after the irreversible processes have begun there will not be a complete return to the same domain structure as before and some magnetization in the direction of the applied field will remain, i.e. we have induced a dipolar remanence. A finite field is then necessary in the opposite direction to reduce the magnetization to zero; this is the coercive field if the magnetization in the forward direction has been taken to saturation. Certain commercially useful alloys have exceedingly low coercive fields. These include supermalloy ($\text{Fe}_{16}\text{Mo}_5\text{Ni}_{79}$) which has a coercivity of $2 \cdot 10^{-3}$ Oe, permalloy ($\text{Fe}_{21.5}\text{Ni}_{78.5}$) with $H_c = 0.05$ Oe. and now some metallic glasses such as the low magnetostrictive alloy of $(\text{Fe}_4\text{Co}_{96})_{75}\text{P}_{16}\text{B}_6\text{Al}_3$ which has a coercive field of ~ 0.013 Oe. However, these are exceptional, involving special preparation techniques, and the value of the coercivity obtained for PdMn is highly unusual and indicative of very small, or zero, anisotropy.

Very little discussion, if any, has been made along these lines to explain the ferromagnetic properties of the low manganese concentration PdMn alloys. A possible

explanation of these ferromagnetic properties can be obtained by considering finite 'chains' of ferromagnetically coupled Mn spins acting in a sense similar to a domain which is broken when two Mn moments are close to one another making an antiparallel alignment between them more favourable. These should then act in an equivalent way to clusters as obtained in the more concentrated spin glasses (see section 1.4.2). On average, therefore, there will not be any overall alignment in zero field but the application of only a small field serves to break a non-aligned portion of a 'chain' at the positions where the ferromagnetic coupling is weak (i.e. where two Mn atoms are nearly close enough for the direct interaction to win out or far enough apart for the change in sign of the conduction electron polarization to occur (see section 1.3.4.)). Thus the sharp rise in the magnetization at low fields is due to the alignment of many of the Mn spins, followed at higher fields by the Mn-Mn antiparallel pairs being broken and the polarization of the Pd host. This process is, therefore, not mediated by the motion of a domain wall, involving the pinning by local anisotropy variations of the wall with the associated irreversibilities, but is essentially reversible due to the apparent lack of anisotropy. Thus, when the field is removed the energy is once again minimized at the relevant Mn-Mn pairs by the flipping over of the spins which were originally in the opposite direction to the applied field.

These clusters, therefore, should have a glass freezing temperature. For these dilute alloys this will be extremely low and the susceptibility will, as the temperature is reduced, reach the limiting value set by the demagnetization factor before this freezing temperature. Now, as the Mn concentration increases, this freezing temperature will increase and we should reach a concentration where this freezing can be seen as a low temperature drop off from the demagnetization limit before the lowest temperature in our apparatus is reached. Well, this is difficult to see either way from our palladium manganese results, but if figures 4.4 and 4.10 are looked at carefully we believe the evidence is here. Figure 4.10 for the Pd 3.6 at%Mn alloy has indications of a low temperature drop off just below 2°K , while the results for the Pd 4.0 at%Mn specimen in figure 4.4 can be seen to give a broader peak than the higher concentration alloys. It is possible to interpret this curve in the following way: firstly, the susceptibility has reached the demagnetization limit by about 2.9°K , remained constant for about 0.3°K and then the low temperature reduction occurs.

This evidence alone is obviously a little thin but a more convincing indication of this effect has recently been published by Verbeek et al. (4.9) for a $(\text{Pd}_{.9965}\text{Fe}_{.0035})_{1-x}\text{Mn}_x$ series of alloys. Here the PdFe matrix is ferromagnetic and the introduction of Mn into this host should be pretty much the same as in pure Pd, except for an increased ferromagnetic behaviour for any given Mn

concentration. This should serve to separate the two effects and push up any low temperature drop off. This is indeed the case. They find that for $0.03 < X < 0.06$ the susceptibility flattens at the demagnetization limit, remains flat for several degrees, with a very clear drop off at lower temperatures.

At higher manganese concentrations in PdMn, the Mn-Mn near neighbour distance decreases so that there are many more neighbours with a preference to align anti-parallel to one another; leading to a greater probability of $J < 0$ exchange coupling and hence shifting the peak in the $P(J)$ curve downwards from a positive value towards zero (i.e. increasing the tendency to spin glass ordering, see section 1.4.1)). In this regime the spin glass freezing temperature has increased to an extent that these spins become frozen at a higher temperature than that necessary for the magnetic susceptibility to reach the demagnetization limit, resulting in the χ peak observed for $C \geq 4.0$ at%Mn. Below the glass freezing temperature the spins are now frozen at zero field, but the application of a magnetic field causes the transition to some more aligned metastable state, the transition proceeding in a viscous way with the rate of transition apparently increasing at larger fields (another point of interest would be to look at the decay of the isothermal remanence induced in these alloys after the application of different fields).

Now, previous high field magnetization measurements by Rault and Burger (4.2) failed to pick up any spin glass properties in PdMn alloys, a transition from ferromagnetic ordering to antiferromagnetism being indicated at about 8 at%Mn. We have made magnetization measurements as a function of field on two alloys just on either side of 4.0 at%Mn. In figure 4.27 we show the magnetization versus field curves for a Pd 3.8 at%Mn disc at several temperatures while similar results for a Pd 4.2 at%Mn sphere are shown in figure 4.28. These are very similar, and no obvious conclusions concerning any differences in the magnetic ordering between the two alloys can be drawn from these curves. These measurements were taken on a similar VSM to the one described in chapter 3, but fitted with a superconducting magnet enabling very high fields to be obtained. The curves were taken in a continuous mode using a feedback circuit in series with the reference coil which alters the current until the reference signal equals the sample signal. In the 4.2 at%Mn alloy, therefore, any time effects at the low temperatures are lost in the continuously increasing magnetization resulting from the sweeping field. The low temperature magnetization thus only shows a decrease when using low fields and if the time effects are beaten by obtaining the reading as quickly after the application of the field as possible.

One further problem has been enhanced by recent preliminary results on the pressure dependence of the ordering temperatures in several of the PdMn specimens

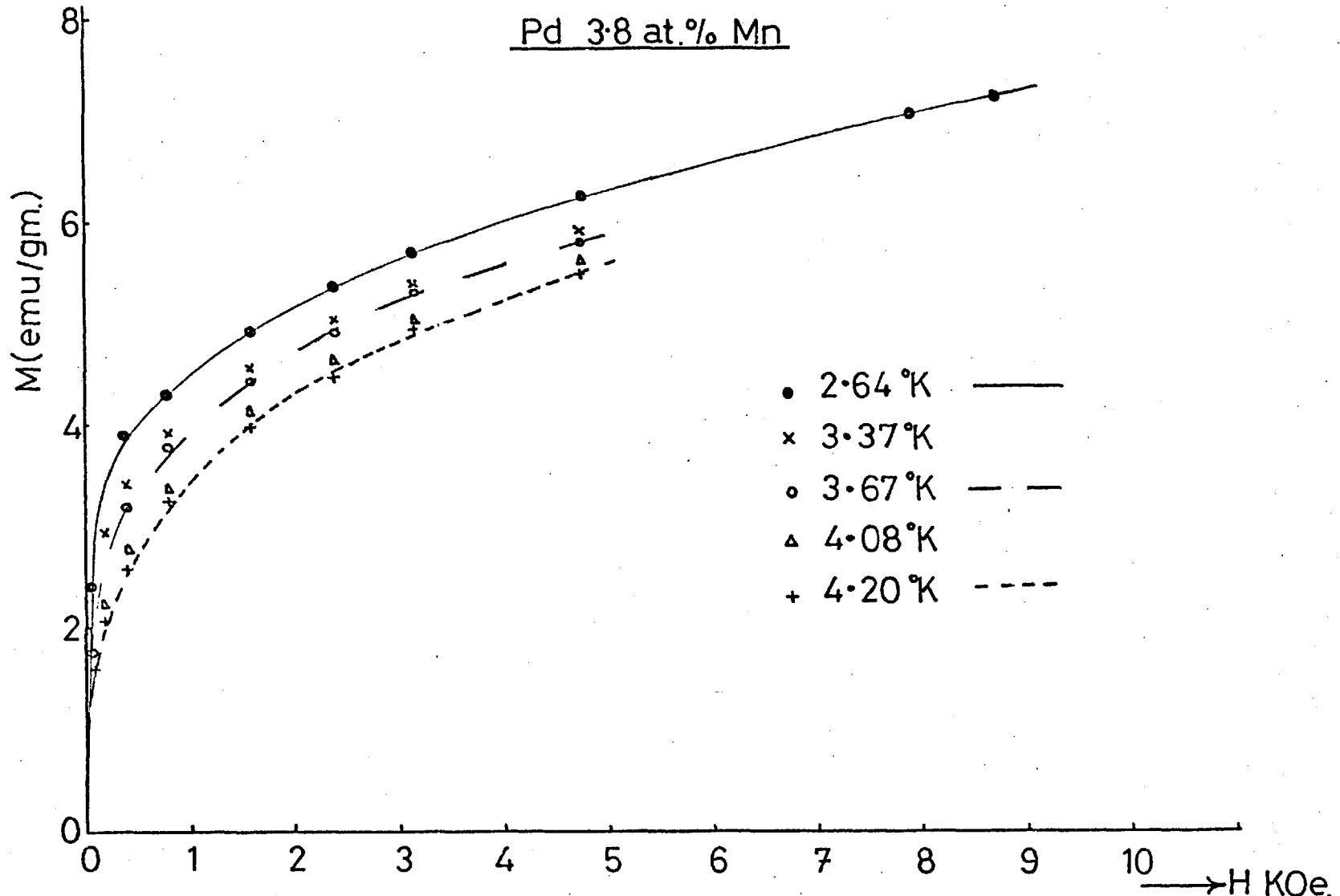


Figure 4.27 : Magnetization vs. field at several temperatures.

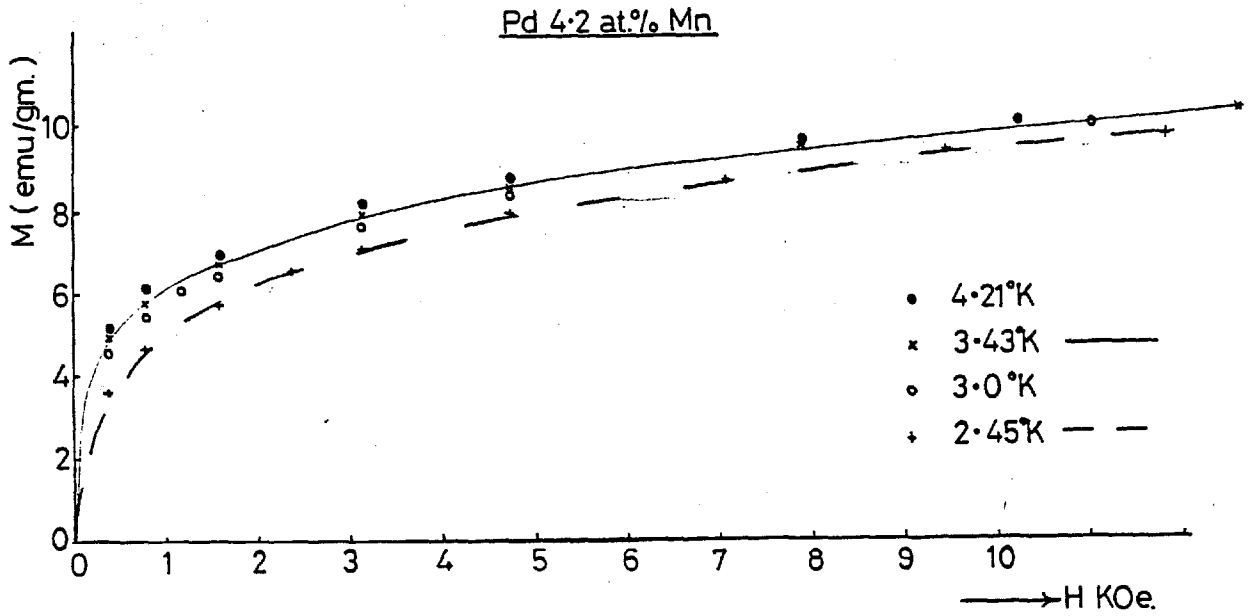


Figure 4.28a: Temperature variation of the Magnetization vs. field curves below 4.2°K.

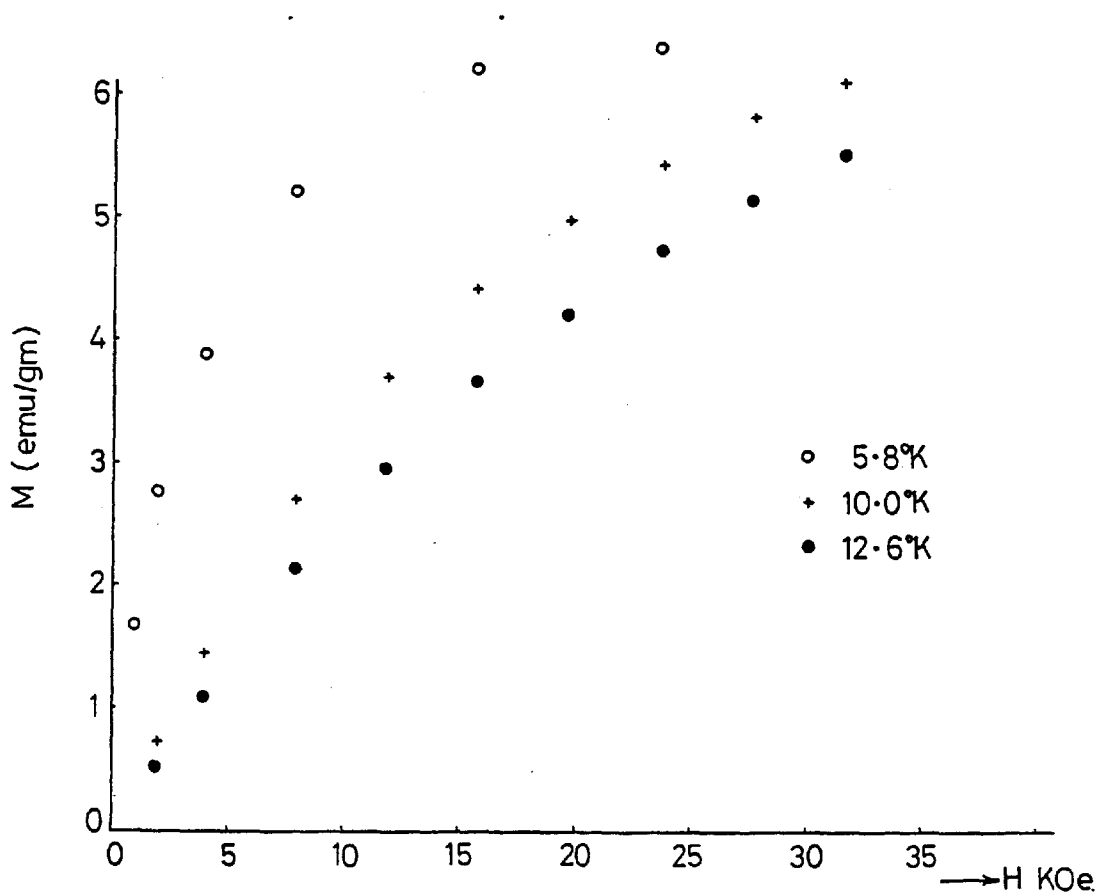


Figure 4.28b: Field dependence of the magnetization for a spherical Pd 4.2 at.% Mn specimen above 4.2°K.

(Guy, private communication). This is related to the long standing uncertainty as to whether a localized or itinerant picture is the more suitable. Some time ago Rhodes and Wohlfarth (4.10) analysed the available susceptibility and magnetization data on many different ferromagnetic systems. They showed that the ratio q_c/q_s reflected whether the localized or itinerant model held in any given system. Here q_c is the magnetic moment as obtained from the Curie-Weiss plots of the high temperature susceptibility data and q_s is the saturation moment per atom in Bohr magnetons. The value of q_c/q_s was 1 for well localized moment systems, no matter what the ordering temperature, but for itinerant systems with ordering temperatures below $1,000^\circ\text{K}$ the ratio q_c/q_s increased the smaller the ordering temperature was. Most alloys fell somewhere on a smooth curve and such a plot of q_c/q_s versus ordering temperature has become known as a Rhodes-Wohlfarth plot. In this original paper, Rhodes and Wohlfarth (4.10) showed that the dilute Pd-based alloys fell on the itinerant curve but many workers since have tended to ignore this fact since the weight of evidence is for a giant moment behaviour involving localized transition metal electrons (Nieuwenhuys 4.11) (the model which we have implicitly favoured in the discussion throughout this chapter and in chapter 2). A recent reappraisal of the method of obtaining q_c/q_s in the Pd alloys (Nieuwenhuys et al. (4.13)) has come down in favour of the localized model for these Pd-based alloys; seemingly solving these differences. However, no sooner are the waters a little

clearer than something tends to muddy them further. The effect of an applied hydrostatic pressure of 11 kbar seems to alter the ordering temperature of the PdMn alloys with $C < 3.8$ at%Mn by over 10% (Guy, private communication). This is more consistent with an itinerant model. However, as this work is very recent and is the source of continuing research, speculation on these preliminary results is a little premature.

To conclude this section, therefore, we have seen how our low field measurements of the magnetization of PdMn alloys have, for the first time, clearly distinguished the spin glass ordering in alloys with 4.0 at%Mn and greater and we have put forward a modified magnetic phase diagram, figure 4.26, with the help of resistivity measurements. We have also discussed many of the still unanswered questions involved in the understanding of the magnetic properties of these alloys and suggested where further information would be useful. There are still many fruits to be picked from the tree of the palladium manganese system.

4.2 Observation of unusual Remanent Behaviour

During the course of the magnetization measurements reported above it was noticed occasionally that an anomalous variation of the magnetization in zero external applied field occurred. After the application of larger fields than the usual measuring field of 2.4 Oe the remanent reading was reduced, Guy and Howarth (4.12).

We investigated the variation of the remanence as a function of the previously applied field for many of the PdMn alloys; typical results being shown in figures 4.29 and 4.30 for a Pd 3.8 at%Mn alloy at 4.2°K and 1.7°K, respectively. These measurements led us to attempt to consider how a reversed remanence could be occurring and this resulted in an extension of the analysis of the signal obtained in the VSM to take account of non-uniformities in the sample magnetization. This re-analysis is given in chapter 5. An extension of this has led to the possibility of using a SQUID magnetometer as a sensitive method of observing non-uniformities in the magnetization of a specimen and in particular to the observation of the sublattice magnetization in a layer antiferromagnet.

It has, however, since become apparent that the original observations of an unusual remanent behaviour in palladium manganese were spurious. Thus, the results given in figures 4.29 and 4.30 are incorrect in that the variation shown is due to the variation of the field at the sample position. The applied field from the helmholtz pair is zero but a stray field is produced by the leads to our diode temperature sensor and this changes after the application of a different field from the Helmholtz coils. This, unfortunately, means that the data obtained on the PdMn alloys, of the signal variation with position in the pick-up coils (see chapter 5), are also incorrect and so the analysis employed on this data is now not relevant.

Figures 4.29-4.30 : Variation of the remanent magnetization of a Pd 3.8 at%Mn alloy, after the application of the fields shown. These curves are now known to occur because of the varying stray field from the diode leads (see the text) and are thus not representative of a reversed dipole as originally thought.

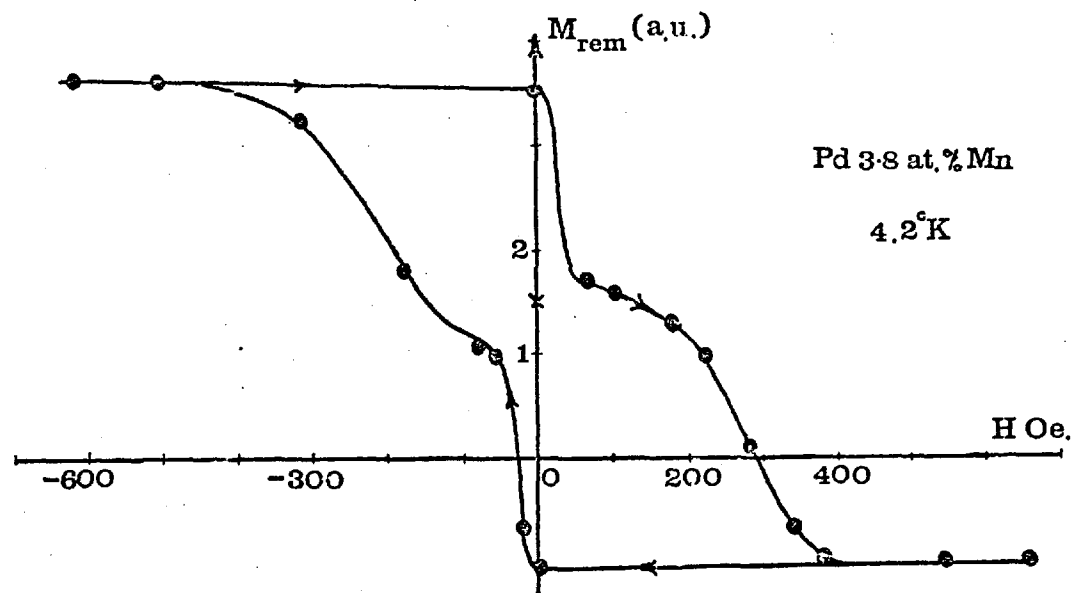


Figure 4.29

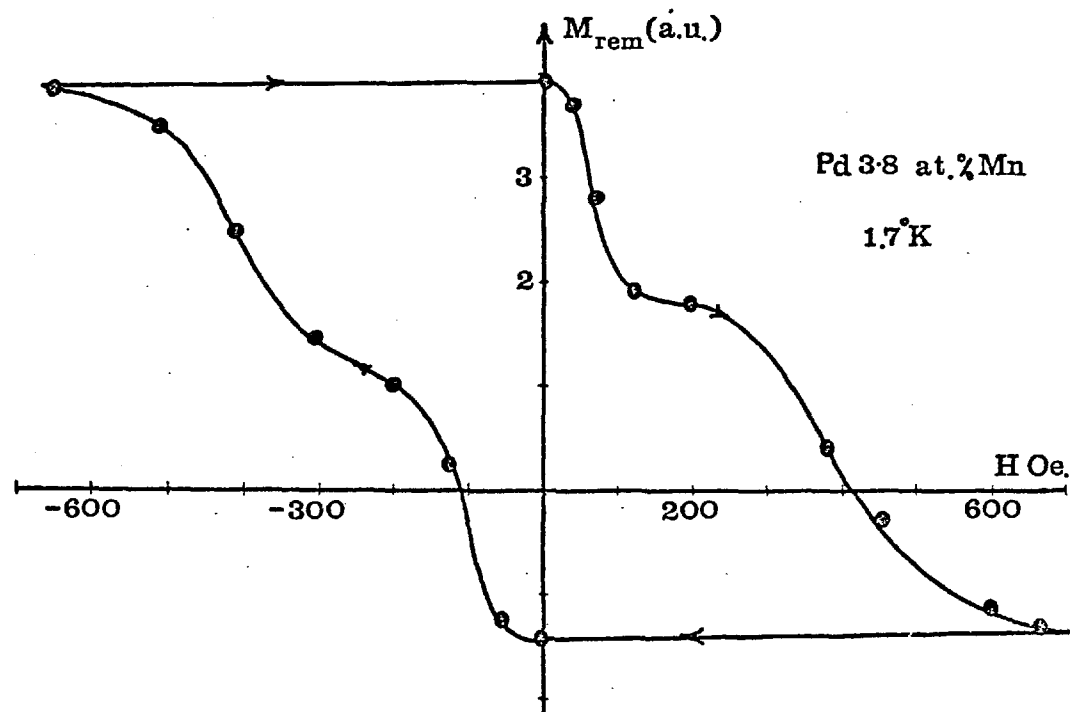


Figure 4.30

However, the basic idea of observation of non-uniform magnetization is correct and so the method of analysis is also included in chapter 5. Even though this is not now applicable to the PdMn data it shows the general method of obtaining the information about the magnitude of the higher magnetic poles present in any sample.

We thus conclude, after all, that the remanence of palladium manganese does not show any unusual negative behaviour but that the original observation and consideration of this spurious effect was useful in leading us onto the work now discussed in chapter 5.

REFERENCES

- 4.1 COLES B.R., JAMIESON H., TAYLOR R.H. and TARI A.
J. Phys. F5, 565 (1975).
- 4.2 RAULT J. and BURGER J.P.
Comptes Rendues 269B, 1085 (1969).
- 4.3 ZIJLSTRA H.
Expt. Methods in Magnetism Vol. II (Amsterdam,
North Holland), (1967).
- 4.4 GUY C.N.
J. Phys. F8, 1309 (1978).
- 4.5 STAR W.M., FONER S. and MCNIFF E.J.
Phys. Rev. B12, 2690 (1975).
- 4.6 KITTEL C. and GALT J.K.
Solid State Physics, Vol. 3, pp. 437-564, Edited
by F. Seitz and D. Turnbull, Academic Press,
N.Y., (1956).
- 4.7 CRAIK D.J. and TEBBLE R.S.
Ferromagnetism and ferromagnetic Domains, Vol. IV
of series of monographs on selected topics in
Solid State Physics, edited by E.P. Wohlfarth,
North Holland, Amsterdam, (1965).
- 4.8 CHIKAZUMI S.
Physics of Magnetism, John Wiley and Sons Inc.,
N.Y., (1964).
- 4.9 VERBEEK B.H., NIEUWENHUYS G.J., STOCKER H. and
MYDOSH J.A.
Phys. Rev. Letts. 40, 586, (1978).
- 4.10 RHODES P. and WOHLFARTH E.P.
Proc. Roy. Soc. (London), A273, 247, (1963).
- 4.11 NIEUWENHUYS G.J.
Adv. Phys. 24, 515, (1975).
- 4.12 GUY C.N. and HOWARTH W.
Amorphous magnetism II, p. 169, edited by R.A. Levy
and R. Hasegawa, Plenum, N.Y., (1977).
- 4.13 VERBEEK B.H., NIEUWENHUYS G.J., STOCKER H. and
MYDOSH J.A.
Phys. Rev. Letts. 40, 586 (1978).

CHAPTER 5

RE-ANALYSIS OF THE VSM SIGNAL FOR NON-UNIFORM MAGNETIZATION

5.1. Introduction

In Section 3.3.1 we saw that the vibration of an infinitesimal dipole induced an emf in a near-by circuit of magnitude

$$\varepsilon = - \frac{d}{dt} \underline{M} \cdot \underline{h}(\underline{r}-\underline{R}) \quad (V.1)$$

For a finite sized sample of magnetization $\underline{M}(\underline{r})$ we obtain;

$$\varepsilon = - \frac{d}{dt} \int \underline{M}(\underline{r}) \cdot \underline{h}(\underline{r}-\underline{R}) dv \quad (V.2)$$

by integrating over the sample volume. If the magnetization is uniform then the analysis is the same as that given in Section 3.4.3(ii), apart from an integration over the sample volume. If, however, the magnetization \underline{M} is not uniform throughout the sample the analysis must be modified. In this case we expand the sensitivity field \underline{h} about the origin in powers of \underline{r} and then relate the series to a multipole expansion of the magnetization $\underline{M}(\underline{r})$ within the sample. Restricting to variations of the z component of the magnetization, for ease of description, and assuming that $M_z(\underline{r})$ has cylindrical symmetry about the z-axis we obtain

$$h_z = \sum_{\ell=0}^{\infty} \frac{1}{\ell!} \left(\frac{\partial^{\ell} h_z}{\partial z^{\ell}} \right)_{z=z_0} r^{\ell} P_{\ell}(\cos\theta) \quad (V.3)$$

Zijlstra, pt.I, p.33 (5.1). Hence, for small amplitude mechanical vibration parallel to the z direction, the emf produced in the circuit is given by;

$$\begin{aligned} \epsilon &= -a\omega \sin\omega t \sum_{\ell=0}^{\infty} \frac{1}{\ell!} \int M_z(r, \theta) r^{\ell} P_{\ell}(\cos\theta) dv \left(\frac{\partial^{\ell+1} h_z}{\partial z^{\ell+1}} \right)_{z=z_0} \\ \epsilon &= -a\omega \sin\omega t \left\{ \int_{z=z_0} M_z dv \left(\frac{\partial h_z}{\partial z} \right) + \int_{z=z_0} M_z z dv \left(\frac{\partial^2 h_z}{\partial z^2} \right) + \right. \\ &\quad \left. \int M_z \frac{(3z^2 - r^2)}{4} \frac{\partial^3 h_z}{\partial z^3} z dv + \dots \right\} \quad (V.4) \end{aligned}$$

Each term in this series represents the amplitude of the induced emf produced by each multipole in the expansion of $M_z(\underline{r})$. If the specimen has multipole strengths $Q_0, Q_1, Q_2,$ etc., the emf induced in the circuit when the sample is vibrated about $z=z_0$ is

$$\epsilon(z_0) = \sum_{\ell=0}^{\infty} \frac{Q_{\ell}}{\ell!} \left(\frac{\partial^{\ell+1} h_z}{\partial z^{\ell+1}} \right)_{z=z_0} (-a\omega \sin\omega t) \quad (V.5)$$

The first term of this series is due to the dipole and is just that obtained in Section 3.4.3(ii). The remaining

terms are due to the higher order magnetic poles and the amplitude of each term, ℓ , is proportional to the magnitude of the ℓ^{th} pole and to the $(\ell+1)^{\text{th}}$ derivative of the sensitivity field, $h_z^{\ell+1}$.

A knowledge of the functions $h_z^{\ell+1}$ forms the basis of the determination of the relative strengths of the multipoles of a given sample magnetic state. For the pick-up coil geometry used in our VSM the first five of these derivatives are calculated, as a function of the position along the z-axis, in Appendix A. The finite size of the sample is taken account of, to first order, by averaging each field derivative calculation over the sample. The results of the calculation for $h_{z_{av}}^1$ to $h_{z_{av}}^5$ (for unit current), averaged over a sample of 2 mm extent in the z direction, are shown in Figures 5.1 to 5.5 respectively, obtained by using the programme given in Appendix B.1.

By measuring $\epsilon(z_0)$, for a range of z_0 , we obtain a function which can be numerically analysed into this linear combination and the Q's determined. It was for this purpose that we connected the coil system to a threaded bar which may be turned outside the cryostat, thus moving the pick-up coil relative to the sample.

5.2. Experimental Verification

To demonstrate the above ideas we show the experimental results for dipole, quadrupole and octupole coil arrays in Figures 5.6, 5.7 and 5.8 respectively. The dipole was wound with seven turns of 48 swg copper wire and had a radius

Figures 5.1-5.5 : The calculated field distribution, for the pick-up coil geometry used in our apparatus, leads to the first five derivatives of the field shown here. These curves were calculated by averaging over a sample of size 2mm. The dots represent the interval over which the calculation (the programme for a Hewlett Packard HP9820 to do this calculation is given in Appendix B1) was performed and the line a smooth curve through these points.

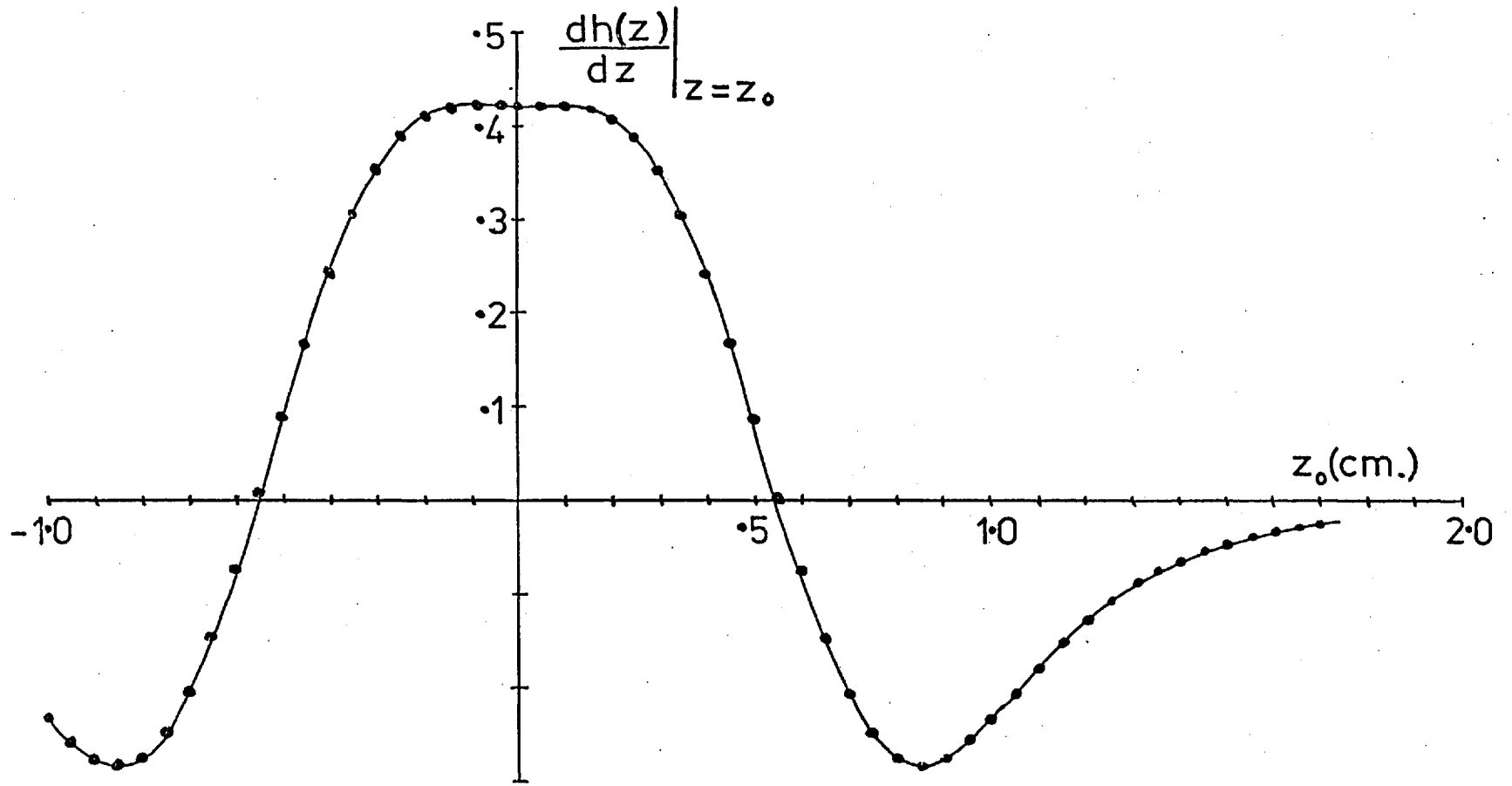


Figure 5.1

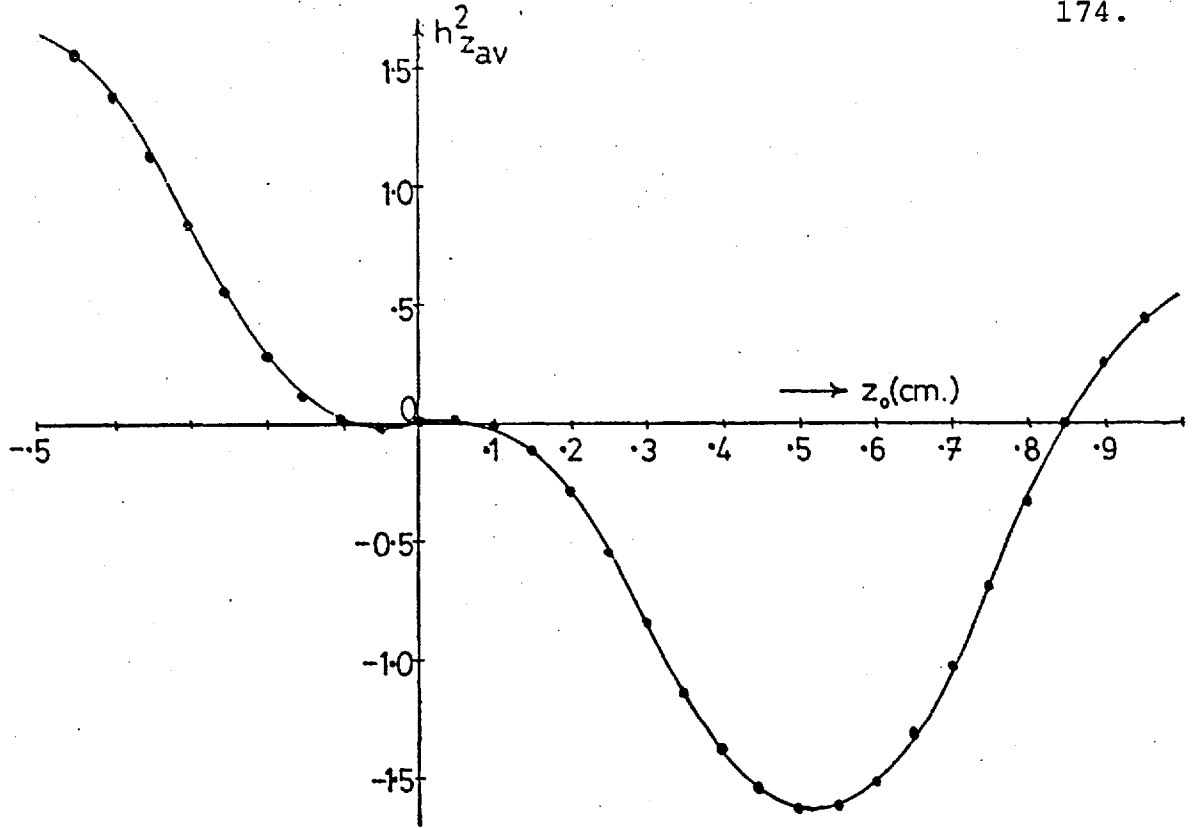


Figure 5.2

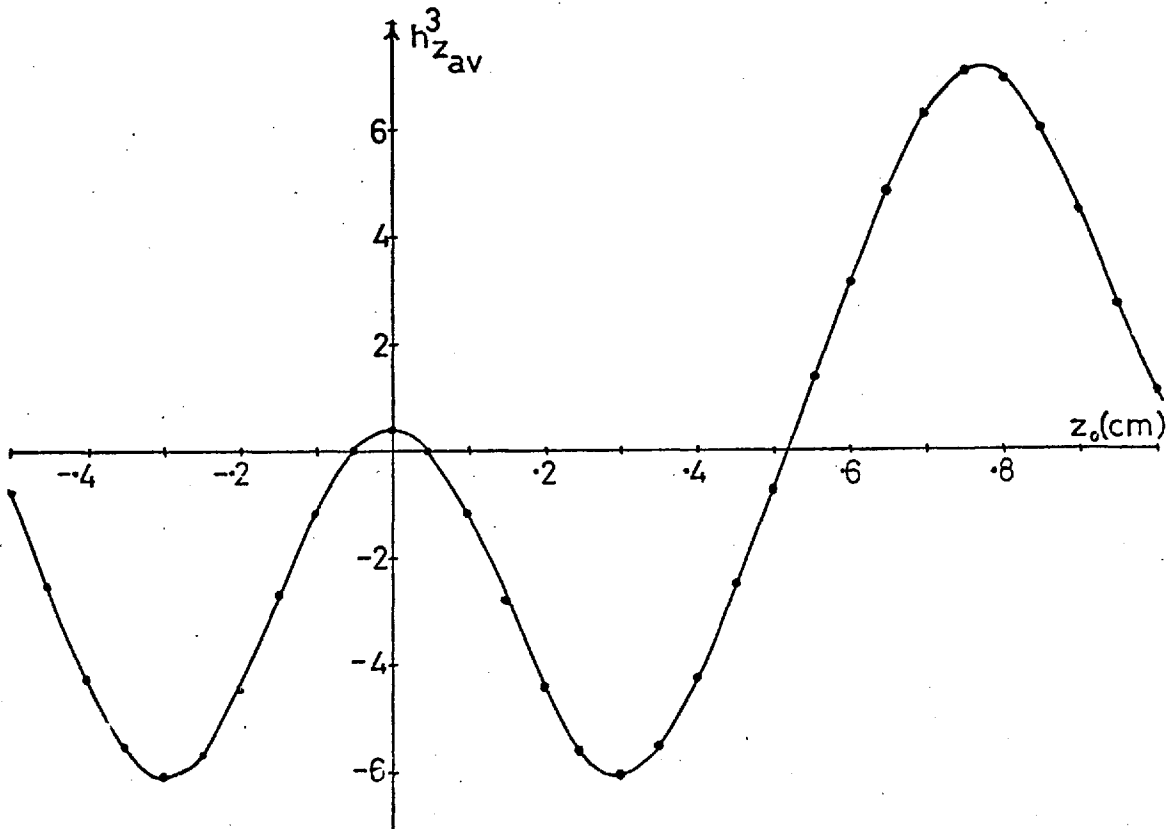


Figure 5.3

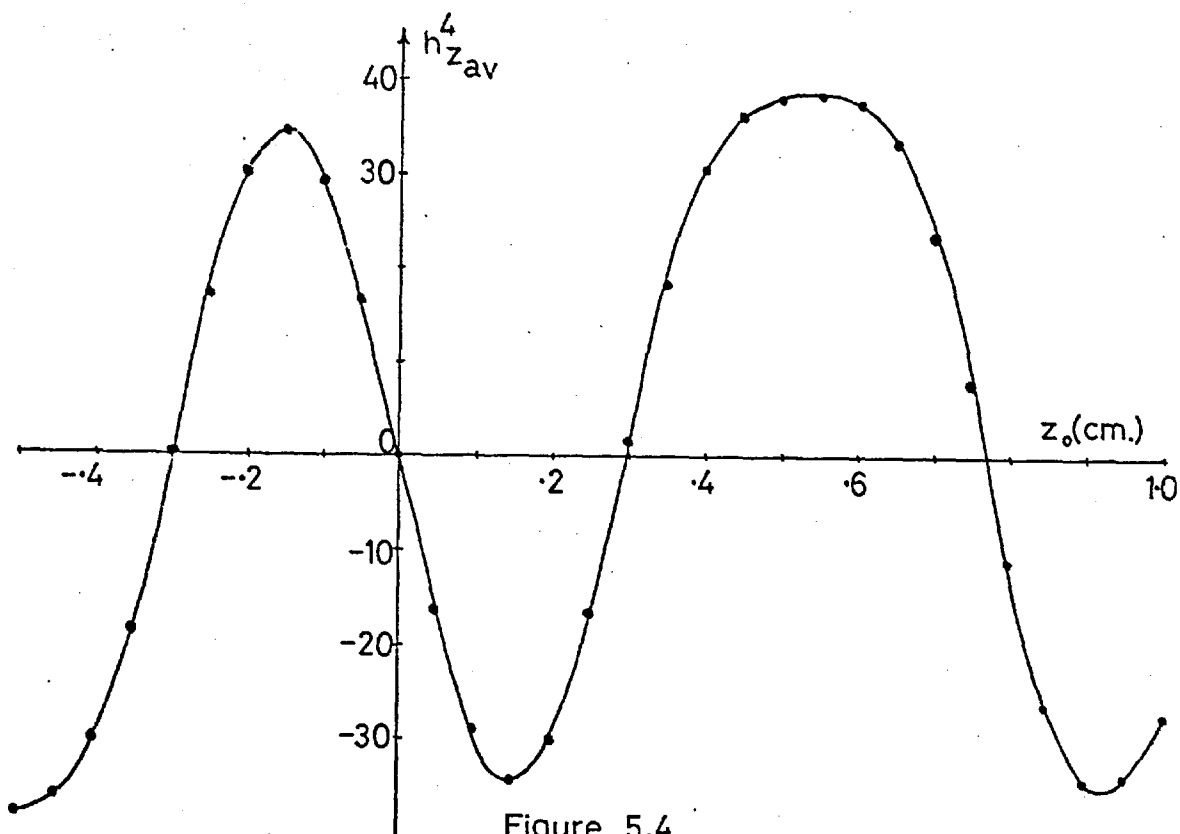


Figure 5.4

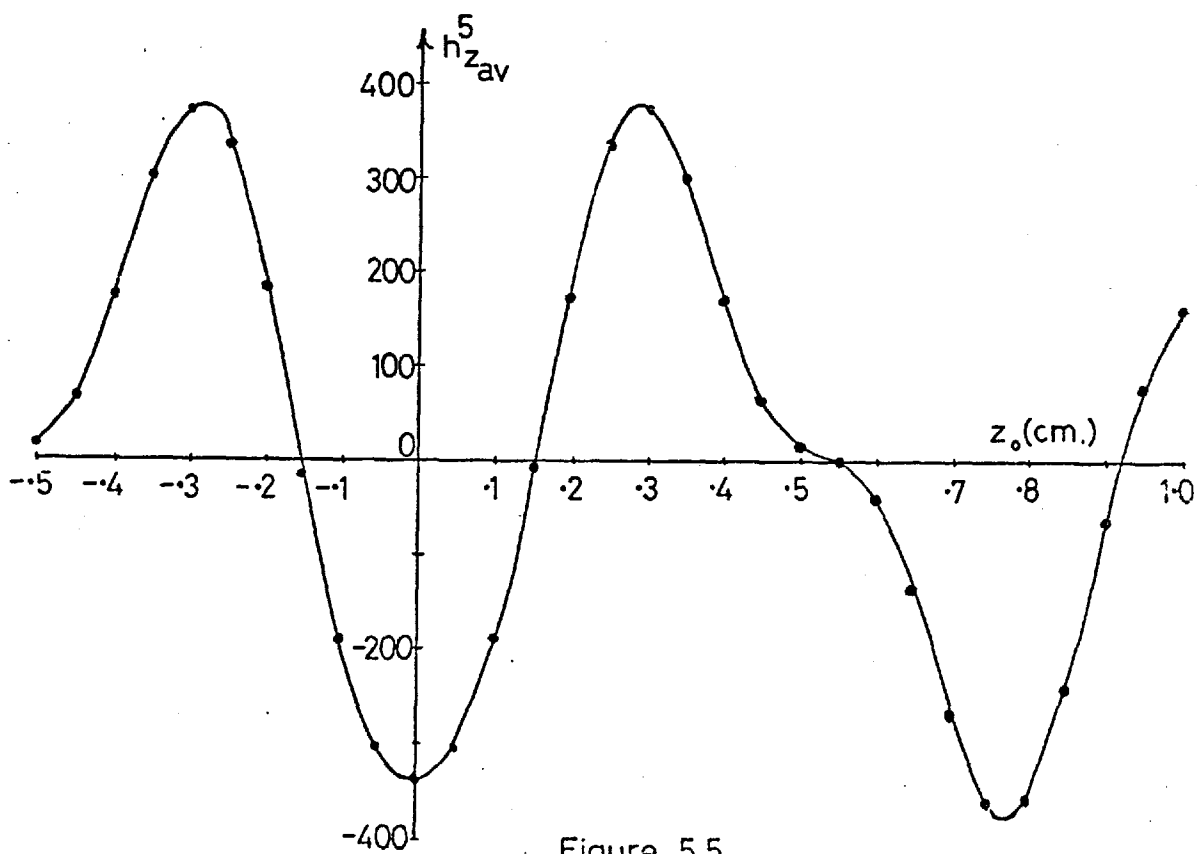


Figure 5.5

of 0.095 cms. The quadrupole was two such dipole coils separated by 0.041 cms and connected in opposite directions while the octupole was made from four equally spaced coils, 0.041 cms apart, connected in the sequence + -- +, where plus represents one direction of winding and minus the opposite direction. A current of 0.1 amp was passed through the coils in each case.

A pure dipole will lead to a signal at $z_0 = 0$ which, from the calibration, can be used to give the magnitude of the dipole moment. A comparison can thus be made between the dipole moment as determined from the apparatus signal and the calculated dipole moment of a coil array, given by;

$$m = n\pi q^2 i / 10$$

where n is the number of turns, q is the coil radius in cms and i amps is the current flowing in the coil. Thus, for a current of 0.1 amp, the dipole moment is $1.98 \cdot 10^{-3}$ emu from this calculation while the signal produced by the coil in the VSM corresponds to a moment of $2.006 \cdot 10^{-3}$ emu.

Pure signals from higher multipoles can be converted to absolute units by the formula

$$Q_l = \frac{l! \epsilon(z_0) \langle h^l(0) \rangle C}{\langle h_z^{l+1}(z_0) \rangle} \quad (V.6)$$

where $\epsilon(z_0)$ is the observed signal strength in apparatus units [the dial setting, K , (Section 3.4.5)] at a given position z_0 and C is the conversion factor for dipoles

Figures 5.6-5.8 : Experimentally obtained curves as our test multipoles are moved through the pick-up coils. Figure 5.6 is for a small single coil representing a dipole moment, figure 5.7 is for two such coils wound in opposite directions to represent a quadrupole moment and figure 5.8 a series of four coils to give an octupole moment. The reference current was 1mA and the values given on the $\epsilon(Z_0)$ axis are the readings of K.

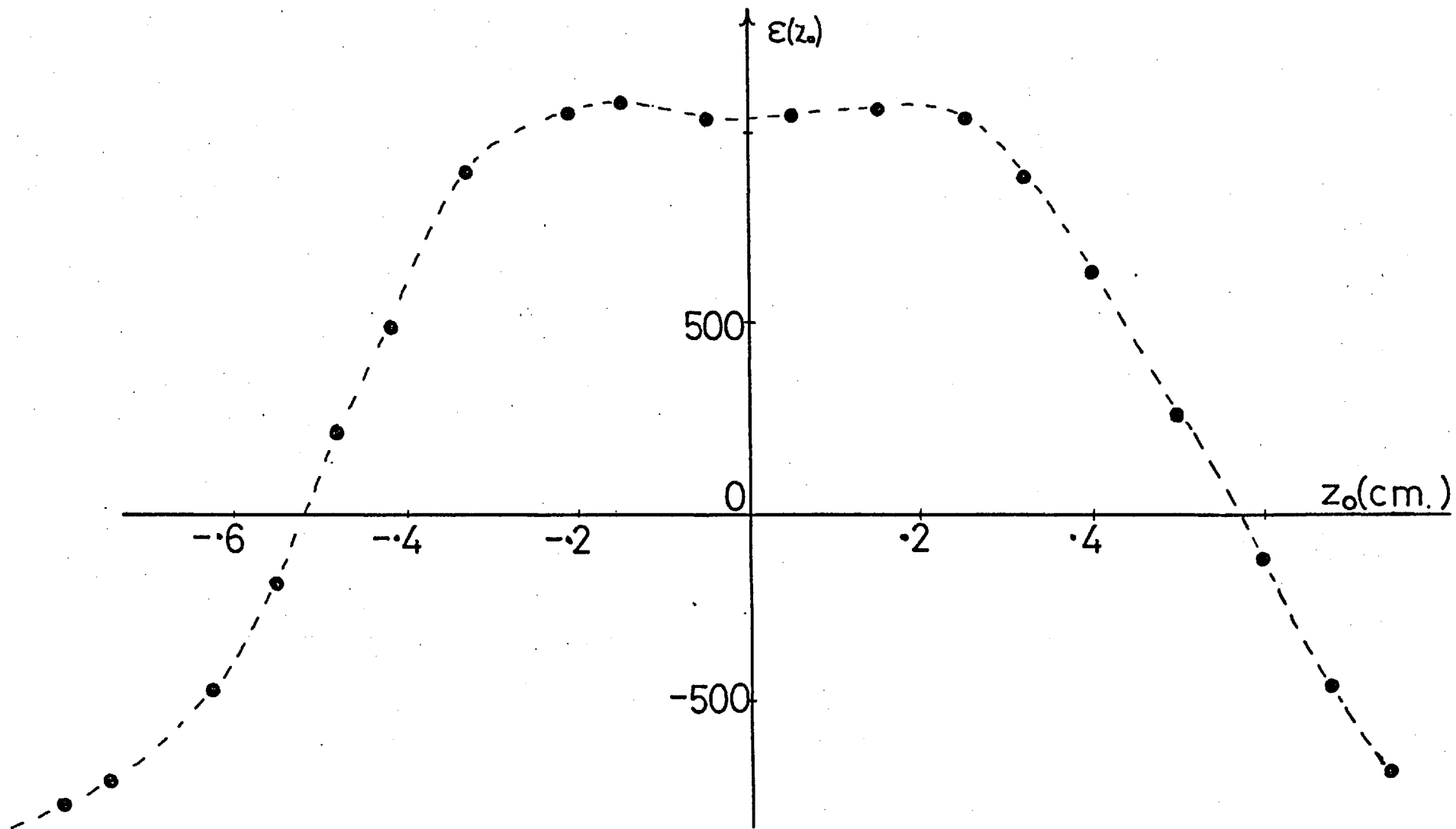


Fig. 56

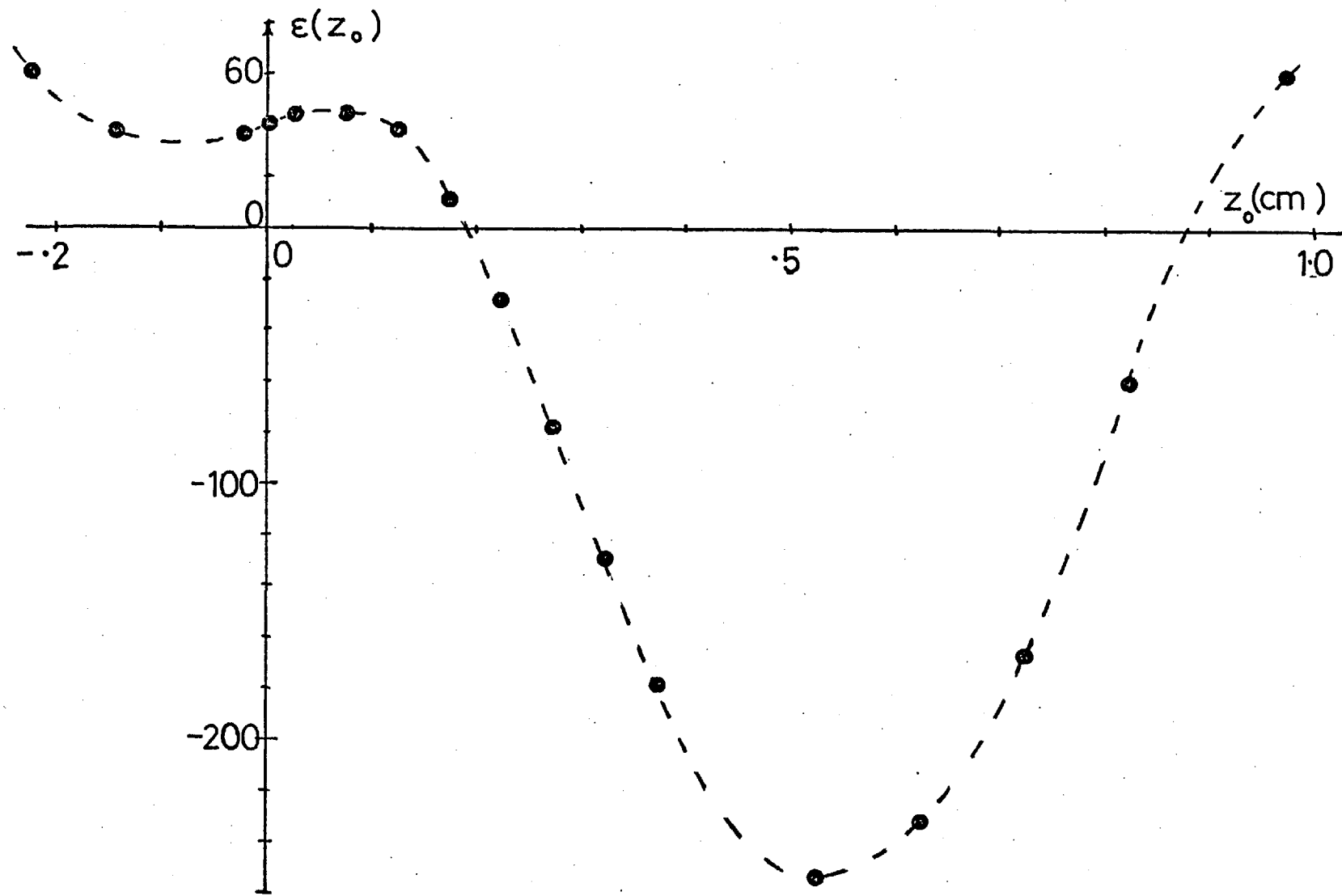


Figure 5.7

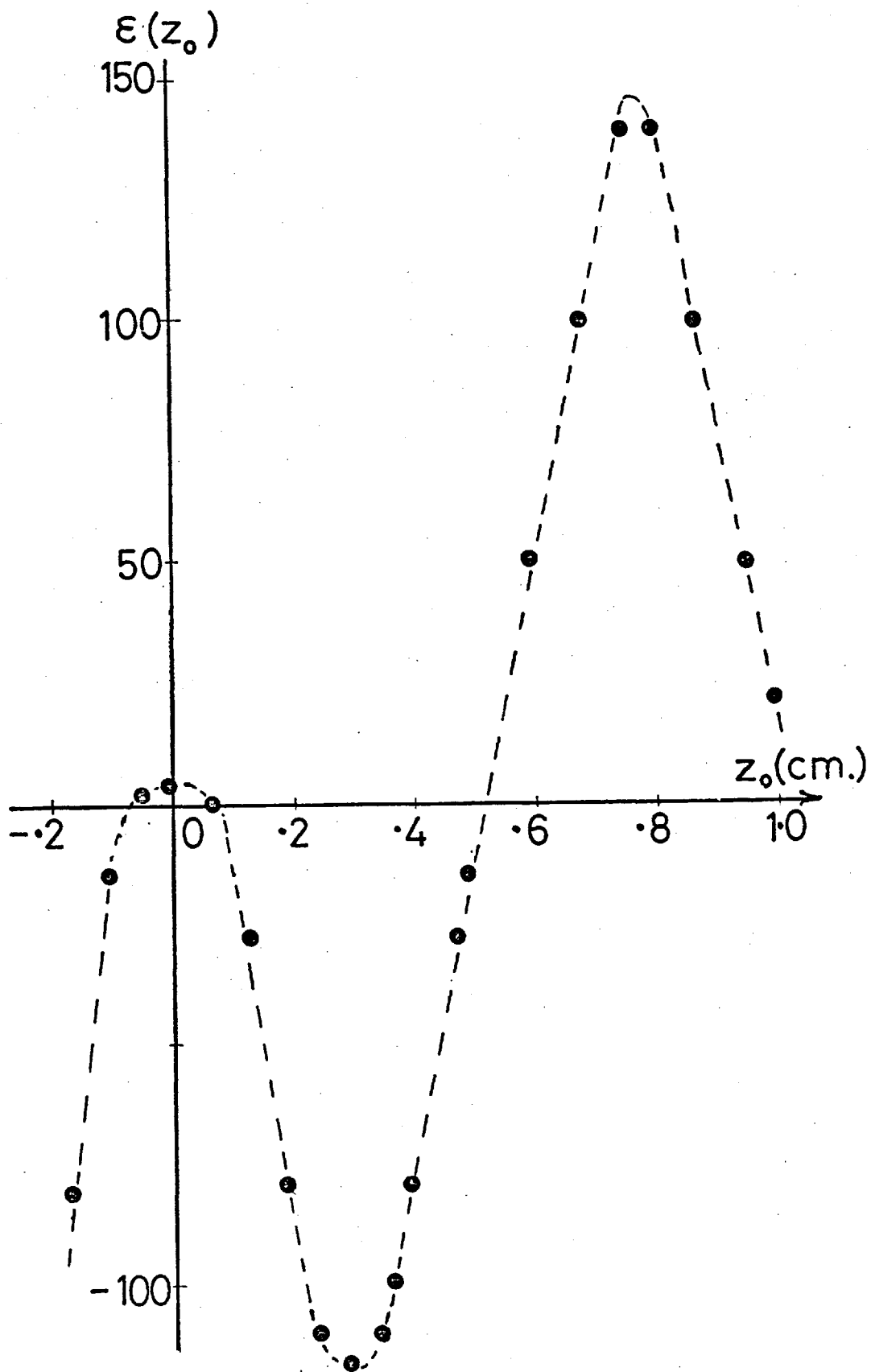


Figure 5.8

between apparatus units and magnetic moment ($= 1.93 \cdot 10^{-6}$). The angular brackets indicate the average value of the field over the sample.

Thus, for the quadrupole and octupole curves (Figures 5.7 and 5.8) we take the position of maximum signal and substitute into Equation (V.6) to obtain the values in brackets in Table 5.1. These are to be compared with the calculated moments for the test coil dimensions, also given in Table 5.1, which are obtained from the formulae

$$\text{Quadrupole moment} = m(2\alpha + \Delta)$$

$$\text{Octupole moment} = 4m(2\alpha + \Delta)^2$$

where 2α is the spacing between the coils and Δ is the coil thickness. For these coils, the seven turns were wound in a single layer and $\Delta = 0.0254$ cms.

TABLE 5.1

	DIPOLE	QUADRUPOLE	OCTUPOLE
Calculated	$1.98 \cdot 10^{-3} \text{ emu}$	$1.315 \cdot 10^{-4} \text{ emu.cm}$	$3.492 \cdot 10^{-5} \text{ emu.cm}^2$
Measured in VSM	$(2.006 \cdot 10^{-3} \text{ emu})$	$(1.332 \cdot 10^{-4} \text{ emu.cm})$	$(3.229 \cdot 10^{-5} \text{ emu.cm}^2)$

Thus, we can see that Figure 5.7 for the quadrupole has the same shape as Figure 5.2 for $h_{z_{av}}^2$ and that Figure 5.8 for the octupole has the same shape as Figure 5.3 for $h_{z_{av}}^3$, as expected from Equation (V.5). These experimental results for the multipoles can be well fitted over the whole range by the appropriate calculated curves, $h_{z_{av}}^{l+1}$,

except for the slight difference in the quadrupole around $z_0 = 0$, which is a small dipolar contribution arising because of the difficulty in winding the two coils exactly the same.

Hence, for this particular pick-up coil geometry, a sample vibrating about the mean position $z_0 = 0$ will produce a signal at the vibration frequency if there is an octupole moment, or higher odd pole, in the sample magnetization. Any misplacement away from the centre will further lead to additional contributions to the signal from the even poles. Thus, we can not relate a signal at $z_0 = 0$ to a dipole moment with any certainty. It should be stressed here that once an external magnetic field is applied the dipolar response to the field is of overwhelming importance and thus the normal magnetization measurements are alright. It is only in the situation where the dipolar magnetization is very small, or zero, that these effects may become important. Remanent signals with extremely low dipolar magnetization are a possible case in question. For such a situation we need to take a plot of the signal variation as the sample position is altered relative to the pick-up coils. These curves then contain the essential information as to the relative contributions from the multipoles present in the sample magnetization. In the following section we present some such plots obtained in our investigation of these ideas and show that the higher pole effects are present in the remanent state signals of certain materials.

5.3. Studies of the Remanent States of Magnetically Ordered Materials

5.3.1. Introduction

All the data presented in this section were obtained on either spherical or disc shaped samples, with a maximum dimension of 2 mm. These restrictions were made in order to eliminate any possible effects of a non-uniform demagnetization field and to ensure that the sample volume moved in a region close to the x-axis where $h_z(x,y)$ was practically constant.

Measurements of $\epsilon(z_0)$ were made in a field of 30 Oe, in all cases, as a check on the possible effects of sample size and shape. This field is sufficient to produce a large uniform magnetization and a comparison between these curves and that of $h_{z_{av}}^1$ would reveal any shape effects in this induced magnetization. In all cases $\epsilon(z_0)$ could be fitted over the measurement range to within $\pm 1\%$ using just $h_{z_{av}}^1$. From this we deduce that the measured $\epsilon(z_0)$ curves obtained from remanent states are not to any significant extent characteristic of a particular specimen shape or size but are characteristic of the internal arrangement of magnetization.

5.3.2. Results for Iron, Nickel and Cobalt

In Figures 5.9, 5.10 and 5.11 we show the curves of $\epsilon(z_0)$, obtained as a function of z_0 , for pure polycrystalline samples of Fe, Ni and Co, respectively, each in the earth's field after previously applying +700 Oe

Figures 5.9-5.11 : Room temperature signal variations as small samples of Fe, Ni and Co, respectively, are moved through the pick up coils. A field of +700 Oe had previously been applied to each sample. The size of the signal for each case is such that 1 on the $\epsilon(z_0)$ axis would be that signal produced at $z_0 = 0$ by a dipole moment of: i) 0.0633 emu/gm for figure 5.9; ii) 0.088 emu/gm for figure 5.10 and iii) 0.12 emu/gm for figure 5.11.

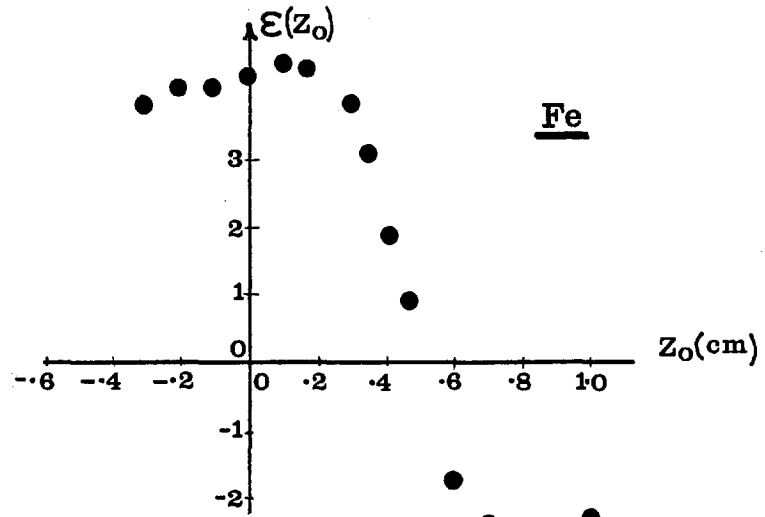


Figure 5.9

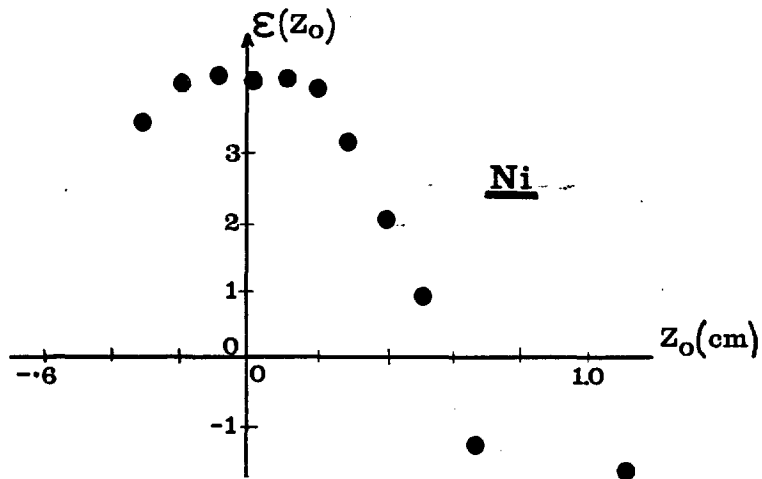


Figure 5.10

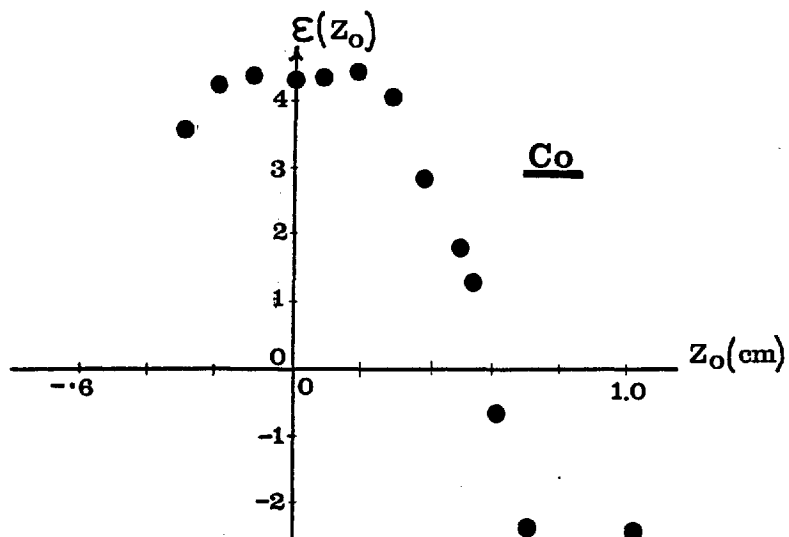


Figure 5.11

to the specimens (+ is an arbitrary notation and represents fields in the same direction as the earth's field). These remanent states are seen to be very nearly dipolar. This, however, is not the case for the remanent states produced by lower reverse fields, in particular, when the material is near the coercive point, the $\epsilon(z_0)$ curve is more complicated, showing clear evidence of higher poles. In Figure 5.12a,b and c we show the data obtained on a spherical sample of Fe with increasing reverse fields, after the initial application of +700 Oe. The dipolar term is reduced by the application of small negative fields until we are left with a more dominant higher pole term which is almost completely reversed after the reverse field has reached 240 Oe. A further increase in this field then results in the dipolar term increasing in the opposite direction to that produced by +700 Oe.

We have, further, examined the $\epsilon(z_0)$ curves produced by the carefully demagnetized states of these materials and have found that there is zero signal for all values of z_0 . This suggests that the higher poles are observed when there is some degree of regularity in the domain structure. After the application of large fields a large fraction of domains are aligned along the z-axis and produce a predominantly dipolar state, while complete demagnetization gives rise to a sufficiently isotropic state for no low order poles to be observed. Between these two extremes we have a state which is partially ordered with respect to the z-axis and this gives rise to higher poles which are clearly

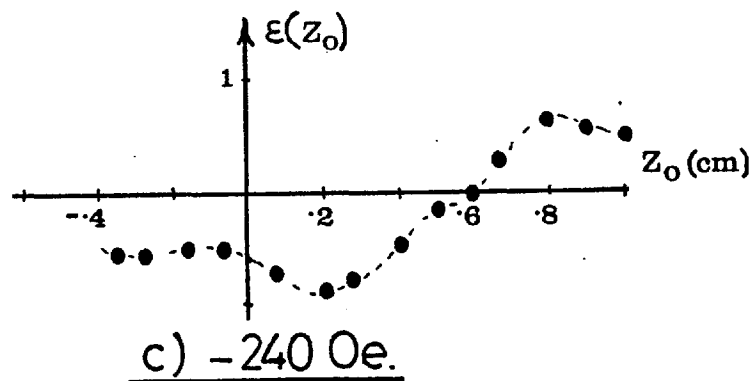
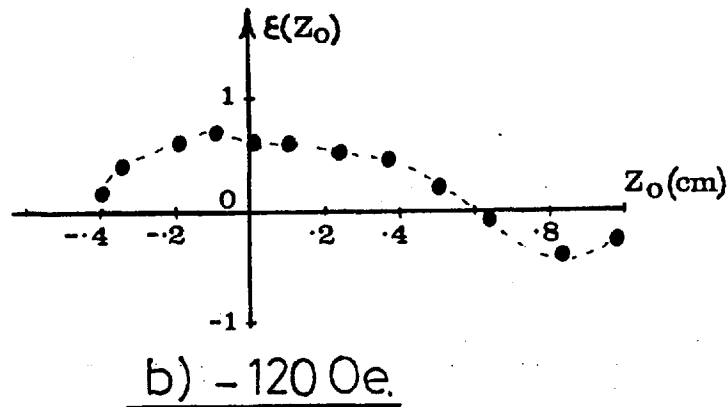
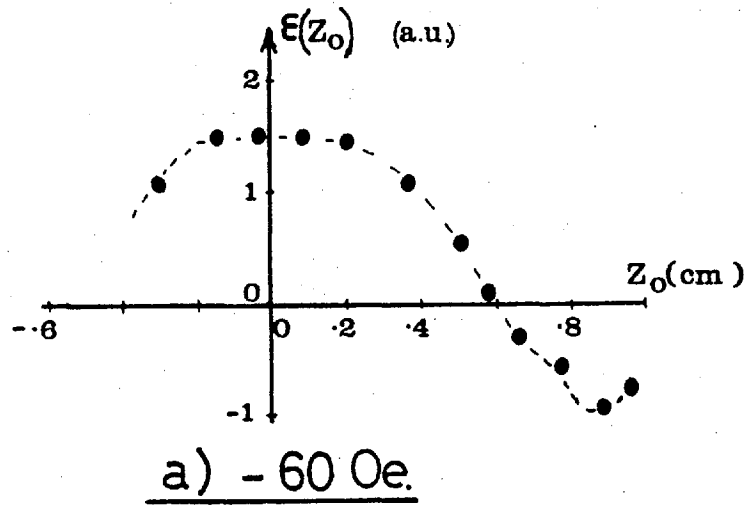


Figure 5.12 : Signal variation as an Fe sample is moved through the pick-up coils, after the previous application of the field shown. 1 on the vertical axis is equivalent to a signal given by a dipole moment of 0.074 emu/gm. at $z_0=0$. These were all at room temperature.

seen in the $\epsilon(z_0)$ curves.

5.3.3. Results on Haematite and Ferrite

Figure 5.13 shows that the remanent state, $\epsilon(z_0)$, curve for a sphere of radio ferrite after the application of +200 Oe is asymmetric about $z_0 = 0$, indicating some quadrupolar contribution. In Figure 5.14 we plot the results for a single crystal of natural, Elba, haematite in the form of a plate. The remanence of the haematite is not affected by the previously applied field for the range of fields available to us. Anisotropy of the remanent state is clearly seen in Figure 5.14a for $c||z$ and Figure 5.14b for $c\perp z$. The former shows a complicated $\epsilon(z_0)$ curve while the latter has a much larger and more nearly dipolar remanence. This haematite specimen has a transition from a canted, high temperature, phase to a collinear antiferromagnetic phase at $220 \pm 5^\circ\text{K}$. A comparison between the curves obtained at 300°K and 77°K (all those discussed above are for room temperature, 300°K) showed that the low temperature state had the main features in it's $\epsilon(z_0)$ variation which were present in the high temperature curves but the values were some ten times lower in the curve taken at liquid nitrogen temperature.

5.3.4. Palladium Alloys

As mentioned at the end of chapter 4, these were the bogus results which started the line of investigation presented in this chapter. We see in figure 5.15 the typical

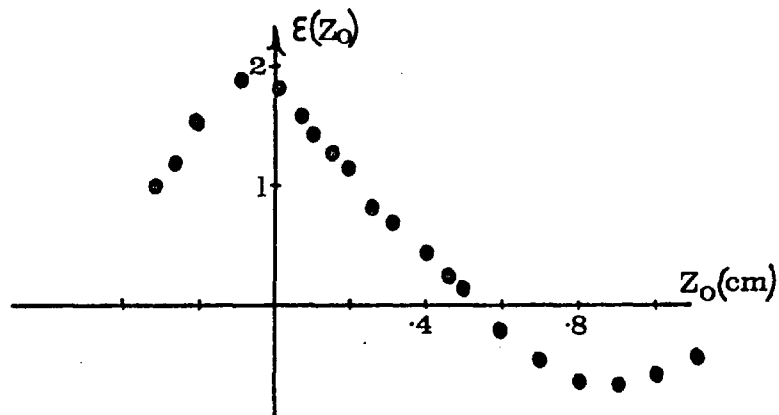


Figure 5.13 : Room temperature signal variation as a function of sample position for a ferrite specimen. 1 on the vertical axis is equivalent to the signal obtained from a dipole moment of 0.02 emu/gm at $z_0=0$.

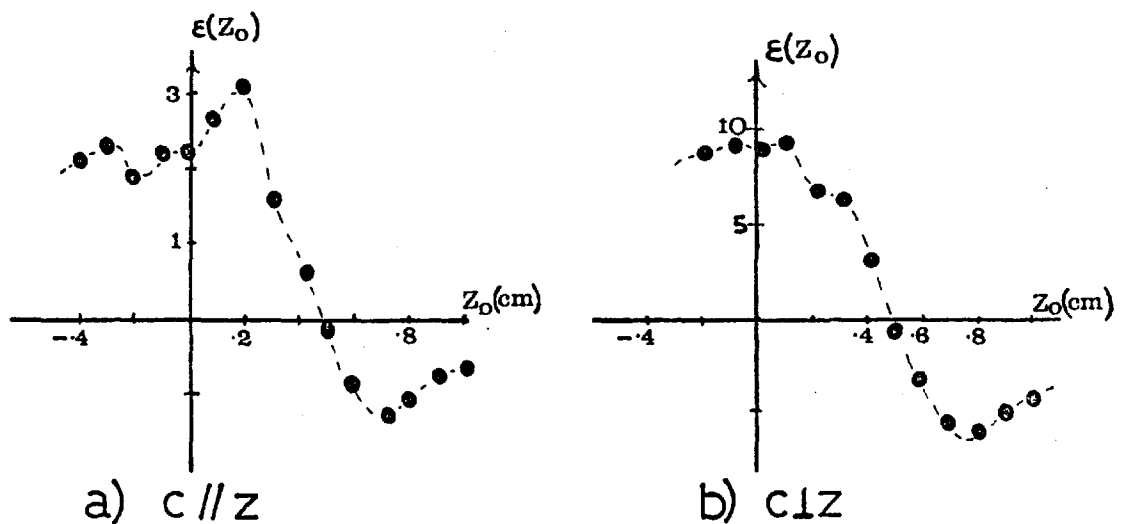


Figure 5.14 : Variation of the room temperature signal as a Haematite specimen is moved through the pick-up coils. A dipole moment of 0.00015 emu/gm would give a signal of 1 on the $\epsilon(z_0)$ axis when positioned at $z_0=0$.

Figure 5.15 : Typical signal variation at 4.2°K as a PdMn specimen is moved through the pick-up coils. Attempted analysis, indicating large 3rd and 5th poles in the multipole expansion, is incorrect as the magnetization was not a truly remanent one.

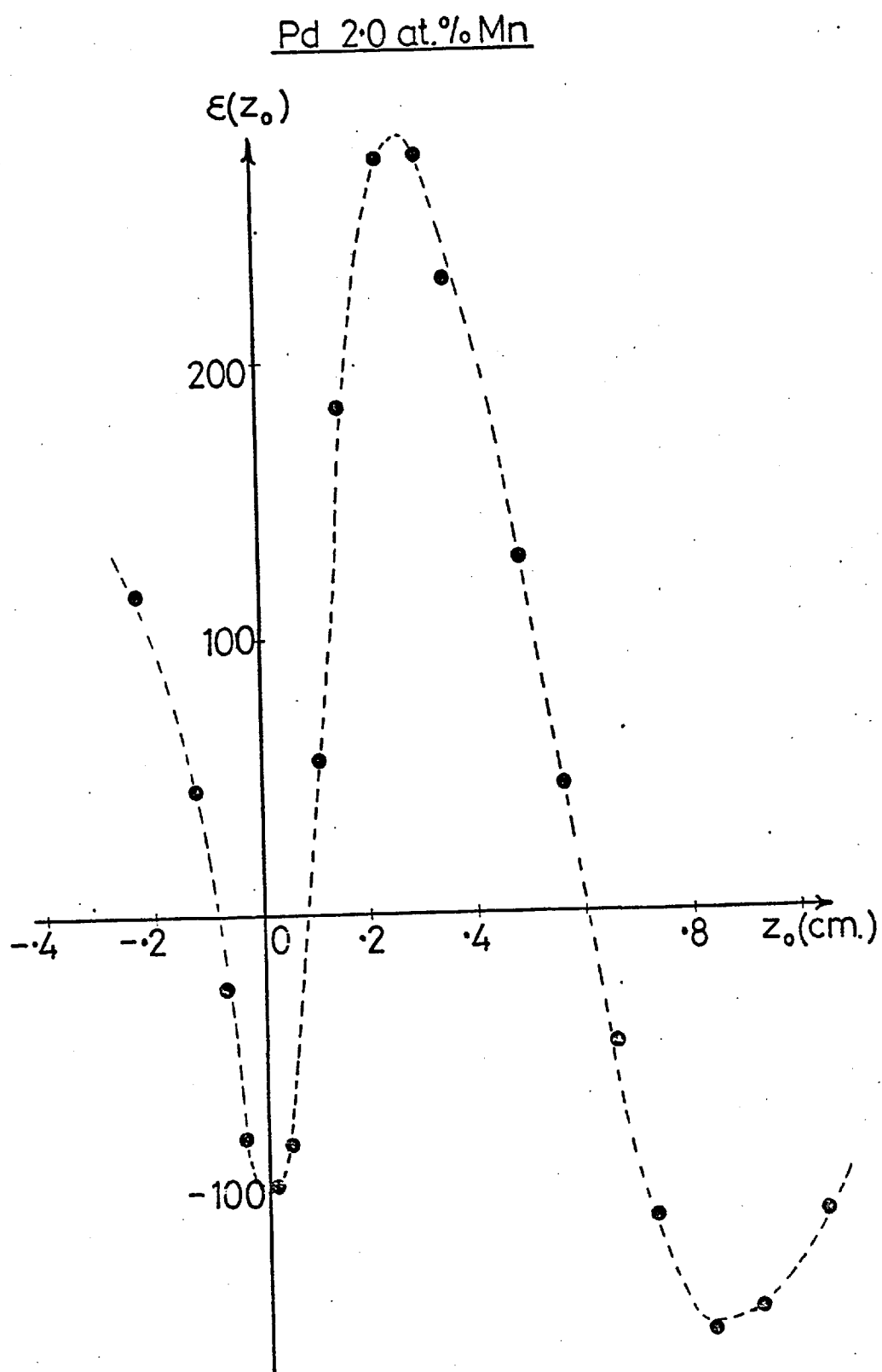


Figure 5.15

sort of signal variation, as a function of Z_0 , originally obtained in the PdMn alloys studied. The curve shown here is for a Pd 2.0 at%Mn specimen at 4.2°K . Now, this looks very much like a combination of high poles, 3rd and 5th mainly, in the multipole expansion and we thought that some unusual circumstance was resulting in their becoming dominant in this system. However, the results obtained for all the PdMn alloys were taken at 4.2°K , or below, and were affected by the stray field produced by the diode leads. When the diode was removed such curves could no longer be repeated; the behaviour showing no noticeable quadrupolar or higher poles to be present in the magnetization (this is not the case for the curves taken in the previous sections, 5.3.3 and 5.3.4 since these were obtained mainly at room temperature).

5.3.5 Discussion

The results of Sections 5.3.2 and 5.3.3 showed that domains in magnetically ordered materials gave rise to higher poles in the remanent state which we could observe directly by use of what has, up until now, been considered an apparatus for the measurement of bulk magnetic properties. This means we have a possible method of observing these more microscopic properties as a function of temperature and field in the same apparatus and at the same time as the measurements of the magnetization are made. This may provide a way of

studying domains in magnetic materials and also since the technique can be applied most conveniently to truly zero field studies, may provide a useful way of studying magnetic phase transitions by observing the changes which occur in the domain structure.

Any sample with a sizeable dipolar remanent magnetization shows a characteristic $\epsilon(z_0)$ variation of the form shown in figure 5.1. When this dipolar signal is reduced towards zero, the possibility of observation of higher pole signals arises. We have seen in sections 5.3.3 and 5.3.4 that such signals become apparent in ferromagnetic materials such as iron when the dipolar magnetization is reduced. The reason why the quadrupolar signal is not larger in the iron sample studied near the coercive point is due to the non-regularity in the size and direction of the domains. If domains of equal size were alternately pointing up and down we should then expect a large quadrupolar signal (see the discussion of the extension of this to alternation on a single spin level, i.e. an anti-ferromagnet, in section 5.5).

In order to make the discussion amenable we restricted the analysis given in section 5.1 to a simplified situation in which only the z component of the magnetization is allowed to vary along the z-axis of the apparatus. In real materials we would seldom encounter such a simplified case and care need be taken in analysing an $\epsilon(z_0)$ curve. We have found

empirically that the cylindrical coil geometry used has some sensitivity to moment variations perpendicular to the Z-axis. This can be readily understood when it is recalled that the sensitivity field \underline{h} must obey the relation $\nabla \cdot \underline{h} = 0$. This leads to relations between higher cross derivatives of the type:

$$\frac{\partial^2 h_z}{\partial z^2} = -2 \frac{\partial^2 h_x}{\partial x \partial z} = -2 \frac{\partial^2 h_z}{\partial x^2}$$

$$\frac{\partial^3 h_z}{\partial z^3} = -2 \frac{\partial^3 h_x}{\partial x \partial z^2} = -2 \frac{\partial^3 h_z}{\partial x \partial x \partial z}$$

These relationships will lead to some ambiguity in the analysis of the $\epsilon(Z_0)$ curves but this problem could be overcome if sample movement along all three axis were possible, allowing plots of (x_0, y_0, Z_0) to be made.

In the following section we restrict ourselves to the simplified situation and discuss a method of analysis of any $\epsilon(Z_0)$ curve to enable numerical information to be obtained about the size of the multipoles in the sample magnetization.

5.4. Numerical Analysis of the $\epsilon(z_0)$ Curves

Since the spatial variation of the signal is just a linear combination of a set of terms related to the magnitude of each multipole in the expansion of the sample magnetization, we should be able to perform an analysis of any general $\epsilon(z_0)$ curve to obtain the relative amounts of these contributions to the total signal. Computationally, this is equivalent to expanding a general vector in terms of a linear combination of basis vectors, where the spatial plots of the field derivatives, $h_{z_{av}}^l$, act as these basis vectors. However, as these functions stand, (Figures 5.1 to 5.5), they are not orthogonal to one another and a deconvolution cannot be uniquely achieved. To overcome this problem, a new set of functions have been formed from the calculated $h_{z_{av}}^l$ functions, but which are orthogonal. These functions, $\phi_1, \phi_2, \phi_3, \phi_4, \phi_5$, are calculated by means of a Gram Schmidt orthonormalization routine and we then make use of a least squares technique to determine the constants in an expansion of the form

$$\epsilon(z_0) = a\phi_1 + b\phi_2 + c\phi_3 + d\phi_4 + e\phi_5 + \quad (V.7)$$

Mathematically, therefore, we have that originally

$$\epsilon(z_0) = Ah_{z_{av}}^1 + Bh_{z_{av}}^2 + \dots \quad (V.8)$$

where A,B, etc are constants related to the magnitude of the appropriate multipole in the sample magnetization. The signal from the higher terms becomes progressively less important so we restrict the analysis to the first five field derivatives for ease of handling. We can, therefore, write Equation V.7 as:

$$\epsilon(z_0) = R\phi \tag{V.9}$$

where $R = (a \ b \ c \ d \ e)$ and $\phi = \begin{pmatrix} \phi_1 \\ \phi_2 \\ \phi_3 \\ \phi_4 \\ \phi_5 \end{pmatrix}$

The Gram Schmidt orthonormalization programme is given in Appendix B2. This programme makes use of a NAG (Numerical Algorithms Group) library file (FO5AAF) and overwrites the five original functions, each split into M equally spaced points over a given region of space (to form the coefficients of an M dimensional vector) by the new, M dimensional, orthogonal vectors. These new vectors are orthogonal over this region of space and so the data for an alloy to be analysed is similarly subdivided into (M-1) regions over this same portion of space. The region over which the analysis was chosen to be carried out was from $z_0 = 0$ to $z_0 = 0.85$ cm, inclusive, taking steps of 0.05 cm. The dimensionality, M, is thus 18 for this particular instance, but can be altered to accommodate data at more frequent intervals or over a wider region if necessary

This Gram Schmidt programme need be used only once to determine the functions ϕ_1 to ϕ_5 . These functions are then incorporated into the least squares procedure programme, given in Appendix B.3, which is used to determine the elements of the matrix, R, in Equation V.9. In particular, this programme has been used on the functions $\epsilon(z_0) = h_{z_{av}}^1$, $\epsilon(z_0) = h_{z_{av}}^2$, etc to determine the elements of the matrices R_1 to R_5 , defined as follows;

$$\begin{aligned}
 h_{z_{av}}^1 &= (a_1 \quad b_1 \quad c_1 \quad d_1 \quad e_1) \phi = R_1 \phi \\
 h_{z_{av}}^2 &= (a_2 \quad b_2 \quad c_2 \quad d_2 \quad e_2) \phi = R_2 \phi \\
 h_{z_{av}}^3 &= (a_3 \quad b_3 \quad c_3 \quad d_3 \quad e_3) \phi = R_3 \phi \\
 h_{z_{av}}^4 &= (a_4 \quad b_4 \quad c_4 \quad d_4 \quad e_4) \phi = R_4 \phi \\
 h_{z_{av}}^5 &= (a_5 \quad b_5 \quad c_5 \quad d_5 \quad e_5) \phi = R_5 \phi
 \end{aligned} \tag{V.10}$$

These values were determined to be;

$$\begin{aligned}
 a_1 &= 1.2747 & b_1 &= c_1 = d_1 = e_1 = 0 \\
 a_2 &= -0.0766 & b_2 &= 0.41511 & c_2 &= d_2 = e_2 = 0 \\
 a_3 &= -0.14507 & b_3 &= -0.0265 & c_3 &= 0.12157 & d_3 &= e_3 = 0 \\
 a_4 &= -0.02608 & b_4 &= -0.08915 & c_4 &= -0.0273 & d_4 &= 0.0598 & e_4 &= 0 \\
 a_5 &= 0.03599 & b_5 &= -0.00212 & c_5 &= -0.0929 & d_5 &= -0.01372 & e_5 &= 0.0229
 \end{aligned}$$

Now, substituting Equation V.10 into Equation V.8 we obtain

$$\epsilon(z_0) = AR_1 \phi + BR_2 \phi + CR_3 \phi + DR_4 \phi + ER_5 \phi \tag{V.11}$$

which with Equation V.9 leads to the required solutions for A,B,C,D and E.

5.5 Sublattice Magnetization Measurements

The determination of the ordered atomic moment in a ferromagnet from bulk measurements depends implicitly on the principle of superposition of electromagnetic fields. If we apply the same principle to a single crystal of an antiferromagnet we are then led to the conclusion that a macroscopic effect should be observed due to the superposition of the fields produced by each cell in the magnetic structure.

Consider the hypothetical layer antiferromagnet, shown in figure 5.16, in which the atomic moment is M and successive layers of N spins are aligned parallel and antiparallel to the Z -axis. If the separation between layers is α and the moment at each site ' i ' is considered to be a point dipole, then the induced emf in the VSM will be (from equation V.4),

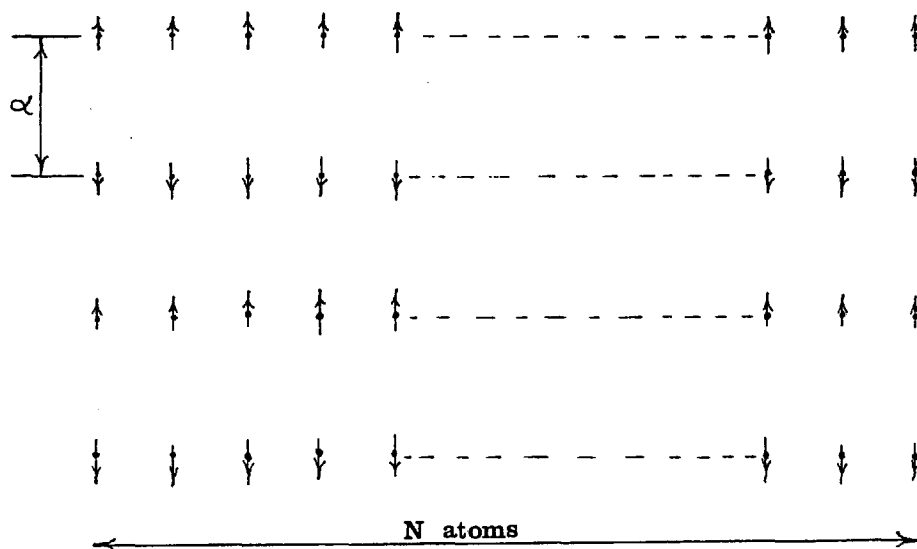


Figure 5.16

$$\epsilon = -a\omega N \sum_{i=0}^{K-1} (M_i) \left(\frac{\partial h_z}{\partial z} \right)_{z=z_0} + \sum_{i=0}^{K-1} (M_i) i\alpha \left(\frac{\partial^2 h_z}{\partial z^2} \right)_{z=z_0} + \dots$$

where we have a total of K layers of N spins along the z -axis. In a macroscopic specimen the two sublattices, 'i' and 'i+1' exactly cancel the z component of magnetization so that the first term is zero leaving just the quadrupole and higher terms. The sum over K layers of the second term gives;

$$N \sum_{i=0}^{K-1} M_i (i\alpha) = \frac{1}{2}(K-1)N|M|\alpha$$

This result can be seen to be correct from the following argument; each pair of sublattices $i, i+1$ forms a quadrupole of strength $Nm\alpha$ and each pair gives an induced signal proportional to $h_{z_{av}}^2$ so that in a region of the sensitivity field where this derivative is slowly varying the contribution from all the pairs of sublattices add constructively to give the total signal shown above. If we suppose that the substance has a cubic chemical symmetry with a repeat of 5\AA and the magnetic repeat along z of 10\AA then for an atomic moment of 1 the quadrupole moment

$$\frac{1}{2}(K-1)N|M|\alpha = \frac{V|M|}{2a^2} = 1.5 \cdot 10^{-8} \text{ emu cm}$$

for a sample volume of $V = 8 \text{ mm}^3$. With the VSM the noise equivalent quadrupole moment is $2 \cdot 10^{-7} \text{ emu cm}$ and thus such a signal could not be detected.

However, the possibility exists to use the much higher sensitivity available from a SQUID magnetometer (see Section 3.3.3). If we assume we have a single turn coil of area 1 cm^2 forming the external coil of a flux transformer we can calculate the flux through the signal coil of a SQUID system. The flux through this coil due to the same volume of the antiferromagnet considered above is;

$$\phi = \sum_i NM'_i \left[h_z + (i\alpha) \left(\frac{\partial h_z}{\partial z} \right)_{z = z_0} + \dots \right]$$

where the sample centre is at z_0 .

Again the first term is zero leaving only the quadrupole and higher terms. Using the same numerical values as above we obtain the 'quadrupole flux'

$$\begin{aligned} \phi_{\text{quad}} &= \frac{1}{2} (K-1) N |M| \alpha \left(\frac{\partial h_z}{\partial z} \right)_{z = z_0} \\ &= 1.5 \cdot 10^{-8} \left(\frac{\partial h_z}{\partial z} \right) \text{ gauss cm}^2 \end{aligned}$$

The maximum gradient of the sensitivity field is at $z_0 = r/2$ (where $r =$ the coil radius) with respect to the coil centre, thus for the one turn coil we have a 'quadrupole flux' of

$$\phi_{\text{quad}} = 1.5 \cdot 10^{-8} \frac{-3\pi}{r^2 \cdot (1.25)^{5/2}} = 2.54 \cdot 10^{-7} \text{ gauss cm}^2$$

This is just over one flux quantum ($\phi_0 = 2.068 \cdot 10^{-7}$ gauss cm²). This has to be compared with the dipoles response at finite temperatures to any residual field trapped in the region of the pick-up coils. If we suppose the specimen has a susceptibility of 10^{-6} emu then the 'dipolar flux' will be

$$\phi = h_z m = \chi H h_{z=\frac{1}{2}r} = 7.2 \cdot 10^{-6} \text{ gauss cm}^2$$

for a trapped flux of 1 Oe.

Clearly to resolve the quadrupole term the trapped flux must be kept small. Improvement in resolution could also be obtained by using an astatic pair of coils which would make h_z zero at $z_0 = r/2$ and increase the derivative term h'_z .

Two types of measurement could be made in this way. The first would be to keep the sample in a fixed position and change the temperature through the Neel point. The second would be more analogous to the VSM measurements, i.e. to move the sample slowly through the coils at a

fixed temperature and to record the flux change as a function of position. This will result in curves which could then be analysed in a similar way to that described in section 5.4.

Guy et al. (5.2) have recently shown that a SQUID magnetometer can indeed be used to directly observe the sublattice magnetization of an antiferromagnet. They were able to pick up a significant quadrupolar signal from a single crystal of MnF_2 and decompose the $\epsilon(Z_0)$ variation obtained into a dipolar contribution and a quadrupolar contribution.

In conclusion, therefore, the work dealt with in this chapter on the possible observation of non-uniformities in the magnetization of samples by means of the VSM and the extension of these ideas to the use of a more sensitive SQUID system have been shown to provide a technique for a future study of anti-ferromagnetic materials and domain structures in ferromagnetic or spin glass alloys.

REFERENCES

- 5.1. ZIJLSTRA H.
Experimental Methods in Magnetism, Vol. I,
(Amsterdam, North Holland), (1967).
- 5.2. GUY C.N., STROM-OLSEN J.O. and COCHRANE R.W.
Submitted to Phys. Rev. Letts.

CHAPTER 6

6.1 Introduction

In this chapter we include a mixture of results obtained on several systems at various times throughout the course of this thesis. These measurements of the low field susceptibilities of a CuMn alloy, several PdFe and PdCo alloys and a couple of PtNi alloys served to investigate certain aspects related either to spin glass properties or to the investigation of the PdMn system. As a result, each in itself is not meant to be a comprehensive discussion of the chosen system but an aid to further elucidate certain points either discussed in section 4.2 or section 4.1.3.

One of the major motivations for initially starting this present low field work was that in 1974 the great effort in the spin glass field was just about taking off and it was still not clear whether the sharp cusps in the a.c. susceptibility were an artefact of the a.c. type of measurement or not. We thus set out to check on systems known to give this behaviour in an a.c. type of measurement by means of our d.c. apparatus.

6.2 Copper Manganese

Dilute alloys of Copper Manganese have been studied extensively (6.1). Manganese atoms in copper display a local moment corresponding to a spin of 2 with $g = 2$ (6.2) and microscopic measurements such as esr and NMR have indicated that both ferromagnetic and antiferromagnetic

interactions between the Mn moments occur (6.2). This is due to the RKKY polarization of the conduction electrons around each Mn moment (see section 1.3.2) and measurements of the bulk properties of dilute CuMn alloys such as the magnetic susceptibility (6.3), resistivity (6.4) and specific heat (6.5), have all been explained in terms of a long-range interaction between the impurities.

Early studies of the susceptibility of CuMn alloys by Owen et al. (6.6) and Kouvel (6.7) gave broad maxima as a function of temperature and the theory by Klein and Brout (6.8) (section 1.4.1) dealing with the statistical mechanics of these dilute alloys was able to explain the $\chi(T)$ results and also the low temperature specific heat results. However, following the discovery that the low-field a.c. susceptibility of certain AuFe alloys exhibited a sharp peak as a function of temperature (Cannella et al. (6.9)) a similar behaviour was found for CuMn alloys, Cannella (6.10). Copper Manganese is now one of the archetype examples of spin glass systems which have been the source of great theoretical attention since the discovery of Cannella et al. (6.9) (see section 1.4.3.).

Cannella (6.10) reported measurements of the a.c. susceptibility of CuMn alloys with 1, 5, 9 and 10 at%Mn and showed that $\log T_g \propto \log C$, where T_g is the glass transition temperature obtained from the peak in the a.c. susceptibility versus temperature curves and C is the concentration of manganese. He further showed that the peak in the more concentrated alloys was considerably rounded in the unannealed (cold worked) state and that

it was only after annealing that the sharp, cusp-like peak in $\chi(T)$ was obtained.

In figure 6.1 we show the low-field d.c. susceptibility of a Cu 2.0 at%Mn alloy. The temperature at which the susceptibility of the annealed alloy peaks is $16.4 \pm 0.2^\circ\text{K}$; this being in good accord with the results of Cannella (6.10). Plots of $\frac{1}{\chi}$ versus temperature for these two curves are shown in figure 6.2. The results for the annealed alloy are linear right down to the temperature of the peak in $\chi(T)$, within the temperature range measured (up to 54°K), while the unannealed specimen shows a deviation from linearity below about 24°K . From the linear portions of these plots the paramagnetic Curie temperature, θ_p , and the effective moment, p_{eff} , have been calculated. Upon annealing, θ_p decreases from 3.5°K to 1.45°K while p_{eff} decreases slightly from 5.61 to 5.49, which is consistent with the occurrence of short range order in the unannealed alloy. Sato et al. (6.11) found evidence from neutron diffraction studies of short range ordering even in dilute CuMn alloys and they discuss the sensitive nature of the magnetic properties to this ordering.

Below the spin glass freezing temperature, Guy (6.12) has reported a shoulder, occurring at approximately $0.6 T_g$, in the low-field d.c. susceptibility of relatively dilute AuFe alloys. Sarkissian (6.13) has also reported a similar behaviour for a ScGd alloy. We see from figure 6.1 that there is a definite shoulder in the $\chi(T)$ curve for the annealed CuMn alloy, the shoulder occurring at

Figure 6.1 : Temperature dependence of the susceptibility of a Cu 2.0 at%Mn alloy as cast (○) and after a heat treatment of 750°C for 17 hours followed by a water quench (●).

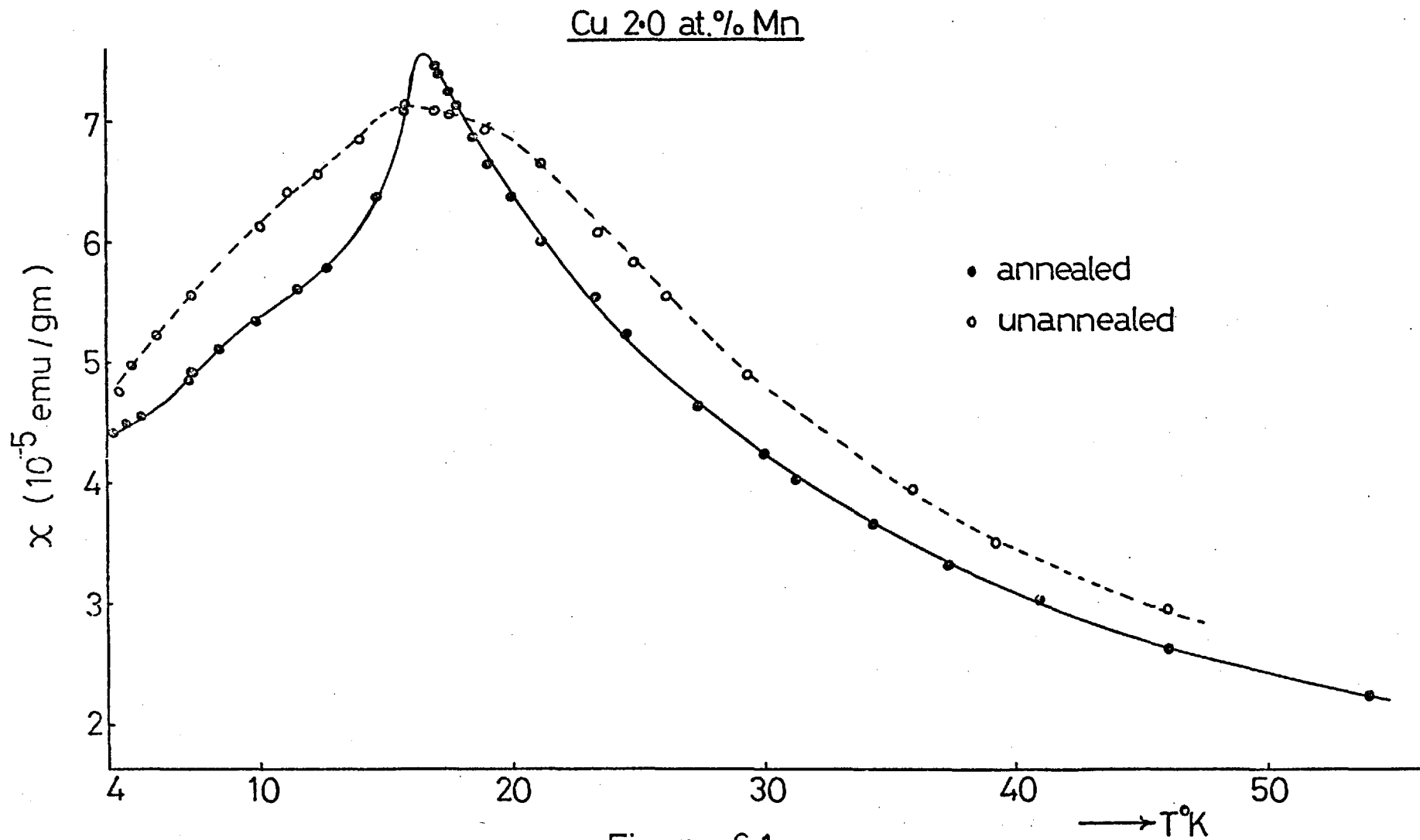


Figure 6.1

Figure 6.2 : Inverse susceptibility versus temperature for the Cu 2.0 at%Mn specimen. For the as cast alloy (O) we obtain $\theta_p = 3.5^\circ\text{K}$ and $p_{\text{eff}} = 5.61$ while after annealing (●) we obtain $\theta_p = 1.45^\circ\text{K}$ and $p_{\text{eff}} = 5.49$.

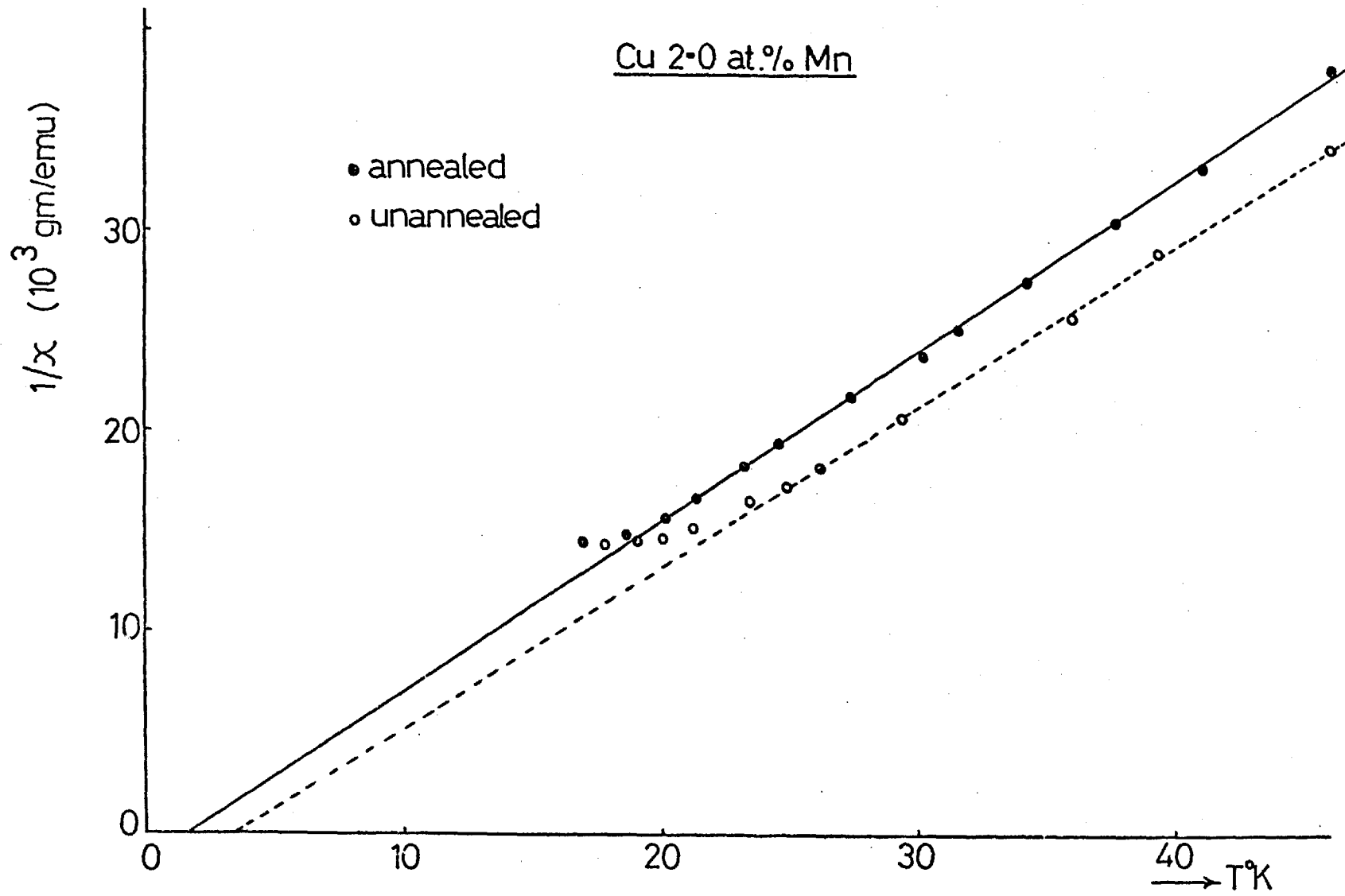


Figure 6.2

about 9°K , but no evidence of this is seen in any of the a.c. susceptibility measurements reported by Cannella (6.10). It is not clear what causes this shoulder but it is most probably due to some characteristic change in the viscous nature of the spin glass which, because of the additional time over which the d.c. measurement is made compared with the a.c. method, becomes more apparent in the d.c. apparatus.

6.3 Palladium Iron and Palladium Cobalt

6.3.1 Results

Both PdFe and PdCo are giant moment systems similar to PdMn, the difference being that at higher solute concentrations the direct interactions between impurity moments are ferromagnetic in these two systems compared with the situation in PdMn, where the Mn-Mn interaction is antiferromagnetic. Ferromagnetism has been reported in PdFe and PdCo alloys down to very low concentrations; 0.01 at%Fe (McDougald and Manuel (6.14)) and 0.1 at%Co (Bozorth et al. (6.15)). However, these results were obtained from high field magnetization measurements and, as we know from the example of PdMn, a spin glass phase can be made to look ferromagnetic when large fields are used. In these giant moment systems we expect a spin glass phase to occur at the very dilute solute concentration end, before ferromagnetism sets in at a concentration high enough to give an infinite chain of neighbouring giant clouds. Chouteau and Tournier (6.16) report evidence for the loss of ferromagnetism below 0.1 at%Fe in PdFe

alloys, but again from high field work, so we have looked at the low field magnetization of dilute alloys by using the Vibrating Sample Magnetometer.

In figure 6.3 we show the magnetization, in an increment of 2.0 Oe (above the earth's magnetic field, the difference of the two readings being taken), for a Pd 0.2 at%Fe alloy in the unannealed state and after heating at 750°C for 18 hours and quenching. The unannealed alloy shows a peak at $2.2 \pm 0.15^\circ\text{K}$ and exhibits time dependent magnetization below this peak while the annealed alloy behaves more ferromagnetically, with a transition temperature of $3 \pm \frac{1}{2}^\circ\text{K}$. This indicates that at this low concentration the disordered alloy is just ferromagnetic but that due to competing antiferromagnetic interactions, arising from the oscillatory nature of the RKKY interaction, we have a complicated situation which is rather dependent on the impurity distribution. The as melted alloy will have some inhomogeneity which leads to spin glass ordering.

From the M-H curves, figure 6.4, we see that the magnetization is essentially reversible, i.e. no large dipolar remanent magnetization occurs. This is very similar to the situation found in the PdMn alloys and the discussion given in section 4.1.3 concerning the unusually small value of the coercivity is also relevant here.

The resistivity of a carefully annealed Pd 0.2 at%Fe alloy was also measured, figure 6.5, from which we can see the large temperature range over which the ordering

Figure 6.3 : Low field magnetization ($\Delta H = 2.0$ Oe) for a Pd 0.2 at%Fe disc. Before annealing, (O) the variation with temperature shows a peak at $\sim 2.2^\circ\text{K}$ with time effects below this temperature while upon annealing at 750°C for 18 hours (●) the magnetization then shows a more ferromagnetic behaviour.

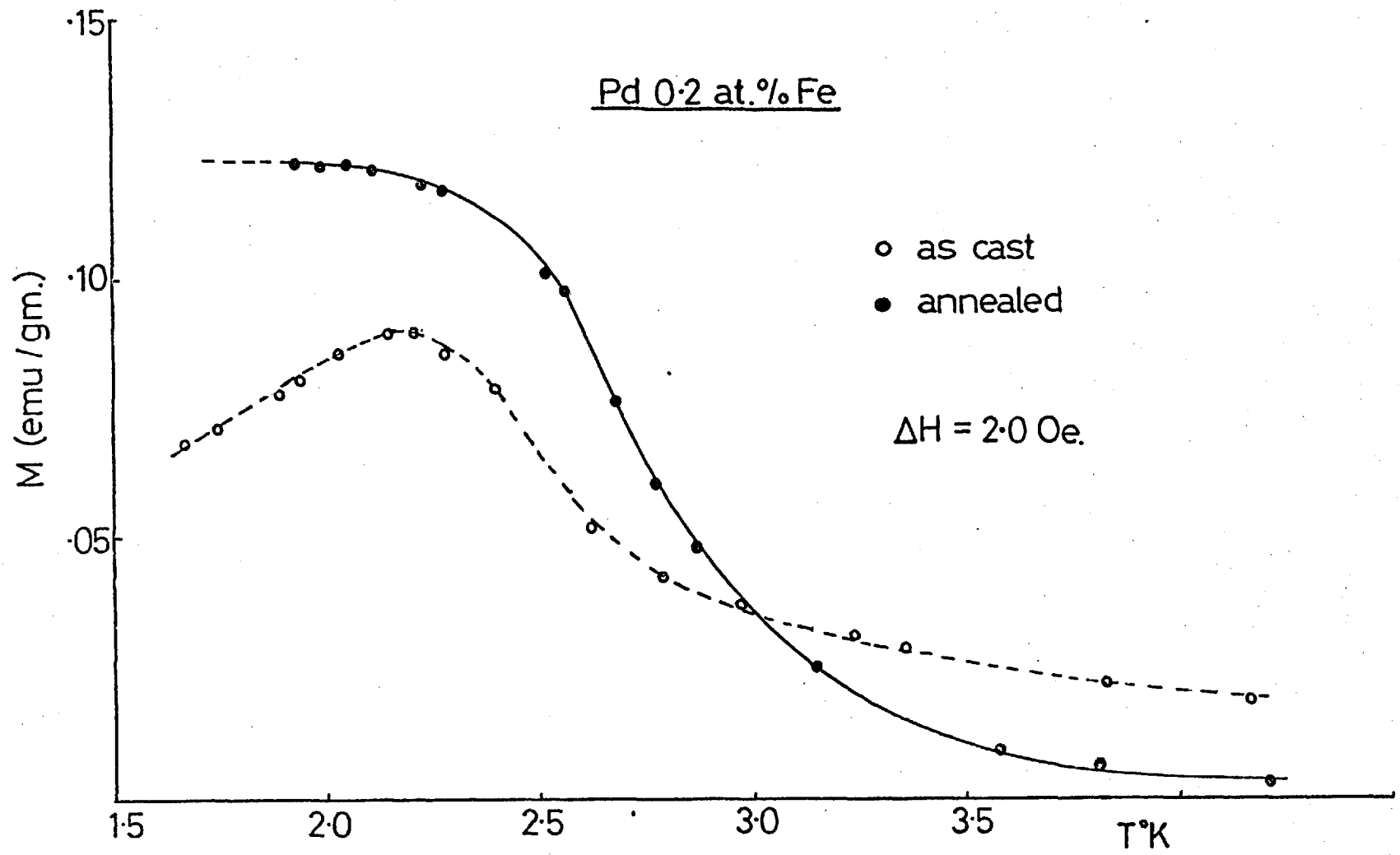


Figure 6.3

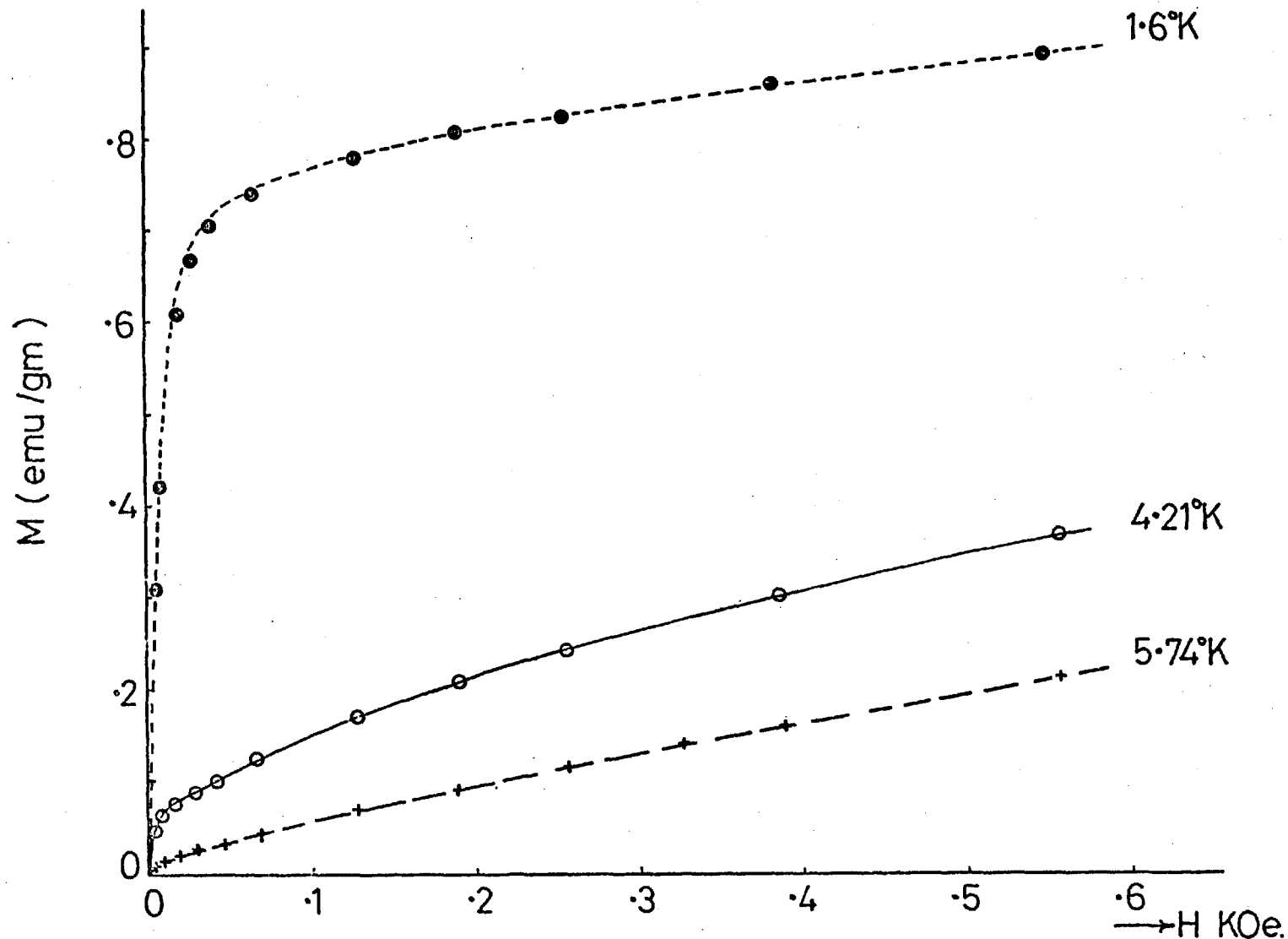


Figure 6.4 : Field dependence of the magnetization for a thin disc Pd 0.2 at.% Fe specimen.

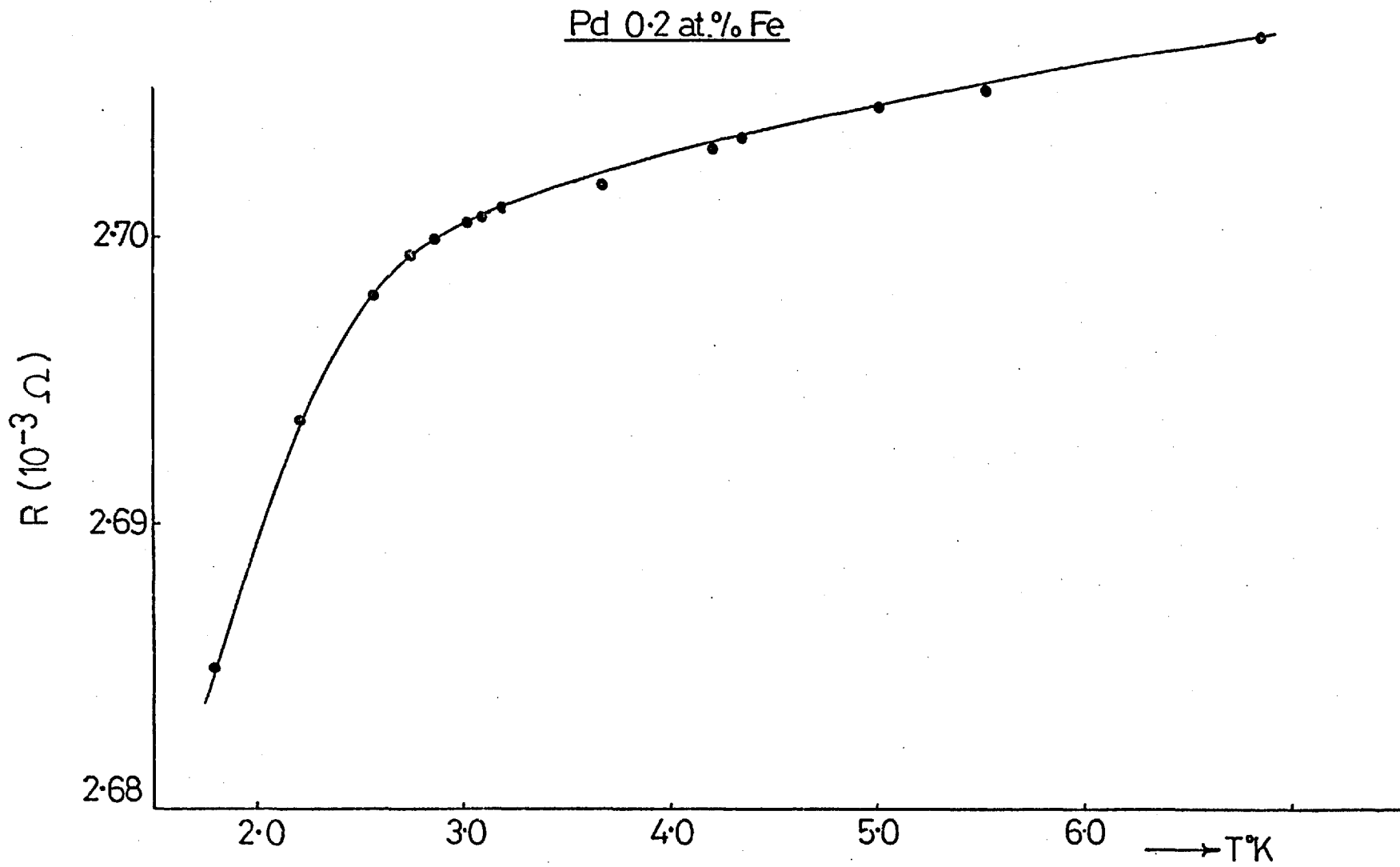


Figure 6.5 : Resistance of a Pd 0.2 at.% Fe sample plotted against temperature.

occurs, in agreement with the broad magnetization versus temperature curve; indicative of the fact that this is not wholly analogous to a standard ferromagnetic transition with a cooperative freezing of the moments parallel to one another at a unique temperature but that rather we have a situation where there is some spread of impurity-impurity interaction strengths and a corresponding spread of temperatures at which neighbouring giant clouds lock ferromagnetically.

The M versus T curve for an annealed disc of Pd 1.5 at%Fe, figure 6.6, shows that the magnetization has reached the demagnetization limit and from the sharp rise we determine a transition temperature of $52 \pm 2^{\circ}\text{K}$. The results before annealing show the same behaviour, indicating that at this concentration ferromagnetism is not so crucially dependent on the solute distribution. Bagguley and Robertson (6.17) obtained a transition temperature of 69°K for a Pd 1.5 at%Fe alloy by means of ferromagnetic resonance measurements. Our result thus falls somewhat lower than this but considering the sharp dependence of the transition temperature on iron concentration and the very wide variation of reported transition temperatures in the PdFe alloys obtained by various methods, Nieuwenhuys (6.18), this is not really surprising.

The magnetization of the annealed Pd 1.5 at%Fe disc is shown in figure 6.7 as a function of applied magnetic field at 4.2°K . As with the Pd 0.2 at%Fe specimen the M-H curve shows little dipolar remanence and has the

Figure 6.6 : Temperature dependence of the magnetization
($\Delta H = 2.0$ Oe) of a Pd 1.5 at%Fe alloy.

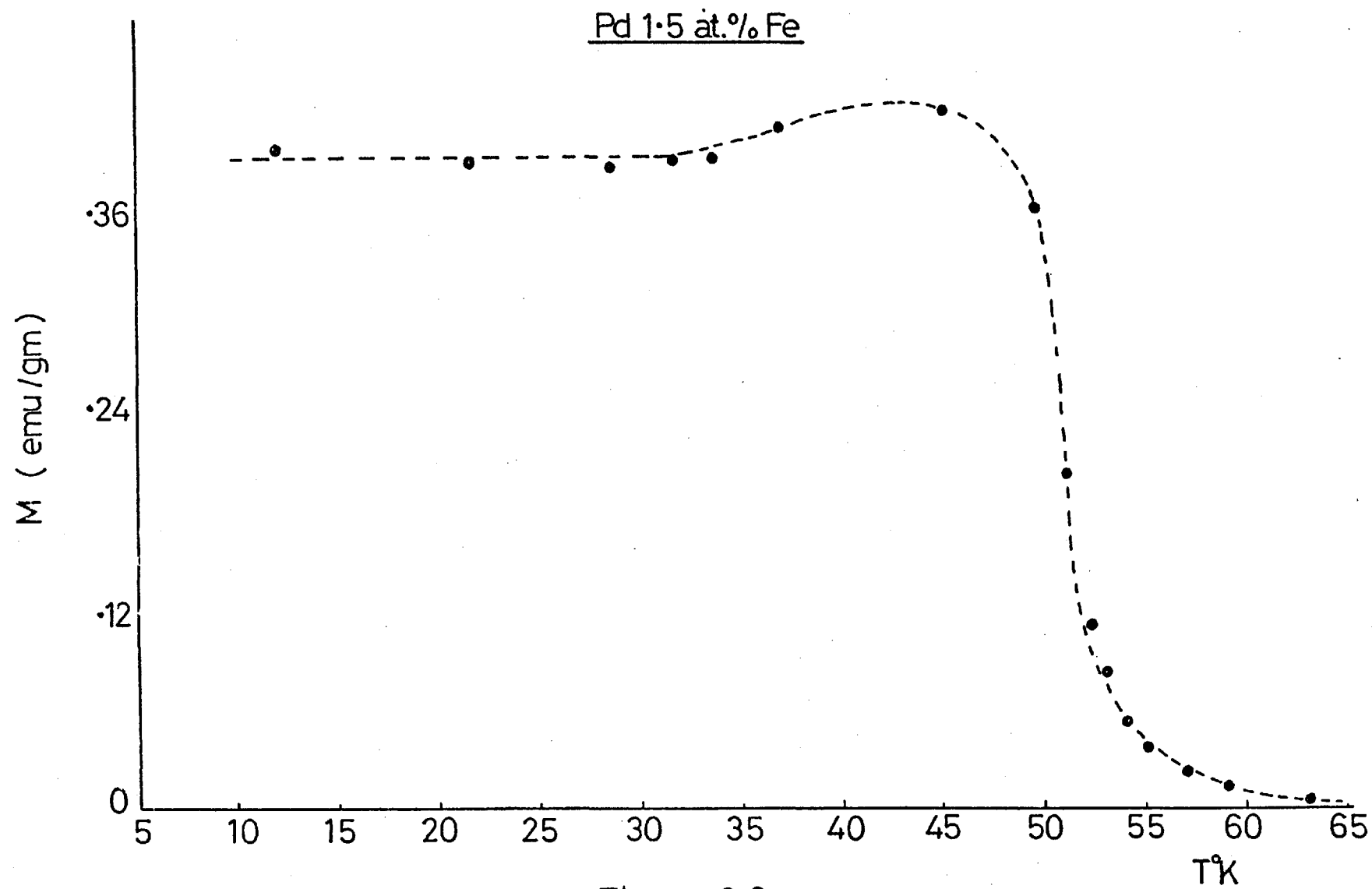


Figure 6.6

Figure 6.7 : Field dependence of the magnetization of the Pd 1.5 at%Fe specimen, at 4.2°K.

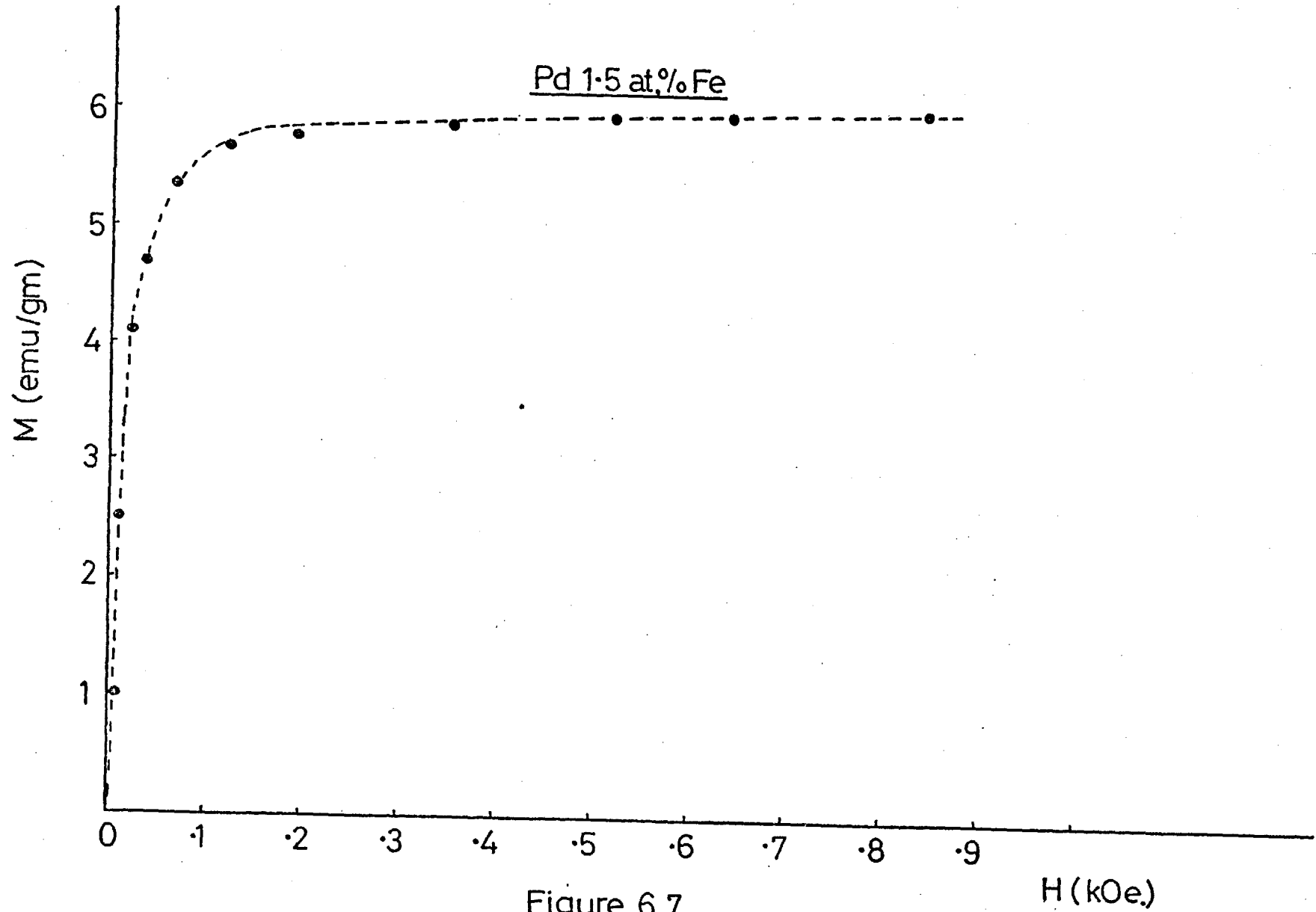


Figure 6.7

same sharp rise up to 50 Oe. followed by a gradual increase for higher fields. The sharp increase is determined by the demagnetization factor, being sharper for the smaller demagnetization factors, and the flattening for both the Pd 0.2 at%Fe alloy and the Pd 1.5 at%Fe alloy corresponds roughly to a moment per impurity atom of $2.2\mu_B$. The magnetization has, however, not fully saturated and high field magnetization measurements lead to a much higher value for the saturation moment per impurity atom.

It was not possible to extend the investigation to lower iron concentrations than 0.2 at%Fe since the transition temperature of interest moves below the minimum of 1.5°K achievable in our apparatus. However, it is clear from the Pd 0.2 at%Fe results that considerable portions of the impurity moments are not close enough to overlap directly with other impurities and thus we have a concentration region where competition of interactions produces a strange mixed region where the magnetic properties are very dependent on the precise distribution of the solute atoms. This is analogous to the PdMn system with manganese concentrations between about 3 and 4 at%.

Recent work by Verbeek et al. (6.19) has shown that the addition of Mn to a Pd 0.35 at%Fe alloy has exactly the same effect as increasing the manganese concentration in PdMn in that the ferromagnetism of the Pd 0.35 at%Fe alloy is broken up by the manganese and a spin glass regime obtained for a manganese concentration greater than

6 at%. Again, the ferromagnetism is broken up inhomogeneously so that a mixed region occurs between the ferromagnetic Pd 0.35 at%Fe alloy and the spin glass regime.

As a contrast, the results for two alloys of PdCo, with 0.3 and 0.58 at%Co, show a different type of behaviour. Nieuwenhuys (6.18) reports magnetization measurements made by Star on a Pd 0.24 at%Co alloy which show a gradual drop as the temperature is increased from 1°K. The effect of decreasing the field is to sharpen the drop to some extent but even in the lowest field used (1 KOe) the magnetization has only reached half the value obtained at 1°K by the time a temperature of 7°K is reached. In figure 6.8 we show the magnetization of a cylindrical Pd 0.3 at%Co sample in an incremental field of 2.0 Oe. Instead of increasing gradually as the temperature is lowered, a fairly sharp increase below 9°K is followed by a peak at about 5°K. However, the actual value of the susceptibility obtained here is much smaller than the demagnetization limit of $\frac{1}{N}$. The reason for this lies in the existence of a large remanent magnetization. After cooling the alloy to 4.2°K in the earth's field a magnetization exists which increases considerably after the application of an external field and its subsequent removal. The remanence reaches a value of 0.25 emu/gm after the largest field available (\sim 700 Oe) is applied. The remanence increases as the temperature is decreased, at 2.2°K the remanence is 0.46 emu/gm. At 4.2°K the coercive field was measured to

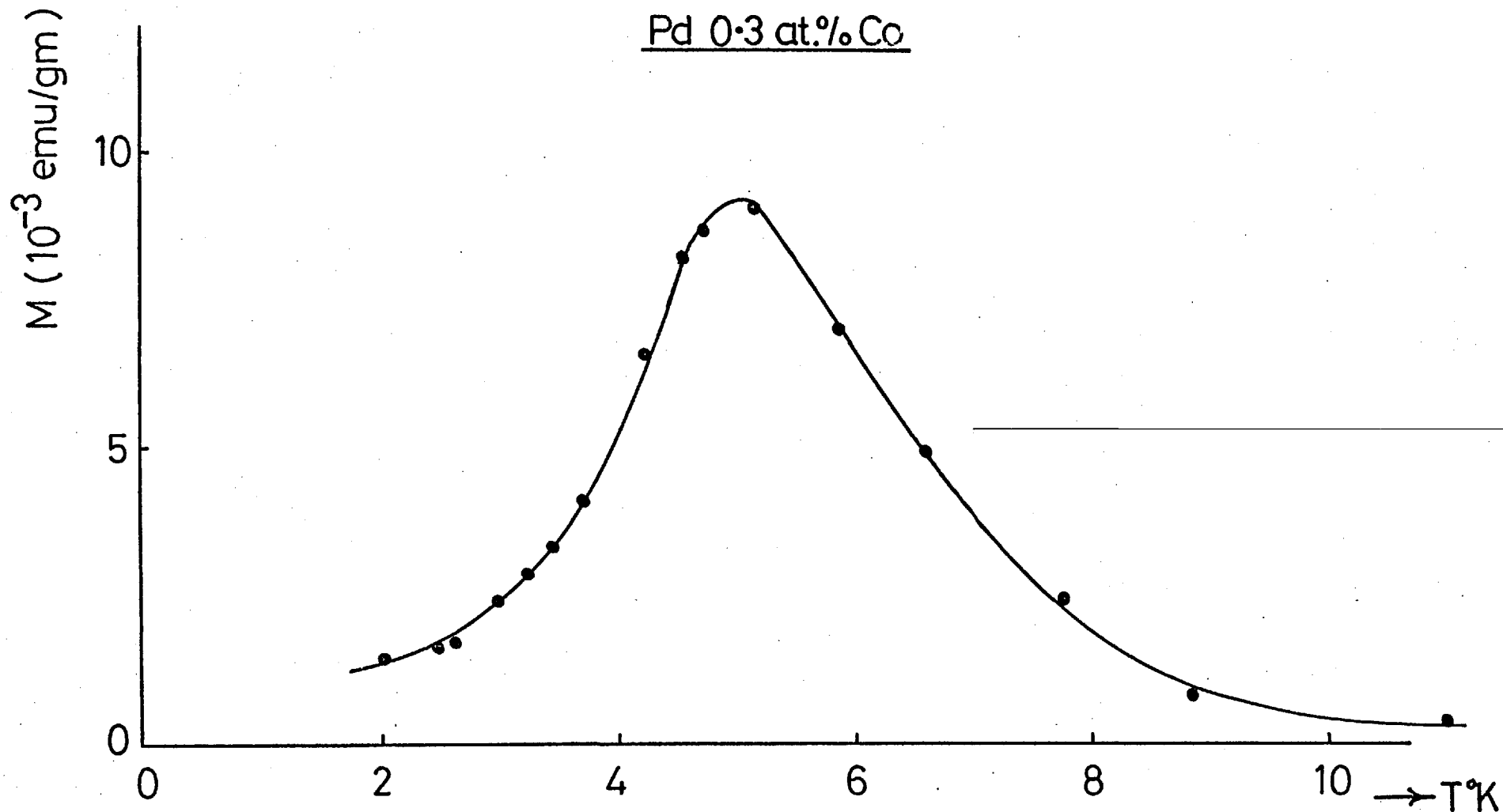


Figure 6.8 : Temperature dependence of the magnetization measured in a field of 2.0 Oe. above the earth's field.

be 40 Oe. while at 2.44°K the coercive field has risen to approximately 120 Oe.

In figure 6.9 we see similar behaviour for the Pd 0.58 at%Co alloy. After cooling to 4.2°K in the earth's field the sample had a magnetization of 0.44 emu/gm. After applying + 40 Oe. this remanence had increased slightly to 0.49 emu/gm. while after + 700 Oe. it had risen to 1.575 emu/gm. The coercive force at 4.2°K was found to be 255 Oe.

6.3.2 Discussion

The curves presented in figures 6.8 and 6.9 are very unusual. This type of variation of the susceptibility with temperature is indicative of a spin glass freezing but the large remanence and lack of time effects below the peak when 2 Oe. is applied indicate that this is not a typical spin glass freezing. However, when a field of 67 Oe was applied the magnetization did show quite a fast increase with time in the Pd 0.58 at%Co alloy. It is thus reasonable to assume that once again we have a field dependence of the time increase, as reported for the PdMn alloys in section 4.1.3, and it seems likely that the nature of the time effects are at the centre of the problem related to the magnetization curves obtained in these Pd based alloys. This would explain the failure of the higher field magnetization measurements on PdCo alloys to see any such low temperature drop in the susceptibility. The lack of any time effects when 2 Oe is applied reflects further

Figure 6.9 : Temperature dependence of the magnetization of a Pd 0.58 at%Co alloy. The applied field was 2.0 Oe above the earth's field so that the susceptibility is merely obtained by dividing the magnetization value by two. Both this alloy, and the Pd 0.3 at%Co alloy of figure 6.8, were in the form of a thin cylinder as they were obtained from resistivity samples. These resistivity samples originated in Orsay and were obtained via Dr. Greig of Leeds University. The exact heat treatment was not known but it may be assumed a standard anneal had been given.

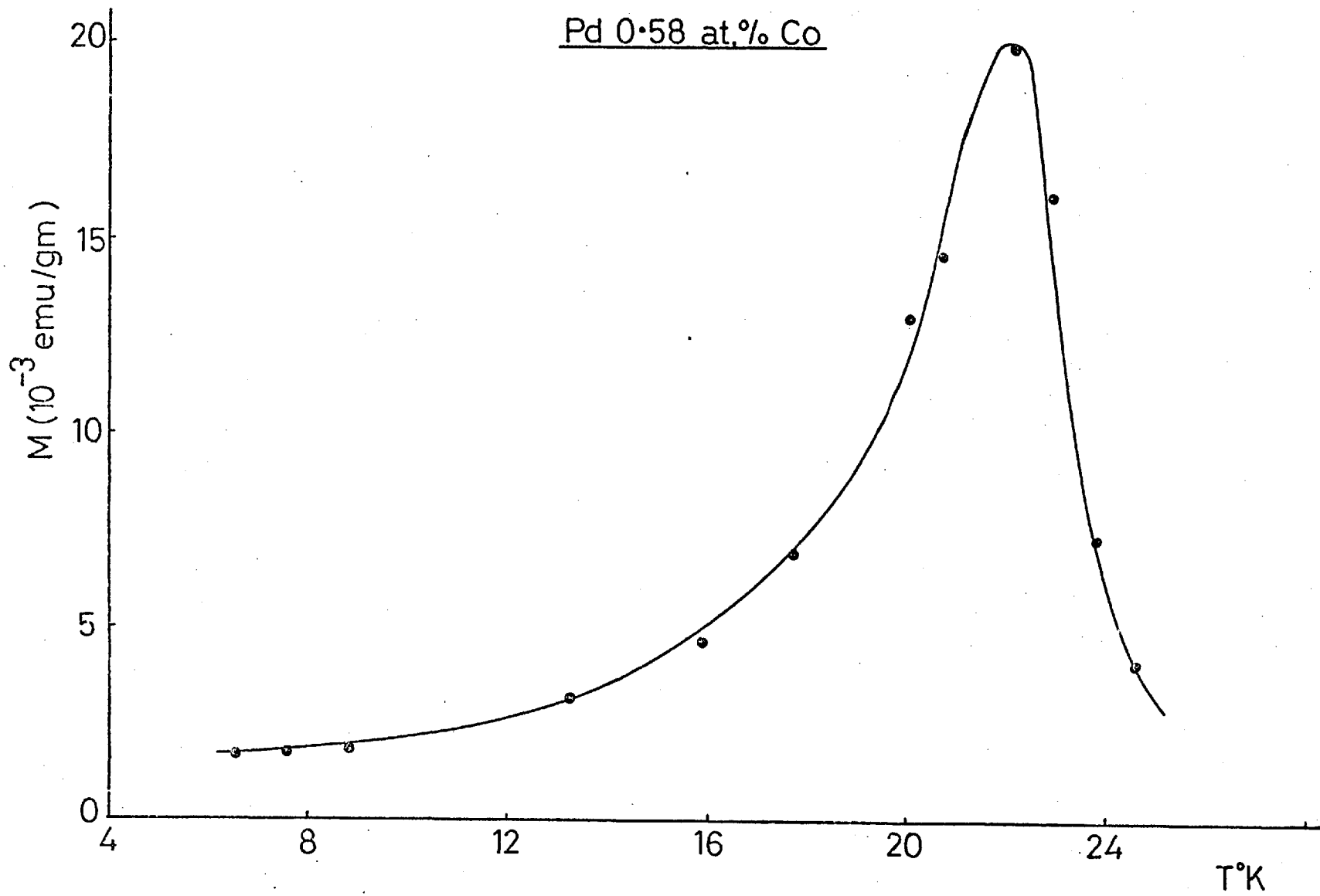


Figure 6.9

the unusual behaviour of these alloys. This may be tied up with the anisotropy which occurs in PdCo. The anisotropy of the resistivity has recently been reported (6.20) and it was argued by these authors that this was evidence for an orbital contribution to the Co moment. This being so, the crystal field at the Co site could result in a single ion anisotropy. This anisotropy is further evidenced in the occurrence of hysteresis in these PdCo alloys, the observation of which, far above the reported Curie temperatures, remains one further problem (for example, Star et al. (6.21) have observed hysteresis in a Pd 0.24 at%Co alloy (reported $T_c \sim 4.16^\circ\text{K}$) at 20°K).

In ordinary ferromagnetic materials the anisotropy goes to zero at T_c so that the sample is 'soft' at T_c but at lower temperatures the anisotropy may increase and thus reduce the initial susceptibility from the demagnetization limit. Hence, even ferromagnetic materials may show a peak in the initial susceptibility (a Hopkinson peak). In dilute ferromagnetic materials there can be a local sort of anisotropy because of the low symmetry around each magnetic site and so if there is a spread of local T_c values along with a rapidly developing magnetic 'hardness' at lower temperatures a superposition of a set of curves could lead to the type of behaviour found for the PdCo alloys studied. Thus, the curves shown in figures 6.8 and 6.9 do not necessarily mean the alloys are not ferromagnetic. However, it is clear that much more work is required in this direction in order to come to any firm conclusions, and we have plans for extending

this investigation in the near future.

6.4 Platinum Nickel

It has generally been accepted that PtNi alloys in the critical concentration region for the onset of ferromagnetism are examples of weak itinerant ferromagnets. These conclusions stem from investigations of the magnetic properties including the effect of an applied hydrostatic pressure on the magnetization (Alberts et al. (6.22), Beille et al. (6.23)) thermal expansivity (Kortekaas et al. (6.24), Franse (6.25)) and volume magnetostriction (Franse (6.25), Kortekaas and Franse (6.26)). However, recent reviews of the dilute alloy problem (Wohlleben and Coles (6.27)) have contended that traditional approaches to moment formation in metals, based on the virtual bound state ideas of Friedel (see chapter 1, section 2), over estimate the itinerant aspect of this problem, and that as a consequence more attention should be paid to ionic like models such as the configuration based approach of Hirst (6.28 and 6.29). We have carried out low field d.c. magnetization measurements on two PtNi alloys containing 40 and 41 at%Ni, concentrations just below the critical concentration for the occurrence of ferromagnetism (= 41.7 at%Ni) and obtained results to support this point of view.

The samples were prepared by arc melting appropriate amounts of pure Ni(3N) and Pt(3N) to form spherical specimens. The magnetization of the 40 at%Ni specimen is shown as a function of temperature in figure 6.10. The

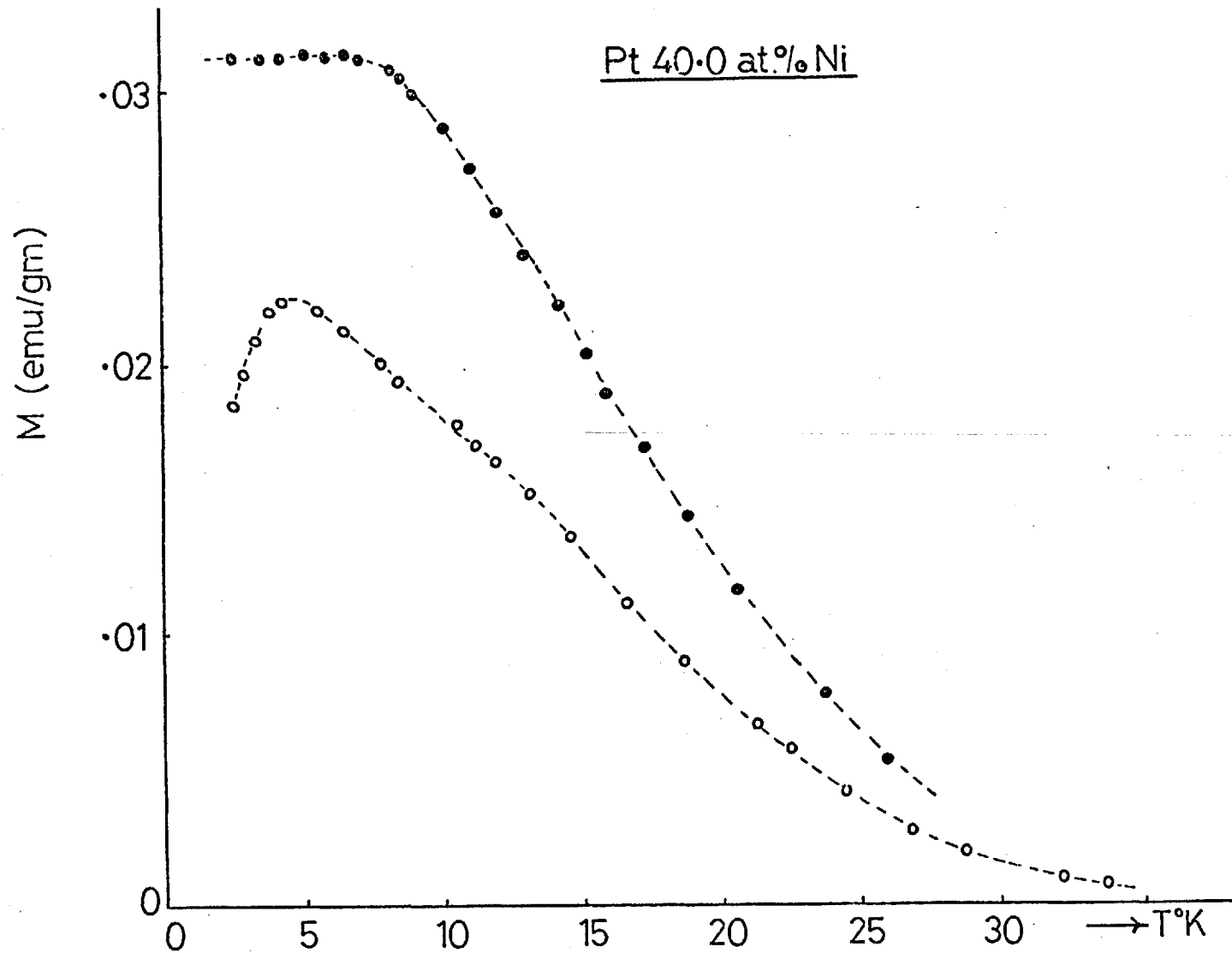


Figure 6.10 : Temperature variation of the magnetization of a Pt 40.0 at.% Ni alloy. • Measured in a field of 2 Oe. after cooling to 21°K in 2 Oe. and warming. ◦ Measured in 2 Oe. after zero field cooling.

sample was first cooled in zero field and the magnetization measured in an applied field of 2 Oe. The sample was then cooled from room temperature to the lowest temperature attainable in the same field of 2 Oe. and the measurements repeated. Similar measurements for the Pt 41 at%Ni alloy are shown in figure 6.11.

We see that when the Pt 41 at%Ni alloy is cooled in zero field, $M(T)$ exhibits a maximum at 5.4°K . Such a temperature dependence of the magnetization indicates spin glass behaviour. When the sample is then field cooled, the maximum disappears and instead $M(T)$ tends to a limiting value below about 11°K . The limiting value of the magnetization reached in the field cooled case is equal to the demagnetization limit for a sphere (the limiting susceptibility for a sphere is 0.2387 emu/c.c.). For PtNi, therefore, with approximately 40 at%Ni this is equivalent to 0.0145 emu/gm), indicative of ferromagnetic ordering. The differences between the field cooled and zero field cooled cases can be understood if there exist magnetic clusters with fairly large moments. The observed behaviour is then comparable with spin glass systems just below the percolation limit for ferromagnetism where large clusters form, each locking at random with respect to one another due to the RKKY coupling between them.

The Pt 40 at%Ni specimen exhibits a similar type of behaviour. When cooled in zero field, the magnetization shows a maximum at 4.3°K . When field cooled it exhibits

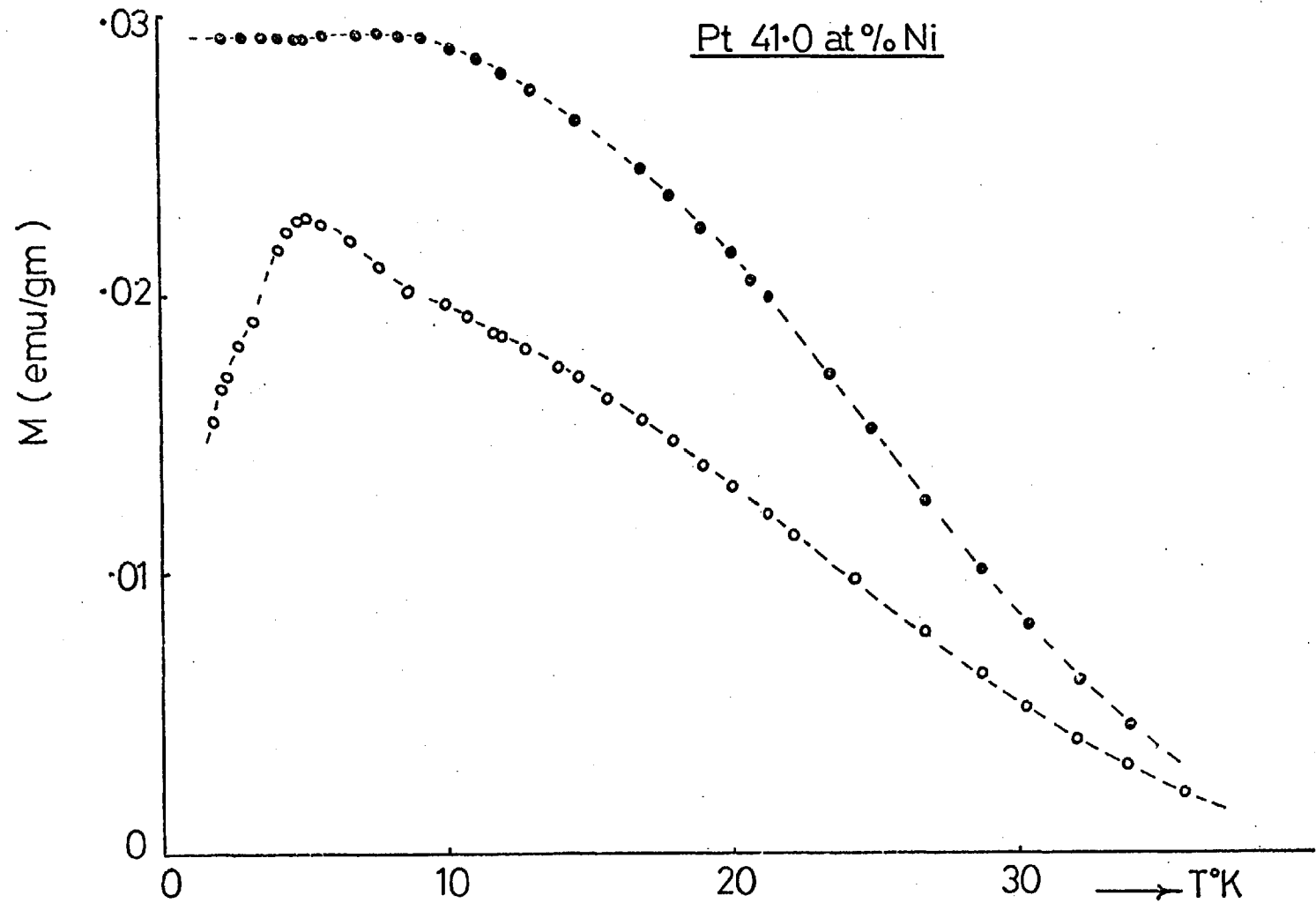


Figure 6.11 : Magnetization versus temperature for Pt 41.0 at.% Ni.

- Measured in 2 Oe. after cooling to 2.1°K in 2 Oe. and warming.
- Measured in 2 Oe. after zero field cooling.

a ferromagnetic character in that the demagnetization limit is reached below 8°K .

In field cooling low concentration spin glasses the magnetization remains constant below T_g , but no increase in the magnetization occurs at this temperature over that for the zero field cooled case. However, for the higher concentration alloys where ferromagnetic clusters form, field cooling has the effect of aligning these large moment clusters to give an apparent ferromagnetic ordering. We believe, therefore, that instead of an explanation in terms of weak itinerant ferromagnetism the approach to ferromagnetic ordering in PtNi can be explained in terms of large ferromagnetic clusters. The approach to ferromagnetism will be inhomogeneous, analogous to the situation in PdNi where local environment effects are operative (Murani et al. (6.30)).

REFERENCES

- 6.1 Van Den BERG G.J.
Prog. Low Temp. Phys., Vol.4, p.194 (1964).
- 6.2 OWEN J., BROWNE M.E., KNIGHT W.D. and
KITTEL C.
Phys. Rev. 102, 1501 (1956).
- 6.3 CAREGA J.A., DREYFUS B., TOURNIER R. and
WEIL L.
Low Temp. Phys. (Proc. Moscow conf. 1966), Vol.10.
- 6.4 NAKAMURA A. and KINOSHITA N.
J. Phys. Soc. Jap. 27, 382 (1969).
- 6.5 Du CHATENIER F.J. and MIEDEMA A.R.
Physica 32, 403 (1966).
- 6.6 OWEN J., BROWNE M.E., ARP V. and KIP A.F.
J. Phys. Chem. Sol. 2, 85 (1957).
- 6.7 KOUVEL J.S.
J. Phys. Chem. Sol. 21, 57 (1961) and Ibid 23,
795 (1963).
- 6.8 KLEIN M.W. and BROUT R.
Phys. Rev. 132, 2412 (1963).
- 6.9 CANNELLA V., MYDOSH J.A. and BUDNICK J.I.
J. Appl. Phys. 42, 1689 (1971).
- 6.10. CANNELLA V.
Amorphous Magnetism, p.195, edited by Hooper H.O.
and De Graaf A.M., Plenum N.Y. (1973).
- 6.11 SATO H., WERNER S.A. and YESSIK M.
AIP Conf. Proc. 5, 508 (1971).
- 6.12 GUY C.N.
J. Phys. F 7, 1505 (1977).
- 6.13 SARKISSIAN B.V.B.
J. Phys. F 7, L139 (1977).
- 6.14 McDOUGALD M. and MANUEL A.J.
J. Appl. Phys. 39, 961 (1968).
- 6.15 BOZORTH R.M., WOLFF P.A., DAVIS D.D., COMPTON V.B.
and WERNICK J.H.
Phys. Rev. 122, 1157 (1961).
- 6.16 CHOUTEAU G. and TOURNIER R.
J. de Physique, Colloque C1, 32, C1-1002 (1971).

- 6.17 BAGGULEY D.M.S. and ROBERTSON J.A.
Physics Letts. A27, 516 (1968).
- 6.18 NIEUWENHUYS G.J.
Adv. in Phys. 24, 515 (1975).
- 6.19 VERBEEK B.H., NIEUWENHUYS G.J., STOCKER H. and
MYDOSH J.A.
Phys. Rev. Letts. 40, 586 (1978).
- 6.20 SENOUSI S., CAMPBELL I.A. and FERT A.
Solid State Commun. 21, 269 (1977).
- 6.21 STAR W.M., FONER S. and McNIFF E.J.
Phys. Rev. B12, 2690 (1975).
- 6.22 ALBERTS H.L., BEILLE J., BLOCH D. and WOHLFARTH E.P.
Phys. Rev. B9, 2233 (1974).
- 6.23 BEILLE J., BLOCH D. and BESNUS M.J.
J. Phys. F4, 1275 (1974).
- 6.24 KORTEKAAS T.F.M., FRANSE J.J.M. and HOLSCHER H.
Phys. Letts. 48A, 305 (1974).
- 6.25 FRANSE J.J.M.
Physica 86-88B, 283 (1977).
- 6.26 KORTEKAAS T.F.M. and FRANSE J.J.M.
J. Phys. F6, 1161 (1976).
- 6.27 WOHLLEBEN D.K. and COLES B.R.
Magnetism, Vol.5, p.3, Edited by Rado G.T. and
Suhl H., Academic press, New York, (1973).
- 6.28 HIRST L.L.
Z. Phys. 241, 9 (1971).
- 6.29 HIRST L.L.
AIP Conf. Proc. 24, 11 (1974).
- 6.30 MURANI A.P., TARI A. and COLES B.R.
J. Phys. F4, 1769 (1974).

CHAPTER 7

Suggestions for further Work

A large number of workers have been contributing to the study of spin glasses in the past two or three years giving a steady addition to the available literature in this field. During the course of this thesis, work in our labs. at Imperial College has added greatly to the advancement of our understanding of these materials, such as the work of Dr. C.N. Guy, who has clearly shown the metastable nature of the spin glass state with respect to an applied magnetic field.

At present, there is still a diversity of opinion as to the crucial question of whether an actual phase transition occurs or not. There is therefore, some further fundamental work to be performed in order to finally clarify this point.

In this thesis, we have been concerned with the important technique of measuring the magnetization of samples in very low fields. Standard measurements of the magnetization of materials have generally been performed in large fields in order to facilitate the measurement but our results have been obtained in fields of about 2 Oe and as such are much more likely to be able to probe the zero field magnetic state, i.e. the intrinsic magnetic order, of the material. We have seen how this is particularly relevant in the study we have made of the PdMn magnetic system. Previous magnetization

measurements were unable to clearly distinguish the change in magnetic ordering of the alloys as the manganese concentration was increased, whereas our low field magnetization measurements show the spin glass nature of those alloys with 4.0 at%Mn and greater. Even though a diverse number of measurements have been made on dilute PdMn alloys ($c < 3.0$) and general agreement over the ferromagnetic and giant moment behaviour exists there are still a lot of unsolved problems. In chapter two we discussed the difficulty in tying together the different types of experimental results, such as the problem of the enhanced g factor obtained from specific heat and the much smaller g factor from esr measurements. Further, the specific heat peaks, lack of magnetization saturation, enhanced forward neutron scattering peaks have all added to the complication of the picture. In chapter 4 we discussed to some extent the problems involved in dealing with dilute alloy ferromagnetism and tried to draw analogies with the situation in standard ferromagnetic theory, dealing with domain formation, in discussing the field dependence of the magnetization of dilute PdMn alloys. The whole area of dilute Pd alloys is still full of uncertainty and a great deal of further attention is needed. In chapter 6 we made a start in studying the PdFe and PdCo low field magnetization and work for the future must centre upon drawing upon the collected knowledge of these systems in order to finally understand the magnetic properties of dilute Pd alloys. For example,

questions as to why and how the differences in the low field magnetization of PdCo and PdFe or PdMn occur, need answering.

Our work on these low field measurements has also indicated that a study of spin glass time effects as a function of field will prove fruitful and dealing further with spin glass effects it will be interesting to be able to extend the type of measurements made here to much lower concentrations, in order to be able to see any change over to a spin glass coupling as the concentration decreases below that necessary for an infinite chain of ferromagnetically coupled moments.

As mentioned in Chapter 4, further work is in progress dealing with the pressure dependence of the ordering in the PdMn alloys, and results in this direction should prove informative.

The work developed in chapter 5, culminating in the proof of the validity of the idea that a SQUID magnetometer may be used to observe the sublattice magnetization of a layer antiferromagnet, also holds great potential for further work.

As is usually the case in research the work presented here is nothing like a closed book and, if anything, suggests much more to be done than at the outset and it will be interesting to look back in five years time to see just how much the picture has changed from that presented here.

APPENDIX A

Consider the pick-up coil arrangement shown in fig.A.1. O is the central point between the two coils and P is a point on the axis, distant Z from O. If a current, i , were to flow in the coils then the field produced at P by the left hand coil is given by

$$H_{zL} = n \int_{\Delta=0}^{\Delta=C} \int_{a=a_1}^{a=a_2} \frac{\frac{1}{2} i a^2}{\left\{ a^2 + \left(\frac{A}{2} + \Delta + Z \right)^2 \right\}^{3/2}} da d\Delta \quad (A.1)$$

where the coil inner radius $R - B = a_1$,

and the coil outer radius $R + B = a_2$

n = no. of turns/unit volume.

Letting $u = A/2 + \Delta + Z$; $du = d\Delta$ and we have :

$$\begin{aligned} H_{zL} &= \frac{1}{2} i n \int_{a=a_1}^{a=a_2} \left[\frac{u}{(a^2 + u^2)^{3/2}} \right]_{u=\frac{A}{2}+Z}^{u=\frac{A}{2}+Z+C} da \\ &= \frac{1}{2} i n \left[\left\{ u \sinh^{-1} \left(\frac{a}{u} \right) \right\}_{u=\frac{A}{2}+Z}^{u=\frac{A}{2}+Z+C} \right]_{a=a_1}^{a=a_2} \quad (A.2) \end{aligned}$$

For the right hand coil we obtain the same expression except $Z \rightarrow -Z$

so that the total field at P is given by evaluating $\left(\frac{1}{2} i n \right) \sinh^{-1} (a/u)$ at eight positions; the four corners 1,2,3,4 of the left hand coil then putting $-Z = Z$ and evaluating at the four corners of the right hand coils, 5,6,7,8 and combining with the appropriate signs.

$$\therefore H_z = \frac{n}{2} i u \sinh^{-1} (a/u) \quad (A.3)$$

By differentiation of this expression we can also show that:

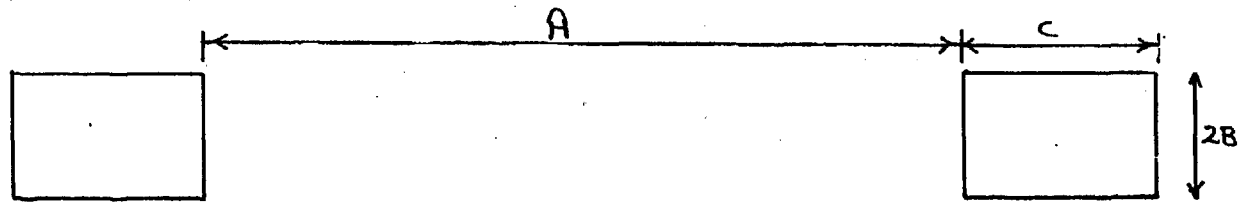
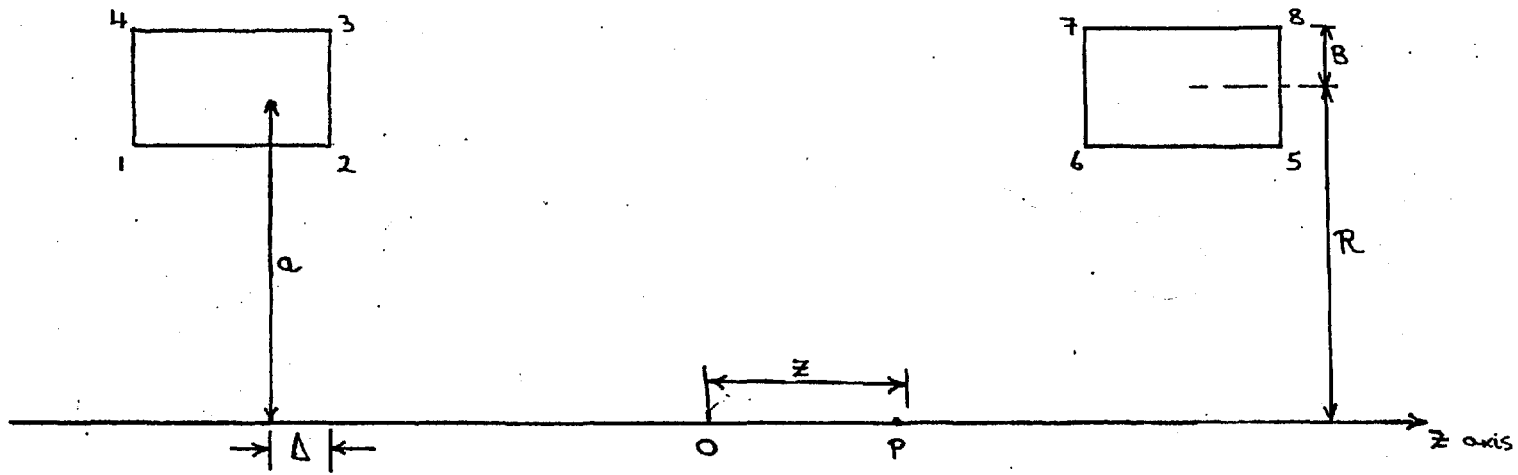


Figure A.1

$$\begin{aligned}
 \text{i)} \quad \frac{dH_z}{dz} &= \frac{1}{2} \operatorname{in} \left[\sinh^{-1} \left(\frac{a}{u} \right) - \frac{a}{(a^2 + u^2)^{\frac{1}{2}}} \right] \\
 &= \frac{1}{2} \operatorname{in} \left[\frac{2H_z}{\operatorname{in} u} + t \right] \quad (\text{A.4})
 \end{aligned}$$

$$\text{where } t = \frac{-a}{(a^2 + u^2)^{\frac{1}{2}}}$$

and further differentiation gives the following :

$$\text{ii)} \quad \frac{d^2 H_z}{dz^2} = \frac{1}{2} \operatorname{in} \left(\frac{t^3}{u} \right)$$

$$\text{iii)} \quad \frac{d^3 H_z}{dz^3} = \frac{1}{2} \operatorname{in} \frac{t^3}{u^2} \left[3t^2 - 4 \right]$$

$$\text{iv)} \quad \frac{d^4 H_z}{dz^4} = \frac{1}{2} \operatorname{in} \frac{t^3}{u^3} \left[15t^4 - 33t^2 + 20 \right]$$

$$\text{v)} \quad \frac{d^5 H_z}{dz^5} = \frac{1}{2} \operatorname{in} \frac{t^3}{u^4} \left[105t^6 - 315t^4 + 324t^2 - 120 \right]$$

each of which are to be evaluated at the eight points in the correct combination.

Appendix B.1 To calculate h_{zav}^1 and modifications for the higher derivatives: (for an HP 9820)

```

0:
ENT A,B,C,X,R22;
0+Y;-1.0+Z;SCL -
1;2;-.5;.5;AXE 0
:0;.5;.1+
1:
0+R1+R2+R3+R5+R6
+R7+R8+R9+R10+R2
6+R27+R51+R52+R4
4+R45+
2:
A+X-B+R51;A+X+B+
R52;Z+A/2+R26;Z+
A/2+C+R27+
3:
IF Y=0;R27+R2;R5
1+R1;GTO 9+
4:
IF Y=1;R26+R2;R5
1+R1;GTO 9+
5:
IF Y=2;R26+R2;R5
2+R1;GTO 9+
6:
IF Y=3;R27+R2;R5
2+R1;GTO 9+
7:
IF Y=4;0+Y;IF
FLG 4;GTO 17+
8:
SFG 4;-Z+Z;GTO 2
+
9:
IF R22=0;GTO 23+
10:
R2+R22/2+R44;r(R
1+R1+R44+R44)+R3
;-R1/R3+R30+
11:
R44*LH ((R1+R3)/
1.0)+R(5+FLG 5)+
12:
IF FLG 5;GTO 14+
13:
SFG 5;-R22+R22;
GTO 10+
14:
-R22+R22;CFG 5;
R5-R6)/R22+R7+
15:
(-1)*Y+R7+R(8+
FLG 4)+R(8+FLG 4
+
16:
Y+1+Y;GTO 3+
17:
CFG 4+
18:
R8+R9+R10;-Z+Z+

```

```

19:
PRT Z;PRT R10;
SPC 1+
20:
PLT Z;R10+
21:
Z+0.1+Z+
22:
IF Z<2;GTO 1+
23:
PRT "R22=0"+
24:
STP +
25:
END +
R344

```

For the higher derivatives

i) for h_{zav}^2 .

line 11: $\ln(R1+R3)+R30 \rightarrow R(5+flg5)$

line 18: $R8-R9 \rightarrow R10$ $-Z \rightarrow Z$

ii) for h_{zav}^3 .

line 11: $1/R44[R30^3]$

iii) for h_{zav}^4 .

line 11: $((R30^3)/(R44 * R44)) * (3(R30^2)-4)$

line 18: $R8-R9 \rightarrow R10$; $-Z \rightarrow Z$

iv) for h_{zav}^5 .

line 11: $(R30^3) * (15R30^4 - 33R30^2 + 20) / (R44^3)$

LIST

```

77/11/15. 16.28.12.
PROGRAM LEASTSQ
00100 PROGRAM LEASTSQ (DH1, DH2, DH3, DH4, DH5, INPUT, OUTPUT,
00120+ TAPE1=DH1, TAPE2=DH2, TAPE3=DH3, TAPE4=DH4, TAPE5=DH5,
00140+ TAPE6=INPUT, TAPE7=OUTPUT)
00160 DIMENSION R(200), Z(5), ZP(5), ZM(5)
00161 DIMENSION XA(30)
00170 INTEGER X
00174 WRITE(7, 15)
00176 15 FORMAT(4X, *THE 18 PTS. TO BE FIT ARE ; *, /)
00199 DO 17 K=1, 3
00200 I=(6.0*K)-5.0
00225 L=I+5
00230 17 READ( , (R(J), J=1, L)
00250 WRITE(7, 438) (R(I), I=1, 18)
00251 438 FORMAT(6F10.6)
00285 DO 888 I=1, 5
00287 888 REWIND I
00300 DO 3 I=19, 36
00320 3 READ(1, 4) R(I)
00340 4 FORMAT(F25.10)
00360 DO 5 I=37, 54
00380 5 READ(2, 4) R(I)
00400 DO 6 I=55, 72
00420 6 READ(3, 4) R(I)
00440 DO 7 I=73, 90
00460 7 READ(4, 4) R(I)
00480 DO 8 I=91, 108
00500 8 READ(5, 4) R(I)
00580 WRITE(7, 819)
00590 819 FORMAT(15X, 25H+*****2X)
00620 DO 99 I=1, 5
00627 A=1.69
00629 S=4.58
00630 B=C=D=0.0
00634 WRITE(7, 91) A, S
00636 91 FORMAT(2X, *STARTING A=*, F4.2, /, *STEP= *, F4.2)
00640 J=1+18
00650 30 X=1
00660 Z(I)=ZM(I)=ZP(I)=0.0
00780 31 Y=R(X)-A*R(X+J)
00800 YP=R(X)-(A+0.0000001)*R(X+J)
00820 YM=R(X)-(A-0.0000001)*R(X+J)
00840 Z(I)=Y+Y+Z(I)
00860 ZP(I)=YP+YP+ZP(I)
00880 ZM(I)=(YM+YM)+ZM(I)
00900 X=X+1
00920 IF(X.GT.18) GO TO 55
00940 GO TO 31
00960 55 TP1=ZP(I)-Z(I)
00980 TP2=Z(I)-ZM(I)
01000 TP=TP1+TP2
01020 IF(TP.GT.0.0) GO TO 82
01040 IF(TP.LT.0.0) GO TO 85
01060 WRITE(7, 408)
01080 408 FORMAT(2X, *SHARP MIN. FOUND*)
01100 GO TO 200
01120 82 IF(TP1) 83, 84, 84
01140 83 A=A+S
01160 B=1
01180 GO TO 97
01200 84 A=A-S
01220 C=1
01240 GO TO 97
01260 85 A=A+(S+2.0)
01280 WRITE(7, 50)
01300 50 FORMAT(2X, *MAX. PT. REACHED*, 2X)
01320 GO TO 30
01340 97 D=B+C
01360 IF(D.EQ.2.0) GO TO 105
01380 GO TO 30
01400 105 S=S/5.0
01420 IF(S.LT.0.000001) GO TO 200
01460 B=C=D=0.0
01500 GO TO 30
01520 200 WRITE(7, 202) A, Z(I)
01540 202 FORMAT(2X, *A= *, E15.8, 10X, *SUM OF SQUARES = *, E15.8)
01560 X=1
01580 501 R(X)=R(X)-A*R(X+J)
01590 X=X+1
01600 IF(X.GT.18) GO TO 99
01620 GO TO 501
01640 99 CONTINUE
01655 WRITE(7, 57)
01657 57 FORMAT(2X, *THE REMAINDER IS*, /)
01660 WRITE(7, 59) (R(I), I=1, 18)
01670 59 FORMAT(5E15.8)
01700 STOP
01800 END
READY.

```